Ingeniería e Investigación
Journal
Abbreviated Journal Title: **Ing. Investig.**

**Editor-in-chief**
Andrés Pavas, Ph.D.

**Editorial Assistants**
Fabián Hernando Ríos, B. Eng.
Ingri Gisela Camacho



**Frequency**
Quarterly, 3 issues per year
April, August and December

**Cover Layout**
Carlos Andrés Ortiz Valle

**Proofreader**
José Daniel Martínez

**Layout Artist**
Patricia Chávez R.

**Photography**
Mauricio Morales Pérez

**For additional information contact**
revii_bog@unal.edu.co
Bogotá - Colombia
December - 2021

# Table of Contents

**Papers published in *Ingeniería e Investigación journal* are abstracted/indexed in**

- Science Citation Index Expanded (SciSearch®), Clarivate Analytics
- Scopus - Elsevier
- Scientific Electronic Library Online - SciELO, Colombia
- Chemical Abstract
- índice de Revistas Latinoamericanas en Ciencias Periódica
- Redalyc-Red de Revistas Científicas de América Latina y el Caribe, España y Portugal
- Dialnet
- Sistema Regional de Información en Línea para Revistas Científicas de América Latina, El Caribe, España y Portugal - Latindex
- Ebsco Publishing
- DOAJ - Directory of Open Access Journals
- Redib - Red Iberoamericana de Innovación y Conocimiento Científico

*Ingeniería e Investigación journal* was created in 1981. This is an entity in charge of spreading the teaching, scientific and technical research developed in the Universidad Nacional de Colombia's Engineering Faculty and other national and international institutions. *Ingeniería e Investigación journal* deals with original, unedited scientific research and technological developments in the various disciplines related to engineering. *Ingeniería e Investigación journal* contributes towards the development of knowledge, generating a global impact on academia, industry and society at large, through an exchange of knowledge and ideas maintaining a set of serious and recognized quality standards.



*Ingeniería e Investigación journal* publications are developed for the academic community who is interested in research and engineering knowledge development. We invite readers to be part of this Journal and participate either as authors, peer reviewers or subscribers.

**For additional information contact:**
www.revistas.unal.edu.co/index.php/ingeinv
E-mail: revii_bog@unal.edu.co
Tel: 57(1) 3 16 5000 Ext. 13674

# Tabla de Contenido

http://dx.doi.org/10.15446/ing.investig.v41n3.97492

Carta al editor

# El COVID-19 está en el aire: ¿por qué seguimos ignorando la importancia de la ventilación?


## Resumen

El principal mecanismo de transmisión del virus SARS-CoV-2 es por vía aérea, particularmente en ambientes interiores mal ventilados. Reconocer la importancia de este mecanismo ha tomado mucho tiempo, a pesar de la evidencia generada por científicos de aerosoles desde una etapa temprana de la pandemia. Por lo tanto, las medidas aplicadas con mayor rigor por la población se han centrado en la desinfección de las superficies, muchas veces de manera exagerada, mientras que las medidas centradas en reducir la concentración de aerosoles en ambientes interiores, tales como una adecuada ventilación y la filtración de aire, han sido promovidas muy tímidamente. Además de los avances en el Plan Nacional de Vacunación, es necesario intensificar las medidas de prevención del contagio para una reapertura de la economía más segura. Es urgente, por lo tanto, educar y generar lineamientos claros para la evaluación y el mejoramiento de la ventilación en espacios interiores.

**Palabras clave:** SARS-CoV-2, COVID-19, transmisión, pandemia, ventilación

Estimado editor,

La pandemia del COVID-19 es la primera causada por un coronavirus que infecta a los humanos, el SARS-CoV-2, el cual inicia su transmisión a través de las células epiteliales del tracto respiratorio (Hu *et al.*, 2021). Desde los primeros informes de casos en Wuhan, China, en enero de 2020, la Organización Mundial de la Salud (OMS) confirmó la transmisión persona a persona y declaró la pandemia en marzo (OMS, 2020a). Desde el inicio de la pandemia, la OMS afirmó que los principales mecanismos de transmisión son gotículas respiratorias producidas al toser o estornudar, así como los fómites, cuando hay contacto con superficies contaminadas (OMS 2020b). De esta manera, las recomendaciones para reducir la transmisión del virus estuvieron enfocadas en la detección y aislamiento de personas con síntomas, el lavado de manos y el distanciamiento social o físico. El posible contagio por superficies contaminadas motivó a la población y las autoridades sanitarias a promover y aplicar medidas exageradas de limpieza y desinfección (Ives, 2021).

En julio de 2020, un grupo de 239 científicos señaló que, durante los primeros seis meses de pandemia, ya había evidencia del papel crucial de un tercer mecanismo de transmisión: los aerosoles. Estos científicos hicieron un llamado a la comunidad médica, así como a las agencias y

Letter to Editor

# COVID-19 Is in the Air: Why Are We Still Ignoring the Importance of Ventilation?


## Abstract

The main transmission mechanism of the SARS-CoV-2 virus is airborne, particularly in poorly ventilated indoor environments. Recognizing the importance of this mechanism has taken a long time, despite the evidence generated by aerosol scientists from an early stage of the pandemic. Hence, measures applied more widely by the population have focused on the disinfection of surfaces, often in an exaggerated way, while measures focused on reducing the concentration of aerosols in indoor environments, such as adequate ventilation and air filtration, have been timidly promoted. In addition to the progress of the National Vaccination Plan, it is necessary to intensify transmission prevention measures for a safer reopening of the economy. It is therefore urgent, to educate and generate clear guidelines for the evaluation and improvement of ventilation in indoor spaces.

**Keywords:** SARS-CoV-2, COVID-19, transmission, pandemic, ventilation

Dear Editor,

The COVID-19 pandemic is the first one caused by a human-infecting coronavirus, SARS-CoV-2, which begins its transmission through the epithelial cells of the respiratory tract (Hu *et al.*, 2021). Since the first case reports in Wuhan, China, in January 2020, the World Health Organization (WHO) confirmed person-to-person transmission and declared a pandemic in March (WHO, 2020a). Since the beginning of the pandemic, the WHO stated that the main transmission mechanisms are respiratory droplets produced by coughing or sneezing, as well as fomites, when there is contact with contaminated surfaces (WHO, 2020b). Thus, the recommendations to reduce the transmission of the virus were focused on the detection and isolation of symptomatic people, hand washing, and social or physical distancing. Potential infection from contaminated surfaces motivated the population and health authorities to promote and apply exaggerated cleaning and disinfection measures (Ives, 2021).

In July 2020, a group of 239 scientists pointed out that, within the first six months of the pandemic, there was already evidence of the crucial role of a third transmission mechanism of the virus: aerosols. They called on the medical community, as well as national and international agencies and authorities, including the WHO, to take preventive measures to reduce airborne transmission (Morawska *et al.*, 2020). Despite the evidence provided by the scientific community, the WHO (2021) recognized the transmission by aerosols only until April 2021. There is still a lack of clarity in the communications of the WHO and health authorities around the world about

autoridades nacionales e internacionales, incluida la OMS, a tomar medidas preventivas para reducir la transmisión aérea (Morawska *et al.*, 2020). A pesar de la evidencia aportada por la comunidad científica, la OMS (2021) reconoció la transmisión por aerosoles solo hasta abril de 2021. Aún falta claridad en las comunicaciones de la OMS y las autoridades sanitarias en todo el mundo sobre la importancia de las medidas que pueden ser más efectivas para reducir el riesgo de transmisión por aerosoles, particularmente en la evaluación y mejora de la ventilación y la filtración de aire en interiores.

Los aerosoles y las gotículas tienen características distintas. Las gotículas tienen un tamaño mayor a 100 µm y, debido a esto, caen rápidamente el suelo con una distancia promedio de 2 m en segundos o unos pocos minutos después de ser exhaladas (al hablar, gritar, cantar, estornudar o toser). Por otro lado, los aerosoles miden menos de 100 µm y también son emitidos al respirar o hablar normalmente. A diferencia de las gotículas, los aerosoles se quedan flotando en el aire, tal como el humo de cigarrillo, pueden permanecer allí por horas, y se acumulan en espacios interiores con mala ventilación (van Doremalen *et al.*, 2020). Entender estas características y aceptar que esta es la ruta predominante de transmisión del SARS-CoV-2 es esencial para controlar la pandemia.

El tímido y tardío reconocimiento de la transmisión por aerosol por parte de la OMS también se reflejó en el reconocimiento tardío por parte de los gobiernos de que los aerosoles son la vía principal de transmisión. Diferentes organizaciones académicas y no gubernamentales han hecho un llamado a los gobiernos para que reconozcan esto y actúen en consecuencia. Grupos académicos de Australia (Health Care Workers, 2021), Inglaterra (Royal College of Nursing, 2021), España (Aireamos, 2021), Canadá y los Estados Unidos, entre otros, han dirigido cartas abiertas a los gobiernos de sus países, abogando por el reconocimiento de la transmisión por aerosol y la implementación de medidas preventivas con énfasis en el uso de tapabocas de alta eficiencia en las poblaciones más expuestas, tales como los trabajadores de la salud, y la evaluación y monitoreo de las condiciones de ventilación en interiores.

En Colombia, un grupo de académicos del Nodo de Salud Ocupacional y Ambiental de Colombia (Nodo SAO Colombia), en una carta abierta al Ministro de Salud y Protección Social con fecha de febrero del 2021, solicitaron considerar esta evidencia y actualizar la Resolución 666 de 2020, que establecía protocolos generales sin hacer mención de la ventilación (Nodo SAO Colombia, 2021). Posteriormente, el Ministerio expidió la Resolución 223 de 2021, que incluía la ventilación como una de las cuatro medidas generales de bioseguridad con más evidencia de contención de la transmisión. Las dos resoluciones anteriores fueron derogadas por la Resolución 777 de 2021, mediante la cual se adoptó el protocolo general de bioseguridad para el desarrollo de actividades económicas, sociales y de Estado, donde se menciona la ventilación como una de las estrategias de control de la transmisión. Esto, sin embargo, fue abordado de una manera muy general, indicando la importancia

the importance of the measures that can be more effective in reducing the risk of aerosol transmission, particularly in the evaluation and improvement of ventilation and indoor air filtration.

Aerosols and droplets have different characteristics. Droplets are larger than 100 µm and, due to their size, they rapidly fall to the floor with an average distance of 2 m in seconds or a few minutes after they are exhaled (when speaking, screaming, singing, sneezing, or coughing). On the other hand, aerosols are less than 100 µm in size and are also emitted when breathing or speaking normally. Unlike droplets, aerosols stay floating in the air, as does cigarette smoke, can linger for hours, and accumulate in indoor spaces with poor ventilation (van Doremalen *et al.*, 2020). Understanding these characteristics and accepting that this is the predominant route of SARS-CoV-2 transmission is essential to controlling the pandemic.

The timid and late recognition of aerosol transmission by the WHO was also reflected in the late recognition by governments that aerosols are the main transmission route. Different academic organizations and non-governmental organizations have called upon governments to acknowledge this and act accordingly. Academic groups from Australia (Health Care Workers Australia, 2021), England (Royal College of Nursing, 2021), Spain (Aireamos, 2021), Canada, and the United States, among others, have addressed open letters to the governments of their countries, advocating for the recognition of aerosol transmission and the implementation of preventive measures with an emphasis on the use of high-efficiency face masks in more exposed populations, such as healthcare workers, and the evaluation and monitoring of indoor ventilation conditions.

In Colombia, a group of scholars from the Global Environmental and Occupational Health Hub (Nodo SAO Colombia), in an open letter to the Minister of Health and Social Protection, dated February 2021, requested to take this evidence into account and update Resolution 666 of 2020, which established general protocols without mention of ventilation (Nodo SAO Colombia, 2021). Subsequently, the Ministry issued Resolution 223 of 2021, which included ventilation as one of the four general biosafety measures with the greatest evidence for the containment of transmission. The two previous resolutions were repealed by Resolution 777 of 2021, through which the general biosafety protocol was adopted for the development of economic, social, and State activities, where ventilation is mentioned as one of the transmission control strategies. This, however, was approached in a very general way, indicating the importance of natural and cross ventilation, but without specific guidelines regarding the need to characterize indoor spaces, measure their capacity for air exchange or renewal, and monitor ventilation. Although the measurement of carbon dioxide ($CO_2$) is currently the best indirect measurement of the quality of indoor ventilation that we have (Peng and Jimenez, 2021), it is not mentioned in the Resolution.

de la ventilación natural y cruzada, pero sin lineamientos específicos en cuanto a la necesidad de caracterizar espacios interiores, de medir su capacidad para el intercambio o renovación de aire y de monitorear la ventilación. Aunque la medición del dióxido de carbono ($CO_2$) es actualmente la mejor medida indirecta de la calidad de ventilación en interiores que tenemos (Peng y Jiménez, 2021), esta se menciona en la Resolución.

En un comentario publicado en abril de 2021 en la revista *The Lancet*, un grupo de investigadores destacados dieron al menos diez razones científicas por las cuales los aerosoles son el mecanismo principal de transmisión del SARS-CoV-2 (Greenhalgh *et al.*, 2021). Entre otras cosas, la evidencia muestra eventos de contagio masivo en espacios cerrados en los cuales se mantuvo el distanciamiento físico y no hubo contacto físico entre personas o con superficies. La evidencia de la transmisión del SARS-CoV-2 por aerosoles ya está disponible y, después de 18 meses de pandemia, no hay dudas de que el virus es aerotransportado (Tang *et al.*, 2021). Entonces, ¿por qué seguimos ignorando la importancia de la ventilación y dudamos ante la evidencia?

Actuar de manera coherente con el hecho de que el SARS-CoV-2 se transmite por el aire implica reconocer y actuar sobre la importancia del uso consistente y apropiado de tapabocas y de garantizar buenas condiciones de ventilación en interiores, donde el aire es compartido por varias personas. También implica informar y educar sobre la importancia de una ventilación adecuada y la manera en que podemos evaluarla y lograrla (Allen e Ibrahim, 2021). Adicionalmente, en el ámbito de los espacios públicos, se deben reforzar las acciones informativas y educativas con lineamientos claros sobre cómo evaluar la calidad de la ventilación y garantizar condiciones mínimas que incluyan el monitoreo de $CO_2$. Mientras estas recomendaciones no se conviertan en lineamientos, es muy difícil que sean adoptadas voluntariamente por establecimientos, instituciones y empresas, a pesar del evidente costo-beneficio de su implementación en el país. Ante esta situación, algunos países europeos como Bélgica y gobiernos locales españoles han comenzado a incluir en sus directrices nacionales la obligación de monitorear el $CO_2$ en establecimientos públicos y de hacerlo visible a sus ocupantes junto con indicadores de límites máximos permisibles (The Irish Times, 2021).

En el regreso a las actividades de trabajo y escuela, que ocurren principalmente en lugares cerrados, donde la gente pasa una cantidad importante de su tiempo, el control de la transmisión del SARS-CoV-2 por medio de una ventilación adecuada adquiere especial importancia (di Gilio *et al.*, 2021).

Hasta el 16 julio de 2021, más de 4,6 millones de casos confirmados y más de 115 333 muertes han sido registradas en Colombia. En marzo de 2021 inició el llamado tercer pico de la epidemia, que ha sido el más largo y severo en cuanto a número de casos, muertes, colapso de servicios hospitalarios, y que se ha producido en medio del descontento social y la introducción de nuevas variantes del SARS-CoV-2. Actualmente, el gobierno está enfocado en el Plan Nacional

In a commentary published in April 2021 in The Lancet journal, a group of leading researchers provided at least ten scientific reasons for which aerosols the predominant transmission mechanism of SARS-CoV-2 (Greenhalgh *et al.*, 2021). Among others, the evidence shows superspreading events in closed spaces in which physical distancing was maintained and there was no physical contact between people or with surfaces. Evidence for the transmission of SARS-CoV-2 by aerosols is already available, and, after 18 months of pandemic, there is no doubt that the virus is airborne (Tang *et al.*, 2021), so why continue to ignore the importance of ventilation and hesitate in the face of the evidence?

Acting consistently with the fact that SARS-CoV-2 is transmitted through the air implies recognizing and acting on the importance of consistent and appropriate use of face masks and guaranteeing good ventilation conditions in indoor spaces, where air is shared by several people. It also implies informing and educating about the importance of adequate ventilation and how we can evaluate and achieve it (Allen and Ibrahim, 2021). Additionally, in the field of public spaces, informational and educational actions need to be reinforced with clear guidelines on how to evaluate the quality of ventilation and guarantee minimum ventilation conditions that include $CO_2$ monitoring. As long as these recommendations do not become guidelines, it is very difficult for them to be voluntarily adopted by establishments, institutions, and companies, despite the evident cost-benefit of their implementation in the country. Faced with this situation, some European countries such as Belgium and local governments in Spain have begun to include, within their national guidelines, the obligation to monitor $CO_2$ in public establishments and make it visible to their occupants with indications of maximum permissible limits (The Irish Times, 2021).

In the return to work and school activities, which mainly occur in closed places, where people spend a significant amount of their time, the control of the transmission of SARS-CoV-2 through adequate ventilation takes on special importance (di Gilio *et al.*, 2021).

Until July 16, 2021, more than 4,6 million confirmed cases and more than 115 333 deaths have been recorded in Colombia. In March 2021, the so-called third epidemic peak in the country began, which has been the longest and most severe in terms of the number of cases, deaths, collapse of hospital services, and which has occurred in the midst social unrest and the introduction of new SARS-CoV-2 variants. The government is currently focused on the National Vaccination Plan, which it is undoubtedly a necessary strategy that needs to advance much more quickly in order to protect a larger portion of the population. However, the government should not lose sight of the fact that the protection provided by vaccines mainly avoids severe cases and deaths, but, although the evidence indicates that vaccines can reduce transmission, they do not eliminate it.

Given the amount of people that are still susceptible to infection and the introduction of the ever-increasing SARS-CoV-2 variants in the country, the purpose of the strategies

de Vacunación, que es sin duda una estrategia necesaria que necesita avanzar mucho más rápido para proteger a una mayor parte de la población. Sin embargo, el gobierno no debe perder de vista del hecho de que la protección que ofrecen las vacunas principalmente evita casos graves y muertes, pero, aunque la evidencia indica que las vacunas pueden reducir la transmisión, estas no la eliminan.

Dada la cantidad de gente que aún es susceptible al contagio y la introducción de las variantes cada vez mayores del SARS-CoV-2 en el país, el propósito de las estrategias debe aspirar a reducir la transmisión y no solo a identificar y tratar casos. Para todas las variantes conocidas, el mecanismo principal de transmisión sigue siendo a través del aire y, por lo tanto, las medidas de prevención son similares y deben basarse en el uso consistente y apropiado de tapabocas, así como en la evaluación, el seguimiento y el mejoramiento de la ventilación en espacios cerrados. Por esta razón, hacemos un llamado a la ciudadanía, sindicatos e instituciones a asumir la importancia de una ventilación adecuada. Solicitamos al gobierno nacional que tome acciones para informar y educar sobre la importancia de la ventilación y definir pautas claras para evaluar, garantizar y monitorear la adecuada ventilación en espacios interiores abiertos al público.

## Referencias


Aireamos (2021). *Carta a los gobiernos sobre prevención de COVID*. https://www.aireamos.org/carta-a-los-gobiernos-sobre-prevencion-de-covid/

Allen, J. G. e Ibrahim, A. M. (2021) Indoor Air Changes and Potential Implications for SARS-CoV-2 Transmission. *JAMA Insights, 325*(20), 2112-2113. 10.1001/jama.2021.5053

van Doremalen N., Morris, D. H., Holbrook, M. G., Gamble, A., Williamson, B. N., Tamin, A., Harcourt, J. L., Thornburg, N. J., Gerber, S. I., Lloyd-Smith, J. O., de Wit, E., and Munster, V. J. (2020). Aerosol and Surface Stability of SARS-CoV-2 as Compared with SARS-CoV-1. *New England Journal of Medicine, 382*(16), 1564-1567. /10.1056/NEJMc2004973

Greenhalgh, T., Jimenez, J. L., Prather, K. A., Tufekci, Z., Fisman, D., y Schooley, R. (2021). Ten scientific reasons in support of airborne transmission of SARS-CoV-2. *The Lancet, 397*(10285), 1603-1605. 10.1016/S0140-6736(21)00869-2

di Gilio, A., Palmisano, J., Pulimeno, M., Cerino, F., Cacace, M., Miani, A. y de Gennaro, G. (2021). $CO_2$ concentration monitoring inside educational buildings as a strategic tool to reduce the risk of SARS-CoV-2 airborne transmission, *Environmental Research*, 202111560. 10.1016/j.envres.2021.111560

Health Care Workers Australia (2021). *National action on aerosol transmission of COVID-19*. https://healthcareworkersaustralia.com/national-action-on-aerosol-transmission-of-covid-19/

Hu, B., Guo, H., Zhou, P., and Shi, Z. L. (2021). Characteristics of SARS-CoV-2 and COVID-19. *Nature Reviews Microbiology, 19*, 141-154. 10.1038/s41579-020-00459-7


should aim to reduce transmission and not only to identify and treat cases. For all known variants, the main transmission mechanism continues to be through the air, and, therefore, prevention measures are similar and should be based on the consistent and appropriate use of face masks, as well as the evaluation, monitoring, and improvement of ventilation in indoor spaces. For this reason, we call upon citizens, unions, and institutions to assume the importance of adequate ventilation. We ask the national government to take action to inform and educate on the importance of ventilation, and to define clear guidelines to evaluate, guarantee, and monitor the adequate ventilation in interior spaces open to the public.

## References


Aireamos (2021). *Carta a los gobiernos sobre prevención de COVID*. https://www.aireamos.org/carta-a-los-gobiernos-sobre-prevencion-de-covid/

Allen, J. G. and Ibrahim, A. M. (2021) Indoor Air Changes and Potential Implications for SARS-CoV-2 Transmission. *JAMA Insights, 325*(20), 2112–2113. 10.1001/jama.2021.5053

van Doremalen N., Morris, D. H., Holbrook, M. G., Gamble, A., Williamson, B. N., Tamin, A., Harcourt, J. L., Thornburg, N. J., Gerber, S. I., Lloyd-Smith, J. O., de Wit, E., and Munster, V. J. (2020). Aerosol and Surface Stability of SARS-CoV-2 as Compared with SARS-CoV-1. *New England Journal of Medicine, 382*(16), 1564-1567. 10.1056/NEJMc2004973

Greenhalgh, T., Jimenez, J. L., Prather, K. A., Tufekci, Z., Fisman, D., and Schooley, R. (2021). Ten scientific reasons in support of airborne transmission of SARS-CoV-2. *The Lancet, 397*(10285), 1603-1605. 10.1016/S0140-6736(21)00869-2

di Gilio, A., Palmisano, J., Pulimeno, M., Cerino, F., Cacace, M., Miani, A., and de Gennaro, G. (2021). $CO_2$ concentration monitoring inside educational buildings as a strategic tool to reduce the risk of SARS-CoV-2 airborne transmission, *Environmental Research*, 202111560. 10.1016/j.envres.2021.111560

Health Care Workers Australia (2021). *National action on aerosol transmission of COVID-19*. https://healthcareworkersaustralia.com/national-action-on-aerosol-transmission-of-covid-19/

Hu, B., Guo, H., Zhou, P., and Shi, Z. L. (2021). Characteristics of SARS-CoV-2 and COVID-19. *Nature Reviews Microbiology, 19*, 141-154. 10.1038/s41579-020-00459-7

Ives M, Mandavilli A. (2020). Si el coronavirus está en el aire, ¿por qué seguimos limpiando superficies interiores?. *New York Times.* https://www.nytimes.com/es/2020/11/23/espanol/coronavirus-desinfectante.html

Morawska, L. and Milton, D. K. (2020). It Is Time to Address Airborne Transmission of Coronavirus Disease 2019 (COVID-19). *Clinical Infectious Diseases, 71*(9), 2311-2313. 10.1093/cid/ciaa939

Ives M, Mandavilli A. (2020). Si el coronavirus está en el aire, ¿por qué seguimos limpiando superficies interiores?. *New York Times.* https://www.nytimes.com/es/2020/11/23/espanol/coronavirus-desinfectante.html

Morawska, L. y Milton, D. K. (2020). It Is Time to Address Airborne Transmission of Coronavirus Disease 2019 (COVID-19). *Clinical Infectious Diseases, 71*(9), 2311-2313. 10.1093/cid/ciaa939

Nodo de Salud Ocupacional y Ambiental de Colombia (Nodo SAO Colombia) (2021). *Carta abierta al Ministro de Salud y Protección Social sobre la actualización de la Resolución 666 de 2020*. https://nodosaocolombia.com/wp-content/uploads/2021/03/2021-COVID-19-Carta-abierta-a-Minsalud-actualizacion-Res-666.pdf

Organización Mundial de la Salud (2020a). *WHO Timeline COVID-19*. https://www.who.int/news/item/27-04-2020-who-timeline---covid-19

Organización Mundial de la Salud (OMS) (2020b). *Modes of transmission of virus causing COVID-19: implications for IPC precaution recommendations: scientific brief*. https://www.who.int/news-room/commentaries/detail/modes-of-transmission-of-virus-causing-covid-19-implications-for-ipc-precaution-recommendations

Organización Mundial de la Salud (OMS) (2021). *Coronavirus disease (COVID-19): How is it transmitted?* https://www.who.int/news-room/q-a-detail/coronavirus-disease-covid-19-how-is-it-transmitted

O'Leary N. (2021) *Belgium imposes ventilation rules for businesses to combat new Covid surge*. The Irish Times. https://www.irishtimes.com/news/world/europe/belgium-imposes-ventilation-rules-for-businesses-to-combat-new-covid-surge-1.4612101

Peng, Z. y Jiménez, J. L. (2021) Exhaled $CO_2$ as a COVID-19 Infection Risk Proxy for Different Indoor Environments and Activities. *Environmental Science & Technology Letters, 8*(5), 392-397. 10.1021/acs.estlett.1c00183

Royal College of Nursing (2021). *Letter to the Prime Minister on protecting health care workers*. https://www.rcn.org.uk/about-us/our-influencing-work/open-letters/letter-to-the-prime-minister-on-protecting-health-care-workers-190221

Tang, J. W., Marr, L. C., Li, Y. y Dancer, S. J. (2021). Covid-19 has redefined airborne transmission. *British Medical Journal, 373*, 913.

**Dr. Néstor Y. Rojas**
Profesor Asociado
Departamento de Ingeniería Química y Ambiental
Universidad Nacional de Colombia
https://orcid.org/0000-0001-7804-0449

**Dra. Laura A. Rodríguez-Villamizar**
Profesora Asociada
Departamento de Salud Pública
Universidad Industrial de Santander
https://orcid.org/0000-0002-5551-2586

Nodo de Salud Ocupacional y Ambiental de Colombia (Nodo SAO Colombia) (2021). *Carta abierta al Ministro de Salud y Protección Social sobre la actualización de la Resolución 666 de 2020*. https://nodosaocolombia.com/wp-content/uploads/2021/03/2021-COVID-19-Carta-abierta-a-Minsalud-actualizacion-Res-666.pdf

Peng, Z. and Jimenez, J. L. (2021) Exhaled $CO_2$ as a COVID-19 Infection Risk Proxy for Different Indoor Environments and Activities. *Environmental Science & Technology Letters, 8*(5), 392-397. https://doi.org/10.1021/acs.estlett.1c00183

Royal College of Nursing (2021). *Letter to the Prime Minister on protecting health care workers*. https://www.rcn.org.uk/about-us/our-influencing-work/open-letters/letter-to-the-prime-minister-on-protecting-health-care-workers-190221

Tang, J. W., Marr, L. C., Li, Y., and Dancer, S. J. (2021). Covid-19 has redefined airborne transmission. *British Medical Journal, 373*, 913.

O'Leary N. (2021) *Belgium imposes ventilation rules for businesses to combat new Covid surge*. The Irish Times. https://www.irishtimes.com/news/world/europe/belgium-imposes-ventilation-rules-for-businesses-to-combat-new-covid-surge-1.4612101

World Health Organization (WHO) (2020a). *WHO Timeline COVID-19*. https://www.who.int/news/item/27-04-2020-who-timeline---covid-19

World Health Organization (WHO) (2020b). *Modes of transmission of virus causing COVID-19: implications for IPC precaution recommendations: scientific brief*. https://www.who.int/news-room/commentaries/detail/modes-of-transmission-of-virus-causing-covid-19-implications-for-ipc-precaution-recommendations

World Health Organization (WHO) (2021). *Coronavirus disease (COVID-19): How is it transmitted?* https://www.who.int/news-room/q-a-detail/coronavirus-disease-covid-19-how-is-it-transmitted

**Dr. Néstor Y. Rojas**
Associate Professor
Department of Chemical and Environmental Engineering
Universidad Nacional de Colombia
https://orcid.org/0000-0001-7804-0449

**Dra. Laura A. Rodríguez-Villamizar**
Associate Professor
Department of Public Health
Universidad Industrial de Santander
https://orcid.org/0000-0002-5551-2586

Research Article / Chemical, Food, and Environmental Engineering https://doi.org/10.15446/ing.investig.v41n3.90349

# Removal of Sulfate Ions by Precipitation and Flotation

## Eliminación de iones sulfato mediante precipitación y flotación

Mario Santander-Muñoz[1], Paola Cardozo-Castillo[2], and Luis Valderrama-Campusano[3]

**ABSTRACT**

The removal of sulfate ions from natural waters, as well as from industrial effluents of different origins, is a problem, considering that most of the proposed processes are inefficient and have a high cost, mainly when reducing the sulfate ion concentration to values below 500 mg.L$^{-1}$ is required. The flotation technique, combined with precipitation, has proven to be efficient for the removal of heavy metal ions. However, there is not enough research to confirm its efficiency for the removal of sulfate ions. This article presents the results of sulfate ion removal from synthetic solutions prepared in an acidic medium, applying the co-precipitation techniques with polyaluminum chloride (PAC) and solid/liquid separation by dissolved air flotation (DAF). The effect of the pH, the [PAC: sulfate ions] ratio, the effect of saturated water flow with air, and the flocculant and collector doses were studied. The achieved results confirm that it is possible to reduce the concentration of sulfate ions from 1 800 to 350 mg.L$^{-1}$ (80% removal) from synthetic solutions by applying the flotation technique combined with precipitation.

**Keywords:** water pollution, sulfate ions, flotation, precipitation

**RESUMEN**

La eliminación de iones sulfatos desde aguas naturales, así como de efluentes industriales de diferentes orígenes, es un problema, considerando que la mayoría de los procesos propuestos son ineficientes y de alto costo, principalmente cuando se requiere reducir la concentración de iones sulfato a valores inferiores a 500 mg.L$^{-1}$. La técnica de flotación combinada con precipitación ha demostrado ser eficiente para la eliminación de iones d metales pesados. Sin embargo, no hay suficientes investigaciones que confirmen su eficiencia para la eliminación de iones sulfato. Este artículo presenta los resultados de la remoción de iones sulfato desde soluciones sintéticas preparadas en un medio ácido, aplicando las técnicas de co-precipitación con policloruro de aluminio (PAC) y separación sólido/líquido mediante flotación por aire disuelto (FAD). Se estudiaron el efecto del pH, la razón [PAC: iones sulfato], el efecto del flujo de agua saturada con aire y las dosis de floculante y colector. Los resultados alcanzados confirman que es posible reducir la concentración de iones sulfato de 1 800 a 350 mg.L$^{-1}$ (80 % de remoción) desde soluciones sintéticas aplicando la técnica de flotación combinada con precipitación.

**Palabras clave:** contaminación de agua, iones sulfato, flotación, precipitación

**Received:** September 4th, 2020
**Accepted:** March 28th, 2021

## Introduction

Sulfate ions are contaminants found in high concentrations in natural waters, as well as in effluents from different industrial processes, including mining acid drainage, acid effluents from copper smelters, water recovered from tailings ponds, and solutions for hydrometallurgical processes (Guerrero-Flores, Uribe-Salas, Dávila-Pulido, and Flores-Álvarez, 2018; Runtti *et al.*, 2017; Silva, Lima, and Leão, 2012). Sulfate ions are not toxic, and sulfur is necessary for several living beings. However, when their concentration in water for human consumption exceeds 600 mg.L$^{-1}$, they cause cathartic effects resulting in the purgation of the digestive tract. According to the World Health Organization (WHO), the maximum tolerable level of sulfate ions in drinking water is 500 mg.L$^{-1}$. Nevertheless, some countries have advised lower values, such as Brazil and the United States of America, both recommending 250 mg.L$^{-1}$ (Fernando, Ashane, Ilankoon, Syed Tauqir, and Yellishetty, 2018; Silva and Rubio, 2011). In Chile, Standard NCH 409/1 establishes that the maximum limit of sulfate ions in water for human consumption must be 500 mg.L$^{-1}$.

Sulfate ion are also the main contributors to the 'mineralization' of water, thus increasing the conductivity and potential corrosion of the receiving bodies. These anions promote corrosion and pickling in pipes, structures, and equipment, making it difficult to recycle and reuse these waters (Dou *et al.*, 2017; Silva *et al.*, 2012; Cao *et al.*, 2011; Rui, Yuanfa, Xingguo, and Jianhua, 2011; Moret and Rubio, 2003).

[1]Ph.D. in Metallurgy Engineering, University of Atacama, Chile. Affiliation: Full Professor, Departament of Metallurgical Engineering.
E-mail: mario.santander@uda.cl
[2]Metallurgy Engineer, University of Atacama, Chile. Affiliation: Researcher, Departament of Metallurgical Engineering. E-mail: paola.cardozo@uda.cl
[3]Ph.D. in Metallurgy Engineering, University of Atacama, Chile. Affiliation: Full Professor, Departament of Metallurgical Engineering.
E-mail: luis.valderrama@uda.cl

**How to cite:** Santander-Muñoz, M., Cardozo-Castillo, P., and Valderrama-Campusano, L. (2021). Removal of Sulfate Ions by Precipitation and Flotation. *Ingeniería e Investigación*, *41*(3), e90349. 10.15446/ing.investig.v41n3.90349

The search for suitable treatment methods for the removal of sulfate ions has been the subject of study by different researchers. Among the broad range of methods studied, biological treatments with sulfate-reducing bacteria, membrane filtration (reverse osmosis and electrodialysis), electrocoagulation, processes based on sorption phenomena (ionic exchange and adsorption/bioadsorption), and chemical precipitation are found (Rumjit *et al.*, 2021; Öztürk and Ekmekçi, 2020; Mamelkina, Tuunila, Sillänpää, and Häkkinen, 2019; Hwang and Jho, 2018; Arahman, Mulyati, Lubis, Takagi, and Matsuyama, 2017; Călinescu *et al.*, 2016; Guimarães and Leão, 2014; Bai *et al.*, 2013; Silva *et al.*, 2012).

Regarding treatment costs, chemical precipitation is the least expensive technique, depending on the reagent used and the effluent physicochemical characteristics (Öztürk and Ekmekçi, 2020; Dou *et al.*, 2017; Telles, Granhen, and Lenzi, 2009). However, it requires an extra operational cost for the generated sludge disposal (Barakat, 2011). According to Ao, Cao, Hong, Wu, and Wei (2020), granular activated carbon (GAC) and anion exchange resins have been widely studied to remove sulfate from industrial wastewater. Nevertheless, GAC has a low adsorption efficiency, while anion exchange resins are too expensive to be utilized in wastewater treatment. On the other hand, Fernando *et al.* (2018) explain that the costs associated with sulfate ion removal using filtration/membrane processes are markedly higher than chemical precipitation. The precipitating reagents traditionally used for the removal of sulfate ions are calcium carbonate and lime to obtain gypsum, barium salts (BaS, $Ba(OH)_2$, or $BaCO_3$) to form barium sulfate, calcium hydroxide, and aluminum hydroxide, thus producing ettringite ($Ca_6Al_2(SO_4)_3(OH)_{12}{\cdot}26H_2O$) (Dou *et al.*, 2017; Cadorin, Carissimi, and Rubio, 2007). However, the precipitation of sulfate ions to form gypsum is not efficient for effluents with concentrations below 1 800 - 2 000 $mg.L^{-1}$ (Cadorin *et al.*, 2007). The formation of barium sulfate (barite) is widely used because it is efficient for the removal of sulfate ions in a wide pH range, and the formed precipitate ($BaSO_4$) has a low solubility. However, the cost of barium salts is high, and barium compounds are carcinogenic (Telles *et al.*, 2009). The production of ettringite for the removal of sulfate ions also allows reducing their concentration to values permitted by environmental regulations. However, for effective removal, an alkaline pH is required (Silva *et al.*, 2012).

Several researchers have proposed to use polyaluminum chloride (PAC) as an alternative reagent, instead of the traditional reagents used for the precipitation of sulfate ions (Silva, Cadorin, and Rubio, 2010; Gao, Zhou, Yue, Liu, and Wang, 2006). PAC can be produced by adding a base to aluminum chloride until the empirical formula of $Al(OH)_n.Cl_{3-n}$ (with $n$ from 1 to 2,5) is obtained (Shen and Dempsey, 1998). PAC is composed of several species of aluminum, and, according to the time it takes for them them to react with the ferron reagent, they are generally divided into $Al_a$ (a monomer that reacts with ferron in 1 minute), $Al_b$ (oligomers and polymers that react with ferron between 1 and 200 minutes), and $Al_c$ (colloidal aluminum species that do not react with ferron) (Shen and Dempsey, 1998; Zhao, Liu, Xu, and Ni, 2009). Studies carried out to analyze the interaction of PAC with sulfate showed that the latter forms soluble complexes with $Al_a$ species, while $Al_b$ and $Al_c$ species react with sulfate to form crystals and amorphous precipitates, respectively. The content of each of the Al species depends on the basicity or molar ratio [Al/OH] (B value). For values of $B = 0$, the species are distributed in 90,1% of $Al_a$ and 9,9% of $Al_b$; and for values of $B = 2{,}5$, the species distribution changes to 7,4% of $Al_a$, 57,5% of $Al_b$, and 35,1% of $Al_c$ (Xu, Wang, and Tang, 2004).

For the removal of aluminum precipitates containing sulfate ions, different methods of solid/liquid separation can be used, for example, sedimentation and dissolved air flotation (DAF). However, flotation compared to sedimentation is a more effective method since it has a higher treatment capacity (40 $m^3.m^{-2}.h^{-1}$), produces less sludge volume, and is efficient for turbidity removal (Jung, Park, Han, and Kim, 2017; Bahadori, A., Zahedi, Zendehboudi, and Bahadori, M., 2013). DAF is a solid/liquid separation method in which microbubbles (with a diameter between 10 and 100 microns) adhere to the solid particles suspended in the liquid, forming aggregates with a density lower than water. Microbubbles are formed by the pressure reduction of a water flow previously saturated with pressurized air, generally above 3 bar (Kurama, Karagüzel, Mergan, and Çelik, 2010). In DAF, the removal of clots or flocs does not necessarily require that they be hydrophobized, given that the formation of aggregates between particles/microbubbles can occur through one of the following mechanisms (Rodrigues and Rubio, 2007): a) bubble entrapment or bubble capture within the flocs or formation of aerated flocs (this phenomenon occurs when microbubbles enter and remain within a floc); b) entrainment of aggregates or flocs by ascending microbubbles (this mechanism occurs when the flocs are loaded onto the microbubbles or the ascending microbubbles remain below a descending floc).

This article reports the results of studies carried out for the removal of sulfate ions from synthetic effluents using PAC as a precipitating reagent and dissolved air flotation for solid/liquid separation.

## Experimentation

### *Materials*

A synthetic solution with a concentration of 1 800 $mg.L^{-1}$ of sulfate ions was prepared by dissolving Merck sodium sulfate (NaSO4) (99% purity) in demineralized water, which had been previously acidified at pH 2. The pH was adjusted with hydrochloric acid (HCl) or sodium hydroxide (NaOH), according to the need of each test, and registered with a Thermo Scientific Orion Star A-series pH-meter. For the precipitation of sulfate ions, aluminum polychloride (PAC ECO-2300) from Ecofast S.A. was used, as well as the ECO-2600, ECO-8065, ECO-5650, and ECO-5350M (cationic), ECO-6750, ECO-6700B, ECO-6700 M (anionic), and ECO-300 (non-ionic) flocculants produced by the same brand, in order to increase the mechanical resistance of the clots (precipitates formed between the different species of aluminum and sulfate ions). The formed flocs were hydrophobized with sodium oleate. The sulfate ion concentration was determined by the gravimetric method by precipitation with barium chloride. The

residual turbidity of the clarified effluent was measured with a HANNA model HI 98703 turbidity meter. The characterization of PAC clots in the absence and presence of sulfate ions was performed in the scanning electron microscope (SEM) from ZEISS, model EVOMA10, and in the Malvern Zeta-Meter 4.0 equipment.

The precipitation tests of sulfate ions with PAC were performed in a glass beaker (500 mL) arranged on top of a magnetic stirrer. The precipitates formed were subsequently separated from the liquid by vacuum filtration using Whatman No. 42 filter paper.

DAF equipment was used for the flotation tests and consisted of a 3 L capacity PVC saturator and a 2 L capacity acrylic flotation cell. The saturator and the flotation cell are connected via a valve that has a plate with a 1 mm diameter center hole. The air to be dissolved was supplied by a Schulz compressor, model 10 BR of 2HP, 200 L capacity, and 9,8 kgf.cm$^{-2}$.

Preliminary DAF tests (not reported here) showed that it is not possible to completely remove the precipitates, even though they were hydrophobized. Through visual inspection, it was determined that the clarified liquid had small precipitates in suspension. Therefore, it was necessary to incorporate a previous flocculation stage to improve flotation efficiency.

The tests were performed in the Jar Test FC4S equipment to determine the type and dose of flocculant. The results of the flocculation tests showed that the ECO-6700B (anionic) and ECO-300 (non-ionic) flocculants, dosed at 11 mg.L$^{-1}$, formed larger floccules (visual inspection) and had a higher sedimentation rate. Subsequently, DAF tests were performed with the two selected flocculants. The flocculation stage was carried out under fast and slow mixing conditions in the flotation cell itself, provided by a Stuart Scientific mechanical stirrer, model SS3.

### *Precipitation test*

Chemical precipitation with PAC was utilized because industrial effluents contain, in addition to sulfate ions, colloidal and suspended solids. Different positively charged polymeric species are produced during PAC precipitation, which are adsorbed without difficulty on the anions and negatively charged particles, forming voluminous clots that can be separated efficiently from the effluent by flotation. In the precipitation tests, 300 mL of synthetic solution contaminated with 1 800 mg.L$^{-1}$ of sulfate ions were used. The effect of pH in the range of 4 to 10 and the effect of the [PAC: sulfate ions] ratio from 1:1 to 9:1 was studied. Tests were performed to determine the effect of pH with a ratio of 8:1, as well as its effect at pH 4,5. In all tests, the artificial effluent contaminated with sulfate ions was agitated at 100 rpm for 8 min, the necessary time to form the precipitates (precipitates formed between the different species of aluminum and the sulfate ions). An aliquot of supernatant liquid was collected and vacuum-filtered once the agitation was completed. The filtered liquid was subjected to chemical analysis to determine the residual concentration of sulfate ions.

### *Flotation test*

DAF was used for solid/liquid separation due to the following advantages on sedimentation and filtration: low operating costs, high pollutant removal efficiency, and high treatment capacity.

Once the optimum parameters for the precipitation stage were defined, flocculation tests were performed to select the type of flocculant (anionic or non-ionic) that would produce the least turbidity in the clarified effluent. Subsequently, DAF studies were carried out to determine the optimum sodium oleate collector dosage from 0 to 25 mg.L$^{-1}$ and the percentage of water saturated with air fed to the flotation cell (% recycling) from 10 to 30%.

The applied methodology was the following: a) the saturator was loaded with 2,25 L of drinking water (75% of the useful volume of the saturator), and 10 L.min$^{-1}$ of air was dissolved during 3 600 s at a constant pressure of 4 kgf.cm$^{-2}$; b) the polymeric species precipitates of aluminum and sulfate ions were formed applying the optimal conditions reached in the precipitation studies (pH 4,5 and [PAC: sulfate ions] ratio equal to 8:1); c) the solution was transferred to the flotation cell, and the clots were flocculated by applying 11 mg.L$^{-1}$ of flocculant (determined in tests performed by Jar Test equipment) under fast mixing conditions (120 rpm) during 180 s (the speed was later reduced to slow mixing conditions of 30 rpm for 1 200 s); d) subsequently, the formed flocs were hydrophobized by applying sodium oleate; e) once the flocs were hydrophobized, the depressurization valve that feeds the flotation cell was opened, and 60 mL of air saturated with water (20% recycling) were added.

After 10 minutes of flotation, the time required for the ascent of the floc/microbubble aggregates of air to the top of the flotation cell, a sample of the clarified effluent was the bottom of said cell to determine the residual turbidity or residual sulfate ion concentration.

## Results and discussion

### *Precipitation of sulfate ions with PAC*

*Effects of pH*: Figure 1 shows the effect of pH on sulfate ion removal via precipitation using a [PAC: sulfate ions] ratio of 8:1. The Figure shows that, at pH 4,5, the concentration of sulfate ions is reduced from 1 800 mg.L$^{-1}$ to 335 mg.L$^{-1}$, which is equivalent to eliminating 81,4% (precipitating together with the colloidal species of PAC). Silva *et al*. (2010) and Xu *et al*. (2004) reported that, at pH 4,5, a higher proportion of sulfate ions is precipitated since $Al_b$ the is predominant species. The optimal pH range for $Al_b$ formation fluctuates between 3,5 and 5. In this pH range, the other aluminum species ($Al_a$ or $Al_c$) tend to hydrolyze and transform into $Al_b$, and the $Al_b$ content increases rapidly with the increment in the molar ratio [OH: Al] (Huang, Tang, Wang, D., Wang, S., and Deng, 2006).

Studies carried out by Wang, Sun, Xu, Tang, and Gregory (2004) showed that the percentage of $Al_a$ increases in the acidic region when the pH decreases, and in the alkaline

region when the pH increases, which would explain why the percentage of sulfate ion removal decreases outside the pH range of 4 to 5.

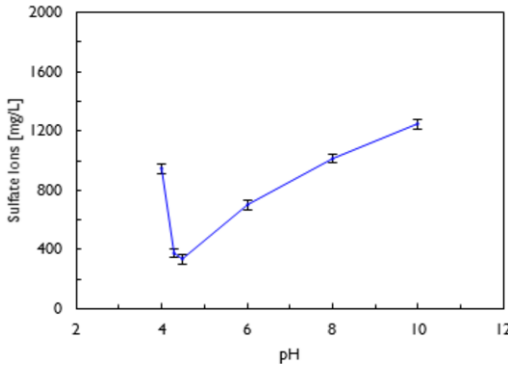


**Figure 1.** Effect of pH on sulfate ion removal using co-precipitation using a [PAC: sulfate ions] ratio of 8:1.
**Source:** Authors

*Effect of the [PAC: sulfate ions] ratio in the precipitation of sulfate ions*: In Figure 2, it can be seen that, by increasing the [PAC: sulfate ions] ratio, the final sulfate ion concentration in the filtered liquid decreases, whereas the sulfate ion concentration decreases from 1 800 mg.L$^{-1}$ to 230 mg.L$^{-1}$ when a ratio equal to 9:1 is used, which is equivalent to a removal percentage of 87%. Studies carried out by Silva *et al.* (2010) with different initial concentrations of sulfate ions, showed that their removal is a function of the [PAC: sulfate ions] ratio; as this ratio increased, the concentration of sulfate ions decreased. When they worked with a ratio of 8:1, the final concentration of sulfate ions was of the order of 500 mg.L$^{-1}$ for an initial concentration of sulfate ions of 1 800 mg.L$^{-1}$. According to these researchers, the efficiency of sulfate ion removal increases because the volume and size of the precipitates formed by PAC hydrolysis products increase as their concentration rises. Results reported by Amaral, Azevedo, Etchepare, and Rubio (2016) revealed that it is enough to use a [$Al^{3+}$ : $S_4^{2-}$] ratio equal to 4:1 to reduce the sulfate ion concentration from 1 800 to 500 mg.L$^{-1}$.

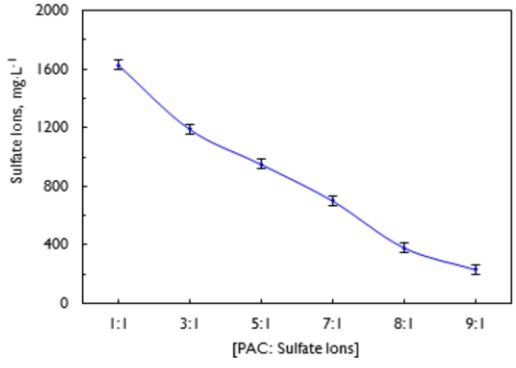


**Figure 2.** Effect of the [PAC: sulfate ions] ratio on the final concentration of residual sulfate ions (initial sulfate ion concentration was equal to 1 800 mg.$^{-1}$, and the pH was 4,5).
**Source:** Authors

*Morphological and chemical characterization of PAC precipitates and sulfate ions:* Figure 3 shows the surface morphology of PAC precipitates in the presence of sulfate ions obtained from the Scanning Electronic Microscope (SEM) equipped to perform an Energy Dispersion Spectrometry (EDS) analysis of x-rays. The precipitates were formed from the co-precipitation of PAC and sulfate ions at pH 4,5 using a [PAC: sulfate ions] ratio equal to 8:1 and an initial concentration of sulfate ions equal to 1 800 mg.L$^{-1}$. The Figure shows the area of a particle demarcated with a white outline, where the EDS analysis was conducted. The results of these analyses presented in Table 1 confirm that the precipitates are formed by aluminum, sulfur, sodium, chlorine, and oxygen from the PAC, $Na_2SO_4$, and NaOH reagents used. The iron traces probably come from external contamination and the carbon from the surface coating used to conduct the analyses.

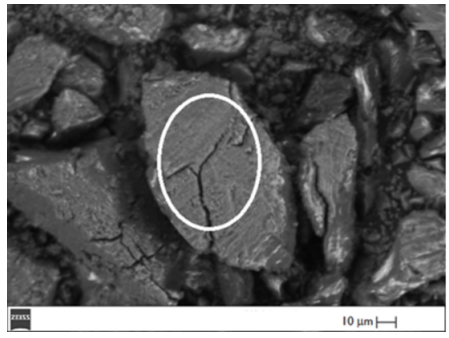


**Figure 3.** Surface morphology of PAC precipitates in the presence of sulfate ions at a pH of 4,5 and a [PAC: sulfate ions] ratio of 8:1.
**Source:** Authors

**Table 1.** Chemical analysis by EDS of PAC precipitates in the presence of sulfate ions

| Element | C(*) | O | Al | S | Cl | Na | Fe |
|---|---|---|---|---|---|---|---|
| Weight % | 12,1 | 45,1 | 31,6 | 9,4 | 1,2 | 0,5 | 0,1 |

**Note:** The high carbon content in the analysis is due to the fact that the precipitates were deposited on a graphite conductive tape.
**Source:** Authors

*Determination of the zeta potential:* The zeta potential was determined as a pH function of the PAC precipitates in the presence and absence of sulfate ions to measure its effect on the electric double layer. As shown in Figure 4, at pH 4,5, the precipitates that were only formed with PAC have a zeta potential of the order of 40 mV, while the precipitates formed from PAC and sulfate ions have a zeta potential of the order of 29 mV. These values allow deducing that the sulfate ions are adsorbed on the precipitates formed with PAC, and the electric double layer is compressed as a consequence of this adsorption. The Figure also shows that the isoelectric point (0,0 mV) is obtained at pH 9 in the presence of sulfate ions, and pH 9,3 in their absence. According to Silva (2011), the alteration of the isoelectric point of the aluminum species as a function of sulfate ion adsorption reveals that the anion adsorption was partially specific on the internal Helmholtz level, which is of a chemical nature.

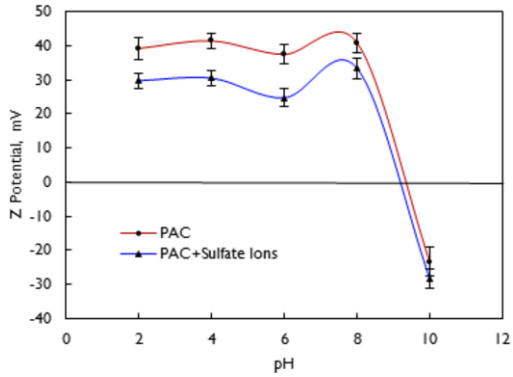


**Figure 4.** Z Potential of PAC precipitates in the presence and absence of sulfate ions (sulfate ion concentration was equal to 1 800 mg.L$^{-1}$, the [PAC: Sulfate ions] ratio was 8:1, and the pH was 4,5).
**Source:** Authors

## *Dissolved Air Flotation*

*Flotation tests to select the type of flocculant*: As noted, preliminary flotation tests showed that aluminum precipitates containing sulfate ions do not float completely. It was verified by visual inspection that the clarification contained a high proportion of suspended precipitates. The application of flocculants (anionic or non-ionic) allowed considerably reducing the number of suspended precipitates. The residual turbidity in the clarified liquid was significantly reduced with both flocculants, as shown in Table 2. The formation of large and porous floccules facilitates the trapping or capture of microbubbles, thus resulting in the formation of aerated floccules, which noticeably improves flotation efficiency (Olivera and Rubio, 2012). Different researchers reported that anionic and non-ionic flocculants are widely used to increase the size of micro-flocs formed with inorganic coagulants and facilitate their subsequent removal through sedimentation, flotation, or filtration techniques (Lee, Robinson, and Chong, 2014; Lee, Morad, Teng, and Poh, 2012; Verma, Dash, and Bhunia, 2012; Ahmad, Wong, Teng, and Zuhairi, 2008). The Table also shows that the non-ionic flocculant produces a clarified effluent with residual turbidity that is lower than the anionic flocculant (46 NTU, and 262 NTU, respectively). It was observed by visual inspection that the flocs formed with the non-ionic flocculant are larger than those formed by the anionic flocculant. This difference in size is possibly due to the different mechanisms of floc formation. According to Bratby (1980) for the case of anionic flocculants applied to colloidal dispersions destabilized by inorganic coagulants, the most suitable mechanism to explain the phenomenon that takes place during the formation of flocs is electrostatic patches, and for non-ionic or charged flocculants of the same sign as colloidal particles, the most suitable mechanism is polymer bridges. One of the main characteristics of this mechanism is the formation of flocs that are more resistant and larger than those generated by the electrostatic patch mechanism (Farrokhpay and Filippov, 2017; Gregory and Baranay, 2011). At pH 4,5, amorphous aluminum precipitates containing sulfate ions have a positive charge (+29 mV).

**Table 2.** DAF tests used to select the type of flocculant

| Flocculant | Initial turbidity (NTU) | Residual turbidity (NTU) | Turbidity removal (%) |
|---|---|---|---|
| ECO-3000 (non-ionic) | 990 | 46 | 95 |
| ECO-6700B (anionic) | 935 | 262 | 72 |

**Note:** The initial concentration of sulfate ions was 1 800 mg.L$^{-1}$, the [PAC: sulfate ions] ratio was equal to 8:1, the pH was 4,5, the flocculent dose was 11 mg.L$^{-1}$, the saturation pressure for DAF was 4 kgf.cm$^{-2}$, and the recycle ratio was equal to 20%.
**Source:** Authors

*Effect of the water flow saturated with air (% recycling):* Figure 5 shows the results of the percentage effect of the water saturated with air fed to the flotation cell. The tests were performed using synthetic effluent contaminated with 1 800 mg.L$^{-1}$ of sulfate ions, a [PAC: sulfate ions] ratio equal to 8:1, pH 4.5, ECO-3000 flocculant dose equal to 11 mg.L$^{-1}$, and a saturation pressure in the FAD equal to 4 kgf.cm$^{-2}$. As shown in the Figure, by increasing the percentage of recycling (water flow saturated with air fed to the flotation cell), the concentration of sulfate ions decreases. This decrease is probably due to the fact that the concentration of microbubbles and the air mass/solid mass ratio increase when increasing the volume of water saturated with air. Flotation efficiency increases when the number of microbubbles increases, due to the probability of collision, adhesion, and the capture of microbubbles in the porous structure of the flocs, thus decreasing their density and increasing their flotation velocity (Jung *et al.*, 2017; Amaral *et al.*, 2016; Ortiz-Oliveros, Flores-Espinosa, Jiménez-Domínguez, Jiménez-Moleón, and Cruz-González, 2012; Al-Shamrani, James, and Xiao, 2002). A removal rate of 70,3% was achieved when tests with 10% of recycling were performed, in comparison with the 81,1% achieved in tests with 30% of recycling.

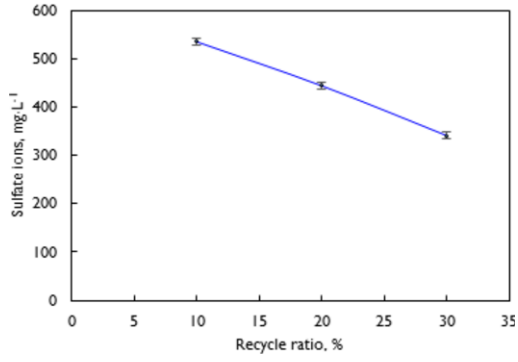


**Note:** The initial concentration of sulfate ions was 1 800 mg.L$^{-1}$, the [PAC: sulfate ions] ratio was equal to 8:1, the pH value was 4,5, the dose of flocculant ECO-3000 was equal to 11 mg.L$^{-1}$, the saturation pressure for DAF was 4 kgf.cm$^{-2}$, and the recycling percentage was equal to 30%.

**Figure 5.** Effect of recycle ratio on the residual sulfate ion concentration in the clarified effluent in DAF tests.
**Source:** Authors

*Effect of sodium oleate concentration*: Figure 6 shows the effect of the hydrophobization of flocs with sodium oleate on

the sulfate ion removal percentage. The tests were performed under the same experimental conditions used to study the effect of the water flow saturated with air except for the recycle ratio, which was kept constant at 30%. The Figure shows that the application of the collector does not reveal a conclusive effect on the percentage of sulfate ion removal. The removal percentage remains at around 81% with and without the addition of 10 mg.L$^{-1}$, and the removal percentage decreases to 76 and 78% with the addition of 5 and 20 mg.L$^{-1}$, respectively. Amaral *et al*. (2016) reported that the application of sodium oleate to hydrophobize flocs formed with PAC in the presence of sulfate ions does not modify the percentage of sulfate ion removal, remaining practically constant at around 80% for the different concentrations of collector applied.

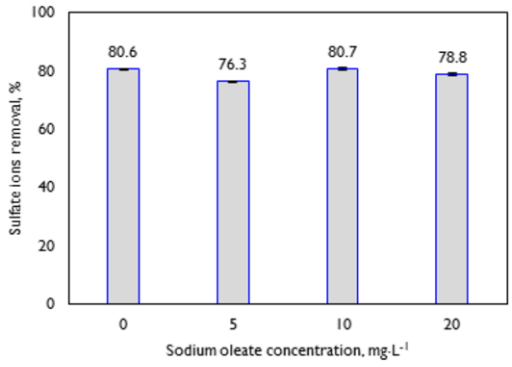


**Note:** The initial concentration of sulfate ions was 1 800 mg.L$^{-1}$, the [PAC: sulfate ions] ratio was equal to 8:1, the pH value was 4,5, the dose of flocculant ECO-3000 was equal to 11 mg.L$^{-1}$, the saturation pressure for DAF was 4 kgf.cm$^{-2}$, and the recycling percentage was equal to 30%.

**Figure 6.** DAF tests to determine the effect of sodium oleate concentration on the percentage of sulfate ion removal.
**Source:** Authors

## Conclusions

The results of this study indicate that the co-precipitation of sulfate ions with polyaluminum chloride (PAC), followed by a flocculation stage with a non-ionic polymer and dissolved air flotation (DAF), proved to be efficient for the removal of sulfate ions from synthetic solutions.

Co-precipitation studies showed that sulfate ion precipitation is highly dependent on pH and the [PAC: sulfate ions] ratio. The concentration of sulfate ions is reduced from 1 800 to 335 mg.L$^{-1}$ at pH 4,5 and with a ratio equal to 8:1. Higher or lower pH values increase their concentration, and higher values of the ratio decrease their concentration. Furthermore, the concentration of sulfate ions is reduced from 1 800 to 230 mg.L$^{-1}$ at pH 4,5 and with a [PAC: sulfate ions] ratio equal to 9:1.

The results of the solid/liquid separation stage showed that, in order to efficiently remove the PAC precipitate containing sulfate ions, it is necessary to include a flocculation stage before flotation. The DAF studies showed that it is possible to reduce the concentration of sulfate ions from 1 800 to 350 mg.L$^{-1}$ (80% removal) when solutions contaminated with sulfate ions were treated under the aforementioned experimental conditions ([PAC: sulfate ions] ratio equal to 8:1, pH 4,5, a non-ionic flocculant dose equal to 11 mg.L$^{-1}$, saturation pressure equal to 4 atm, and 30% recycle ratio in the DAF).

## Acknowledgements

The authors are grateful for the financial support provided by the Directorate of Research of the University of Atacama through the funding of the DIUDA-22252 research project. The authors also thank Mr. Bruno Zazzali for his support in the experimental development of this work, as well as Miss Evelyn Cárdenas for the translation of this article.

## References

Ao, H., Cao, W., Hong, Y., Wu, J., and Wei, L. (2020). Adsorption of sulfate ion from water by zirconium oxide-modified biochar derived from pomelo peel. *Science of the Total Environment, 708*, 135092. 10.1016/j.scitotenv.2019.135092

Ahmad, A. L., Wong, S. S., Teng, T. T., and Zuhairi, A. (2008). Improvement of alum and PACl coagulation by polyacrylamides (PAMs) for the treatment of pulp and paper mill wastewater. *Chemical Engineering Journal, 137*(3), 510-517. 10.1016/j.cej.2007.03.088

Al-Shamrani, A. A., James, A., and Xiao, H. (2002). Separation of oil from water by dissolved air flotation. *Colloids and Surfaces A: Physicochemical and Engineering Aspects, 209*(1), 15-26. 10.1016/S0927-7757(02)00208-X

Amaral, J., Azevedo, A., Etchepare, R., and Rubio, J. (2016). Removal of sulfate ions by dissolved air flotation (DAF) following precipitation and flocculation. *International Journal of Mineral Processing, 149*, 1-8. 10.1016/j.minpro.2016.01.012

Arahman, N., Mulyati, S., Lubis, M. R., Takagi, R., and Matsuyama, H. (2017). Removal profile of sulfate ion from mix ion solution with different type and configuration of anion exchange membrane in electrodialysis. *Journal of Water Process Engineering, 20*, 173-179. 10.1016/j.jwpe.2017.10.007

Bahadori, A., Zahedi, G., Zendehboudi, S., and Bahadori, M. (2013). Estimation of air concentration in dissolved air flotation (DAF) systems using a simple predictive tool. *Chemical Engineering Research and Design, 91*(1), 184-190. 10.1016/j.cherd.2012.07.004

Bai, H., Kang, Y., Quan, H., Han, Y., Sun, J., and Feng, Y. (2013). Treatment of acid minedrainage by sulfate reducing bacteria with iron in bench scale runs. *Bioresource Technology, 128*, 818-822. 10.1016/j.biortech.2012.10.070

Barakat, M. A. (2011). New trends in removing heavy metals from industrial wastewater. *Arabian Journal of Chemistry, 4*(4), 361-377. 10.1016/j.arabjc.2010.07.019

Bratby, J. (1980). *Coagulation and flocculation: with an emphasis on water and wastewater treatment*. Croydon, UK: Uplands Press Ltd.

Cadorin, L., Carissimi, E., and Rubio J. (2007). *Avances en el tratamiento de aguas ácidas de minas* [Paper presentation]. Scientia et Technica Año XIII, No. 36, Pereira, Colombia.

Călinescu, O., Marin, N. M., Ioniță, D., Pascu, L. F., Tudorache, A., Surpățeanue, G., Badea, I. A., and Aboul-Enein, H. Y. (2016). Selective removal of sulfate ion from different drinking waters. Environmental Nanotechnology, Monitoring and Management, 6, 164-168. 10.1016/j.enmm.2016.10.004

Cao, W., Dang, Z., Zhou, X., Yi, X., Wu, P., Zhu, N., and Lu, G. (2011). Removal of sulphate from aqueous solution using modified rice straw: preparation, characterization and adsorption performance. *Carbohydrate Polymers, 85*(3), 571-577. 10.1016/j.carbpol.2011.03.016

Dou, W., Zhou, Z., Jiang, L., Jian, A., Huang, R., Tian, X., Zhang, W., and Chen, D. (2017). Sulfate removal from wastewater using ettringite precipitation: Magnesium ion inhibition and process optimization. *Journal of Environmental Management, 196*, 518-526. 10.1016/j.jenvman.2017.03.054

Farrokhpay, S. and Filippov, L. (2017). Aggregation of nickel laterite ore particles using polyacrylamide homo and copolymers with different charge densities. *Powder Technology, 318*, 206-213. 10.1016/j.powtec.2017.05.021

Fernando, M. Ashane, W., Ilankoon, I. M. S. K., Syed Tauqir, H., and Yellishetty, M. (2018). Challenges and opportunities in the removal of sulphate ions in contaminated mine water: A review. *Minerals Engineering, 117*, 74-90. 10.1016/j.mineng.2017.12.004

Gao, B., Zhou, W., Yue, Q., Liu, L., and Wang, Y. (2006). Al-Ferron kinetics and quantitative calculation of Al(III) species in polyaluminum chloride coagulants. *Colloids and Surfaces A: Physicochemical and Engineering Aspects, 278*(1-3), 235-240. 10.1016/j.colsurfa.2005.12.024

Guerrero-Flores, A. D., Uribe-Salas, A., Dávila-Pulido, G. I., and Flores-Álvarez, J. M. (2018). Simultaneous removal of calcium and sulfate ions from flotation water of complex sulfides. *Minerals Engineering, 123*, 28-34. 10.1016/j.mineng.2018.04.024

Gregory, J. and Barany, S. (2011). Adsorption and flocculation by polymers and polymer mixtures. *Advances in Colloid and Interface Science, 169*(1), 1-12. 10.1016/j.cis.2011.06.004

Guimarães, D. and Leão, V.A. (2014). Batch and fixed-bed assessment of sulphate removal by the weak base ion exchange resin Amberlyst A21. *Journal of Hazardous Materials, 280*, 209-215. 10.1016/j.jhazmat.2014.07.071

Huang, L., Tang, H., Wang, D., Wang, S., and Deng, Z. (2006). Al(II1) speciation distribution and transformation in high concentration PACl solutions. *Journal of Environmental Sciences, 18*(5), 872-879. 10.1016/S1001-0742(06)60007-7

Hwang, S. K. and Jho, E. H.(2018). Heavy metal and sulfate removal from sulfate-rich synthetic mine drainages using sulfate reducing bacteria. *Science of the Total Environment, 635*, 1308-1316. 10.1016/j.scitotenv.2018.04.231

Iakovleva, E., Mäkilä, E., Salonen, J., Sitarz, M., and Sillanpää, M. (2015). Industrial products and wastes as adsorbents for sulphate and chloride removal from synthetic alkaline solution and mine process water. *Chemical Engineering Journal, 259*, 364-371. 10.1016/j.cej.2014.07.091

Jung, J., Park, H., Han. M., and Kim, T. (2017). Importance of Bubble Bed Characteristics in Dissolved-air-flotation. *KSCE Journal of Civil Engineering, 22*, 2214-2118. 10.1007/s12205-017-1540-7

Kijjanapanich, P., Do, A. T., Annachhatre, A. P., Esposito, G., Yeh, D. H., and Lens, P. N. L. (2014). Biological sulfate removal from construction and demolition debris leachate: effect of bioreactor configuration. *Journal of Hazardous Materials, 269*, 38-44. 0.1016/j.jhazmat.2013.10.015

Kurama, H., Karagüzel, C., Mergan, T., and Çelik, M. S. (2010). Ammonium removal from aqueous solutions by dissolved air flotation in the presence of zeolite carrier. *Desalination, 253*(1-3), 147-152. 10.1016/j.desal.2009.11.017

Lee, K. E., Morad, N., Teng, T. T., and Poh, B. T. (2012). Development, characterization and the application of hybrid materials in coagulation/flocculation of wastewater: a review. *Chemical Engineering Journal, 203*, 370-386. 10.1016/j.cej.2012.06.109

Lee, C. S., Robinson, J., and Chong, M. F. (2014). A review on application of flocculants in wastewater treatment. *Process Safety and Environmental Protection, 92*(6), 489-508. 10.1016/j.psep.2014.04.010

Mamelkina, M. A., Tuunila, R., Sillänpää, M., and Häkkinen, A. (2019). Systematic study on sulfate removal from mining waters by electrocoagulation. *Separation and Purification Technology, 216*, 43-50. 10.1016/j.seppur.2019.01.056

Moret, A. and Rubio, J. (2003). Sulphate and molybdate ions uptake by chitin-based shrimp shells. *Minerals Engineering, 16*(8), 715-722. 10.1016/S0892-6875(03)00169-9

Oliveira, C. and Rubio, J. (2012). A short overview of the formation of aerated flocs and their applications in solid/liquid separation by flotation. *Minerals Engineering, 39*, 124-132. 10.1016/j.mineng.2012.05.024

Ortiz-Oliveros, H. B., Flores-Espinosa, R. M., Jiménez-Domínguez, H., Jiménez-Moleón, M. C., and Cruz-González, D. (2012). Dissolved air flotation for treating wastewater of the nuclear industry: preliminary results. *Journal of Radioanalytical and Nuclear Chemistry, 292*, 957-965. 10.1007/s10967-012-1682-5

Öztürk, Y. and Ekmekçi, Z. (2020). Removal of sulfate ions from process water by ion exchange resins. *Minerals Engineering, 159*, 106613. 10.1016/j.mineng.2020.106613

Parker, D. R. and Bertsch, P. M. (1992). Identification and Quantification of the "Al13" Tridecameric Polycation Using Ferron. *Environmental Science and Technology, 26*(5), 908-914. 10.1021/es00029a006

Rodrigues, R. T. and Rubio, J. (2007). DAF - dissolved air flotation: potential applications in the mining and mineral processing industry. *International Journal of Mineral Processing, 82*(1), 1-13. 10.1016/j.minpro.2006.07.019

Rui, D., Yuanfa, L., Xingguo, W., and Jianhua, H. (2011). Adsorption of sulfate ions from aqueous solution by surfactant-modified palygorskite. *Chemical Engineering Journal, 56*(10), 3890-3896. 10.1021/je200544n

Rumjit, N. P., Samsudin, N. A., Low, F. W., Thomas, P., Lai, C. W, Chellam, P. V., Johan, M. R. B., Lime, Y. C., Amin, N., and Tiong, S. K. (2021). Kinetic and isotherm studies on adsorptive removal of sulfates by cotton shell derived biochar: Recovery of sulfates from marcasite soil. Sustainable *Chemistry and Pharmacy, 20*,100361. 10.1016/j.scp.2020.100361

Runtti, H., Tynjälä, P., Tuomikoski, S., Kangas, T., Hu, T., Rämö, J., and Lassi, U. (2017). Utilisation of barium-modified analcime in sulphate removal: Isotherms, kinetics and thermodynamics studies. *Journal of Water Process Engineering, 16*, 319-328. 10.1016/j.jwpe.2016.11.004

Shen, Y. and Dempsy, B. A. (1988). Synthesis and speciation of polyluminum chloride for water treatment. *Environment International, 24*(8), 890-910. 10.1016/S0160-4120(98)00073-7

Silva, A. M., Lima, R. M. F., and Leão, V.A. (2012). Mine water treatment with limestone for sulfate removal. *Journal of Hazardous Materials, 221-222*, 45-55. 10.1016/j.jhazmat.2012.03.066

Silva, R. and Rubio, J. (2011). *Sulphate ions removal from aqueous solution II. Separation from coal effluents using aluminium bearing salts* [Paper presentation]. 2° Seminario Internacional en Asuntos Ambientales en la Industria Minera, Santiago, Chile.

Silva, R. (2011). Interações de íons sulafto com sais de aluminio e soluções ácidas. Estudos Básicos e aplicações Ambientais (Ph.D. Thesis, UFRGS, Porto Alegre, Brasil). https://www.Lume.ufrgs.br/handle/10183/35631

Silva, R., Cadorin, L., and Rubio, J. (2010). Sulphate ions removal from an aqueous solution: I. Co-precipitation with hydrolysed aluminium-bearing salts. *Minerals Engineering, 23*(15), 1220-1226. 10.1016/j.mineng.2010.08.016

Telles, C., Granhen, C. R., and Lenzi, E. (2009). Sulfate removal from waste chemicals by precipitation. *Journal of Environmental Management, 90*(1), 504-511. 10.1016/j.jenvman.2007.12.006

Verma A. K., Dash R. R., and Bhunia, P. (2012). A review on chemical coagulation/flocculation technologies for removal of colour from textile wastewaters. *Journal of Environmental Management, 93*(1), 154-168. 10.1016/j.jenvman.2011.09.012

Wang, D., Sun, W., Xu, Y., Tang, H., and Gregory J. (2004). Speciation stability of inorganic polymer flocculant–PACl. *Colloids and Surfaces A: Physicochemical and Engineering Aspects, 243*(1-3), 1-10. 10.1016/j.colsurfa.2004.04.073

Xu, Y., Wang, D., and Tang, H. (2004). Interaction of PACls with sulfate. *Journal of Environmental Sciences, 16*(3), 420-422. https://pubmed.ncbi.nlm.nih.gov/15272715/

Zhao, H. Liu, C., Xu, Y., and Ni, J. (2009). High-concentration polyaluminum chloride: Preparation and effects of the Al concentration on the distribution and transformation of Al species. *Chemical Engineering Journal, 155*(1-2), 528-533. 10.1016/j.cej.2009.08.007

Research Article / Chemical, Food, and Environmental Engineering https://doi.org/10.15446/ing.investig.v41n3.87537

# Batch Conversion of Methane to Methanol Using Copper Loaded Mordenite: Influence of the Main Variables of the Process

## Conversión de metano a metanol por lotes usando mordenita intercambiada con cobre: influencia de las variables principales del proceso

Hebert Rodrigo Mojica Molina[1], Marlene González Montiel[2], and Amado Enrique Navarro Frómeta[3]

**ABSTRACT**

Due to the demands of oxygenated derivatives of hydrocarbons for the industry, the methane ($CH_4$) to methanol (MeOH) conversion through solid-state catalysis is a current topic, with definite questions and specific challenges. This work shows a statistical model that predicts the quantity of methanol produced through a batch conversion process employing copper-exchanged mordenite in accordance with a full factorial experimental design. Synthesis was performed through solid-state ion exchange from $Cu(acac)_2$ and $NH_4$-Mordenite, obtaining weight percentages (%Cu) of 1%, 3%, and 5%, which was followed by activation through calcination at a range of temperatures (Tcal) between 300-500 °C, as well as a reaction with methane under 2-10 bar pressure (P) in static conditions employing a batch reactor. The quantities of MeOH produced, and their yields were determined through a gas chromatography and mass spectrometry analysis of the reaction samples. Finally, the role and contribution of each of the variables considered in the conversion process were analyzed. By using a nonlinear model, a quadratic dependence with %Cu and P in the studied range of the variables was found, as well as a linear dependence with Tcal. Finally, for this experiment, the highest yields (μmol/g) were obtained with the following conditions: %Cu = 3 %, P = 6 bar, and Tcal = 400 °C.

**Keywords:** methane, methanol, mild conditions, copper mordenite, solid-state ion exchange, activation temperature, methane pressure, copper weight percent

**RESUMEN**

Debido a la demanda de derivados oxigenados de hidrocarburos para la industria, la conversión de metano ($CH_4$) a metanol ($CH_3OH$) por medio de catálisis en estado sólido es una cuestión de actualidad, precisa y con retos específicos. Este trabajo muestra un modelo estadístico que predice la cantidad de metanol producido por un proceso de conversión por lotes empleando mordenitas intercambiadas con cobre de acuerdo con un diseño experimental factorial. La síntesis fue realizada por intercambio iónico en estado sólido a partir de $Cu(acac)_2$ y $NH_4$-Mordenita, obteniendo porcentajes de intercambio en peso de Cobre (%Cu) de 1 %, 3 % y 5 %, seguido de una activación por calcinación en el rango de temperaturas (Tcal) de 300-500 °C, así como una reacción con metano en el rango de presiones de 2-10 bar (P) bajo condiciones estáticas con un reactor por lotes. Las cantidades de MeOH producidas y sus rendimientos fueron determinados usando análisis de cromatografía de gases y espectrometría de masas de las muestras de la reacción. Finalmente se analizaron el papel y la contribución de cada una de las variables consideradas en el proceso de conversión. Usando un modelo no lineal, se encontró una dependencia cuadrática del %Cu y P en el rango estudiado de cada variable, así como una dependencia lineal con Tcal. Finalmente, para este experimento, los mayores rendimientos (μmol/gr) se obtuvieron con las siguientes condiciones: %Cu=3 %, P = 6 bar y Tcal = 400 °C.

**Palabras clave:** metano, metanol, condiciones suaves, mordenita de cobre, intercambio iónico en estado sólido, temperatura de activación, presión de metano, porcentaje de peso de cobre

**Received:** May 22nd, 2020
**Accepted:** March 20th,2021

[1]Bachelor in Physics, BUAP, México. Ph.D. Candidate in Advanced Technology, Centro de Investigación en Ciencia Aplicada y Tecnología Avanzada. Affiliation: Ph.D. student, IPN, México. E-mail: hmojicam1900@alumno.ipn.mx
[2]Bachelor in Physics, UPITA-IPN. Master in Advanced Technology, CICATA-IPN. Ph.D. in Advanced Technology, Centro de Investigación en Ciencia Aplicada y Tecnología Avanzada, México. Affiliation: CONACyT-Fellowship, CICATA, U. Legaria, IPN, México. E-mail: mgonzalezmo@conacyt.mx
[3]Bachelor in Chemistry, Universidad de la Habana, Cuba. Ph.D. in Chemical Sciences in Petroleum and Chemistry Azizbekov Institute, Azerbaijan. Affiliation: Research Professor, UTIM, México. E-mail: navarro4899@gmail.com

## Introduction

MeOH is a very important raw material for the chemical industry, with an increasing demand for a wide variety of

**How to cite:** Mojica-Molina, H. R., González-Montiel, M., and Navarro-Frómeta, A. E. (2021). Batch Conversion of Methane to Methanol Using Copper Loaded Mordenite: Influence of the Main Variables of the Process. *Ingeniería e Investigación*, *41*(3), e87537. 10.15446/ing.investig.v41n3.87537

applications (Dalena *et al.*, 2018; Hammond, Conrad, and Hermans, 2012). $CH_4$ is one of the most important fossil fuels in the planet, which is not fully exploited because of the economical unsuitability of the synthetic pathway from syngas to produce the required quantities of MeOH (Burnett *et al.*, 2019; Jovanovic *et al.*, 2020). Therefore, the direct conversion of $CH_4$ to MeOH has been a long-standing challenge in the field of catalysis (Tomkins, Ranocchiari, and van Bokhoven, 2017). Normally, MeOH is synthesized in different ways, such as $CO_2$ hydrogenation and synthesis gas production (Abashar and Al-Rabiah, 2018; da Silva, 2016). Many efforts have been made to control the completion of the reaction up to the exact level of MeOH formation, in order to avoid overoxidation and its byproducts, *e.g.*, carbon oxides or formic acid (Narsimhan *et al.*, 2015; Schwarz, 2011). It is assumed that a continuous process for direct methane to methanol conversion will ultimately be limited to achieving high methanol selectivity at low methane conversions (Latimer, Kakekhani, Kulkarni, and Nørskov, 2018). Thus, the search for catalysts and reaction conditions for this process is a topical issue. A wide variety of materials have been developed as catalysts for this reaction, including copper-exchanged zeolites and mordenite (Burnett *et al.*, 2019; Lomachenko *et al.*, 2019; Tomkins *et al.*, 2016; Wulfers, Teketel, Ipek, and Lobo, 2015). These kinds of materials are synthesized from different copper precursors. Zeolites with different frameworks and physical-chemical properties are used, as well as a variety of ionic exchange methods (aqueous, solid, and gaseous) (Zakaria and Kamarudin, 2016). These kinds of materials are inspired by the activity of Particulate Methane Monooxygenase (pMMO), which is a metalloenzyme found in methanotrophs, capable of oxidizing $CH_4$ with very high efficiency at room conditions (Banerjee, Proshlyakov, Lipscomb, and Proshlyakov, 2015; Sharma, Poelman, Marin, and Galvita, 2020). The functioning of these enzymes is given by a combination of specific copper active sites and biological-chemical processes (Balasubramanian and Rosenzweig, 2007; Yoshizawa and Shiota, 2006). Copper active sites have been broadly studied. Based on pMMO, it has been proposed that stable copper monomers, dimers, and trimmers in different configurations are able to activate methane C-H bonding due to the favourable electronic environment generated (Grundner *et al.*, 2015; Newton, Knorpp, Sushkevich, Palagin, and van Bokhoven, 2020; Palagin, Knorpp Pinar, Ranocchiari, and van Bokhoven, 2017; Sushkevich, Palagin, and van Bokhoven, 2018). Furthermore, through various reaction mechanisms, these sites assist methane oxidation up to its specific point. Even though it has been possible to almost reproduce specific, reactive to $CH_4$, copper active sites in the framework structure of exchanged zeolites, their yield and selectivity are still low (Jovanovic *et al.*, 2020; Newton *et al.*, 2020). In this context, different reaction conditions and steps within the processes have been studied to increase the quantity of MeOH produced.

Copper mordenite has been reported as one of the most efficient inorganic materials, with applications in $CH_4$ to MeOH conversion under mild conditions (Álvarez, Marín, and Ordóñez, 2020; Burnett *et al.*, 2019; Tomkins *et al.*, 2016; Wulfers *et al.*, 2015). Furthermore, it has been linked to the solid-state ion exchange synthesis method with a higher amount of MeOH production (Sainz-Vidal, Balmaseda, Lartundo-Rojas, and Reguera, 2014). Normally, experiments are focused on continuous flow reaction systems (Grundner *et al.*, 2015; Sushkevich *et al.*, 2018; Tomkins *et al.*, 2017, 2019), but a static system (batch reactor) still offers a broad field to be studied, relating to the material behavior at different reaction conditions. Besides describing an experiment and predicting the results, the construction of a mathematical model allows understanding of the role played by variables, which can be modified in every reaction. It is possible to understand if and how much they are related, as well as the way in which they affect experiment performance. Herein, with the objective of elucidating the role of variables on MeOH yields, the influence of the percentage of copper charge, the temperature of activation, and methane reaction pressure in a batch process are studied using a full factorial experiment design. The choice of these variables was made according to previously reported studies, in which, starting with different copper ion exchange amounts, specific activation temperatures produce different reactive sites with various populations in the mordenite framework where the conversion process takes place. Furthermore, methane pressure is a manageable variable in batch experiments that indirectly allows the study of the interaction of a material with a gas phase, thus influencing MeOH yields (Álvarez *et al.*, 2020; Kim *et al.*, 2017; Tomkins *et al.*, 2016). sectionExperimental section

Ammonium mordenite with a 20:1 (Silicon: Aluminium, $SiO_2$: $Al_2O_3$) mole ratio from Alfa Aesar, denoted as $NH_4$-Mordenite, and copper (II) acetylacetonate (> 99,9%) from Sigma Aldrich as a metal ion source, denoted as Cu-$(acac)_2$, were employed in the synthesis of materials.

*Synthesis of materials:* The solid-state ion-exchange method was chosen, using a planetary ball mill, to obtain homogeneous samples and control the energy applied to the samples. This is very difficult to reach if an Agate mortar and arm force are used. 0,9 grams of $NH_4$-Mordenite with 0,0387 grams, 0,1269 grams, and 0,2334 grams of Cu-$(acac)_2$ were grinded for 60 minutes to obtain three samples with a copper weight percentage of 1, 3, and 5, labeled as CuMor 1%, CuMor 3%, and CuMor 5%, respectively. These weight percentages were corroborated in the activated samples by inductively coupled plasma-optical emission spectrometry (ICP-OES).

*Activated materials:* The milled samples were dried at 70 °C for 24 hours, kept in a silica desiccator, and calcined in a muffle with airflow. Two samples (CuMor 1% and CuMor 5%) were calcined separately at 200 °C and 500 °C, thus obtaining four activated samples, labeled as CuMorO 1% 200, CuMorO 1% 500, CuMorO 5% 200 and CuMorO 5% 500. Also, CuMor 3%, calcined at 400°C (CuMorO 3% 400), was obtained.

*Experimental design:* A complete $2^k$ factorial experimental design with the variables and levels shown in Table 1 was used.

**Table 1.** Definition of variables according to the experimental design

| Variable | -1 | 0 | 1 |
|---|---|---|---|
| Calcination Temperature, °C | 300 | 400 | 500 |
| Cu wt % in the catalyst | 1 | 3 | 5 |
| Methane pressures, bar | 2 | 6 | 10 |

**Source:** Authors

*Methanol obtention:* Reactions were conducted in a 500 mL batch reactor (Parr Instruments, USA). 0,25 grams of each sample sieved through a < 200 µm mesh reacted with methane at the design pressure. The reactor was heated at a rate of 2 °C/min up to 200 °C and maintained at this temperature for 2 hours. After this time, it was cooled to room temperature.

*Sample analysis*: The resulting material was dispersed in 1 mL of water and stirred vigorously for 30 minutes to extract the formed methanol. The liquid phase was centrifuged, filtrated, and preserved in vials at 4 °C until the chromatographic analysis was carried out. Before the analysis, 1 µL of isopropyl alcohol (IOH) was added to each sample as an internal standard. The GC-MS analysis was carried out in a Clarus SQ 680 GC, coupled to a Clarus SQ 8T MS, using a PE-WAX (Perkin Elmer, Boston, MA, USA) capillary column (50 m x 0,25 mm i.d. x 0,25 µm phase thickness). The temperature program was set as follows: 40 °C for 8 min, 20 °C/min up to 80 °C, 40 °C/min up to 90 °C, and 50 °C/min up to 180 °C. The injection temperature was 150 °C, and helium was used as carrier gas (1,5 mL $min^{-1}$). The mass spectrometer was operated in electron impact mode (70 EV), with selective ion monitoring (m/z 29, 31, 43, 45, 46, 58, 59, and 60; dwell time 0,05 s), keeping the chromatograph interphase and the source temperature at 280 °C. Quantitation of MeOH (mz 29+31) and IOH (m/z 45) was performed using a five-point calibration curve (R > 0,99) and areas of specific ions mass-chromatograms.

*Statistical Analysis:* Analysis of the experimental design, general analysis of variance (ANOVA), and nonlinear regressions were performed with Statistica V 13.3 (TIBCO Software Inc., 2017).

## Results and discussion

Starting with a $2^k$ factorial experimental design, as mentioned, two central points and a random point were included. In Table 2 is summarized the experimental conditions employed and methanol yields obtained according to the experimental design described in previous section.

It should be noted that no other compounds besides MeOH were detected in the chromatographic analysis. The obtained amount of MeOH is in the same order of magnitude with those reported in the literature (Tomkins *et al.*, 2016, 2019; Wulfers *et al.*, 2015), but much less compared with cycling continuous flow processes (Álvarez *et al.*, 2020; Burnett *et al.*, 2019; Jovanovic *et al.*, 2020; Ma *et al.*, 2020). Likewise, a dependency on Cu wt % of catalyst was observed (Figure 1) with a similar tendency to the work reported by Le *et al.* (2017) and Oord, Schmidt, and Weckhuysen (2018). Particularly, the samples with 1% and 3% Cu wt reported an increasing tendency of MeOH obtention, but samples with 5% Cu wt showed a decreased performance. This can be explained by stoichiometric calculations, in which a maximum ion exchange between 4 and 5 copper percent is evident, depending on the chemistry of mordenite and copper precursor used. More copper ions than are possible to insert into the mordenite framework tend to form different species that, at the temperatures employed in this work, did not contribute to forming MeOH (Tomkins *et al.*, 2017). Similarly, the results in Table 2, expressed in µmol/µmol Cu, show a behavior similar to that reported in the literature, that is, lower quantities of copper loaded into the mordenite framework display a better performance in MeOH obtention (Le *et al.*, 2017).

**Table 2.** Experimental design and amount of methanol obtained in moles per gram of catalyst (µmol/g) and moles per copper loaded moles (µmol Met/mol Cu)

| Samples | Cu wt % | Activation Temperature | Pressure | µmol/g | µmol Met/mol Cu |
|---|---|---|---|---|---|
| cu1t300p10 | -1 | -1 | 1 | 11,215 | 0,0713 |
| cu1t300p2 | -1 | -1 | -1 | 4,732 | 0,0301 |
| cu1t500p10 | -1 | 1 | 1 | 20,732 | 0,1317 |
| cu1t500p2 | -1 | 1 | -1 | 17,289 | 0,1099 |
| cu5t300p10 | 1 | -1 | 1 | 15,636 | 0,0199 |
| cu5t300p2 | 1 | -1 | -1 | 3,098 | 0,0039 |
| cu5t500p10 | 1 | 1 | 1 | 21,206 | 0,0270 |
| cu5t500p2 | 1 | 1 | -1 | 8,460 | 0,0108 |
| cu3t400p6a | 0 | 0 | 0 | 24,745 | 0,0524 |
| cu3t400p6b | 0 | 0 | 0 | 29,840 | 0,0632 |
| cu1t500p6 | -1 | 1 | 0 | 6,596 | 0,0419 |

**Source:** Authors

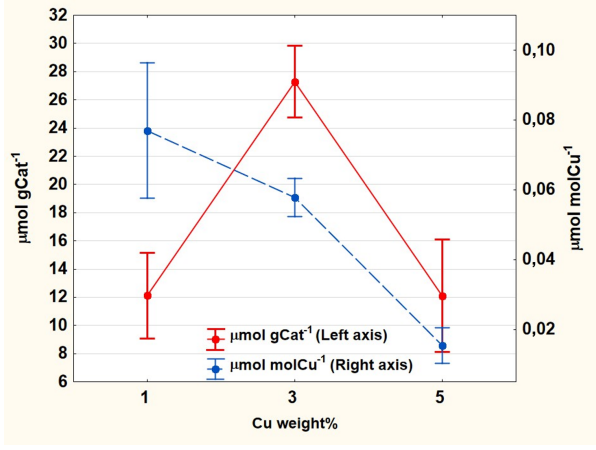


**Figure 1.** Mean values and standard errors of MeOH obtained against copper weight percent.
**Source:** Authors

The complex dependency of μmol/g yield is shown in Figure 2, in which partial minimal square adjusted surface graphics can be appreciated. It is observable that quadratic relations are needed. Certainly, the analysis of complete factorial experimental design $2^k$, with a pair of central points, does not show a significative influence by any variable, nor a suitable adjustment, if the curvature (Curv) parameter is not considered in the analysis design. After eliminating the non-significative effects, a model was obtained with an intercept in which only the variables Tcal, P, and Curv were significant.

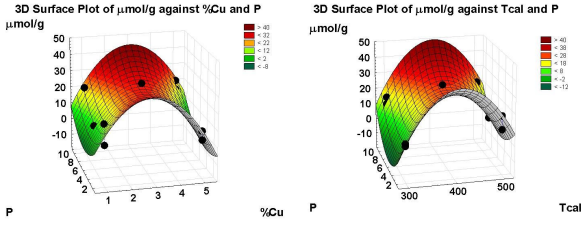


**Figure 2.** Yield dependence with respect %Cu, Tcal, and P.
**Source:** Authors

It must be noted that, at this stage, comparing the obtained and predicted data, the model does not offer sufficient certainty. At this point, a main effects ANOVA shows the global influence of variables in MeOH obtention in the studied range. The different behavior of each variable can be appreciated in Figure 3.

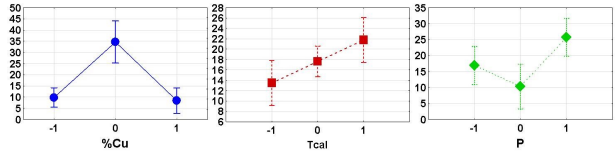


**Figure 3.** Yield dependence with different values of variables used in the experiment, according to the experimental design (vertical bars denote 0,95 confidence intervals).
**Source:** Authors

3 %Cu wt, Tcal = 500°C, and P = 10 bar are the best conditions in each of the global analysis per variables. 3 %Cu wt has a maximum yield because it contains a greater population of active sites than 1% Cu wt, which is made evident by the amount of copper ion charged in the materials. Also, it is greater than 5 %Cu wt due to a stoichiometric limitation (Dyballa *et al.*, 2019; Pappas *et al.*, 2017) that favors the formation of copper species which do not participate in methane oxidation. Considering the molecular shape of $NH_4$-mordenite and the substitution of ammonium ions by copper (II) ions, the stoichiometric rate of maximum ion exchange is between 4 and 5%, depending on the mordenite's molecular formula.

Tcal = 500 °C favors the oxidation of the material, the elimination of residual organic compounds, and the production of specific active sites (Groothaert, Smeets, Sels, Jacobs, and Schoonheydt, 2005; Sheppard, Hamill, Goguet, Rooney, and Thompson, 2014). Temperatures of 300, 400, and 500 °C follow a growing trend, suggesting that higher temperatures favor the formation of a higher populations of reactive copper sites in mordenite (Sainz-Vidal *et al.*, 2014; Vanelderen *et al.*, 2014), associated with the amount of MeOH obtained. Activation at higher temperatures allowed us to confirm that organic material from acetylacetonate disappears, and that activation at lower temperatures does not remove it at all.

The MeOH yield has a peculiar dependence on P, showing a minimum at P = 6 atm. Pressures of 10 bar are related to a higher concentration of $CH_4$ and greater interaction between $CH_4$ and the material. In our experiments, a better yield was obtained at 2 bars, rather than at a 6 bar $CH_4$ pressure. Higher $CH_4$ conversion at lower pressures is a desired feature, and the better response at high pressures is an expected and usual aspect.

As mentioned above, the experimental model with curvature does not offer a good enough explanation to the influence of the variables on the MeOH yield. Therefore, a polynomial regression was employed with the coded values of the variables, in which the quadratic influence of %Cu and P was observed with a good description of results. The quadratic term for Tcal was zeroed with the statistical package. Figure 4 shows how far away the experimental data are from those predicted by the proposed model.

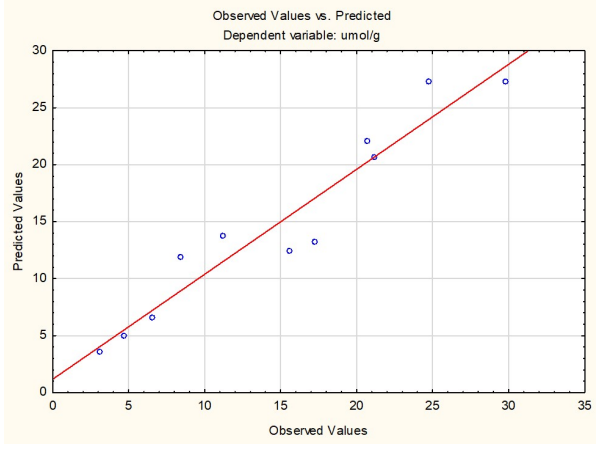


**Figure 4.** Predicted vs. obtained results by the polynomial regression model.
**Source:** Authors

Finally, to verify the goodness of the quadratic model, and to obtain the model coefficients based on the real values of the variables, a nonlinear estimation was performed using Equation 1, considering that the yield has a quadratic dependence on %Cu and P, and a linear dependence on Tcal, as it was obtained with the quadratic regression. It was observed, as expected, that residuals are like those obtained with the previously discussed model. The coefficients A, B, C, L, Q, and R in Table 3 were obtained using the Levenberg-Marquardt estimation method of the statistical package.

$$Yield = A + B\ \%Cu + C\ (\%Cu)^2 + L\ Tcal + Q\ P + R\ P^2 \quad (1)$$

All terms were considered because the entire p-values of the coefficients were under 0,05. In Table 3, the estimate values of coefficients according to the nonlinear model, which are represented in Equation 1, can also be observed.

**Table 3.** Estimated values of coefficients accordingly to the nonlinear model

| | Estimate | Standard error | t-valued f = 5 | p-value |
|---|---|---|---|---|
| A | -12,7498 | 4,753433 | -2,68224 | 0,043703 |
| B | 35,8928 | 4,635228 | 7,74348 | 0,000574 |
| C | -5,9719 | 0,788338 | -7,57536 | 0,000636 |
| L | 0,0331 | 0,008428 | 3,92458 | 0,011131 |
| Q | -7,7347 | 2,106922 | -3,67107 | 0,014427 |
| R | 0,5358 | 0,174697 | 3,06712 | 0,027875 |

**Source:** Authors

This nonlinear model allows a good description of the experimental points in terms of the real values of the studied variables.

## Conclusions

A nonlinear statistical model of a batch reaction of methane to methanol direct conversion employing copper mordenite as the catalyst is proposed, which describes with good accuracy the experimental results of the yield of methanol production. The model adequately confirms what is seen in Figures1 and 3, that is, very high or very low values of a copper-loaded percent can lead to a decrease in the yield, which is a fact that has been observed in practice. The maximum value at 3% Cu wt can be explained according to the formation process of copper mordenite, with the maximum stoichiometric copper percent ranging between 4 and 5%, depending on the exact mordenite molecular framework unity and precursor of copper employed. Higher amounts of Copper-loaded into mordenite (> 5% Cu wt) may have a negative effect on methanol production with the conditions applied in the experiments. This suggests the important role of the catalyst stoichiometry in the yield of methanol production. On the other hand, pressure behaved as expected, and higher pressure means bigger concentration and contact between methane and material and, consequently, a major probability of interaction of methane with the mordenite's active sites. At lower pressures, the interaction is reduced and, as a result, decreases the amount of methanol produced. However, the material still produces good enough quantities, suggesting that pressure does not have such a great impact in methanol production within the range studied. Within global analysis, the mordenite's calcination temperature had a linear behavior at higher temperatures, and a higher yield of methanol was obtained. However, in relation to the copper-loaded amount, this variable seems to have a low influence on the experimental results, as is suggested by its linear contribution to the model. To the best of our knowledge, a nonlinear model that describes the yields of the batch direct conversion of methane to methanol has not been proposed, which gives practical value to the results herein obtained from an engineering point of view. More experimental data are needed to improve the accuracy of the model and to expand the studied variable ranges.

## Acknowledgements

The authors thank the Energy Conversion and Storage National Laboratory (LNCAE-IPN) and the University of Izúcar de Matamoros (UTIM) for the equipment support and materials provided, as well as the National Council for Science and Technology of the Mexican government (CONACyT) for the doctorate student scholarship provided.

## References

Abashar, M. E. E., and Al-Rabiah, A. A. (2018). Investigation of the efficiency of sorption-enhanced methanol synthesis process in circulating fast fluidized bed reactors. *Fuel Processing Technology, 179*, 387-398. 10.1016/j.fuproc.2018.07.028

Álvarez, M., Marín, P., and Ordóñez, S. (2020). Direct oxidation of methane to methanol over Cu-zeolites at mild conditions. *Molecular Catalysis, 487*, 110886. 10.1016/j.mcat.2020.110886

Balasubramanian, R., and Rosenzweig, A. C. (2007). Structural and Mechanistic Insights into Methane Oxidation by Particulate Methane Monooxygenase. *Accounts of Chemical Research, 40*(7), 573-580. 10.1021/ar700004s

Banerjee, R., Proshlyakov, Y., Lipscomb, J. D., and Proshlyakov, D. A. (2015). Structure of the key species in the enzymatic oxidation of methane to methanol. *Nature, 518*, 431-434. 10.1038/nature14160

Burnett, L., Rysakova, M., Wang, K., González-Carballo, J., Tooze, R. P., and García-García, F. R. (2019). Isothermal cyclic conversion of methane to methanol using copper-exchanged ZSM-5 zeolite materials under mild conditions. *Applied Catalysis A: General, 587*, 117272. 10.1016/j.apcata.2019.117272

da Silva, M. (2016). Synthesis of methanol from methane: Challenges and advances on the multi-step (syngas) and one-step routes (DMTM). *Fuel Processing Technology, 145*, 42-61. 10.1016/j.fuproc.2016.01.023

Dalena, F., Senatore, A., Basile, M., Knani, S., Basile, A., and Iulianelli, A. (2018). Advances in Methanol Production and Utilization, with Particular Emphasis toward Hydrogen Generation via Membrane Reactor Technology. *Membranes, 8*(4), 98. 10.3390/membranes8040098

Dyballa, M., Pappas, D. K., Kvande, K., Borfecchia, E., Arstad, B., Beato, P., Olsbye, U., and Svelle, S. (2019). On How Copper Mordenite Properties Govern the Framework Stability and Activity in the Methane-to-Methanol Conversion. *ACS Catalysis, 9*(1), 365-375. 10.1021/acscatal.8b04437

Groothaert, M. H., Smeets, P. J., Sels, B. F., Jacobs, P. A., and Schoonheydt, R. A. (2005). Selective Oxidation of Methane by the Bis(μ-oxo)dicopper Core Stabilized on ZSM-5 and Mordenite Zeolites. *Journal of the American Chemical Society, 127*(5), 1394-1395. 10.1021/ja047158u

Grundner, S., Markovits, M. A. C., Li, G., Tromp, M., Pidko, E. A., Hensen, E. J. M., Jentys, A., Sanchez-Sanchez, M., and Lercher, J. A. (2015). Single-site trinuclear copper oxygen clusters in mordenite for selective conversion of

methane to methanol. *Nature Communications, 6*, 7546. 10.1038/ncomms8546

Hammond, C., Conrad, S., and Hermans, I. (2012). Oxidative methane upgrading. *ChemSusChem, 5*(9), 1668-1686. 10.1002/cssc.201200299

Jovanovic, Z. R., Lange, J.-P., Ravi, M., Knorpp, A. J., Sushkevich, V. L., Newton, M. A., Palagin, D., and van Bokhoven, J. A. (2020). Oxidation of methane to methanol over Cu-exchanged zeolites: Scientia gratia scientiae or paradigm shift in natural gas valorization? *Journal of Catalysis, 385*, 238-245. 10.1016/j.jcat.2020.02.001

Latimer, A. A., Kakekhani, A., Kulkarni, A. R., and Nørskov, J. K. (2018). Direct Methane to Methanol: The Selectivity–Conversion Limit and Design Strategies. *ACS Catalysis, 8*(8), 6894-6907. 10.1021/acscatal.8b00220

Le, H. V., Parishan, S., Sagaltchik, A., Göbel, C., Schlesiger, C., Malzer, W., Trunschke, A., Schomäcker, R., and Thomas, A. (2017). Solid-State Ion-Exchanged Cu/Mordenite Catalysts for the Direct Conversion of Methane to Methanol. *ACS Catalysis, 7*(2), 1403-1412. 10.1021/acscatal.6b02372

Lomachenko, K. A., Martini, A., Pappas, D. K., Negri, C., Dyballa, M., Berlier, G., Bordiga, S., Lamberti, C., Olsbye, U., Svelle, S., Beato, P., and Borfecchia, E. (2019). The impact of reaction conditions and material composition on the stepwise methane to methanol conversion over Cu-MOR: An operando XAS study. *Catalysis Today, 336*, 99-108. 10.1016/j.cattod.2019.01.040

Ma, C., Tan, X., Zhang, H., Shen, Q., Sun, N., and Wei, W. (2020). Direct conversion of methane to methanol over Cu exchanged mordenite: Effect of counter ions. *Chinese Chemical Letters, 31*(1), 235-238. 10.1016/j.cclet.2019.03.039

Narsimhan, K., Michaelis, V. K., Mathies, G., Gunther, W. R., Griffin, R. G., and Román-Leshkov, Y. (2015). Methane to Acetic Acid over Cu-Exchanged Zeolites: Mechanistic Insights from a Site-Specific Carbonylation Reaction. *Journal of the American Chemical Society, 137*(5), 1825-1832. 10.1021/ja5106927

Newton, M. A., Knorpp, A. J., Sushkevich, V. L., Palagin, D., and van Bokhoven, J. A. (2020). Active sites and mechanisms in the direct conversion of methane to methanol using Cu in zeolitic hosts: a critical examination. *Chemical Society Reviews, 49*(5), 1449-1486. 10.1039/C7CS00709

Dolivos-Suarez, A. I., Szécsényi, À., Hensen, E. J. M., Ruiz-Martinez, J., Pidko, E. A., and Gascon, J. (2016). Strategies for the Direct Catalytic Valorization of Methane Using Heterogeneous Catalysis: Challenges and Opportunities. *ACS Catalysis, 6*(5), 2965-2981. 10.1021/acscatal.6b00428

Oord, R., Schmidt, J. E., and Weckhuysen, B. M. (2018). Methane-to-methanol conversion over zeolite Cu-SSZ-13, and its comparison with the selective catalytic reduction of NOx with NH3. *Catalysis Science and Technology, 8*(4), 1028-1038. 10.1039/C7CY02461D

Palagin, D., Knorpp, A. J., Pinar, A. B., Ranocchiari, M., and van Bokhoven, J. A. (2017). Assessing the relative stability of copper oxide clusters as active sites of a CuMOR zeolite for methane to methanol conversion: size matters? *Nanoscale, 9*(3), 1144-1153. 10.1039/C6NR07723D

Pappas, D. K., Borfecchia, E., Dyballa, M., Pankin, I. A., Lomachenko, K. A., Martini, A., Signorile, M., Teketel, S., Arstad, B., Berlier, G., Lamberti, C., Bordiga, S., Olsbye, U., Lillerud, K. P., Svelle, S., and Beato, P. (2017). Methane to Methanol: Structure–Activity Relationships for Cu-CHA. *Journal of the American Chemical Society, 139842*, 14961–14975. 10.1021/jacs.7b06472

Sainz-Vidal, A., Balmaseda, J., Lartundo-Rojas, L., and Reguera, E. (2014). Preparation of Cu-mordenite by ionic exchange reaction under milling: A favorable route to form the mono-(μ-oxo) dicopper active species. *Microporous and Mesoporous Materials, 185*, 113-120. 10.1016/j.micromeso.2013.11.009

Schwarz, H. (2011). Chemistry with methane: Concepts rather than recipes. *Angewandte Chemie - International Edition, 50*(43), 10096-10115. 10.1002/anie.201006424

Sharma, R., Poelman, H., Marin, G. B., and Galvita, V. V. (2020). Approaches for Selective Oxidation of Methane to Methanol. *Catalysts, 10*(2), 194. 10.3390/catal10020194

Sheppard, T., Hamill, C. D., Goguet, A., Rooney, D. W., and Thompson, J. M. (2014). A low temperature, isothermal gas-phase system for conversion of methane to methanol over Cu–ZSM-5. *Chemical Communications, 50*(75), 11053-11055. 10.1039/C4CC02832E

Sushkevich, V. L., Palagin, D., and van Bokhoven, J. A. (2018). The Effect of the Active-Site Structure on the Activity of Copper Mordenite in the Aerobic and Anaerobic Conversion of Methane into Methanol. *Angewandte Chemie - International Edition, 57*(29), 8906-8910. 10.1002/anie.201802922

Tomkins, P., Mansouri, A., Bozbag, S. E., Krumeich, F., Park, M. B., Alayon, E. M. C., Ranocchiari, M., and Vanbokhoven, J. A. (2016). Isothermal Cyclic Conversion of Methane into Methanol over Copper-Exchanged Zeolite at Low Temperature. *Angewandte Chemie - International Edition, 55*(18), 5467–5471. 10.1002/anie.201511065

Tomkins, P., Ranocchiari, M., and van Bokhoven, J. A. (2017). Direct Conversion of Methane to Methanol under Mild Conditions over Cu-Zeolites and beyond. *Accounts of Chemical Research, 50*(2), 418-425. 10.1021/acs.accounts.6b00534

Tomkins, P, Mansouri, A., L. Sushkevich, V., van der Wal, L. I., Bozbag, S. E., Krumeich, F., Ranocchiari, M., and van Bokhoven, J. A. (2019). Increasing the activity of copper exchanged mordenite in the direct isothermal conversion of methane to methanol by Pt and Pd doping. *Chemical Science, 10*(1), 167-171. 10.1039/C8SC02795A

Vanelderen, P., Vancauwenbergh, J., Tsai, M.-L., Hadt, R. G., Solomon, E. I., Schoonheydt, R. A., and Sels, B. F. (2014). Spectroscopy and Redox Chemistry of Copper in Mordenite. *ChemPhysChem, 15*(1), 91-99. 10.1002/cphc.201300730

Wulfers, M. J., Teketel, S., Ipek, B., and Lobo, R. F. (2015). Conversion of methane to methanol on copper-containing small-pore zeolites and zeotypes. *Chemical Communications, 51*(21), 4447-4450. 10.1039/C4CC09645B

Yoshizawa, K. and Shiota, Y. (2006). Conversion of Methane to Methanol at the Mononuclear and Dinuclear Copper Sites of Particulate Methane Monooxygenase (pMMO): A DFT and QM/MM Study. *Journal of the American Chemical Society, 128*(30), 9873-9881. 10.1021/ja061604r

Zakaria, Z. and Kamarudin, S. K. (2016). Direct conversion technologies of methane to methanol: An overview. *Renewable and Sustainable Energy Reviews, 65*, 250-261. 10.1016/j.rser.2016.05.082

Research Article / Case report / Civil and Sanitary Engineering https://doi.org/10.15446/ing.investig.v41n3.87737

# Cost Forecasting of Public Construction Projects Using Multilayer Perceptron Artificial Neural Networks: A Case Study

## Previsión de costos de proyectos de construcción pública utilizando Redes Neuronales Artificiales de Perceptrón Multicapa: un estudio de caso

Alcineide Pessoa[1], Gean Sousa[2], Luiz Maurício Furtado Maués[3], Felipe Campos Alvarenga[4], and Débora de Gois Santos [5]

**ABSTRACT**

The execution of public sector construction projects often requires the use of financial resources not foreseen during the tendering phase, which causes management problems. This study aims to present a computational model based on artificial intelligence, specifically on artificial neural networks, capable of forecasting the execution cost of construction projects for Brazilian educational public buildings. The database used in the training and testing of the neural model was obtained from the online system of the Ministry of Education. The neural network used was a multilayer perceptron as a backpropagation algorithm optimized through the gradient descent method. To evaluate the obtained results, the mean absolute percentage errors and the Pearson correlation coefficients were calculated. Some hypothesis tests were also carried out in order to verify the existence of significant differences between real values and those obtained by the neural network. The average percentage errors between predicted and actual values varied between 5% and 9%, and the correlation values reached 0,99. The results demonstrated that it is possible to use artificial intelligence as an auxiliary mechanism to plan construction projects, especially in the public sector.

**Keywords:** public undertakings, costs, artificial neural network

**RESUMEN**

La ejecución de proyectos de construcción del sector público a menudo requiere el uso de recursos financieros no previstos durante la fase de licitación, lo que genera problemas de gestión. Este estudio tiene como objetivo presentar un modelo computacional basado en inteligencia artificial, específicamente en redes neuronales artificiales, capaz de pronosticar el costo de ejecución de proyectos de construcción de edificios públicos educativos brasileños. La base de datos utilizada en el entrenamiento y prueba del modelo neuronal se obtuvo del sistema en línea del Ministerio de Educación. La red neuronal utilizada fue un perceptrón multicapa como algoritmo de retropropagación optimizado por el método de descenso de gradiente. Para evaluar los resultados obtenidos, se calcularon los errores porcentuales absolutos medios y los coeficientes de correlación de Pearson. También se llevaron a cabo algunas pruebas de hipótesis con el fin de verificar la existencia de diferencias significativas entre los valores reales y los obtenidos por la red neuronal. Los errores porcentuales promedio entre los valores predichos y reales variaron entre el 5 % y el 9 %, y los valores de correlación alcanzaron el 0,99. Los resultados demostraron que es posible utilizar la inteligencia artificial como mecanismo auxiliar para la planificación de proyectos de construcción, especialmente en el sector público.

**Palabras clave:** empresas públicas, costos, red neuronal artificial

**Received:** May 28th, 2020
**Accepted:** March 28th, 2021

## Introduction

In emerging countries, the final cost of public works is often significantly higher than the amount arranged in the bidding (Bucciol, Chillemi, and Palazzi, 2013; Wanjari and Dobariya,

[1]Civil Engineering, Federal University of Maranh˜ao (UFMA), Brazil M.Sc. in Civil Engineering, Federal University of Pará (UFPA), Brazil. Affiliation: Ph.D. student, Federal University of Pará (UFPA), Brazil. Email: alcineidedutra@hotmail.com
[2]Mathematical, Federal University of Pará (UFPA), Brazil. PhD., Electrical Engineering,Federal University of Maranhão (UFMA), Brazil. Affiliation: Associate Professor, Institute of Technology, Federal University of Maranhão (UFMA), Brazil. Email: gean.sousa@ufma.br
[3]Civil Engineering, Federal University of Pará (UFPA), Brazil. Ph.D. Federal University of Pará (UFPA), Brazil. Affiliation: Ph.D., Associate Professor, Institute of Technology, Federal University of Pará (UFPA), Brazil. Email: maues@ufpa.br
[4]Civil Engineering, Federal University of Pará (UFPA), Brazil. MSc., Institute of Technology, Federal University of Pará (UFPA),Brazil.Affiliation: M.Sc., Engineer, Federal University of Pará (UFPA), Brazil.
Email: felipealvarenga.eng@hotmail.com.br
[5]Civil Engineering,Federal University of Sergipe (UFS),Brazil. Ph.D., Federal University of Santa Catarina, Brazil. Affiliation: Ph.D., Associate Professor, Department of Civil Engineering, Federal University of Sergipe (UFS), Brazil.
Email: deboragois@yahoo.com.br

**How to cite:** Pessoa, A., Sousa, G., Maués, L., Alvarenga, F., and Santos, D. (2021). Cost forecasting of Public Construction Projects Using Multilayer Perceptron Artificial Neural Networks: A Case Study. *Ingeniería e Investigación*, *41*(3), e87737. https://doi.org/10.15446/ing.investig.v41n3.87737

2016). In Brazil, for example, Alvarenga (2019) showed that 61.89% of the works of the Federal Government regarding education completed between 2006 and 2017 had a cost addition. In India, Wanjari and Dobariya (2016) found that about 57% of 410 projects had their costs increased.

It is worth mentioning, however, that requests for an increase in the initial budgeted amounts for carrying out public construction works is not only a problem in the Brazilian or Indian context. Countries like Portugal, Indonesia, Ghana, the West Bank, and Jordan have also experienced this problem (Monteiro, 2010; Kaming, Olomolaiye, Holt, and Harris, 1997; Famiyeh, Amoatey, Adaku, and Agbenohevi 2017; Mahamid, 2018; Hyari, Al-Daraiseh, and El-Mashaleh, 2016). However, in Brazil, when it comes to public works, cost overrun values cannot exceed 25% in new constructions (Brasil, 1993).

Additional costs in construction projects can cause serious problems for the contractor and even require the interruption of the work due to lack of resources (TCU, 2018). An alternative to mitigate this type of problem is to accurately forecast the real costs of the undertaking, that is, predicting the real cost can promote better planning and avoid later problems.

The possibility of presenting a mechanism capable of predicting the real value of a governmental undertaking, and thus contributing to the planning of costs of public construction works in Brazil, is the main motivation of this research. Our main hypothesis is that a computational model based on artificial neural networks (ANNs) is able to learn patterns in such a way that it can predict the real costs of a construction based on information contained in the bidding contracts.

The hypothesis raised here has also been the object of study in the field of engineering. Hyari *et al.* (2016), for example, proposed a model based on machine learning, more specifically on neural networks, to predict the costs of engineering services. Shahandashti and Ashuri (2016) used vector error correction models to predict highway construction costs, and Lu, Luo, and Zhang (2011) used genetic algorithms to the same end.

By using multivariate approximation, Shahandashti and Ashuri (2013) presented a model capable of predicting the construction cost index (CCI). This index is a North American cost indicator published monthly by Engineering News-Record (ENR). Ugur (2017) used neural models to predict costs of public undertakings and evaluated their training and test results using the $R^2$ metric, which, in the case of training, was 0,97 and in the test was 0,89.

Although several works have aimed at predicting costs in public projects, it is important to note that the proposed models are usually trained to meet the peculiarities of each problem, that is, a model that obtained good results in the building of highways will not necessarily have good results predicting costs in the construction of schools, and the model trained in India may not have the same performance in Brazil. Therefore, it is in this context that this research was conducted, with the objective of presenting a computational model based on artificial intelligence, precisely on ANNs, capable of forecasting the cost of executing public educational building construction projects in Brazil. The model presented herein aims to assist managers in the planning and budgeting of construction projects contracted by federal agencies. The model is also intended to present the smallest possible error between collected and predicted data.

## Cost forecasting for public construction projects

The administration of public construction projects comprises stages that go from the elaboration of the engineering project up to the conclusion and delivery of the work. This includes budgeting, bidding, contracting, and execution phases. However, it is in the budgeting phase that it is possible to determine, through cost forecasting, whether a particular undertaking is feasible (Paula and Garcia, 2012).

Cost has been an important variable for contracting companies to carry out public works through a bidding process. However, Tisaka (2006) points out that choosing a company based only on the lowest price is not the best criterion when it comes to achieving the objectives of said process. This choice, based on the lowest cost criterion, levels the quality of the construction downward. In the context of public construction works, there are several examples of bids whose work did not start, was poorly finished, or even dropped altogether (Borba and Marinho, 2019; Cunha and Caffé Filho, 2019; Jorge and Ribeiro, 2006; Oliveira, 2016; Tisaka, 2006). When on hold, these projects can bring several problems for public administration, which implies losses for taxpayers.

A possible flaw in the management that may cause uncontrolled costs directly influences the final results of the project (Silva, Corrêa, and Ruas, 2018). The public sector, for example, has difficulty completing works such as the construction of kindergartens, schools, hospitals, sport courts, basic sanitation systems, roads, ports, and airports (TCU, 2018).

In 2006, upon realizing the difficulties public authorities face to conclude the execution of construction projects, the Federal Court of Auditors (TCU) carried out a survey to diagnose the situation of unfinished public works. The audited works were mostly linked to the executive branch.

A set of 400 unfinished construction projects was presented in the TCU report (2018). The total cost attributable to these projects amounted to R$ 3,5 billion. Of the 400 works, 130 were carried out directly by the federal government and 270 by states and municipalities, but all used federal resources. Figure 1 shows the causes of stoppage hitherto identified in the report by the Court of Auditors.

In Figure 1, it can be seen that the main cause for stoppage of the works analyzed by the TCU's Court of Auditors was budgetary problems. As Paula and Garcia (2012) state,

the ability to predict construction costs can result in more accurate proposals.

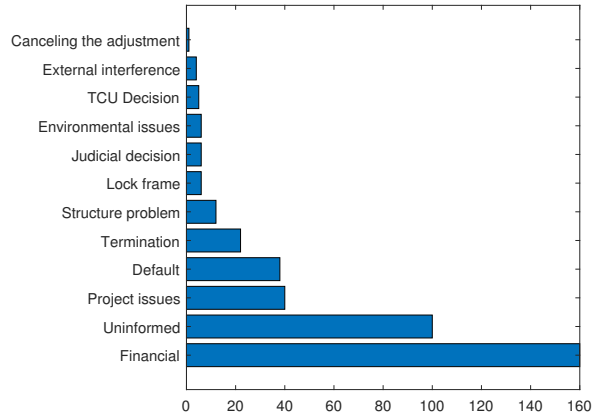


**Figure 1.** Causes of work stoppage.
**Source:** TCU (2018)

Given that budget is an important factor in the stoppage of public construction projects, it is expected that mechanisms to help decision makers to forecast real costs before starting a work may be developed in relation to financial issues, so as to diminish the probability of interruptions. These premises endorse the importance of developing a computational model capable of forecasting the real cost of public undertakings.

## Artificial Neural Networks - ANN

Artificial neural networks are computational models inspired by the functioning of the nervous system, namely the functioning of neurons (Silva, Spatti, and Flauzino, 2016). Neurons are cells capable of perceiving changes in the environment, maintaining communication with each other through chemical and/or electrical processes, as well as commanding bodily responses (Bear, Connors, and Paradiso, 2002).

Communication between neurons and information processing essentially depends on three integral parts: dendrites, cell body (or soma), and axon. Similarly, the functioning of an artificial neuron occurs involving the following integrating parts: the synaptic weights, sum, and activation functions. The relationship between these parts can be seen in Figure 2.

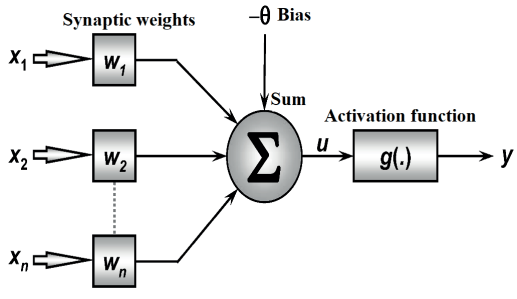


**Figure 2.** Artificial neuron.
**Source:** Silva *et al.* (2016)

The mathematical operations that characterize the functioning of the neuron begin with the multiplication of each input $x_j$ (connected to the neuron $k$ in $j$) and multiplied by the synaptic weight $w_{kj}$). After the multiplications, an adder is activated, transforming the set of multiplications into a linear combination Σ. The result of the linear combination $u_k$, plus a bias $b_k$, is applied to an activation function $g(\cdot)$ (Silva *et al.*, 2016).

Mathematically, the functioning of an artificial neuron is given in Equations (1) and (2).

$$u_k = \sum_{1}^{m} w_{kj} x_j \tag{1}$$

$$y_k = g(u_k + b_k) \tag{2}$$

Haykin (2001) defines the architecture of an ANN as the way in which neurons are arranged together or structured in layers. The existence of at least one layer between the inputs and the output layer of an ANN is what characterizes a multilayer network. Among these multilayer networks, the Multilayer Perceptron (MLP) type stands out (Figure 3). Multilayer Perceptron networks are applicable to several types of problems, such as approximation of functions, forecasting, and optimization.

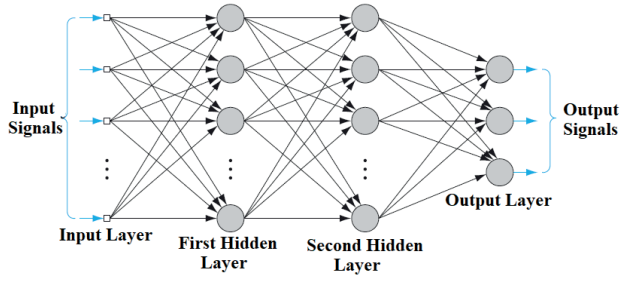


**Figure 3.** Multilayer Perceptron (MLP).
**Source:** Haykin (2001)

The use of an MLP network for a given project requires the designer to define the specifications (topology) of the network beforehand. This includes, for example, the number of input signals, the number of hidden layers, the number of neurons in each hidden layer, and the number of neurons in the output layer. There are no pre-established rules for choosing the network topology. This choice depends on the problem in question and is usually chosen through computational tests (Rocha, 2018).

The training of an MLP-type network is carried out through supervised learning and the error backpropagation algorithm. This algorithm is based on the error correction learning rule and consists of two phases: propagation (forward phase) and backpropagation (backward phase) (Haykin, 2001).

In the propagation phase, the input signals are multiplied by the synaptic weights, applied to the adder to form a linear combination, and the result is applied to an activation function. This process is carried out on all neurons and on

all layers until reaching the output layer (Silva *et al.*, 2016). When the process reaches the output layer, the result is examined to check for the existing error between the network output and the desired signal (Haykin, 2001; Rocha, 2018; Batista, 2012).

The error obtained in the propagation phase is used to update the weights of the MLP layers, so that this update is made starting at the last layer until it reaches the first one. This process of updating of weights is known as backpropagation (Haykin, 2001). Figure 4 shows the operation of the backpropagation algorithm in an MLP network.

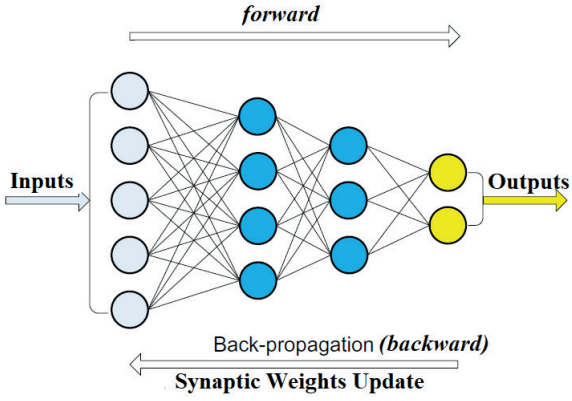


**Figure 4.** Backpropagation algorithm.
**Source:** Adapted from Asteris *et al.* (2016)

In short, the successive application of the forward and backward phases implies the minimization of error and consequent convergence of the network (Silva *et al.*, 2016). Optimization methods are applied for derivation of the iterative expressions for updating weights.

## Materials and method

After the first contacts with works on cost forecasting models for public projects, we noticed that there were gaps to be filled internationally, mainly with regard to issues related to Brazilian projects. As a matter of fact, it is common that contractors request additional, not originally foreseen values during the execution of works contracted by the public power.

According to Alvarenga (2021), out of the total public construction projects linked to educational institutions completed between December, 2006, and August, 2017, 61,89% required additional costs. It can be seen, then, that requests for additional items are, in fact, an important problem because they hinder the planning and execution of state constructions. It is then in the attempt of assisting the planning of government agencies that this work proposes the use of a computational model to forecast the final cost of public construction works.

To achieve the objectives proposed in this work, two types of variables were defined. The first, a dependent variable, is the one we want to model and predict what values it would assume when information about it is missing. The dependent variable in this research was the final cost of each construction project.

The second type of variable consisted of the characteristics of the projects available to users of the model. These were called independent variables and consisted of the following: the area of the facility to be constructed, the number of inspections, the estimated budgeted cost, and the contracted cost. These variables were chosen because information about them is available for projects on the platform of the Ministry of Education (MEC).

In terms of the methodological framework, this research can be classified as explanatory in terms of the objectives and quantitative with respect to the approach, with an *ex-post facto* design as to the procedures adopted for data collection.

### *Database*

The data used in the modeling process were obtained from an online platform of the MEC (MEC,2019). This platform is called the Integrated Monitoring, Execution and Control System (SIMEC). Authorization from MEC was requested to access the data because these are not public domain data. A complete description of the methodological acquisition procedure and an analysis of this database can be found in the work of Alvarenga (2019). The data used in the present work were provided by this researcher.

In order to avoid a high number of renovation and adaptation projects in the sample, the following filters were applied in the listing of projects: projects that were 100% completed, projects with costs above R$ 1 000 000,00, and projects in federal universities, federal institutes, and university hospitals. In the first filtering, a total of 2178 contracts were considered for the composition of the database, broken down into 109 universities and university hospitals in 27 federation units located in 460 municipalities.

The sample composition was quite diverse and included information on constructions carried out in several Brazilian municipalities in all regions of the country. The completion of the works took place in the period between December, 2006, and August, 2017, and the report was extracted from the system in early September of 2017. Out of the total data, 11% refer to works carried out in the North of Brazil, 22% in the South, 27% in the Northeast, 27% in the Southeast, and 13% in the Midwest. (Alvarenga, 2019).

A second filtering was applied in order to find only samples that contained information on both dependent and independent variables to be used in the modeling process. After performing this second filtering, the database was reduced to 1094 samples, which were then used for modeling.

### *Modeling*

The modeling process sought to be in line with the concepts of experimentation, abstraction, resolution, validation, and modification presented by Bassanezi and Ferreira (1988). The modeling phase was therefore carried out in three stages: choice of the type of ANN and construction of the algorithm,

specifications and training of the ANNs, and testing of the networks.

*Choice of type of ANN and construction of the algorithm*

The choice of the type of ANN usually depends on the problem to be modeled. MLP networks are commonly used for forecasting problems. Thus, a MLP network was chosen for cost forecasting in the context of this study. It was also decided that an algorithm would be written to carry out the MLP training and testing phases.

It is worth noting that the choice of the number of separate samples for training and testing does not come from statistical methodologies, but from tests related to the learning capacity of the ANN, that is, it depends on the problem to be solved. In some problems, this separation can occur according to the ratio of 70/30 (70% for training and 30% for testing), or even 90/10 (90% for training and 10% for testing).

The topological characteristics of the network regarding the number of layers, learning rate, stopping criteria, number of neurons in each layer, and bias were defined based on various training runs and the validation of the network.

It is also worth mentioning that there are no mathematical mechanisms for defining the characteristics of the network, thus giving an empirical character to this choice. After conducting several training sessions with different topologies, the best results were chosen, and the respective topologies were presented.

Before carrying out the training of an ANN, it is always advisable to normalize the data, so as to limit them to the interval [0,1] (Doğan, Arslan, and Ceylan, 2015). One way to achieve this normalization is to use Equation (3).

$$A_n = \frac{A_i - \min(A)}{\max(A) - \min(A)}. \quad (3)$$

where $A_n$ is the normalized sample, $A_i$ is the original sample, and $\min(A)$ and $\max(A)$. These are the lowest and highest value among all samples of the variable to be normalized, respectively.

The specifications used in the ANN for cost forecasting were: four inputs, one hidden layer, eight neurons in the hidden layer, and one output (cost). Figure 5 illustrates the ANN's topology and training process in cost prediction.

The value predicted by the network in each loop is compared with the measured value. Therefore, it was defined as a criterion for stopping the network when the difference between the error of one looping and the other one is not less than $10^{-7}$. Otherwise, the network continues to update the synaptic weights.

*ANN testing*

The testing phase of the ANN for cost forecasting consists of applying the forward phase of the backpropagation algorithm only once in new data. This phase differs from the training phase in that only one looping is performed without updating weight; the weights used are those obtained during training, and the calculated error is analyzed for model validation purposes. Figure 6 shows how the ANN testing process for cost forecasting takes place.

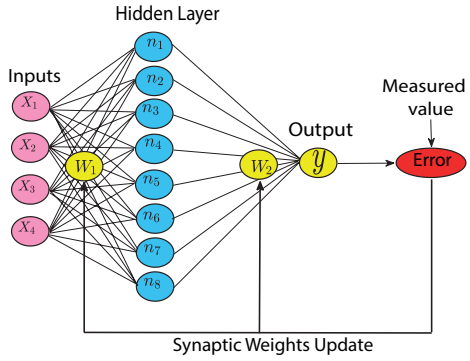


**Figure 5.** Topology of the network used to predict public work costs.
**Source:** Authors

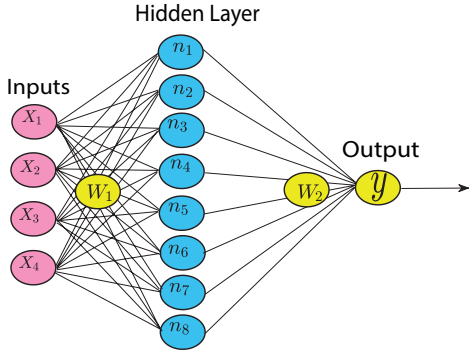


**Figure 6.** Network topology used to validate the cost prediction model.
**Source:** Authors

*Model Evaluation and statistical analysis*

Before performing the evaluations of the results, the sample values were denormalized according to Equation (4).

$$A_i = A_n[\max(A) - \min(A)] + \min(A). \quad (4)$$

For the results of the presented models, we analyzed the statistical characteristics of both the training and test phases. These analyses consisted of evaluations using accuracy and correlation measurements, as well as hypothesis tests.

With the values calculated by the neural networks, the mean absolute percentage error (MAPE) between the outputs of the network and the real values were calculated. MAPE is mathematically defined according to Equation (5) (Belalia *et al.*, 2017; Maués, 2017).

$$MAPE = \frac{100}{n}\sum_{i=1}^{n}\left|\frac{X_i - Y_i}{X_i}\right| \quad (5)$$

where $X_i$ is the measured or observed value (real value); $Y_i$ is the respective approximation to $X_i$, obtained through the mathematical model; and $n$ is the number of samples evaluated. The MAPE was used to verify the accuracy (or assertiveness)of the model, and it was determined from the

percentage of predicted values belonging to the interval [$L_s$,$L_i$] defined by Equations (6) and (7) (Maués, 2017).

$$L_s = V_R(1 + MAPE), \quad (6)$$

$$L_i = V_R(1 - MAPE). \quad (7)$$

In these Equations, $L_s$ and $L_i$ are the upper and lower limits of the assertiveness range, respectively, and $V_R$ is the real value of the database.

A correlation analysis was also carried out to verify if there was a linearity relationship between the predicted and real values. In addition to the accuracy and correlation estimates, comparisons were made between the box plots of the actual values and the values obtained by the models in order to graphically verify differences between the analyzed samples.

As graphic analyses alone are not enough to infer the existence or not of differences between the sets of the analyzed samples, it was necessary to carry out hypothesis tests. First, the Kolmogorov-Smirnov test was performed to infer the type of data distribution. The test revealed that samples did not come from a normal distribution. Then, the Mann Whitney test was carried out to check for significant differences between the real values and those obtained by the neural models (Bussab and Morettin, 2003).

## Results

The simulations performed aimed to predict the final costs of construction projects. First, the network training was carried out to update the synaptic weights with the purpose of minimizing the error between the network output and the real values. In the second phase, the weights obtained in the training were used to test and validate the model.

The results obtained for cost forecasting in the training and testing of the ANN are presented in the following subsections, as well as the hypothesis tests and the correlation test between values obtained by the network and the real ones.

### *Training of the ANN for cost forecasting*

The input variables used in the training phase were the area of the facility to be constructed, the number of inspections, the estimated budgeted cost, and the contracted cost. The topology of the network used is described in Table 1.

**Table 1.** ANN Topology

| Topological item | Amount |
|---|---|
| Appetizer | 4 |
| .pdf Hidden layers | 1 |
| .pdf Neuron in the hidden layer | 8 |
| .pdf Learning rate | 0,5 |
| .pdf Activation function | Sigmoid |
| .pdf RNA type | Multilayer Perceptron |
| .pdf Algorithm | Backpropagation |

**Source:** Authors

994 of the total of 1094 samples were randomly selected and used to carry out the training of the neural network. A MAPE equal to 9,62% was obtained. From the MAPE value, an interval was established to calculate the accuracy. Of the 994 values referring to the total cost of the works used in the training of the ANN, 878 were within the established interval, that is, the model obtained an accuracy of 88,33% in the training phase. An overview of the value sets within and outside the established interval is presented in Figure 7.

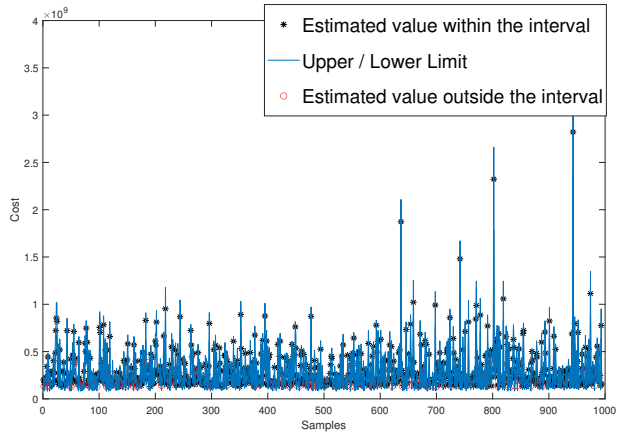


**Figure 7.** Results of the training phase of the ANN for cost forecasting.
**Source:** Authors

A subset of samples is presented in in Figure 8 to better understand the relationship between the estimated values and the error interval established for the analysis of the model. However, in the presented samples, it appears that the estimated values that do not belong to the error interval are visibly close to the upper or lower limit.

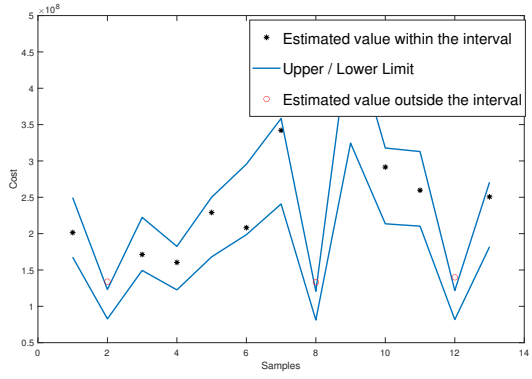


**Figure 8.** Results of the ANN training phase for cost forecasting (some samples).
**Source:** Authors

The main objective of the training phase of an MLP-type ANN is to find the weight matrices that minimize the error between the real values and the network's output. If the weight matrices are known, the neural model can be applied to new data, and the results can then be extrapolated. With that in mind, the following are the synaptic weight matrices obtained in the training process for cost forecasting:

$$w_1 = \begin{bmatrix} 0{,}10 & 0{,}58 & -0{,}08 & 2{,}08 & 0{,}45 \\ 0{,}21 & 0{,}25 & 0{,}37 & 1{,}08 & 0{,}99 \\ -0{,}82 & 0{,}43 & 1{,}20 & -0{,}25 & 0{,}47 \\ 0{,}77 & 0{,}77 & 0{,}58 & -0{,}06 & 0{,}77 \\ -0{,}33 & -0{,}25 & 3{,}16 & 7{,}74 & -0{,}00 \\ 0{,}16 & -0{,}22 & 1{,}05 & 0{,}88 & 0{,}62 \\ 1{,}58 & -0{,}17 & -0{,}39 & 2{,}07 & -0{,}40 \\ 1{,}43 & 0{,}02 & 0{,}11 & 1{,}36 & -0{,}26 \end{bmatrix}$$

and

$$w_2^T = \begin{bmatrix} 5{,}03 \\ 1{,}45 \\ 0{,}44 \\ -1{,}62 \\ -0{,}41 \\ 4{,}36 \\ 0{,}12 \\ 2{,}35 \\ 1{,}56 \end{bmatrix}$$

where $w_1$ represents the weights of the first layer and $w_2$, the second layer. It is important to note that the number of lines of $w_1$ corresponds to the number of neurons in the hidden layer, whereas the number of columns is equal to the number of inputs plus 1 (bias). The dimensions of $w_2$ refer to the number of output variables (row) and the number of neurons in the hidden layer plus 1 (columns).

### *Testing of the ANN for cost forecasting*

The test of the neural model was performed using the matrices presented above. 100 samples were separated and used for this phase. It is worth mentioning that the samples for both training and testing were randomly chosen.

The MAPE value found in the testing phase was 9,14% and thus, in an analogous way to what was done in the training, an interval was established to check the accuracy of the model. Ninety samples were within this interval, that is, the accuracy in the testing phase was 90%. In Figure 9, it is possible to see which estimated values were within and which were outside the interval.

An interesting observation to make when analyzing Figure 9 is that there are almost no values with great differences concerning the error limits. This suggests that the trained model has a strong generalization 'power'.

### *Statistical analysis of cost forecasting*

In this subsection, a statistical analysis is presented which considers the calculation of Pearson's correlation coefficient, the characteristics of the distributions of the real and the network output values, and the hypothesis tests.

The correlation between the network output values and the measured values was 0,9921 in the training phase and 0,9912 in the testing phase. The correlation analysis is important, as it demonstrates the extent to which two variables are linearly related. Figure 10 shows the relationship between

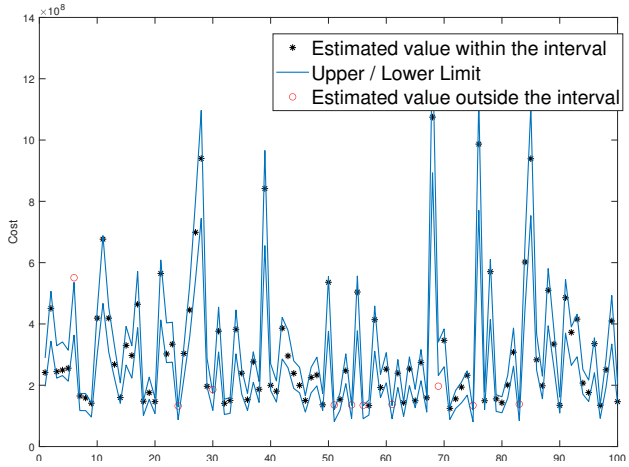


**Figure 9.** Results of the ANN test phase for cost forecasting.
**Source:** Authors

the analyzed variables and the line that best approximates them for the training and the testing phases.

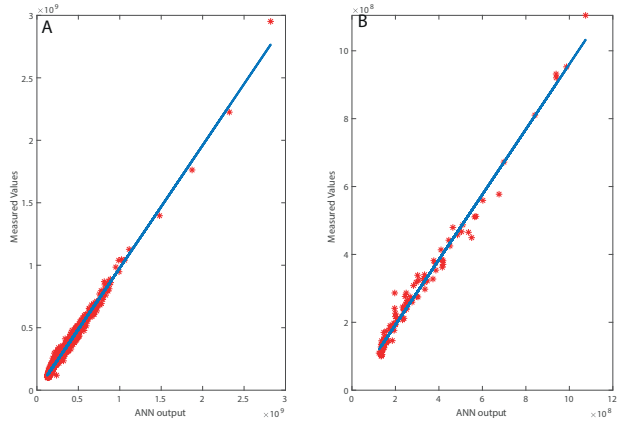


**Figure 10.** Correlation between the measured values and the ANN output: A) Training phase, B) Test Phase.
**Source:** Authors

The high correlation obtained both in the training and test phases of the network means that there is a linear relationship between the real values and those obtained by the network. This fact corroborates the results related to the small number of values outside the error range.

The fact that there is a linear relationship between the real and the network output data shows that, in this particular case, in addition to small percentage error, there is a relationship of proportionality between variables. This trend indicates that, when a real value increases (or decreases), the network result also increases (or decreases). This analysis is important, as it can encourage further research on models complementary to ANN (to create a hybrid model). That is to say, the ANN output data can be used as an input to another model and generate enhanced results. As for the 'behavior' in terms of distribution, the box plots in Figure 11 show how the data in the training and testing phases are distributed around the median.

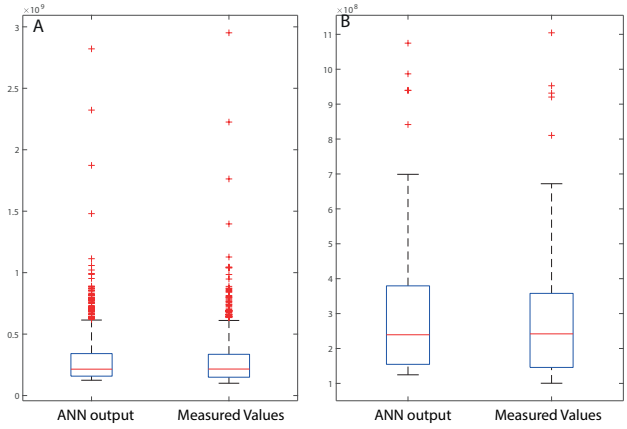


**Figure 11.** Distribution of measured values and ANN output for cost forecasting: A) Training phase, B) Test Phase.
**Source:** Authors

The distributions shown in Figure 11 allow inferring and assuming that there is not 'much difference' between the sets. However, measurements and the application of techniques are needed to verify whether or not there are significant differences between values coming from the ANN and the real values. To achieve this goal, hypothesis tests were performed. First, the Kolmogorov-Smirnov normality test was carried out using the network output values and measured values in the two phases (training and testing) of the construction of the proposed model.

Results of the tests in all data sets pointed to the rejection of the null hypothesis (normal data), with a significance level of 5%. As the null hypothesis was rejected, that is, the data did not come from a normal distribution, the Mann-Whitney U test was applied to verify the existence of significant differences.

The Mann-Whitney U test was applied to the results obtained in the training and in testing phases for the case of cost forecasting. In the training phase, the test showed that the hypothesis that the network output and real values are samples of distributions with equal medians should be rejected at the significance level of 5% ($p$-value = 0,0307). In the testing phase, the results pointed to the non-rejection of this hypothesis ($p$-value = 0,555).

### *Estimating the total cost of the construction based on the forecast of cost overruns*

During the development of this study, we noticed possibility of obtaining a system capable of estimating the final cost of the construction projects based on the forecast of overruns. This system consists of training an ANN whose desired output is the cost overrun. After the neural model provided such value, it was added to the contracted value, thus leading to the total cost of the work. This procedure is summarized in Figure 12.

Table 2 shows the values of the main evaluative metrics regarding the total cost prediction of the work from the additive values provided by the ANN.

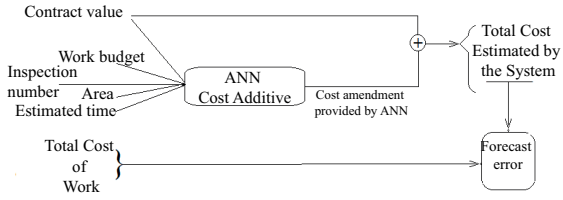


**Figure 12.** Total cost forecast through forecast of cost overruns.
**Source:** Authors

**Table 2.** Results obtained for training data

| Metric | Value |
|---|---|
| MAPE | 5,97% |
| Assertiveness | 95,54% |
| Correlation | 0,99 |

**Source:** Authors

Results obtained in the testing phase of the total cost forecast of the work based on cost overrun values are shown in Table 3.

**Table 3.** Results obtained for testing data

| Metric | Value |
|---|---|
| MAPE | 5,27% |
| Assertiveness | 96,25% |
| Correlation | 0,99 |

**Source:** Authors

In view of the results presented in Tables 2 and 3, it is evident that the methodology based on the use of the system proposed in Figure 12 presents relatively better results than those obtained with the use of the model directly trained for cost forecasting.

These error percentages of cost forecasting are promising and demonstrate that this research brings an important contribution to the proposal of collaborations aimed at improving the planning process of construction projects, given that, according to Hyari *et al.* (2016), conceptual cost estimates relying on traditional methods are inherently associated with high percentage errors, usually in the range between 20,8 and 27,9%.

For comparison purposes, one can observe the results obtained by Hyari *et al.* (2016), who carried out a similar work, applying a neural model to forecast costs. They obtained 28,2% of MAPE (testing phase). However, it is important to note an important difference between their work and ours, namely the amount of values available for training the network, as it is known that the performance of ANNs increases with the amount of training samples. That is, as the number of samples used in the present study is much greater than those used by Hyari *et al.* (2016), better results were expected.

As the weight matrices were made available in the text, the forecasting model can be implemented in more popular software such as Microsoft Excel, and thus be used by

engineering professionals (even without any knowledge of ANNs) in their professional practice, provided they have access to the network. Furthermore, this model can be 'embedded' in electronic devices such as computers and cellphones.

## Discussion

As it can be seen, the results obtained in the ANN training phase showed two important points regarding the building of the model. The first is that the low error value indicates that the training algorithm converged because the goal of training is to find the synaptic weights that minimize the error.

The second point to be highlighted about the results of the training phase is that the accuracy of the model reached a percentage close to 90%. This demonstrates that, although the data were collected from different Brazilian cities and, therefore, represent different realities, the algorithm kept the vast majority of forecasts within the interval established by MAPE values. The good results regarding the percentage error and the MAPE in the training phase are of great importance. However, it is in the testing phase that the model can be analyzed more carefully.

When observing results of the testing phase, the mistake of extolling the "low" error value (MAPE = 9,14%) may be incurred. However, Alvarenga (2021) demonstrated that, for values used in the database, the average percentage cost overrun was 15,14%, that is to say, without considering any computational mechanism, the original budget has an error of approximately 15% on average.

Bearing in mind that the reduction of error from 15,14 to 9,14% is not as drastic as expected, the forecast system, also based on ANNs, was presented in this work (Figure 12). Thereupon, considering the mentioned system, an error of only 5,27% was observed. This error value stimulates the application of the proposed system in the practice, as it can, in fact, assist the person responsible for the budgetary planning of public construction works.

In addition to an error of relatively less than 9,14%, the presented system has a high accuracy, that is, few works in practice can be expected to have a budget forecast outside the established range of more or less 5%. This fact can increase confidence when approving resources for the execution of state undertakings. This budgetary safety, obtained through the presented system, can translate into a reduced number of paralyzed projects or reduced loss of public money.

Notwithstanding the promising results, some limitations, typical of ANN-based models, and which can be the subject of future research, must be mentioned. One of them is the fact that this computational mechanism is based on pattern learning, which means that it is uncertain whether the system presented in this research, trained with Brazilian data, will have the same success if applied in other countries.

Another limitation of ANN-based models is that they require an extensive data set for training, therefore restricting their applicability to some specific problems. However, it is worth mentioning that the data set used in this research overcame this limitation, for the algorithm converged to a satisfactory error value.

## Conclusions

The success of construction projects generally depends on good planning. In public sector construction works, however, poor planning is commonplace, especially in emerging countries. In this context, one of the factors observed to contribute to inefficient execution of the plan is the lack of mechanisms capable of predicting the real cost of undertakings.

Aiming to provide more credible estimates of real values necessary for the completion of governmental projects, computational models based on the functioning of neurons were proposed in this work. The main purpose of using such models is to collaborate with the planning of public construction or renovation projects.

The neural model used in the cost forecast obtained a learning process that, when applied to new samples, resulted in a percentage error of 9,14%. This demonstrates that the use of artificial intelligence in this type of problem can help to improve the planning phase. When the cost overrun forecast was combined with the final cost forecast, it was found that the total cost forecasting model was improved, and the results were reduced to errors of 5%.

It is notable, therefore, that the ANN-based modeling technique can be used as an auxiliary tool in the pricing of projects and thus improve the planning of public agencies responsible for construction or renovation projects, as the cost forecasting model showed average percentage errors between 5 and 9%.

Bearing in mind that the presented model mirrors a wide reality in several Brazilian states with an assertiveness of 96,25%, it can be said that it can be adopted in developing countries that have similar characteristics to those of Brazil.

## Acknowledgements

The authors thank the support of the Coordination for the Improvement of Higher Education Personnel (CAPES) in Brazil.

## References

Alvarenga, F. C. (2019). *Análise das causas de aditivos de custo e de prazo em obras públicas de instituicões federais de ensino* [Master's thesis]. Universidade Federal do Pará. http://repositorio.ufpa.br/jspui/handle/2011/11129

Alvarenga, F. C., Maués, L. M. F., Santos Júnior, P. C. D., and Macedo, A. N. (2021). Alteracões de custo e prazo em obras públicas. *Ambiente Construído, 21*(1), 161-180. 10.1590/s1678-86212021000100500

Asteris, P. G., Kolovos, K. G., Douvika, M. G., and Roinos, K. (2016). Prediction of self-compacting concrete strength

using artificial neural networks. *European Journal of Environmental and Civil Engineering, 8189*(November), 1-21. 10.1080/19648189.2016.1246693

Bassanezi, R. and Ferreira, W. (1988). *Equacões Diferenciais com Aplicacões*. São Paulo, Brazil: Harbra.

Batista, C. F. B. (2012). *Solucões de Equacões Diferenciais Usando Redes Neurais de Múltiplas camadas com os métodos da Descida mais íngreme e Levenberg - Marquardt* [Master's thesis]. Universidade Federal do Pará.

Bear, M. F., Connors, B. W., and Paradiso, M. A. (2002). *Neurociências: Desvendando o Sistema Nervoso* (2nd edition). Porto Alegre, Brazil: Artmed.

Belalia, O., Bakhta, D., Mohamed, B., and Arezki, G. (2017). Prediction of properties of self-compacting concrete containing fly ash using artificial neural network. *Neural Computing and Applications, 28*(1), 707-718. 10.1007/s00521-016-2368-7

Borba, R. T. R. and Marinho, M. (2019). Estatísticas dos Contratos de Obras Públicas no Estado de Pernambuco. *Revista de Engenharia e Pesquisa Aplicada, 4*(3), 52-66. 10.25286/repa.v4i3.994

Brasil.Lei 8.666 de 21 de Junho de 1993. Regulamenta o art. 37, inciso XXI, da Constituição Federal, institui normas para licitações e contratos da Administração Pública e dá outras providências. Diário Oficial (Separata), 1993-06-26. http://www.planalto.gov.br/ccivil_03/leis/l8666compilado.htm

Bucciol, A., Chillemi, O., and Palazzi, G. (2013). Cost overrun and auction format in small size public works. *European Journal of Political Economy, 30*, 35-42. 10.1016/j.ejpoleco.2013.01.002

Bussab, W. de O. and Morettin, P. A. (2003). *Estatística Básica* (5th edition). São Paulo, Brasil: Saraiva.

Cunha, W. S., and Caffé Filho, H. P. (2019). Management of Public Works: Logistics more suited to the fulfillment of planned deadlines. *Revista de Psicologia, 13*(45), 77-89. 10.14295/idonline.v13i45.1823

Doğan, G., Arslan, M. H., and Ceylan, M. (2015). Statistical feature extraction based on an ANN approach for estimating the compressive strength of concrete. *Neural Network World, 25*(3), 301. 10.14311/NNW.2015.25.016

Elmousalami, H. H. (2020). Artificial Intelligence and Parametric Construction Cost Estimate Modeling: State-of-the-Art Review. *Journal of Construction Engineering and Management, 146*(1), 03119008. 10.1061/(ASCE)CO.1943-7862.0001678

Famiyeh, S., Amoatey, C. T., Adaku, E., and Agbenohevi, C. S. (2017). Major causes of construction time and cost overruns: A case of selected educational sector projects in Ghana. *Journal of Engineering, Design and Technology, 15*(2), 181-198. 10.1108/JEDT-11-2015-0075

Haykin, S. (2001). *Redes Neurais: Princípios e Prática* (2nd edition). Porto Alegre, Brasil: Bookman.

Hyari, K. H., Al-Daraiseh, A., and El-Mashaleh, M. (2016). Conceptual Cost Estimation Model for Engineering Services in Public Construction Projects. *Journal of Management in Engineering, 32*(1), 1-9. 10.1061/(ASCE)ME.1943-5479.0000381

Jorge, R. and Ribeiro, B. (2006). Possibilidades de atuação do Poder Legislativo frente à questão das obras inacabadas. *Revista do TCU, 107*(2006), 95-100. https://revista.tcu.gov.br/ojs/index.php/RTCU/article/view/510

Kaming, P. F., Olomolaiye, P. O., Holt, G. D., and Harris, F. C. (1997). Factors influencing construction time and cost overruns on high-rise projects in Indonesia. *Construction Management and Economics, 15*(1), 83-94. 10.1080/014461997373132

Lu, Y., Luo, X. Y., and Zhang, H. (2011). A gene expression programming algorithm for highway construction cost prediction problems. *Journal of Transportation Systems Engineering and Information Technology, 11*(6), 85-92. 10.1016/S1570-6672(10)60150-X

Mahamid, I. (2018). Critical Determinants of Public Construction Tendering Costs. *International Journal of Architecture, Engineering and Construction, 7*(1). 10.7492/ijaec.2018.005

Maués, M. (2017). *Modelo para Estimar o Prazo de Execucão de Obras Residenciais Verticais-Por meio da Lógica Fuzzy* [Master's thesis]. Universidade Federal do Maranhão. http://repositorio.ufpa.br/jspui/handle/2011/9877

MEC. Ministério da Educação. (2019). *Sistema Integrado de Monitoramento Execucão e Controle*. http://simec.mec.gov.br/login.php

Monteiro, M. O. (2010). *Processos de obras de infra-estruturas viárias municipais: uma análise dos desvios de custo e de prazo* [Doctoral dissertation]. Universidade de Trás-os-Montes e Alto Douro, Vila Real.

Oliveira, T. D. (2016). *Improbidade administrativa e seus efeitos nos casos de desvio de recursos públicos nas obras inacabadas e contratadas pelo poder público* [Undergraduate's thesis].Centro Universitário Tabosa de Almeida. http://repositorio.asces.edu.br/bitstream/123456789/656/1/Concluida%20Thiago%20%281%29.pdf

Rocha, P. L. (2018). Reconhecimento de Voz utilizando Seleção Dinâmica de Redes Neurais. Universidade Federal do Maranhão.

Santos, A. de P. and Garcia, L. E. M. (2012). Orçamento executivo como ferramenta do processo de planejamento e controle de custos de obras públicas. *Revista Gestão e Políticas Públicas, 2*(1), 40-67. https://www.revistas.usp.br/rgpp/article/view/97850

Shahandashti, S. M. and Ashuri, B. (2013). Forecasting engineering news-record construction cost index using multivariate time series models. *Journal of Construction Engineering and Management, 139*(9), 1237-1243. 10.1061/(ASCE)CO.1943-7862.0000689

Shahandashti, S. M. and Ashuri, B. (2016). Highway Construction Cost Forecasting Using Vector Error Correction Models. *Journal of Management in Engineering, 32*(2), 1-8. 10.1061/(ASCE)ME.1943-5479.0000404

Silva, I. N., Spatti, D., and Flauzino, R. (2016). *Redes Neurais Artificiais para Engenharia e Ciências Aplicadas: Curso Prático* (2nd edition). São Paulo, Brazil: Artliber.

Silva, M. A. O., Corrêa, L. R., and Ruas, A. X. A. (2018). Gerenciamento De Projetos Na Construção Civil: Tempo, Custo e Qualidade. *Construindo, 10*, 1-20. http://revista.fumec.br/index.php/construindo/article/view/5034

TCU. Tribunal de Contas da União (2018). *Relatório de Auditoria elaborado pelo Ministério da Economia*.

Tisaka, M. (2006). *Orcamento na construcão civil consultoria, projeto e execucão*. São Paulo, Brasil: Pini.

Ugur, L. (2017). A Neuro-Adaptive Learning (NAL) approach about costs of residential buildings. *Acta Physica Polonica A*, 132(3), 585-587. 10.12693/APhysPolA.132.585

Wanjari, S. P. and Dobariya, G. (2016). Identifying factors causing cost overrun of the construction projects in India. *Sadhana - Academy Proceedings in Engineering Sciences, 41*(6), 679-693. 10.1007/s12046-016-0498-3

Zanella, L. C. H. (2011).*Metodologia de Pesquisa* (2nd edition). Florianópolis: Departamento de Ciências da Administração. Universidade Federal de Santa Catarina / Sistema UAB.

Research Article / Case report / Civil Engineering https://doi.org/10.15446/ing.investig.v41n3.90430

# Characterization of High-Rise Reinforced Concrete Buildings Located in Antofagasta, Chile, by Means of Structural Indexes

## Caracterización de edificios altos de hormigón armado ubicados en la ciudad de Antofagasta, Chile, a través de índices estructurales

Juan Andrés Music Tomicic[1] and Felipe Ignacio Soto Ramírez[2]

**ABSTRACT**

This study aims to characterize a series of high-rise reinforced concrete wall buildings located in Antofagasta, Chile, by means of a set of structural indexes commonly used in professional activities in our country and recommended by researchers. To this effect, a total of eight buildings was analyzed, from which, based on their architectural plans and engineering drawings, a series of properties was determined, such as wall and floor area, among others. Additionally, a modal spectral analysis was carried out according to the current Chilean regulations (NCh 433Of.1996Mod.2009 and DS 61) by means of the ETABS software. Next, eleven structural indexes were selected and determined, which are related to stiffness, structural redundancy, and ductility, with the purpose of making a seismic qualification. The obtained values indexes provide information about the expected structural performance of the buildings under a major seismic event. Finally, correlations between the different indexes were established.

**Keywords:** structural indexes, seismic performance, NCh433Of.1996Mod.2009, DS 61 MINVU

**RESUMEN**

El presente estudio busca caracterizar un conjunto de edificios altos estructurados en base a muros de hormigón armado, ubicados en la ciudad de Antofagasta-Chile, mediante un conjunto de índices estructurales comúnmente usados en la práctica profesional en nuestro país y sugeridos por investigadores. Para esto, se analizaron ocho edificios en total, a los cuales, a partir de los planos de arquitectura y estructurales, se les determinó un conjunto de propiedades tales como el área de muros y pisos, entre otros. Además, se les realizó un análisis modal espectral según la normativa chilena vigente (NCh 433Of.1996Mod.2009 y DS 61) mediante el programa ETABS. A continuación, se seleccionaron y determinaron once índices estructurales relacionados con la rigidez, redundancia estructural y ductilidad, con el fin de realizar una calificación sísmica. Los valores obtenidos aportan información sobre el posible comportamiento estructural que podrían tener los edificios frente a un evento sísmico severo. Finalmente, se establecieron correlaciones entre los diferentes indicadores.

**Palabras clave:** índices estructurales, desempeño sísmico, NCh433Of.1996Mod.2009, DS 61 MINVU

**Received:** September 10th, 2020
**Accepted:** April 5th, 2021

## Introduction

Chile, located in South America, between the Pacific Ocean and Andes mountain range, has historically suffered the effects of the subductive movement of the Nazca Plate while interacting with the South American Plate, thus generating not only large earthquakes, but also destructive tsunamis.

The greatest earthquake ever recorded in Chile and the world occurred in Valdivia in 1960, with a moment magnitude (Mw) of 9,5. The latest major earthquake in Chile occurred in 2010 with a Mw = 8,8, which affected the south and central regions, which amounts to more than 40% of the population, including important cities such as Santiago, Viña del Mar, and Concepción. A total of four buildings (between 4 and 18 stories) collapsed, and 40 buildings were severely damaged. Due to this, several changes to the Chilean seismic code were proposed (Lagos *et al.*, 2012). The return period of major earthquakes in the territory has made the Chilean practice to assume that at least one big event will occur during the structure's lifetime.

In the northern region of the country, a large earthquake occurred in Antofagasta in July 30th, 1995, with a Mw = 8,0.

The real estate boom that started in 1995 and the high cost of the land in the city generated a significant growth in the construction of high-rise buildings. Nowadays, there are more than 150 buildings of 10 stories or more in Antofagasta.

In this study, eight reinforced concrete buildings were analyzed. Eleven structural indexes related to stiffness,

[1]Structural Civil Engineer, Universidad de Chile, Chile, Affiliation: Full Professor, Department of Civil Engineering, Universidad Católica del Norte, Antofagasta, Chile. E-mail: jmusic@ucn.cl
[2]Civil Engineer, Universidad Católica del Norte, Chile, Affliation: Proyect Engineer, Dimecpro Ingeniería SPA, Chlie E-mail: felipeisotor@gmail.com

**How to cite:** Music, J. and Soto, F. (2021). Characterization of High-Rise Reinforced Concrete Buildings Located in Antofagasta, Chile, by Means of Structural Indexes. *Ingeniería e Investigación*, *41*(3), e90430. 10.15446/ing.investig.v41n3.90430

structural redundancy, and ductility were determined. The purpose was to obtain a seismic qualification of the buildings in order to get information on the expected structural performance against major earthquakes.

## Structural indexes

After each earthquake that produces damage to the infrastructure of the country, the performance of its structures is analyzed with the purpose of taking actions for future events.

In Chile, experience in building performance under seismic events is vast. This performance has been correlated with structural indexes, establishing ranges of values that assure a good seismic behavior (Guendelman, T., Guendelman, M., and Lindenberg, 1997; Henoch, Lindenberg, Guendelman, T., and Guendelman, M., 2010; Lagos *et al.*, 2012; Guendelman, T., Medina, Guendelman, M., and Figueroa, 2017).

For this research, eleven structural indexes were selected. This sought to measure different parameters that affect the performance of a reinforced concrete building and allow performing seismic qualification.

These structural indexes can be classified into two groups: stiffness indexes and structural redundancy and ductility demand indexes.

### *Stiffness indexes*

*Building total height/period of first uncracked translational mode of vibration*

This index is related to the lateral stiffness of the building (Guendelman *et al.*, 1997).

To obtain this value, a modal spectral analysis is carried out to determine the different modes of vibration of the buildings.

This index is determined as follows:

$$\text{X} - \text{Direction} \rightarrow \frac{H}{T_x^*} \tag{1}$$

$$\text{Y} - \text{Direction} \rightarrow \frac{H}{T_y^*} \tag{2}$$

where $H$ is the total height of the building, and $T^*$ is the uncracked period of vibration with the largest mass participation in the direction of analysis.

*Height of the building above the ground level/period of first uncracked translational mode of vibration*

This index is also related to the lateral stiffness of the building (Guendelman *et al.*, 1997).

The use of the height-above-the-ground level instead of the total height of the building is due to the fact that it better represents the vibrational properties of the building.

This index is determined as follows:

$$\text{X} - \text{Direction} \rightarrow \frac{H_0}{T_x^*} \tag{3}$$

$$\text{Y} - \text{Direction} \rightarrow \frac{H_0}{T_y^*} \tag{4}$$

where $H_0$ is the total height of the building above the ground level, and $T^*$ is the uncracked period of vibration with the largest mass participation in the direction of analysis.

*Height of the building above ground level/period of first cracked translational mode of vibration*

This index is related to the residual lateral stiffness of the building after a large earthquake (Lagos *et al.*, 2012).

This index is determined as follows:

$$\text{X} - \text{Direction} \rightarrow \frac{H_0}{T_{ag_x}^*} \tag{5}$$

$$\text{Y} - \text{Direction} \rightarrow \frac{H_0}{T_{ag_y}^*} \tag{6}$$

where $H_0$ is the total height of the building above the ground level, and $T^*_{ag}$ is the cracked period of vibration with the largest mass participation in the direction of analysis.

According to the current Chilean seismic codes, the cracked period with the largest mass participation can be determined as 1,5 times the uncracked period of the mode with the largest mass participation.

*Performance index*

This index is related to the lateral stiffness of the building (Lagos *et al.*, 2012).

$$d_{\max} = 1000\frac{\delta_u}{H_o} \tag{7}$$

where $\delta_u$ is the lateral displacement at the top of the building, defined in DS 61 MINVU (2011), and $H_0$ is the total height of the building above the ground level.

*The lateral displacement at the top of the building is determined as follows:*

$$\delta_u = 1{,}3\ S_{de}\left(T_{ag}^*\right) \tag{8}$$

where $S_{de}$ is the elastic displacement response spectrum from DS 61 MINVU (2011).

*Maximum inter-story drift measured in the center of mass*

This index is related to the lateral stiffness of the building (Guendelman *et al.*, 1997).

$$\text{X} - \text{Direction} \rightarrow \max\begin{cases}\frac{1000(\delta_{k+1}-\delta_k)_{CMxx}}{h_{(k+1-k)}}\\ \frac{1000(\delta_{k+1}-\delta_k)_{CMxy}}{h_{(k+1-k)}}\end{cases} \tag{9}$$

$$\text{Y} - \text{Direction} \rightarrow \max\begin{cases}\frac{1000(\delta_{k+1}-\delta_k)_{CMyy}}{h_{(k+1-k)}}\\ \frac{1000(\delta_{k+1}-\delta_k)_{CMyx}}{h_{(k+1-k)}}\end{cases} \tag{10}$$

where $\delta_{k+1}$ is the lateral displacement in the center of mass of the story $k+1$, $\delta_k$ is the lateral displacement in the center of mass of the story $k$, and $h_{(k+1+k)}$ is the height between story $k+1$ and story $k$.

The Chilean seismic code limits this index to 2,0‰.

*Maximum inter-story drift measured in points located on the most unfavorable position*

This index is related to the torsional rigidity of the building (Guendelman *et al.*, 1997).

$$\text{X} - \text{Direction} \rightarrow \max\left\{\begin{array}{l}\frac{1000\left[(\delta_{(k+1)P}-\delta_{(k)P})_{xx}-(\delta_{(k+1)CM}-\delta_{(k)CM})_{xx}\right]}{h_{(k+1-k)}}\\ \frac{1000\left[(\delta_{(k+1)P}-\delta_{(k)P}-\delta_{(k+1)CM})_{xy}-(\delta_{(k)CM})_{xy}\right]}{h_{(k+1-k)}}\end{array}\right. \quad (11)$$

$$\text{Y} - \text{Direction} \rightarrow \max\left\{\begin{array}{l}\frac{1000\left[(\delta_{(k+1)P}-\delta_{(k)P})_{yy}-(\delta_{(k+1)CM}-\delta_{(k)CM})_{yy}\right]}{h_{(k+1-k)}}\\ \frac{1000\left[(\delta_{(k+1)P}-\delta_{(k)P}-\delta_{(k+1)CM})_{yx}-(\delta_{(k)CM})_{yx}\right]}{h_{(k+1-k)}}\end{array}\right. \quad (12)$$

where $\delta_{(k+1)P}$ is the lateral displacement of point $P$ of story $k+1$, $\delta_{(k)P}$ is the lateral displacement of point $P$ of story $k$, $\delta_{(k+1)CM}$ is the lateral displacement of center of mass of story $k+1$, $\delta_{(k)CM}$ is the lateral displacement of center of mass of story $k$, and $h_{(k+1+k)}$ is the height between stories $k+1$ and $k$.

### *Structural redundancy and ductility demand indexes*

*Total area of walls on the first floor/total area of first floor*

This index aims to monitor shear stress in the walls produced by seismic loads (Lagos *et al.*, 2012).

$$d_{1S} = \frac{A_w}{A_f} \quad (13)$$

where $A_w$ is the area of walls on the first floor in each direction of analysis, and $A_f$ is the total area of the first floor.

*Total area of walls on the first floor / Total seismic weight above first floor*

This index aims to monitor the level of compression load on the walls (Lagos *et al.*, 2012).

$$d_{2C} = \frac{A_w}{P_f} \quad (14)$$

where $A_w$ is the area of walls on the first floor in each direction of analysis, and $P_f$ is the total seismic weight above the first floor, defined by article 5.5.1 of NCh433. The Chilean standard limits the compression load on the wall to $0{,}35\ f'_C\ A_g$.

*Total area of walls on the first floor/cumulative plan area of the stories above first floor*

This index, similar to the previous one, aims to monitor the compression load on walls (Lagos *et al.*, 2012).

$$d_{3C} = \frac{A_w}{A_{cumulated}} \quad (15)$$

where $A_w$ is the area of walls on first floor in each direction of analysis, and $A_{cumulated}$ is the cumulative plan area of the stories above first floor.

*Effective spectral reduction factor*

This index is related to the ductility demand of the building (Lagos *et al.*, 2012).

$$R^{**} = \frac{Qe}{1{,}4\ Qd} \quad (16)$$

where $Q_e$ is the elastic seismic base shear determined using the elastic response spectrum, and $Q_d$ is the design's seismic base shear, determined by using the design spectrum as indicated in DS 61 MINVU (2011).

*Modified ductility displacement index*

To understand this index, it is necessary to define how ductility is calculated. By definition, ductility is the ultimate displacement divided by the yield displacement, as indicated below:

$$\mu^*_\Delta = \frac{\delta_u}{\delta_y} \quad (17)$$

The yield displacement is often unknown, since it is necessary to perform a static nonlinear analysis to determine it.

Therefore, a modified index for the displacement ductility ratio is calculated considering the yield displacement as 1,4 times the design's lateral displacement (Lagos *et al.*, 2012).

According to the above, the index is determined as follows:

$$\mu^*_\Delta = \frac{\delta_u}{1{,}4\ \delta_d} \quad (18)$$

where $\delta_u$ is the design's lateral displacement on the top of the building as defined in DS 61 MINVU (2011), and $\delta_d$ is the design's lateral displacement on the top of the building, determined with the elastic design response spectrum reduced by factor $R^{**}$, *i.e.*, $S_{ae}/R^{**}$.

## Ranges of selected structural indexes

The range adopted for each index is shown in Table 1 (Lagos *et al.*, 2012; Guendelman *et al.*, 2017).

## Selected buildings and seismic analysis

### *Selected buildings*

In this study, eight reinforced concrete buildings were analyzed with the selected indexes. Photos and typical plan views of the buildings are shown in Figures 1 and 2.

## Modelling

The analyzed buildings are high-rise reinforced concrete buildings. Their structural system consists of reinforced concrete shear walls in both directions and reinforced concrete slabs in all levels.

**Table 1.** Range of structural indexes

| Structural Index | Normal Range | Out of range but acceptable | Out of range |
|---|---|---|---|
| Building total height/period of first uncracked translational mode of vibration | 40 - 80 [m/s] | 20 - 40 [m/s]<br>80 - 150 [m/s] | < 20 [m/s]<br>> 150 [m/s] |
| Height of the building above the ground level/period of first uncracked translational mode of vibration | 32 - 64 [m/s] | 16 - 32 [m/s]<br>64 - 120[m/s] | < 16 [m/s] > 120 [m/s] |
| Height of the building above ground level/period of first cracked translational mode of vibration | 21 - 43 [m/s] | 11 - 21 [m/s]<br>43 - 80 [m/s] | < 11 [m/s] > 80 [m/s] |
| Performance index | ≤ 10 | 10 - 15 | > 15 |
| Maximum inter-story drift measured in the CM | ≤ 2,0 | | > 2,0 |
| Maximum inter-story drift measured on points located on the most unfavorable position | ≤ 1,0 | | > 1,0 |
| Total area of walls on the first floor/total area of first floor | ≥ 2% | | < 2% |
| Total area of walls on the first floor/total seismic weight above first floor | 0,001 - 0,002 [$m^2$/ton] | | < 0,001 [$m^2$/ton] > 0,002 [$m^2$/ton] |
| Total area of walls on the first floor/cumulative plan area of the stories above first floor | ≥ 0,1% | | < 0,1% |
| Effective spectral reduction factor | ≤ 4 | 4 - 6 Pushover analysis | > 6 Dynamic non-linear analysis |
| Modified ductility displacement index | Still undefined by the authors of the indexes | | |

**Source:** Lagos *et al.* (2012); Guendelman *et al.* (2017).


**Figure 1.** Photos of the buildings, fundamental period, and design lateral displacement at the roof in each direction.
**Source:** Authors

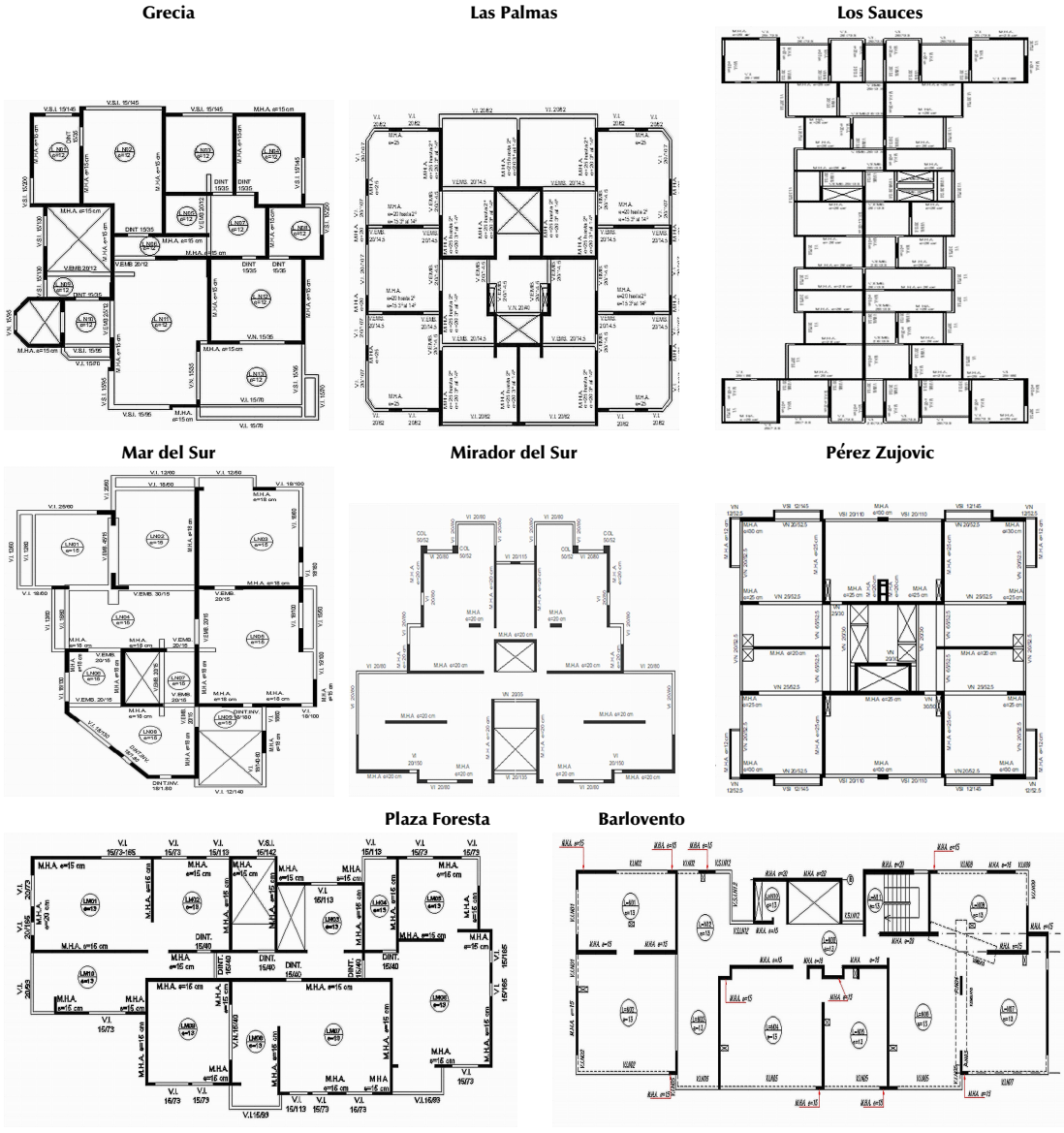


**Figure 2.** Typical plan view of buildings.
**Source:** Authors

**Table 2.** Seismic analysis of the buildings

| Building | Stories | Number of modes to obtain 90% of the total mass | $T_x^*$ [seg] | Mass participation in X-Direction [%] | $T_y^*$ [seg] | Mass participation in Y-Direction [%] | Type of Soil |
|---|---|---|---|---|---|---|---|
| **Grecia** | 12 + 1 | 20 | 0,507 | 56,2 | 0,407 | 61,7 | Type A |
| **Las Palmas** | 14 + 1 | 9 | 0,484 | 47,1 | 0,535 | 70,2 | Type A |
| **Los Sauces** | 15 + 0 | 9 | 0,356 | 70,8 | 0,443 | 34,1 | Type A |
| **Mar del Sur** | 13 + 0 | 12 | 0,715 | 61,0 | 0,466 | 66,3 | Type A |
| **Mirador del Sur** | 15 + 1 | 9 | 0,539 | 36,8 | 0,769 | 68,6 | Type A |
| **Pérez Zujovic** | 27 + 1 | 22 | 1,151 | 61,1 | 1,632 | 61,8 | Type B |
| **Plaza Foresta** | 17 + 1 | 13 | 0,476 | 36,4 | 0,753 | 63,2 | Type A |
| **Barlovento** | 15 + 1 | 17 | 0,377 | 31,6 | 0,754 | 49,5 | Type A |

**Source:** Authors

**Table 3.** Results for the structural indexes

| Structural Index | $H/T^*$ [m/s] | | $H_0/T^*$ [m/s] | | $H_0/T^*_{ag}$ [m/s] | | 1000 $\delta_u/H_0$ | | 1000 $\Delta_{CM}$ | | 1000 $\Delta_P$ | | $d_{1S}$ [%] | | $d_{2C}$ [m²/ton] | | $d_{3C}$ [%] | | $R^{**}$ | | $\mu^*_\Delta$ [%] | |
|---|---|---|---|---|---|---|---|---|---|---|---|---|---|---|---|---|---|---|---|---|---|---|
| **Building** | X-Dir. | Y-Dir. | X-Dir | Y-Dir. | X-Dir | Y-Dir. | X-Dir | Y-Dir. | X-Dir | Y-Dir. | X-Dir | Y-Dir. | X-Dir | Y-Dir. | X-Dir | Y-Dir. | X-Dir | Y-Dir. | X-Dir | Y-Dir. | X-Dir | Y-Dir. |
| **Grecia** | 66,5 | 82,8 | 59,9 | 74,9 | 39,9 | 49,7 | 2,54 | 1,96 | 0,269 | 0,174 | 0,133 | 0,029 | 2,16 | 3,90 | 0,002 | 0,004 | 0,19 | 0,35 | 3,30 | 4,13 | 3,2 | 4,1 |
| **Las Palmas** | 79,7 | 72,1 | 72,9 | 65,9 | 48,6 | 44,0 | 2,07 | 2,33 | 0,201 | 0,242 | 0,045 | 0,058 | 2,16 | 3,31 | 0,002 | 0,003 | 0,17 | 0,25 | 4,11 | 3,92 | 5,2 | 4,9 |
| **Los Sauces** | 106,3 | 85,4 | 106,3 | 85,4 | 70,9 | 57,0 | 1,32 | 1,74 | 0,101 | 0,162 | 0,028 | 0,046 | 2,81 | 3,66 | 0,002 | 0,003 | 0,2 | 0,26 | 5,24 | 4,13 | 7,0 | 5,3 |
| **Mar del Sur** | 46,4 | 71,2 | 44,3 | 68,0 | 31,0 | 47,5 | 3,51 | 2,10 | 0,417 | 0,197 | 0,253 | 0,052 | 2,25 | 4,12 | 0,002 | 0,004 | 0,18 | 0,34 | 2,84 | 4,06 | 4,2 | 4,6 |
| **Mirador del Sur** | 76,8 | 53,8 | 69,6 | 48,8 | 46,4 | 32,5 | 2,21 | 3,40 | 0,285 | 0,397 | 0,487 | 0,119 | 2,54 | 2,64 | 0,002 | 0,002 | 0,18 | 0,19 | 2,53 | 2,90 | 3,3 | 4,0 |
| **Pérez Zujovic** | 64,7 | 45,6 | 54,2 | 38,2 | 36,2 | 25,5 | 4,45 | 5,49 | 0,554 | 0,844 | 0,072 | 0,218 | 3,43 | 3,08 | 0,001 | 0,001 | 0,19 | 0,11 | 2,50 | 1,86 | 4,2 | 3,3 |
| **Plaza Foresta** | 98,5 | 62,2 | 91,8 | 57,9 | 61,2 | 38,7 | 1,64 | 2,84 | 0,175 | 0,691 | 0,233 | 0,350 | 2,06 | 2,38 | 0,002 | 0,003 | 0,2 | 0,23 | 3,32 | 2,70 | 5,3 | 3,1 |
| **Barlovento** | 109,9 | 54,9 | 101,9 | 51,0 | 67,9 | 34,0 | 1,42 | 3,23 | 0,354 | 0,585 | 0,458 | 0,317 | 2,84 | 1,73 | 0,006 | 0,004 | 0,58 | 0,36 | 2,68 | 2,53 | 3,1 | 3,0 |

Normal Range | Acceptable but out of range | Out of Range

**Source:** Authors

Buildings were modelled using the ETABS software. Shear walls were modelled as shell elements; beams and columns as frame elements without rigid offsets; and slabs as shell elements. All members were rigidly connected, as their ends and walls were fixed at the base. The properties of the elements are based on their gross dimensions. On each level, a rigid diaphragm was considered with 3 degrees of freedom per joint (two translations and one rotation).

The model of each building includes the underground levels, but not soil-structure interaction was considered.

### *Seismic analysis*

A linear elastic modal spectral analysis was carried out in ETABS according to the provisions of the Chilean seismic codes (NCh433Of96.Mod.2009 and DS61 MINVU 2011). The seismic mass considered included all dead loads plus 25% of live loads.

Table 2 shows the uncracked periods of vibration and the corresponding associated mass participation in each direction of analysis.

## Results

Tables 3 and 4 show the results of the structural indexes for each selected building, classified according to the ranges as normal, acceptable but out of range, and out of range.

**Table 4.** Number of indexes in each range

| Building | Normal Range | | | Acceptable but out of range | | | Out of Range | | |
|---|---|---|---|---|---|---|---|---|---|
| | X-Dir. | Y-Dir. | Total | X-Dir. | Y-Dir. | Total | X-Dir. | Y-Dir. | Total |
| **Pérez Zujovic** | 10 | 10 | 20 | 0 | 0 | 0 | 0 | 0 | 0 |
| **Mirador del Sur** | 7 | 9 | 16 | 3 | 1 | 4 | 0 | 0 | 0 |
| **Mar del Sur** | 11 | 5 | 16 | 0 | 3 | 3 | 0 | 1 | 1 |
| **Plaza Foresta** | 6 | 9 | 15 | 3 | 0 | 3 | 1 | 1 | 2 |
| **Grecia** | 9 | 5 | 14 | 1 | 4 | 5 | 0 | 1 | 1 |
| **Barlovento** | 7 | 7 | 14 | 3 | 0 | 3 | 1 | 2 | 3 |
| **Las Palmas** | 7 | 7 | 14 | 3 | 2 | 5 | 0 | 1 | 1 |
| **Los Sauces** | 5 | 5 | 10 | 4 | 4 | 8 | 1 | 1 | 2 |

**Source:** Authors

### *Correlations between structural indexes*

In this part of the study, an analysis is carried out to find correlations between structural indexes for the set of buildings. This analysis was performed only for those buildings funded on bedrock, so the Pérez Zujovic building was not considered.

In order to consider correlations between indexes as valid, the correlation coefficient should be equal to or greater than 0,8 for a positive slope and -0,8 in the case of negative slope.

Table 5 shows the analyzed variables, the correlation coefficients, and the equations found.

**Table 5.** Correlations between structural indexes

| Correlation | Correlation coefficient | Equation |
|---|---|---|
| $d_{max} - H_0/T^*$ | −0,847 | $1000(\delta_u/H_0) = 0{,}001(H_0/T^*)^2 - 0{,}2(H_0/T^*) + 10{,}9$ |
| $R^{**} - T^*$ | −0,658 | $R^{**} = -3{,}7\ T^* + 5{,}46$ |
| $R^{**} - H_0/T^*$ | 0,652 | $R^{**} = -0{,}0005(H_0/T^*)^2 + 0{,}11(H_0/T^*) - 1{,}35$ |
| $R^{**} - H_0/T^*_{ag}$ | 0,439 | $R^{**} = -0{,}0005(H_0/T^*_{ag})^2 + 0{,}11(H_0/T^*_{ag}) - 1{,}35$ |
| $\mu^*_\Delta - T^*$ | −0,499 | $\mu^*_\Delta = 8{,}03\ T^{*2} - 13{,}3\ T^* + 8{,}98$ |
| $\mu^*_\Delta - R^{**}$ | 0,768 | $\mu^*_\Delta = 0{,}35\ R^{**2} - 1{,}47\ R^{**} + 5{,}073$ |

**Source:** Authors

## Conclusions

In this study, a total of eleven structural indexes were determined for eight reinforced concrete buildings located in Antofagasta, Chile, to determine their seismic qualification. The conclusions of this study are:

All analyzed building complied with the restrictions of the lateral seismic displacement stated in the actual Chilean seismic code.

Six out of eight buildings have the density of walls in compression index out of range. This implies that the walls of the first floor of these buildings might be subjected to high compression stresses. Since 2011, Chilean regulations limit the compression stress on walls on all floors to 0,35 $f'_c\ A_g$. Both Mirador del Sur and Pérez Zujovic are the only buildings with that index in the normal range.

The structural response index ($H_0/T^*$) has a good relationship with the performance target index, defined as $\delta_u/H_o$, according to SEAOC VISION 2000 (1995). In buildings with a $H_0/T^*$ greater than 75 m/s, a value lower than 0,002 for $\delta_u/H_o$ was obtained. Previous studies indicate that, in this case, an elastic overall seismic response is expected for the building supported on bedrock. However, in terms of individual elements, an inelastic behavior may occur.

In four of the buildings, the values of $R^{**}$ are in the range of 4-6. According with the Chilean experience, it is necessary to perform an analysis according to the demand-capacity procedure, where the demand is determined by using the elastic acceleration response spectrum defined in the current Chilean seismic code. To do so, the Capacity Spectral Method (CEM) may be used, which requires a static nonlinear analysis (pushover).

From the correlation study between structural indexes for all buildings on ground type A (bedrock with $V_{s30} \geq 900$ m/s$^2$), the best result is for the correlation between $d_{\max}$ and $H_0/T^*$.

## References


Calderón, J. (2007). *Actualización de tipologías estructurales usadas en edificios de hormigón armado en Chile* [Undergraduate Thesis, Universidad de Chile]. http://repositorio.uchile.cl/handle/2250/104697

Cornejo, F. and Music, J. (2011). Comparación de resultados del perfil bio-sísmico aplicando las disposiciones de NCh 433Of.96Mod.2009, Decreto 117 y Decreto 61 a edificios de Antofagasta. *Revista de Ingeniería Innova, 2,* 83-98.

DS No. 61 MINVU. (2011). Reglamento que fija el diseño sísmico de edificios y deroga Decreto No. 11, de 2010 (in Spanish), Ministerio de Vivienda y Urbanismo. Diario oficial 13 de diciembre del 2011. https://www.bcn.cl/leychile/navegar?idNorma=1034101

Guendelman, T., Guendelman, M., and Lindenberg, J. (1997). *Perfil Bío-Sísmico de Edificios* [Conference presentation], Séptima Jornada Chilenas de Sismología e Ingeniería Antisísmica, La Serena, Chile.

Guendelman, T., Medina, F., Guendelman, M., and Figueroa, L. (2017). Perfil Bío-Sísmico 3.0. *Anales del Instituto de Ingenieros de Chile, Revista Chilena de Ingeniería, 129*(3), 75-84.

Henoch, R., Lindenberg, J., Guendelman, T., and Guendelman, M. (2010). *Perfil Bío-Sísmico de Rascacielos* [Conference presentation], Décimo Congreso Chileno de Sismología e Ingeniería Sísmica, Santiago, Chile.

Lagos, R., Kupfer, M., Lindenberg, J., Bonelli, P., Saragoni, R., Guendelman, T., Massone, L., Boroschek, R., and Yañez, F. (2012). Seismic Performance of High-rise Concrete Buildings in Chile. *International Journal of High-Rise Buildings, 1*(3), 181-194.

López, C. and Music, J. (2016). Análisis del período y desplazamiento de edificios de hormigón armado considerando distintos grados de rigidez en sus elementos resistentes. *Revista Obras y Proyectos 19*, 33-47. https://scielo.conicyt.cl/pdf/oyp/n19/art03.pdf

Official Chilean Standard (2010) NCh 433.Of96 Modifcada 2009, Earthquake Resistant Design of Building (in English), Instituto Nacional de Normalización, INN.

Ríos, H. (2006). *Perfil Bío-Sísmico de Edificios representativos de la construcción en altura de la ciudad de Antofagasta* [Undergraduate Thesis, Universidad Católica del Norte].

Structural Engineers Association of California (SEAOC) (1995). Performance Based Seismic Engineering of Building VISION 2000.

Soto, F. (2020). *Características y determinación de índices estructurales en edificios altos de hormigón armado ubicados en la ciudad de Antofagasta* [Undergraduate Thesis, Universidad Católica del Norte].

Research Article / Short Article / Electrical, Electronic, and Telecommunications Engineering

https://doi.org/10.15446/ing.investig.v41n3.85377

# Current Innovation Sources Driving The Spanish Electric Power Sector

## Principales fuentes de innovación que están impulsando el sector de energía eléctrica en España en la actualidad

Pablo de Mergelina[1] and Isaac Lemus-Aguilar[2]

**ABSTRACT**

Renewable energy is not simply the cornerstone of a transition, but an entire electric power revolution. However, which are the technologies with which power companies are going to redesign the electricity industry? Interviews were conducted with innovation managers of the biggest power companies in Spain to shed some light on the innovation sources upon which the electric power system of the future is based. The results revealed that renewable electricity represents a complete paradigm shift. Until now, the system's net electricity balance has been achieved by adjusting power generation to its demand. However, in a renewable system, electricity generation is limited by and depends on environmental resources, so it cannot be sufficiently controlled to meet the demand at all times. Therefore, it is the electricity consumption that must be adjusted to generation. It was concluded that there are currently nine innovation sources that are redesigning the industry: renewable energy, energy storage systems, electric vehicles, Industry 4.0, smart grids, blockchain, distributed and self-consumption generation, smart client, and demand side response. Moreover, it was found that system regulations established by governments, business sustainability plans, and open innovation by startups play key roles in the development of innovation.

**Keywords:** innovation, electric power, Spain, innovation sources

**RESUMEN**

Las energías renovables no son simplemente la piedra angular de una transición, sino de toda una revolución eléctrica. Sin embargo, ¿cuáles son las tecnologías con las que las compañías eléctricas van a rediseñar la industria eléctrica? Se realizaron entrevistas a los responsables de innovación de las principales compañías eléctricas en España con el objetivo de arrojar luz sobre las fuentes de innovación en las que se basa el sistema eléctrico del futuro. Los resultados revelaron que las energías renovables suponen un cambio completo de paradigma. Hasta ahora, el balance de energía neto del sistema se alcanza ajustando la generación de energía a la demanda. Sin embargo, en un sistema renovable, la generación de electricidad está limitada por y depende de los recursos medio ambientales, por lo que no se puede controlar lo suficiente para satisfacer la demanda en todo momento. Por lo tanto, es el consumo de energía el que se debe ajustar a la generación. Se concluyó que actualmente existen nueve líneas de innovación que están rediseñando la industria: las energías renovables, los sistemas de almacenamiento de energía, el vehículo eléctrico, la Industria 4.0, las redes inteligentes, el *blockchain*, la generación distribuida y autoconsumo, el *smart client* y el control de la demanda. Asimismo, la regulación del sistema establecida por los gobiernos, los planes de sostenibilidad de las empresas y la innovación abierta protagonizada por las *startups* tienen un papel fundamental en el desarrollo de la innovación.

**Palabras clave:** innovación, energía eléctrica, España, fuentes de innovación

**Received:** February 27th, 2021
**Accepted:** April 6th, 2021

## Introduction

The development of technology, industrial advancements, new methodologies, and other discoveries evolve exponentially throughout the world, including the electric power sector. The political engine (such as the SDG 2030) is crucial for the development of renewable energies, but it is not the only factor. Countries that promote and drive different factors have a more successful development pace, thus becoming a fundamental part for the development of each technology to generate a set of appropriate drivers such as tax incentives or greater regulatory flexibility, among many others (Darmani, Arvidsson, Hidalgo, and Albors, 2014). The transition to renewable energy depends on governments, citizens, and industries: "businesses can't thrive unless the planet and society do so as well. The opposite is also true – we can't build a prosperous future without the resources and innovation that

[1] Industrial Engineer, Universidad Politécnica de Madrid, and M.Sc. in Productivity and Personal Development, Universidad de Alcalá. Affiliation: Researcher, Universidad Politécnica de Madrid. E-mail: p.demergelina@alumnos.upm.es
[2] Ph.D. in Management and Economics, Politecnico di Milano, and Ph.D. in Industrial Engineering, Universidad Politécnica de Madrid. Affiliation: Assistant Professor and IMIM Program Coordinator, Universidad Politécnica de Madrid and Lecturer, University of Sussex Business School, Science Policy Research Unit.
E-mail: isaac.lemus@upm.es, i.lemus-aguilar@sussex.ac.uk

**How to cite:** de Mergelina, P. and Lemus-Aguilar, I. (2021). Current Innovation Sources Driving The Spanish Electric Power Sector. *Ingeniería e Investigación*, *41*(3), e85377. 10.15446/ing.investig.v41n3.85377

businesses provide" (Winston, 2014). Companies are one form of important change leadership towards a more efficient and sustainable social model. As for the future of the electric power industry, it is within companies, and particularly in their business models, where the real power for change lies.

Additionally, one should bear in mind that more developments can be achieved by innovating the different parts of the business than just by innovating energy sources. Moreover, "business model innovation may achieve what technological and product innovation have long failed to deliver" (Girotra and Netessine, 2011, p. 7). Therefore, because of the importance of business models, the objective of this research is to identify the main sources of innovation for electric power companies, given that business models and interests are crucial for understanding innovation and energy transitions.

## *Theoretical framework*

To this effect, it is vital to recall the concept of business model, in order to know the particularities of Spanish electricity regulations and to be aware of the current innovation sources in the sector. In this way, we can investigate which sources of innovation will be used by the Spanish electricity sector to innovate its business models within the current regulations.

In one of its simplest definitions, "business models are stories that explain how an enterprise works" (Magretta, 2002, p. 1). A business model is the set of main activities, key decisions, and hypotheses that are dependent on each other and theoretically determine the functioning of a company, as well as its behavior in environment matters. Therefore, a business model is an essential instrument to manage a company. Innovation in business models refers to changes in these decisions: what is offered, when are decisions be made, by whom, and why (Girotta and Netessine, 2014). Innovation in business models encompasses the redesign of any part that determines the operation of the company with a clear objective: to gain a competitive edge. If a business model is the stories that tell how a company works, innovation is to rewrite any of those stories.

The legislation of the Spanish electricity grid constitutes an electric power system composed of six agents (Figure 1):

1. electricity producers (left),
2. distributors (3),
3. retailers (right),
4. system operators (1, 2),
5. market operators (4, 5),
6. and industry supervisors (6).

The last three agents are public designation bodies. In Spain, the electricity sector is mostly integrated –approximately 80%– by five major companies: *Endesa*, *Iberdrola*, *Naturgy*, *EDP* and *Viesgo*. They have established an oligopolistic system.

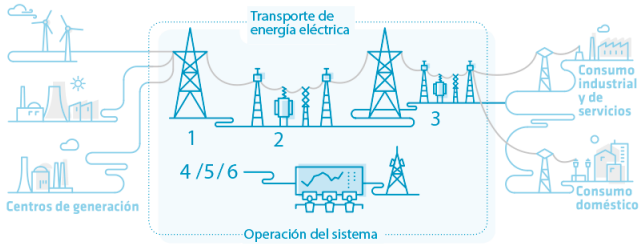


**Figure 1.** Electrical system Scheme.
**Source:** Red Eléctrica de España (n.d.).

The first three agents amount to 65% of the market share (Consejo Económico y Social, 2018).

During a review of the current literature regarding the opportunities presented by the electricity sector, the following innovation sources were identified: renewable energies, energy storage systems, big data and Internet of Things, self-sufficiency and mini grids, electric vehicle, customer as generator, and blockchain.

According to Ritcher (2013), most authors consider renewable energies as a disruptive technology that will significantly change the industry of electricity. The main drawback of renewable energies is the dependence and uncertainty of generation, which results in the need for additional grid flexibility.

New battery and energy storage technologies not only grant part of that flexibility, but also enable the consumer to store their own energy (de Roca, 2018). As stated by Engelken, Römer, Drescher, and Welpe, "load management and storage are other opportunities repeatedly mentioned in the renewable energy sector" (2015, p. 804). Energy decentralization can be considered as one of the most promising sources of innovation in the electricity industry, enabling ideas such as "prosumers, self-supply or even partial energy autarky" (Engelken, *et al.*, 2015, p. 804).

Likewise, smart grid solutions that provide greater flexibility by controlling demand response offer another wide range of business opportunities (Lee, Kao, and Yang, 2014; Loebbecke and Picot, 2015; Engelken, *et al.*, 2015). Smart grids are, in their simplest definition, the complete control of the network regarding both information and operation. They are essentially based on two technologies: Big Data and Internet of Things (Loebbecke and Picot, 2015). This gives way to the participation of customers as generators. This dual nature of the customer is clearly seen in the vehicle to grid (V2G) idea. Electric car batteries present the opportunity to serve as short-term storage to stabilize the grid. (Engelken, *et al.*, 2015). According to Cotteleer and Sniderman (2017), the Fourth Industrial Revolution, also known as Industry 4.0 (which includes virtual reality, augmented reality, artificial intelligence or the Internet of Things, among others), is changing the way businesses operate.

Finally, Preukschat (2017) explains that blockchain is an infrastructure that allows you to build on top of the internet

and create another layer on top of which people are going to be able to exchange value with each other. Therefore, blockchain will affect how electricity is tracked and exchanged in the electricity sector (Vega and López-Bueno, 2017).

## Methodology

Initially, a survey was chosen as the ideal methodology for data collection, and a questionnaire was designed. The surveys were to be sent to the innovation departments of the leading companies in the sector. Nevertheless, this methodology could not guarantee the validity, reliability, comprehensiveness, accuracy, integrity, and timeliness of the data, nor did it ensure a minimum response rate. Moreover, surveys have the added drawback that they might condition participants' responses. For this reason, considering that the study aims to seek out new sources of innovation, the questions of this exploratory study needed to be open-ended, and the structure of the interview had to be flexible to small order changes, that is, to the omission of certain questions or inclusion of others. Therefore, a semi-structured interview stood out as the optimal data collection methodology (Saunders, Lewis, and Thornhill, 2009).

This research gathered data on electricity innovation sources by interviewing representatives from Spanish electricity companies, which are called 'interviews with experts' in the literature.

On one hand, the best sources of information are guaranteed. The objects of this research are the sources and paths of innovation in the electricity sector, and these innovations are exactly those that are developed and implemented by the companies. Then, there could be no better source of information than those managers of innovation in the companies themselves; they are the ones who identify, analyze, and decide which innovations to develop. Moreover, in Spain, the leading companies are the ones that invest the most in R&D, the ones with the greatest impact on the sector with their novelties, and the ones that know the most about innovation paths, not only through their own research but also by offering themselves as incubators for startups. On the other hand, it must be acknowledged that this methodology has its limitations, mainly in the generalizability of the data.

To achieve validity, the following minimum requirements were established: data was collected from three out of the top five electricity companies about power capacity, power annually generation, clients, and sales in Spain. These three companies represent 60% of the electricity sector, if it is assumed that all five companies have the same weight within the oligopoly.

All of the three interviewed companies performed generation, distribution, and retail activities in the electric sector. The participants interviewed are the heads of the innovation departments of their respective companies (Table 1). The interviews were conducted face-to-face during the second quarter of 2019 and lasted one hour on average.

**Table 1.** Companies interviewed and position of innovation experts

| | Company 1 | Company 2 | Company 3 |
|---|---|---|---|
| **Activities** | Generation, distribution, and retail | Generation, distribution, and retail | Generation, distribution, and retail |
| **Expert position** | Head of Idea Hub | Member of innovation startup program | InnovaHub Leader |
| **Number of employees** | > 6 000 | > 6 000 | > 6 000 |
| **Number of customers** | 3-12 m | 3-12 m | 3-12 m |
| **Generation capacity** | > 15 m GW | > 15 m GW | > 15 m GW |
| **EBITDA** | 2-5 billion euros | 2-5 billion euros | 2-5 billion euros |

**Source:** Authors

## Results

All innovation sources found on interviews are discussed hereunder. Table 2 shows innovation sources by company.

**Table 2.** Interview results about main innovation sources for Spanish major energy power companies at present

| | Interview A | Interview B | Interview C |
|---|---|---|---|
| **Renewable energies** | X | X | X |
| **Energy storage systems** | X | X | |
| **Electric vehicle** | X | X | X |
| **Industry 4.0** | X | X | X |
| **Smart grids** | | X | |
| **Distributed generation and self-consumption** | | X | X |
| **Demand side response** | | X | |
| **Blockchain** | X | | X |

**Source:** Authors

Renewable energy has been the trigger for the entire energy industry revolution, and renewable energies are at the heart of it, responding to the prevailing need for energy autarky, unlimited resources, and sustainable generation. Renewable sources, such as photovoltaic panels or micro-hydro power plants, make the idea of self-sufficiency a reality both at the particular and community levels, thus constituting mini-grids, and they invite a virtual disconnection from the network. However, this has a substantial limitation: electricity production cannot be controlled. Dependence on natural resources requires a dispersed, geographically distributed generation infrastructure, as well as weather forecasting activities to estimate electricity production. This prediction of electricity supply becomes a primary task when generation cannot be controlled to establish the net electricity balance. Big data is the technology that makes this possible. Large data analysis not only allows for a prediction of power generation, but also of consumption, and this demand prediction is a key activity. In short, renewable energy does not have sufficient flexibility, and it is necessary to estimate supply and demand.

At this point, energy storage manifests itself as a solution to the limitation of renewable generation. Next-generation batteries or new energy storage systems give the system the ability to store electricity in overproduction cycles and to supply energy stored in cycles in which the generation is not sufficient to meet demand. Also, next-generation batteries drive the development and implementation of the electric vehicle. Sustainable mobility has an immense social electrification potential since it is one of the customer's assets of the future (smart client).

Blockchain is an open, distributed, immutable ledger that can record transactions between two parties efficiently and in a verifiable and permanent way. It also facilitates the process of tracking assets in a network. An asset can be tangible or intangible. Virtually anything of value can be tracked and traded within a blockchain network (Iansiti and Lakhani, 2017). Regarding the renewable origin of electricity, certificates of origin (CoO) are a decisive resource for retailers. Although certificates such as guarantees of origin or green certificates already exist, new certificates of origin are being developed from blockchain.

Industry 4.0 constitutes telecommunications technologies, virtual reality, augmented reality, artificial intelligence, the Internet of Things, drones, satellites, and big data. Industry 4.0 is the first source of innovation in automating activities and optimizing processes. Drones and satellite imaging, alongside artificial intelligence, facilitate the automation of processes, essentially those related to asset and infrastructure maintenance. The Internet of Things defines a digital and intelligent client, and new digital products reveal a virtually unlimited data source. Analyzing this data using big data provides a deeper understanding of the customer and business model, yielding information that aids decision-making. Grid monitoring with digital assets results in smart grids.

Smart grids, in their simplest definition, enable complete technical control of the electricity network. Besides, network sensing and continuous analysis of the status of distribution assets allows for predictive maintenance of infrastructures. Complete technical control of the distribution network opens doors to a multipoint customer conception, that is, to the customer's ability to consume electricity from different points and be identified as the same customer. This multipoint client nature can be applied even in the opposite direction, in other words, that the same client can act as a generator from different points on the grid. Additionally, complete network control is an indispensable aspect for distributed generation and mini-grids. On the other hand, smart grids allow virtual disconnection, understanding this as decoupling from the network temporarily, as long as it is beneficial to the system or the mini-grid. On the other hand, smart grids are unfailing to demand side response because demand cannot be controlled without controlling consumer access to the grid.

Similarly, if smart grids are the complete technical control of the network, blockchain is conceived as its complete economic control. Blockchain enables economic transactions in a decentralized manner between individuals, as well as guaranteeing their security and reliability. Moreover, total economic control of the grid enables the multipoint nature of the smart client in monetary terms, the virtual disconnection of distributed generation, and the demand side response.

The decentralization of electricity generation is both an opportunity and a direct consequence of renewable energy. Distributed generation or mini-grids consist of smaller and more concentrated systems of electricity generation, distribution, and consumption. When this dimension is reduced to the maximum, self-sufficiency is reached at an individual level. Self-consumption and self-sufficiency products provide power generation capacity to customers, which results in customers behaving as power generators for the system.

Up to this point, the future electricity customer has been defined as an intelligent customer, a fully digitized, large electricity consumer of multipoint nature and generating capacity. This is the definition of smart client.

Strictly speaking, the demand side response is not a source of innovation but the natural response to flexibility required by renewable generation. Renewable energy is a game changer when it comes to establishing the inescapable balance of net electricity. Until now, power generation has been adapted to consumption; but, from now on, it is electricity consumption that must be adapted to a renewable generation that cannot be controlled. Therefore, the prediction of market supply and demand with big data analysis, as well as absolute control of the network thanks to smart grids and blockchain, becomes the cornerstone to control electricity demand. Thus, the concept of smart client proposes new business models to control electricity consumption. An example of these are aggregators. The separate consumption of particular loads has no significant effect on demand. However, aggregators are business models that consist of grouping a large number of loads, so that controlling all of them as a set is relevant to controlling demand. Furthermore, if aggregators were not only able to direct the consumption of loads but could group and orchestrate the batteries of the electrical system, such as electric cars batteries with the technology Vehicle to Grid (V2G), the problem of flexibility in renewable electricity could be solved.

All these current innovation sources driving the Spanish electric power sector are depicted in Figure 2. Each of these technologies are lines of innovation in themselves for electricity companies in Spain and are potential sources for originating new business models. However, each of them is also a source of innovation that helps solve the challenges and limitations of the others. These relationships and sources of innovation are made clear with outgoing arrows that end at their receivers.

### *Agents, opportunities, and barriers*

This study reveals what are the main agents of the electric revolution in Spain. If governments, citizens, and businesses are the three fundamental pillars of the transition to renewable energy (Winston, 2014), they materialize in the regulation of the system, companies' sustainability policies, and open innovation.

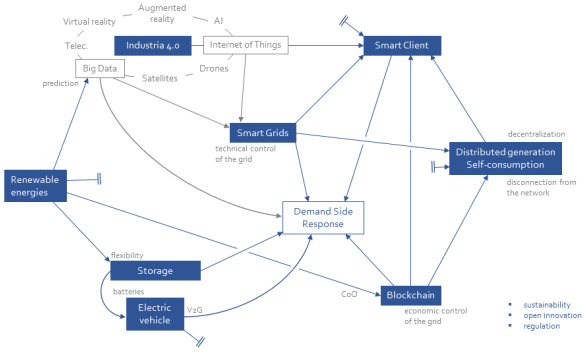


**Figure 2.** Main innovation sources for Spanish major energy power companies at present.
**Source:** Authors

Inasmuch as no company wants to develop new products or processes in an uncertain and unregulated policy framework that may subsequently prohibit or jeopardize the advances made, stable legislation is essential to enable and drive innovation in the sector. In this way, legislation, especially the lack of regulation, acts as a barrier to each of these lines of innovation. Governments and regulatory agencies hold the key to spur companies to research, develop, and implement innovation. For instance, companies in Spain do not venture to use unattended drones on a large scale to inspect the condition of high and medium voltage power lines because no legal framework has yet been defined to regulate unattended drone flights.

Renewable brand value is one of the increasingly relevant intangible resources, where power companies find new opportunities and strategies such as certifying the renewable origin of electricity. The rise of renewable energy, its dissemination in society, and the growing concern of citizens about the environment is the impetus of all companies to take sustainable measures. Sustainability plans are deployed as a corporate strategy to increase and reinforce brand value. Power Purchase Agreements (PPAs) with big brands are a clear example of this.

Finally, the conception of open innovation is at the heart of the entire industry's technological development. Large power companies find in startups the opportunity to innovate. Innovation managers explain how larger power companies are not agile enough to develop innovation sources. However, they can welcome, finance, and accelerate the ideas that arise from startups, universities, or innovation centers, thus resulting in innovations accessible to the entire market. Open innovation has been found to be a joint technological development of the entire industry.

## Conclusions

This study concludes that the main innovation sources for power companies in Spain are renewable energy, energy storage systems, electric vehicles, Industry 4.0, smart grids, blockchain, distributed generation and self-consumption, smart clients, and demand side response.

The main agents driving innovation are industry regulations established by governments, citizen-driven business sustainability plans, and startups featuring open innovation.

Each and every one of these technologies is a line of innovation in itself for power companies in Spain, and they are potential sources to originate new business models. Each of them is also a source of innovation that helps solve the challenges and limitations of others.

### *Criticism and reflection*

All innovation sources can renew a part of the electricity sector and the companies' business models. Renewable energy is driving a shift in the main generation resources, and big data analysis enables the shift from fossil fuels to information as a key resource for power generation. In hypothetical terms, if smart grids, together with blockchain, gave rise to a smart client, able to generate and consume electricity interchangeably from any point of the grid, this client would not have a role different than that of power plants. That is, both generators and customers can generate and consume electricity, and they only differ in their dimensions and proportions. However, they are ultimately seen from the network as peer agents. Additionally, all these technologies, together with the treatment of large amounts of information as a core, can discover new horizons to achieve system net electricity balance at every moment. These innovation sources can lead to different ways of doing things, as well as to change the functioning of the market. A real and current example of this kind of approach are mini-grids, a new way to structure the network. Nevertheless, new is not synonymous with better. In a first approximation, a system structured in mini-grids, even though it may have advantages in certain specific situations, a single and meshed network has much greater stability.

Reversing the thought process and, instead of looking at business model parts that can be innovated with the identified technologies and innovation sources, paying attention to model parts that are not the target of innovation, it is found that the industry of electricity will continue to use physical lines of transport and distribution, that is, through cables. Currently, technologies such as inductive charging transfer are already in place to charge mobile devices wirelessly. Is it not possible that in the future electricity could be transported and distributed wirelessly? What if electricity, as well as other kinds of energy, was transported?

In Spain, the power industry finds, in these innovation sources as a whole, the opportunity to redesign the entire system: the agents, the market, the operation, etc. It is time to decide what structure and operation the electricity sector will have in the coming decades. There is an opportunity to nationalize or liberalize the sector; to redefine the functions of the system operator and the market operator; to opt for a single network or a mini-grid-structured grid; to determine a new algorithm for net electricity balance, supply-demand marriage, and electricity pricing; or to continue with the same system. All approaches to the system are valid; each has its own advantages and disadvantages. It is now, when the

innovation sources give the possibility to innovate the system, that it is time to decide what the Spanish electric system wants, without being afraid of change. Once the innovation sources have redesigned the industry, what forces will drive a new change in the energy power industry?

## References


Asociación de Empresas de Energías Renovables. (2017). *Estudio del Impacto Macroeconómico de las Energías Renovables en España*. Madrid, Barcelona, Spain: Asociacio´n de Empresas de Energías Renovables.

Bughin, J., Chui, M., and Manyika, J. (2010). Clouds, big data, and smart assets: Ten tech-enabled business trends to watch. *McKinsey Quarterly*. https://www.mckinsey.com/industries/technology-media-and-telecommunications/our-insights/clouds-big-data-and-smart-assets-ten-tech-enabled-business-trends-to-watch#

Bürer, M. and Wüstenhagen, R. (2009). Which renewable energy policy is a venture capitalist's best friend? Empirical evidence from a survey of international cleantech investors. *Energy Policy, 37*, 4997-5006. 10.1016/j.enpol.2009.06.071

Bürger, C. and Weinmann, J. (2017). The 3 Stages of a Country Embracing Renewable Energy. *Harvard Business Review*. https://hbr.org/2017/04/the-3-stages-of-a-country-embracing-renewable-energy

Consejo Económico y Social. (2018). *Informe 04/2017 El sector eléctrico en España*. Madrid, Spain: Consejo Económico y Social.

Cotteleer, M. and Sniderman, B. (2017). *Forces of change: Industry 4.0*. New York, NY: Deloitte Services LP.

Darmani, A., Arvidsson, N., Hidalgo, A., and Albors, J. (2014). What drives the developement of renewable energy technologies? Toward a typology for the systemic drivers. *Renewable and Sustainable Energy Reviews, 38*, 834-847. 10.1016/j.rser.2014.07.023

de Roca, A. (2018). *El modelo de negocio de las compañías eléctricas: nuevos actores, nuevos roles, nuevas reglas*. https://www.magnuscmd.com/es/el-modelo-de-negocio-de-las-companias-electricas-nuevos-actores-nuevos-roles-nuevas-reglas/

de Roca, A. (2019). *Magnus Commodities, Garantías de Origen (GdO)*. https://www.magnuscmd.com/es/garantias-de-origen-gdo/

Engelken, M., Römer, B., Drescher, M., and Welpe, I. M. (2015). Comparing drivers, barriers, and opportunities ofbusiness models for renewable energies: A review. *Renewable and Sustainable Energy Reviews, 60*, 795-809. 10.1016/j.rser.2015.12.163

Girotra, K. and Netessine, S. (2011). How to Build Risk into Your Business Model. *Harvard Business Review*. https://hbr.org/2011/05/how-to-build-risk-into-your-business-model

Girotta, K. and Netessine, S. (2014). Four Paths to Business Model Innovation. *Harvard Business Review*. https://hbr.org/2014/07/four-paths-to-business-model-innovation

Iansiti, M. and Lakhani, K. R. (2017). The Truth About Blockchain. *Harvard Business Review*. https://hbr.org/2017/01/the-truth-about-blockchain

Lee, J., Kao, H.-A., and Yang, S. (2014). Service innovation and smart analytics for Industry 4.0 and big data environment. *Procedia CIRP, 16*, 3-8. 10.1016/j.procir.2014.02.001

Loebbecke, C. and Picot, A. (2015). Reflections on societal and business model transformation arising from digitization and big data analytics. *Journal of Strategic Information Systems, 24*(3), 149-157. 10.1016/j.jsis.2015.08.002

Magretta, J. (2002). Why Business Model Matters. *Harvard Business Review*. https://hbr.org/2002/05/why-business-models-matter

Preukschat, A. (2017). *Blockchain. La revolución industrial de internet*. Barcelona, España: Grupo Planeta.

Red Eéctrica de España (n.d). *Conócenos/Actividades de negocio/Negocio eléctrico en España*. https://www.ree.es/es/conocenos/actividades-de-negocio/negocio-electrico-en-espana

Ritcher, M. (2013). Business model innovation for sustainable energy: German utilities and renewable energy. *Energy Policy, 62*, 1226-1237. 10.1016/j.enpol.2013.05.038

Saunders, M., Lewis, P., and Thornhill, A. (2009). *Research Methods for Business Students* (5th edition). Harlow, UK: Pearson Education Limited.

United Nations (2015). *Transforming our world: the 2030 Agenda for Sustainable Development*. New York, NY: United Nations.

Vega, G. and López-Bueno, O. (2017). 'Blockchain': la tecnología que va a cambiar tu vida. *El País*. https://elpais.com/retina/2017/03/30/tendencias/1490871615_134683.html

Winston, A. (2014). Two Forces Moving Business Closer to Climate Action. *Harvard Business Review*. https://hbr.org/2014/09/two-forces-moving-business-closer-to-climate-action

Research Article / Industrial Engineering https://doi.org/10.15446/ing.investig.v41n3.87761

# Design of Comminution Plants in the Ceramic Industry Using a Simulation-based Optimization Approach

## Diseño de una planta de molienda para la industria de cerámica mediante un enfoque de optimización basado en simulaciones

Ignacio Ortiz de Landazuri Suárez[1] and María-José Oliveros Colay[2]

**ABSTRACT**

In many cases, the design process of a structural ceramic comminution plant typically consists of an 'expert designer' who makes decisions using intuitive criteria to select commercial equipment. This paper proposes a simulation-based optimization approach to help decision-making. The complexity of the problem lies in selecting the model and amount of equipment for each stage at the lowest cost while simultaneously satisfying a previously fixed production and granulometry. The proposed approach is based on a genetic algorithm to generate solutions and facilitate the optimization process, together with discrete simulation to evaluate the performance of the comminution process according to its service level. To evaluate the algorithm, different problems, whose parameters are based on the requirements of the ceramic industry, are solved and analyzed.

**Keywords:** comminution, equipment selection, genetic algorithm, simulation

**RESUMEN**

En muchos casos, el proceso de diseño de una planta estructural de molienda para la industria de la cerámica consiste en un "diseñador experto" que utiliza criterios intuitivos para seleccionar equipos comerciales. Este artículo propone un enfoque de optimización basado en simulación para ayudar en la toma de decisiones. La complejidad del problema radica en seleccionar el modelo y número de equipos en cada etapa por el costo más bajo y, simultáneamente, satisfacer producción y granulometría fijadas previamente. El enfoque propuesto se basa en un algoritmo genético para generar soluciones y facilitar el proceso de optimización, junto con un modelo de simulación para evaluar el rendimiento del proceso de molienda de acuerdo con su nivel de servicio. Para evaluar el algoritmo, se resuelve y analizan diferentes problemas cuyos parámetros se basan en los requerimientos de la industria cerámica.

**Palabras clave:** molienda, selección de equipos, algoritmo genético, simulación

**Received:** May 30th, 2020
**Accepted:** March 26th, 2021

## Introduction

Comminution is commonly defined as the reduction in the average particle size of solid materials. It is usually performed via crushing, grinding, cutting, vibrating, among others (Martins, 2016). These processes are commonly used in the mining, pharmaceutical, food, chemical, recycling (Kruszelnicka, 2020), and ceramic industries.

The structural ceramic industry is dedicated to the procurement of bricks, tiles, and refractories (Cely-Illera, 2016). Most companies operating in this sector obtain their raw materials from quarries close to their installations, regardless of whether these quarries belong to them or to third parties. Untreated clay obtained from quarries is transported by truck to the company site, where it is unloaded and stored for later use (Regional Activity Centre for Cleaner Production, 2006).

During the grinding process, untreated clay acquired directly from the quarry is milled to obtain raw material with the necessary grain-size distribution and texture for subsequent shaping. Two methods can be used to achieve this: the dry method and the semi-wet method. This study focuses on the dry method, since hard clays are best prepared in installations by using it. This type of system ensures that a significant proportion of fine particles is obtained, which can then be moistened more easily and quickly, thus resulting in a highly homogenous mass with high plasticity. As a result, a better finish and a stronger product are obtained.

In the structural ceramic industry, crushers, box feeders, hammer mills, and conveyor belts are common machines used in the comminution process. Although it seems straightforward at first, the sheer number of combinations of all the parameters to consider makes it extremely likely that erroneous estimates will be made, as well as glossing over

[1] Industrial Engineer, Zaragoza University. Affiliation: R&D Manager, Tezasa, Spain. E-mail: iols@me.com
[2] Industial Engineer, Universidad de Zaragoza, Spain. M.Sc. Industrial Engineering, Universidad de Zaragoza, Spain. Affiliation: Associate Professsor, Universidad de Zaragoza, Spain. E-mail: mjoliver@unizar.es

**How to cite:** Ortiz-Landazuri, I., and Oliveros, M. J., (2021). Design of Comminution Plants in the Ceramic Industry Using a Simulation-based Optimization Approach. *Ingeniería e Investigación*, *41*(3), e87761. 10.15446/ing.investig.v41n3.87761

the best possibilities. There is a need to develop valuable tools to aid decision-making in real-world problems that are usually solved only by experience (Pradenas-Rojas and Passicot-Guzmán, 2017). The aim of this study is to optimize the selection of the necessary equipment in the comminution of structural ceramics, considering the desired level of production at the lowest possible investment cost.

It is possible to find decision-making processes similar to those presented in this paper in the field of maintenance management applied to grinding processes (Barberá-Martinez, Viveros-Gunckel, González-Prida-Díaz, and Mena, 2014), as well as in the equipment selection process (Musingwini, 2016). However, in the mining industry, much of this type of processes used to be carried out experimentally despite the costs derived from decision-making (Burt and Caccetta, 2018). Moreover, in the structural ceramic industry, it is difficult to find studies focused on the selection of equipment, perhaps because this kind of product has a lower added value.

To optimize a process, it is necessary to be able to simulate and evaluate the behavior of the industrial plant in order to ensure that there are no bottlenecks or unnecessary oversizing. These simulations are common in other fields (Lin and Chen, 2015) and, although there are commercial programs for the crushing process, they are usually focused on the mining industry (such as JKSimMetTM, USIM PACTM, and ModSimTM) and are steady-state simulators. Even though they are adequate in several circumstances, they are unable to simulate transient states and may lead to erroneous estimates (Asbjörnsson, Hulthén, and Evertsson, 2013).

Discrete event simulators have been proven to measure the efficiency of in-plant logistics (Seebacher, Winkler, and Oberegger, 2015). Recently, a modular system has been reported, developed using MATLAB/Simulink to simulate the comminution circuits applied to the mining sector (Légaré, Bouchard, and Poulin, 2016). Negahban and Smith (2014) provide an excellent review of discrete event simulation publications with a particular focus on applications in manufacturing.

Later in this paper, it will be made evident that it is impossible to evaluate all feasible solutions in a short period of time. Therefore, it is necessary to look for optimization algorithms that allow finding an optimal solution in a reasonable period of time. Guerrero, Sotelo-Cortés, and Romero-Mota (2018) use a multi-objective model based on mixed integer programming, combining optimization and simulation techniques. We have chosen a genetic algorithm (GA) approach in this work. GAs are based on the mechanisms of natural evolution which were originally proposed by John Holland (Holland, 1975). A GA is a strategy that employs random choices to guide a highly exploitative search, striking a balance between exploration of the feasible domain and exploitation of good solutions. An example of the combination of GA and simulation applied for facility layout problems can be seen in the work by Wang, Yan, Zhang, Shangguan, and Xiao (2008), where the objective function is the material handling cost.

Note that a previous study applied GAs to optimization problems involving comminution processes and is closely related to the problem that affects the subject of this work (Farzanegan and Mirzaei, 2015). Another study applied it in a crushing plant using commercial machines from the Sandvik Company (Derpich, Munoz, and Espinoza, 2019).

This study improves upon existing methods in the literature by optimizing the entire design of a comminution process, rather than just the parameters that control a previously defined process. This design includes the selection of the equipment at each stage, as well as the values of its main parameters to facilitate optimal operation. Therefore, we have programmed a GA that designs the process and a simulator that evaluates the design proposed by the algorithm.

The aim of this work is to facilitate decision-making in the process of selecting equipment for the ceramic industry, looking for the optimal combination of machinery that meets the desired production and granulometry at minimum cost.

## Description of the problem

### *Process description*

Figure 1 shows the 5 stages of a basic dry grinding process. This type of process is used in the structural ceramic industry when the clay moisture is less than 10-12%. Comminution in a dry grinding process is typically performed in two stages, using a crusher and a hammer mill consecutively to achieve the optimum granulometry needed in the extruder. The extruder needs a continuous flow of material, while the crusher receives a batch flow. The raw material extracted from the quarry is dosed into the crusher via a dumper truck or wheel loader every time the hopper reaches a previously stipulated level.

There are feeders with hoppers between these machines in order to avoid bottlenecks and homogenize material flow.

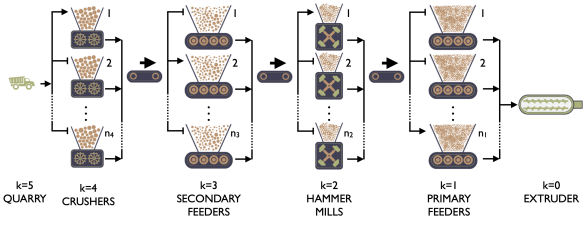


**Figure 1.** Comminution basic stages of a dry grinding process.
**Source:** Authors

Each stage has a number of identical equipment ($n_k$), and each equipment consists of one machine ($M_k$) and one hopper ($T_k$). A particular machine model can be fitted with different types of hoppers. Storage capacity increases with height, but the total height (machine plus hopper height) is limited by the inside height of the factory. $PS_k$ is the stage production (t/h) and $P_k$ (t/h) is the equipment production in stage $k$; thus $PS_k = n_k P_k$.

Every machine has a short conveyor that feeds the main conveyor, which brings the material to the next stage. If there is more than one machine at this stage, another reversible conveyor is needed to feed the hoppers one by one. The

main conveyor belt moves material between the stages. Their speed and inclination are design parameters and depend on the chosen model. The length is determined by the height of the equipment that receives material, and the width is calculated to ensure that the capacity is enough to carry the maximum output that the stage can produce. The value of material waste during transport between stages is typically 5% or less of the material moved at each stage.

The extruder or stage $k = 0$ is the process client. It kneads the clay with water to obtain the desired shape through extrusion and vacuum. This equipment needs a continuous and uninterrupted material flow with a fixed granulometry. The client determines both parameters: $PS_{k=0} = PS_0$ (t/h) and $\Phi_{k=0} = \Phi_0$ (mm).

Primary feeders or PFs ($M_1$) dose the exact production required in the extruder. Each feeder draws a variable production $P_{k=1}$ (t/h) from its hopper. The total stage production must be equal to $PS_0$, but the production of each feeder may vary within a range according to material availability.

Hammer mills, or HMs, ($M_2$) break the material to decrease its granulometry. The diameters of screen holes are fixed to match the granulometry needed in the extruder ($\Phi_2 = \Phi_0$). HM model production is fixed, and the overall production sent to PFs is the result of multiplying the number of active HMs (the ones with material in their hoppers) by their nominal productions. They stop once PF hoppers are full and run again when some of their levels are below a reserve level, which is usually 40% of their capacity, and all available HMs send material to the corresponding PF hopper.

Secondary feeders or SFs ($M_3$) feed HMs in a similar manner as PFs do, although they do not necessarily feed the exact amount of material that HMs produce. Once all the HM hoppers are full, the feeders stop and resume when a hopper reaches the reserve level. Material flow must be equal to or higher than the amount needed by the HMs in order to receive sufficient material in a timely manner every time they are set in motion. This parameter, called 'production multiplier' must be considered in the design process.

Crushers ($M_4$) decrease the grain size of the raw material stored in their hoppers $T_4$. The diameter of the raw material, $\Phi_5$, is an initial condition of the problem. Otherwise, the diameter from the material that goes out of the crusher, $\Phi_4$, varies between a set of values. This is important because the selected size influences the work done by the HM.

Stage 5 models the way in which trucks or wheel loaders directly transport the raw material from the quarry. Batch process size, number, and tempo depend on hopper capacity, $T_4$. In this work, we have decided that the simulator should use the wheel loader when the capacity of the hopper is small, and dumper trucks in the rest of the cases. The average charge cycle time has been considered to be 5 and 20 minutes, respectively.

### *Process parameters*

The main parameters that control the process are demanded by the client: extruder continuous production, $PS_0$ (t/h), and extruder granulometry, $\Phi_0$ (mm). Other parameters affecting the performance of the plant are raw materials granulometry at the quarry, $\Phi_5$ (mm), and available height inside the factory, $H$ (m).

Bulk density $\rho$ is a significant factor because clay is a granular material, and its density depends on particle size. Equation 1 defines a linear relationship between $\Phi_{80}$ (the diameter below which 80% of material passes) and density based on a company experimental dataset. Therefore, density grows as grain size decreases, and the material becomes more compact. This indicates that the flow demanded by the extruder ($m^3$/h) is lower than the flow of clay at the entrance.

$$\rho\left[\frac{t}{m^3}\right] = 1{,}60144 - 0{,}00114\ \emptyset_{80}\ [mm] \tag{1}$$

Considering these parameters and available commercial models, the designer defines a set of machines and hoppers for each stage and chooses a specific one from these sets. Let $M_k = \{1 \ldots q_k\}$ be the set of feasible machines in stage $k$ ($k = 1 \ldots 4$) with $q_k$ as the maximum number of selectable machines. $T_{ik,k}$ is the set of feasible hoppers for each machine in stage $k$, with $i_k \in M_k$. Therefore, the problem is to select the machine and hopper model in each stage $k$, as well as their respective numbers. The decision variables are as follows:

1. $x_i^k$ the machine model that equals 1 if the model that occupies position $i$ in $\{M_k\}$ is selected;
2. $y_{i,j}^k$, the hopper model that equals 1 if the model that occupies position $j$ in $\{T_{i_k,k}\}$ is selected;
3. and $n_k$, the number of equipment (machines plus hopper) in each stage.

As comminution is generally done in two stages, it is necessary to define the output diameter at the crusher, $\Phi_k = 4$. As the possibilities are many, a set $\{B\}$ of $b_{\max}$ dimensions is defined with the most common values. The second variable is the production multiplier for the secondary feeder, which is limited to a set $\{A\}$ of $a_{\max}$ dimensions with values between 1 and 2. The production value given by these feeders is the theoretically necessary production at the extruder stage multiplied by factor $a$.

## Optimization approach

### *Genetic algorithm*

Design experts, depending on their subjective experiences, typically judge a huge combination of feasible solutions to select an optimal solution. But not all solutions are really feasible. Thus, some solutions tend to be over-dimensioned if the designer is focused on reliability, while some solutions

lead to a lack of production if the designer is focused on cost. Hence, each solution needs to be simulated to evaluate its performance, but this is time-intensive and not feasible.

A GA has been developed to solve this problem. The goal is to find an optimal equipment set that minimizes installation costs while ensuring a feasible solution (extruder continuous production and granulometry, as well as maximum installation height). Each solution is codified as an integer 14-dimensional vector, and gene value indicates the positions of selected elements in the set. Thus, the chromosome structure is $\{n_{k=1}, i_{k=1}, j_{k=1}, n_{k=2}, i_{k=2}, j_{k=2}, a, n_{k=3}, i_{k=3}, j_{k=3}, n_{k=4}, i_{k=4}, j_{k=4}, b\}$, where $n_k$ is the number of equipment (machine and hopper) corresponding to block $k$; $i_k$ is the position of machine model in set $\{M_k\}$; $j_k$ is the position of the hopper model in set $\{T_{ik,k}\}$; $a$ is the position of the production multiplier parameter in $\{A\}$; and $b$ is the position of the selected diameter $k = 4$ in $\{B\}$. All values range between 1 and 5.

The goal is to minimize all equipment costs, $C_{equip}$, expressed by Equation 2. The cost of machines and hoppers at every stage $k$, is defined by $Cm_k^i$ and $Ch_{ik}^j$, where $n_k$ is the number of machines, $Cc_{k+1,k}$ is the cost of the conveyor, and $nc_{k+1,k}$ is the number of conveyors.

$$C_{equip} = \sum_{k=1}^{4} n_k \left(Cm_k^i + Ch_{ik}^j\right) + \sum_{k=0}^{4} nc_{k+1,k} Cc_{k+1,k} \qquad (2)$$

The flowchart of the genetic algorithm schema is shown in Figure 2. The GA starts with a randomly generated population, the Basic-Population (BP), of feasible *Npop*-solutions whose fitness is evaluated (Equation 3). Then, a new population is formed by selecting individuals from this BP to create the offspring of a subsequent generation. Every basic solution has a predetermined probability $p_c$ ($p_c = 0{,}8$) to belong to a parent population. Subsequently, a best-worst crossover operator is applied to establish parent-chromosome pairs and generate two offspring from each couple. Each offspring gene is randomly selected from one of the parents. After the crossover, the mutation operation is carried out. A chromosome of the offspring population is selected for the mutation operation with probability $p_m$ ($p_m = 0{,}3$), and the values of 3 genes change randomly. Each of these solutions is evaluated in a computer model specially designed to simulate its behavior. A solution is rejected if it is unfeasible.

The algorithm selects the best solutions (parents, offspring and muted) to survive, and it updates the BP. Additionally, a heuristic technique is applied to improve the quality of BP solutions. The method consists of randomly choosing a block or stage ($k = 1 \ldots 4$) and changing all parameters of the selected block. Finally, the last iteration step is to choose the best solution and finish the improvement method for this iteration. The best feasible solution is selected when the maximum number of iterations is reached.

## *Model simulation*

Apparently, the problem and the solution proposed by the algorithm seem simple, given the fact that there are no components of variability in the system (it is assumed that, at the entrance, the clay has the same particle size, times are fixed, etc.). However, when the behavior of the different equipment is simulated and the evolution of hopper levels over time is evaluated, this behavior becomes dynamic and seemingly chaotic.

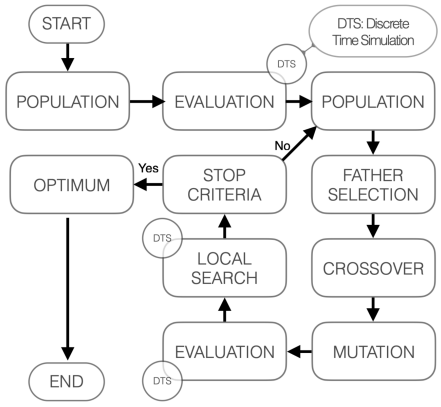


**Figure 2.** Genetic algorithm schema.
**Source:** Authors

The operation of each stage is conditioned by both the anterior and subsequent stages, and the flows take time to stabilize. It is therefore difficult to predict where and when bottlenecks can be found, and the existence or not of oversized elements. Figure 3 illustrates the evolution of the capacity ($m^3$) of a hopper of feeder. Initially, the hopper is full and begins to empty in a linear manner, but soon the behavior becomes chaotic when the material demand and filling cycle have different and chaotic periods. Some examples of this type of behavior can be found in the works by Légaré *et al.*, (2016) and Li, Evertsson, Lindqvist, Hulthén, and Asbjörnsson (2018).

Therefore, we have designed a simulation model to evaluate the operation of the installation over a sufficiently long period of time, in order to ensure that the model reaches all states. The process starts with all the hoppers full at maximum capacity, and the extruder starts by requesting material from previous stages. The model continuously evaluates the flow of material that reaches the extruder, $PR_T$ (t/h), and compares it to $PS_0$ (t/h), the design parameter. The relationship between $PR_T$ and $PS_0$ is the Service Level ($SL_R$).

The simulation model has been programmed in Matlab© and, in addition, another parametric model was built using WitnessPwF© to validate the results. The results of the two approaches are very similar, and the differences are not significant. Finally, the Matlab-based model was included because the computational time to evaluate each solution was lower.

Early results show that a cheaper installation cost can be achieved if constraints are relaxed by allowing production ($PR_T$) to be below what is initially required ($PS_0$) at certain times. Therefore, it has been decided to widen the search space with those solutions that were close to the desired level of service, $SL_T$. We do not rule out solutions that fall short of it, but we penalize ($PE$) them proportionally to how

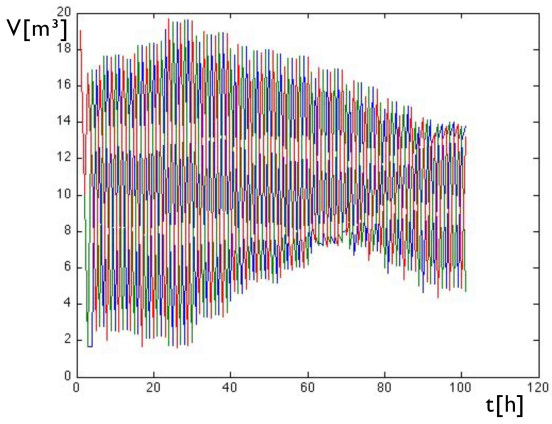


**Figure 3.** Capacity ($m^3$) vs. time (h) in a feeder hopper.
**Source:** Authors

close they are (Equation 3). This way, SL, far from being a restriction, became part of the fitness. Then, the fitness function became as the one defined in Equation (4).

$$PE = \begin{cases} 1 & SL_R \geq SL_T, \\ 1 + 100 \log\left(\frac{SL_T}{SL_R}\right) & SL_R < SL_T, \end{cases} \quad (3)$$

$$C = C_{equip} PE \quad (4)$$

For example, Figure 4 illustrates the evolution of the SL (%) of a facility when $PS_0 = 100$ t/h. Initially, the installation was perfectly balanced, but there were actually small imbalances caused by the excessive production of the crusher.

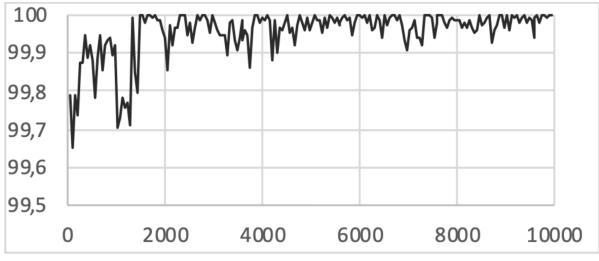

**Figure 4.** Service Level (%) for $PS_0 = 100$ t/h.
**Source:** Authors

After several rounds of testing, the simulation time will be at least 50 hours for all states to appear; the necessary warm-up period is 5 hours. Thus, the computing time to simulate each GA proposal is 40 seconds.

## Results and discussion

### *Computational results*

The algorithm was implemented in the industry to validate its performance. Usually, the ceramic industry production values range between 50 and 150 t/h, so machines are sized to meet these requirements. However, there are cases where much larger productions are needed, where success business stories to compare are much more limited. Thus, 8 levels of extruder production (25-50-100-150-200-250-300-400 t/h) and 2 levels of particle size reduction (125,5/1 and 81,2/10) have been identified, and the number of experiments is 16.

Taking these requirements into account, available commercial models were selected. The models and parameters used in this study were based on the real-world equipment of a company located in Zaragoza Spain, dedicated to the design and manufacturing of machinery for the treatment and preparation of clay in the ceramic industry. Table 1 shows various parameters such as the range of flow rate, capacity, and cost of feasible equipment at every stage. To facilitate the comparison of results, the set of machines and hoppers for each stage was the same for all experiments. Note that the selectable models at feeder stages are identical. On the other hand, crusher machines have higher flow rates than hammer mill models because of the presence of waste material between stages, and because the material is compacted as the process progresses.

**Table 1.** Data to design ceramic industry

| |
|---|
| **Stage 2: Hammer Mills** |
| No. models: 25 (5 HMs and 5 hoppers) |
| Q [$m^3$/h]: 22 - 63 |
| Capacity [$m^3$]: 1,4 - 4,67 |
| Cost [€]: 76 105 - 15 0674 |
| **Stage 4: Crusher** |
| No. models: 25 (5 crushers and 5 hoppers) |
| Q [$m^3$/h]: 25 - 114 |
| Capacity [$m^3$]: 0,41 - 28,73 |
| Cost [€]: 42 460 - 122 420 |
| Output diameter at the crusher [mm]: 24 - 60 |
| **Stages 1 and 3: Feeder** |
| No. models: 25 (5 Feeders and 5 Hoppers) |
| Q [$m^3$/h]: 10/40 - 90/120 |
| Capacity [$m^3$]: 1,34 - 67,08 |
| Cost [€]: 32 000 - 61 139 |
| Production multiplier of secondary feeder, PM: 1 - 2 |
| **Belt conveyor** |
| Cost = fixed term proportional to number of conveyors between stages plus variable term depending on the length and width |

**Source:** Tezasa (www.tezasa.com).

Otherwise, the caudal output at the crusher, $Q_{CRUSHER}$, is subjected on $k = 4$, and it increases with the diameter (the $Q_k = 4$ interval in Table 1 is for the minimum diameter, $k = 4 = 24$ mm). The hammer mills caudal, $Q_{k=2}$, is not directly influenced by particle size and production, but hammer velocity, inlet position, breaker gap, infeed granulometry, screen size, and others have minimum influences on this parameter. To simplify the model, a constant and independent production were considered.

The numerical experiments were performed on a Windows 7 PC with an Intel® Core$^{TM}$ i7-6800K CPU@3.4GHz and 16GB RAM. The GA and code for the simulation model were written in MATLAB©.

**Table 2.** Best results of the instances: cost

| No | $PS_0$ t/h | $\Phi_{in}/\Phi_{out}$ mm/mm | Cost M€ | Primary Feeder ($k$ = 1) | | Hammer Mills ($k$ = 2) | | Secondary Feeder ($k$ = 3) | | Crusher ($k$ = 4) | |
|---|---|---|---|---|---|---|---|---|---|---|---|
| | | | | n | Cost M€ | n | Cost M€ | n | Cost M€ | n | Cost M€ |
| **1** | 25 | 125,5/1 | 211 | 1 | 32 | 1 | 76,1 | 1 | 32 | 1 | 42,5 |
| **2** | 25 | 81,2/10 | 211 | 1 | 32 | 1 | 76,1 | 1 | 32 | 1 | 42,5 |
| **3** | 50 | 125,5/1 | 245 | 1 | 32 | 1 | 94,6 | 1 | 32 | 1 | 42,5 |
| **4** | 50 | 81,2/10 | 244 | 1 | 32 | 1 | 94,6 | 1 | 32 | 1 | 42,5 |
| **5** | 100 | 125,5/1 | 375 | 1 | 39 | 1 | 145 | 1 | 39 | 1 | 70,3 |
| **6** | 100 | 81,2/10 | 374 | 1 | 39 | 1 | 145 | 1 | 39 | 1 | 70,3 |
| **7** | 150 | 125,5/1 | 576 | 1 | 45 | 2 | 130 | 1 | 45 | 1 | 93,8 |
| **8** | 150 | 81,2/10 | 573 | 1 | 45 | 2 | 130 | 1 | 45 | 1 | 73,3 |
| **9** | 200 | 125,5/1 | 760 | 2 | 39 | 2 | 145 | 2 | 39 | 2 | 70,3 |
| **10** | 200 | 81,2/10 | 758 | 2 | 39 | 2 | 145 | 2 | 39 | 2 | 70,3 |
| **11** | 250 | 125,5/1 | 990 | 2 | 45 | 3 | 145 | 2 | 45 | 2 | 73,3 |
| **12** | 250 | 81,2/10 | 987 | 2 | 45 | 3 | 145 | 2 | 45 | 2 | 73,3 |
| **13** | 300 | 125,5/1 | 1 048 | 3 | 39 | 3 | 145 | 2 | 45 | 2 | 73,3 |
| **14** | 300 | 81,2/10 | 1 044 | 3 | 39 | 3 | 145 | 2 | 45 | 2 | 73,3 |
| **15** | 400 | 125,5/1 | 1 418 | 3 | 45 | 4 | 145 | 3 | 45 | 3 | 73,3 |
| **16** | 400 | 81,2/10 | 1 413 | 3 | 45 | 4 | 145 | 3 | 45 | 3 | 73,3 |

**Source:** Authors

**Table 3.** Best results of the instances: configuration

| No | Primary Feeder ($k$ = 1) | | Hammer Mills ($k$ = 2) | | Secondary Feeder ($k$ = 3) | | | Crusher ($k$ = 4) | |
|---|---|---|---|---|---|---|---|---|---|
| | Q m³/h | Cap m³ | Q m³/h | Cap m³ | PM m³ | Q m³/h | Cap m³ | Cap m³ | $\Phi_4$ mm |
| **1** | 10-40 | 1,34 | 22 | 1,4 | 1 | 10-40 | 1,34 | 0,41 | 24 |
| **2** | 10-40 | 1,34 | 22 | 1,4 | 1 | 10-40 | 1,34 | 0,41 | 24 |
| **3** | 10-40 | 1,34 | 32 | 1,85 | 1 | 10-40 | 1,34 | 0,41 | 48 |
| **4** | 10-40 | 1,34 | 32 | 1,85 | 1 | 10-40 | 1,34 | 0,41 | 48 |
| **5** | 50-80 | 3,94 | 63 | 2,16 | 1 | 50-80 | 3,94 | 0,87 | 48 |
| **6** | 50-80 | 3,94 | 63 | 2,16 | 1 | 50-80 | 3,94 | 0,87 | 48 |
| **7** | 70-100 | 6,12 | 50 | 1,87 | 1 | 70-100 | 6,12 | 6,18 | 48 |
| **8** | 70-100 | 6,12 | 50 | 1,87 | 1 | 70-100 | 6,12 | 4,37 | 60 |
| **9** | 50-80 | 3,94 | 63 | 2,16 | 1,1 | 50-80 | 3,94 | 0,87 | 48 |
| **10** | 50-80 | 3,94 | 63 | 2,16 | 1,1 | 50-80 | 3,94 | 0,87 | 48 |
| **11** | 70-100 | 6,12 | 63 | 2,16 | 1,1 | 70-100 | 6,12 | 4,37 | 48 |
| **12** | 70-100 | 6,12 | 63 | 2,16 | 1,1 | 70-100 | 6,12 | 4,37 | 48 |
| **13** | 50-80 | 3,94 | 63 | 2,16 | 1,1 | 70-100 | 6,12 | 4,37 | 60 |
| **14** | 50-80 | 3,94 | 63 | 2,16 | 1,1 | 70-100 | 6,12 | 4,37 | 60 |
| **15** | 70-100 | 6,12 | 63 | 2,16 | 1,1 | 70-100 | 6,12 | 4,37 | 60 |
| **16** | 70-100 | 6,12 | 63 | 2,16 | 1,1 | 70-100 | 6,12 | 4,37 | 60 |

**Source:** Authors

To simulate each solution, simulation time was set to 50 h with a 5 h warm-up period; the computational time was around 38 s per solution. The average computing time to make the prescribed iterations prescribed was 6,7 h, and the algorithm evaluated approximately 630 solutions. Each test instance was solved 8 times, and the best results are listed in Tables 2 and 3.

Table 2 shows the best result's configuration and cost. The first three columns define the numeration and settings of the experiment. Column 4 refers to the cost (M€) of the best solution found among the eight solutions obtained. Columns 5 and 6 refer to the primary feeder stage ($k$ = 1), listing the number of machines and unitary cost of the equipment (M€). The rest of the columns contain similar information for the hammer mills ($k$ = 2), secondary feeder ($k$ = 3), and crusher ($k$ = 4) stages.

Table 3 displays the number of machines, flow rate, and capacity of the best solutions for all stages. The results suggest that the installation cost is strongly related to production, and the cost of all stages rise as $PS_0$ increases. When scenarios with the same productions are compared, it is made evident that the value of the particle size reduction is not relevant. Hence, the algorithm proposes identical configurations (number and type of machine and hopper) for

each level of extruder production, even when the particle size reduction changes, except in the case of crushers ($PS_0$ = 150 t/h). The conveyors cause small differences (note that installation cost decreases, as expected, but only 0,5% of the maximum); as clay is more compact, conveyors are narrower and cheaper.

Analyzing the configuration of each stage, the algorithm proposes high production HMs and medium-low production crushers. On the other hand, hoppers of all stages and experiments are as small as possible, to ensure equipment height is as short as possible, which allows for shorter and cheaper conveyors to be used. Finally, note that size reduction in the first crushing stage, $IN$ - $k$ = 4, is the least possible. Moreover, $k$ = 4 takes medium to high values, which are independent of the initial and final granulometry. In this way, the crusher processes as much material as possible, although the crushing is not so severe.

Figure 5 shows, for each production level, the individual cost (M€) of every stage including conveyors, calculated through Equation 2 and disaggregated by stages. As expected, the cost of all blocks increases as production rises.

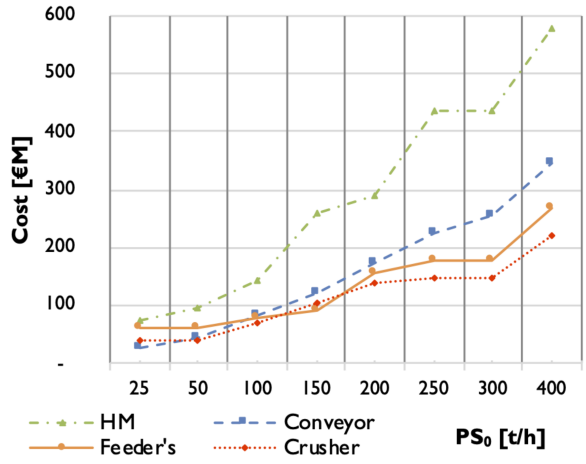


**Figure 5.** Cost of every stage.
**Source:** Authors

Figure 6 displays the cost relative to the global cost for each problem (%), and a particular emphasis is given to the relative cost of hammer mills. On the other hand, conveyors account for 20-25% of installation costs, although this cost is not considered during product design, given that they are considered to be an auxiliary system.

Figure 7 shows cost relative to $PS_0$. Relative cost is very high for small $PS_0$ values because of oversized equipment; at higher productions, the relative cost does not change so much, and these small differences are due to the discretization of equipment parameters (capacity, flow, and cost).

### *Algorithm vs. industry*

The solutions provided by the GA are similar to those adopted in ceramic industries, but some interesting alternatives appear in the design of facilities.

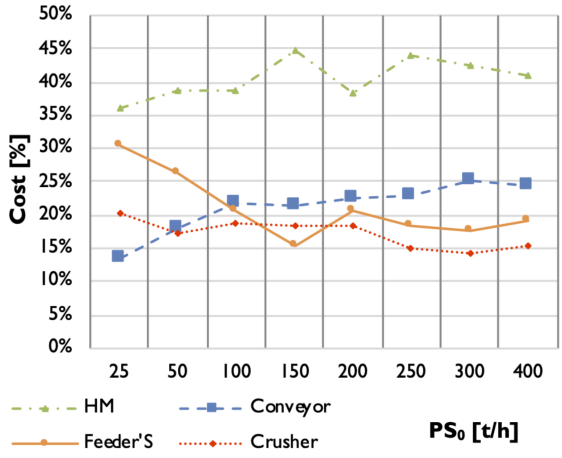


**Figure 6.** Cost relative of every stage.
**Source:** Authors

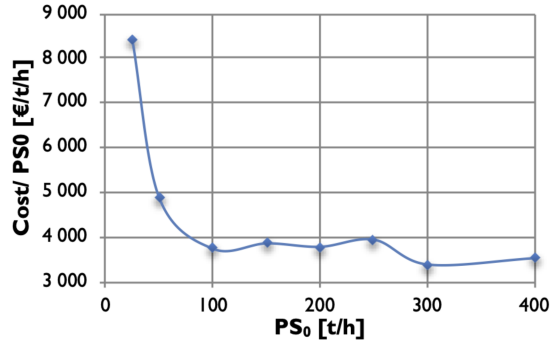


**Figure 7.** Cost [€/t] VS Production [t/h].
**Source:** Authors

Normally, hoppers are placed as high as possible, except at the hammer mills stage. This decision is usually made because of doubts that the line is not balanced and properly dimensioned. This results in conveyor belts that are much longer and need a larger area for the comminution zone, thus increasing the cost of hoppers and especially belts, which can represent 40% of the installation investment. Additionally, this over-dimensioning also causes an increase in energy consumption.

Finally, it is worth noting that this work has been approximated in the most realistic way possible, using commercial equipment with sizes and prices related to the relevant industry. For large production cases, the capacities of hammer mills are insufficient, and a higher capacity model needs to be developed.

## Conclusions

In this paper, we parameterized and characterized the comminution process of ceramics, where the dry grinding process was carried out with two machines: crusher and hammer mill. We proposed a simulation-optimization-procedure-based GA to obtain an economical solution to the problem of equipment selection. In this study, we considered the cost of all the

installation equipment and the ratio between the actual and demanded production at the extruder during the considered period of time.

To assess the feasibility of the solution, it was necessary to develop a simulation model that, via time discretisation, calculated the obtained production and material granulometry, as well as the service level. Because of the high computation times needed to evaluate production, it was necessary to consider different strategies in the GA, including local improvement to select an optimal solution in a shorter time. Finally, the proposed method has been tested with a variety of real-world problems faced by the ceramic industry, evaluating how the cost of the plant and the type of equipment is distributed in each block or stage. Such calculations can be done for a wide range of combinations of machines and hoppers, with respect to both number and sizes.

Regarding the obtained results, it should be noted that the installation cost is strongly related to production, but not to the particle size reduction. We would also like to highlight the need for hoppers of all stages and experiments to be as small as possible, in order to ensure that the equipment is as short as possible, and, therefore, allows for the use of shorter and cheaper conveyors.

The capacity of the system presented in this article to design comminution plants has been proven. Finding the best possible solution that fits with the needs of the client presents possibilities of new ways of working that would allow companies to overcome the bias that an expert may have when designing new plants for the structural ceramic industry. Future work should incorporate more complex grinding processes and energy consumption into this method.

## Funding

This research did not receive any specific grant from funding agencies in the public, commercial, or non-profit sectors.

## References

Asbjörnsson, G., Hulthén, E., and Evertsson M. (2013). Modelling and simulation of dynamic crushing plant behavior with MATLAB/Simulink. *Minerals Engineering*, *43-44*, 112-120. 10.1016/j.mineng.2012.09.006

Barberá-Martinez, L., Viveros-Gunckel, P., González-Prida-Díaz, V., and Mena, R. (2014). Influence of the input load on the reliability of the grinding line. A case study. *Revista DYNA*, 89(5), 560-568. 10.6036/7013

Burt, C. N. and Caccetta, L. (2018). Literature review. In Burt, C. N. and Caccetta, L. (Eds.) *Equipment Selection for Mining: with Case Studies* (pp. 25-51). New York, NY: Springer. 10.1007/978-3-319-76255-5_3

Cely-Illera, L. (2016). Raw materials for the ceramics industry from norte de santander. I. Mineralogical, chemical and physical characterization. *Revista Facultad de Ingeniería - Universidad de Antioquia, 80*(2016), 31-37. 10.17533/udea.redin.n80a04

Derpich, I., Munoz, N., and Espinoza, A.(2019). Improving the productivity of the copper mining process in the Chilean copper industry. *Croatian Operational Research Review, 10*(2), 227-240. 10.17535/crorr.2019.0020

Farzanegan, A. and Mirzaei, Z. S. (2015). Scenario-Based Multi-Objective Genetic Algorithm Optimization of Closed Ball-Milling Circuit of Esfordi Phosphate Plant. *Mineral and Extractive Metallurgy Review*, *36*(2), 71-82. 10.1080/08827508.2013.868348

Guerrero, W. J., Sotelo-Cortés, L. A., and Romero-Mota E. (2018). Simulation-optimization techniques for closed-loop supply chain design with multiple objectives. *Revista DYNA, 35*(206), 202-210. 10.15446/dyna.v85n206.70596

Holland, J. (1975). *Adaptation in Natural and Artificial Systems.* Ann arbour, MI: The University of Michigan Press.

Kruszelnicka, W. (2020). New model for ecological assessment of comminution process in energy biomass processing chain. *E3S Web of Conferences*, *154*, 1-21. 10.1051/e3sconf/202015401001

Légaré, B., Bouchard, J., and Poulin. (2016). A Modular Dynamic Simulation Model for Comminution Circuits. *IFAC-PapersOnLine, 49*(20), 19-24. 10.1016/j.ifacol.2016.10.090

Li, H., Evertsson, M., Lindqvist, M., Hulthén, E., and Asbjornsson, G. (2018). Dynamic modeling and simulation of a SAG mill-pebble crusher circuit by controlling crusher operational parameters. *Minerals Engineering, 127*, 98-104. 10.1016/j.mineng.2018.07.010

Lin, J. T. and Chen, C.-M. (2015). Simulation optimization approach for hybrid flow shop scheduling problem in semiconductor back-end manufacturing. *Simulation Modelling Practice and Theory*, *51*, 100-114. 10.1016/j.simpat.2014.10.008

Martins, S. (2016). Size-energy relationship in comminution, incorporating scaling laws and heat. *International Journal of Mineral Procesing, 153*, 29-43. 10.1016/j.minpro.2016.05.020

Musingwini, C. (2016). Mine Planning and Equipment Selection (MPES 2015). *Journal of the Southern African Institute of Mining and Metallurgy, 116*(9), 809-820. http://www.scielo.org.za/scielo.php?script=sci_arttext&pid=S2225-62532016000300001

Negahban, A. and Smith, J. S. (2014). Simulation for manufacturing system design and operation: Literature review and analysis. *Journal of Manufacturing Systems*, *33*(2), 241-261. 10.1016/j.jmsy.2013.12.007

Pradenas-Rojas, L. and Passicot-Guzmán, P. (2017). Optimizing the use of cranes and trucks in forestry operations. *Revista DYNA, 84*(201), 172-179. 10.15446/dyna.v84n201.52739

Regional Activity Centre for Cleaner Production (RAC/CP). (2006). Phases in the manufacture of ceramic products. In RAC/CP (Eds.) *Pollution Prevention in the Structural Ceramics Sector*, (pp. 45-52). http://www.cprac.org/docs/ceramicaestr_ang.pdf

Seebacher, G., Winkler, H., and Oberegge,r B. (2015). In-plant logistics efficiency valuation using discrete event simulation. *International Journal of Simulation Modelling, 14*(2015), 60-70. 10.2507/IJSIMM14(1)6.289

Wang, G., Yan, Y., Zhang, X., Shangguan, J., and Xiao, Y. (2008). A simulation optimization approach for facility layout problem. In IEEE (Eds.) 2008 IEEE *International Conference on Industrial Engineering and Engineering Management*, IEEM 2008. 10.1109/IEEM.2008.4737966

Research Article / Industrial Engineering https://doi.org/10.15446/ing.investig.v41n3.83763

# The Influence of Safety Climate, Motivation, and Knowledge on Worker Compliance and Participation: An Empirical Study of Indonesian SMEs

## La influencia del clima, la motivación y el conocimiento de seguridades en el cumplimiento y la participación de los trabajadores: un estudio empírico de PyMEs en Indonesia

Nachnul Ansori[1], Ari Widyanti[2], and Yassierli[3]

**ABSTRACT**

In the workplace, safety behavior has been regarded as an important safety performance factor that is generally expressed based on the degree of safety compliance and worker participation. Previous studies have proposed several models for Small and Medium Enterprises (SMEs), but the human factor and situation-related matters seem yet to be included. This study aims to investigate the role of motivation and knowledge (as person-related constructs) and safety climate (as a situation-related construct) in SMEs' compliance and participation. Based on a more comprehensive model, a questionnaire was constructed and distributed to 23 Indonesian metal manufacturing SMEs. The results showed that safety climate positively influenced safety knowledge, motivation, compliance, and participation. Safety knowledge and motivation were found to mediate the relationship between safety climate and behavior (*i.e.*, compliance and participation). Safety knowledge only affected compliance, while motivation influenced compliance and participation. This study suggests that SMEs should consider situation-related constructs (safety climate) and person-related constructs (motivation and knowledge) to improve their safety behavior.

**Keywords:** safety compliance, safety motivation, safety participation, safety climate, safety knowledge, SMEs

**RESUMEN**

En el lugar de trabajo, el comportamiento de seguridad ha sido considerado como un factor importante del rendimiento de seguridad que se expresa generalmente en función del grado del cumplimiento de seguridad y de la participación de los trabajadores. Estudios anteriores han propuesto varios modelos del comportamiento de seguridad para las pequeñas y medianas empresas (PyMEs), pero el factor humano y los asuntos relacionados con la situación parecen no estar incluidos todavía. Este estudio tiene como objetivo investigar el papel de la motivación y del conocimiento (constructos relacionados con la persona) y el clima de seguridad (constructo relacionado con la situación) en el cumplimiento y la participación de las PyMEs. Basado en un modelo más integral, se construyó un cuestionario que se distribuyó a 23 PyMEs indonesias de fabricación de metales Los resultados mostraron que el clima de seguridad influyó positivamente en el conocimiento, la motivación, el cumplimiento y la participación de seguridad. Se encontró que el conocimiento y la motivación de seguridad median en la relación entre el clima de seguridad y el comportamiento (es decir, cumplimiento y participación). El conocimiento de seguridad solo afectó el cumplimiento, mientras que la motivación influyó en el cumplimiento y la participación. Este estudio sugiere que las PyMEs tienen que considerar constructos relacionados con la situación (clima de seguridad) y constructos relacionados con la persona (motivación y conocimiento) para mejorar su comportamiento en materia de seguridad.

**Palabras clave:** cumplimiento de seguridad, motivación de seguridad, participación en seguridad, clima de seguridad, conocimiento de seguridad, PyMEs

**Received:** November 28th, 2019
**Accepted:** February 26th, 2021

[1]Faculty of Industrial Technology, Institut Teknologi Bandung, Indonesia. Industrial Engineering Department, Universitas Trunojoyo Madura, Indonesia. Affiliation: Ph.D. student of Faculty of Industrial Technology, Institut Teknologi Bandung, Indonesia. Email nachnulansori@students.itb.ac.id, nachnul@gmail.com
[2]Faculty of Industrial Technology, Institut Teknologi Bandung, Indonesia. Affiliation: Associate professor at Industrial Engineering and Management, Institut Teknologi Bandung. E-mail: widyanti@mail.ti.itb.ac.id
[3]Faculty of Industrial Technology, Institut Teknologi Bandung, Indonesia. Affiliation: Professor at Faculty of Industrial Technology, Institut Teknologi Bandung. E-mail: yassierli@ti.itb.ac.id

## Introduction

According to Geller (2001), safety behavior is an important aspect of workplace safety. Al-Hemoud and Al-Asfoor (2006) reported that 80% of accidents are triggered by unsafe

**How to cite:** Ansori, N., Widyanti, A., and Yassierli (2021). The Influence of Safety Climate, Motivation, and Knowledge on Worker Compliance and Participation: An Empirical Study of Indonesian SMEs. *Ingeniería e Investigación*, *41*(3), e83763. 10.15446/ing.investig.v41n3.83763

behaviors, while unsafe conditions cause the remaining 20%. Khandan, Maghsoudipour, Vosoughi, and Kavousi (2013) stated that approximately 86-96% of industrial workplace accidents occur due to unsafe behaviors. Therefore, adopting an appropriate safety behavior tends to reduce the number of accidents and lost work time (Seo, Lee, Kim, and Jee, 2015). Improving in this regard is required to prevent unexpected or undesirable events (Xu and Shi, 2017), so there is a noticeably negative relation between safety behavior and accidents (Wallace, 2016).

Safety behavior reflects the safe practices that workers need to embrace to evade accidents (Panuwatwanich, Al-Haadir, and Stewart, 2016). Safety participation and compliance are generally used to describe the adopted level or extent of safety behavior (Neal, Griffin, and Hart, 2000). Safety participation is based on worker involvement, efforts, programs, and initiatives to improve workplace safety. Safety compliance refers to the state of observing established safety procedures, standards, and regulations at workplace (Neal *et al.*, 2000).

Safety behavior can be improved by modifying its influencing factors, which are individual (person-related) and organizational (situation-related) (Christian, Bradley, Wallace, and Burke, 2009). Reports showed that organizational factors affect individual determinants, which impacts safety behavior (Neal *et al.*, 2000). Moreover, safety training and regulations, worker participation, and supervisor support are aspects of safety climate.

There have been studies on safety behavior, but only few of them have comprehensively looked at person-related and situation-related factors in this context. Among the individual factors are safety motivation and knowledge, while organizational factors include safety climate. It should be noted that safety behavior has a direct impact on safety outcome (accidents, injury, etc.), which is influenced by both person-related and situation-related factors (Christian *et al.*, 2009). Safety motivation is defined as the workers' eagerness to adopt safety measures in work areas (Neal and Griffin, 2006). It is an individual-level variable that is expected to be widely shared within organizational units (Kopelman, Brief, and Guzzo, 1990). Meanwhile, safety knowledge shows the level of worker awareness related to practices involved in occupational safety (Vinodkumar and Bhasi, 2010). It improves job-specific and non-job-specific task proficiencies (Campbell, McCloy, Oppler, and Sager, 1993). Results from several similar studies reported that safety motivation positively influences safety behavior (Shin, Gwak, and Lee, 2015; Amponsah-Tawaih and Adu, 2016; Panuwatwanich *et al.*, 2016; Baser, Ture, Abubakirova, Sanlier, and Cil, 2017; Mohammadfam, Ghasemi, Kalatpour, and Moghimbeigi, 2017). Person-related factors were reported to be the key determinants that influence safety behavior.

Conversely, situation-related factors include safety climate and leadership (Christian *et al.*, 2009). According to Neal and Griffin (2006), a safety climate is a shared awareness of procedures, wisdom, and practices related to safety in the workplace. It is an individual-level variable expected to be widely shared within organizational units (Kopelman *et al.*, 1990). Several studies reported that safety climate influences safety behaviors (Shin *et al.*, 2015 and Panuwatwanich *et al.*, 2016) and is depicted by safety communication and systems, including training that influences safety behavior (Shin *et al.*, 2015). Panuwatwanich *et al.* (2016) reported that safety climate is described by management commitment and communication, competence, personal appraisal of risk, work pressure, safety rules, and procedures.

More specifically, regarding Small and Medium Enterprises (SMEs), several studies showed that the dimensions of safety climate (represented by management commitment, safety training, regulations, communication, and worker involvement) have a direct effect on safety behavior (Hong, Surienty, and Hung, 2011; Saat, Subramaniam, and Shamsudin, 2016; Subramaniam, Shamsudin, Zin, Ramalu, and Hassan, 2016). This means that, in SMEs, these dimensions directly affect safety behavior. However, these studies did not include safety knowledge and motivation in their models.

SMEs have a unique safety climate, which is why their safety behavior characteristics may also be unique and influenced by the relationship between workers, as well as their relationships with their employers (owners), in order to avoid social hierarchy (Marlow and Patton, 2002; Sørensen, Hasle, and Bach, 2007; Croucher, Stumbitz, Quinlan, and Vickers, 2013), since the nature of the interaction between workers and employers during operational activities (Legg, Olsen, Laird, and Hasle, 2015) and any firm-related cordial relationships among them lead to a paternalistic culture in safety management (Croucher *et al.*, 2013). The owners are the manager, regardless of their experiences or educational background (Croucher *et al.*, 2013). Therefore, the safety climate that describes the workers' shared perceptions regarding a safe atmosphere is highly influenced by the owner's subjectivity. Subsequently, safety practices tend to be compromised (Kheni, Gibb, and Dainty, 2010), irrespective of whether the workers have adequate knowledge and motivation.

As a developing country, the number of accidents in Indonesia is still high, and increases have been reported during the last three years, which seems to be related to poor safety measures (Huda, Sukmawati, and Sumertajaya, 2016). In this study, we focused on metal manufacturing SMEs, which were selected due to their significant contribution to the nation's economic growth (Harncharoen, Isahak, Kaewboonchoo, Low, and Ratanasiripong, 2016). Additionally, the number of accidents that occur in this industry is quite high (Suprianto and Evendi, 2015; Ansori, Widyanti, and Sutalaksana, 2018), which is mostly due to a lack of safety behavior of the workers' part.

Safety behavior model for metal-mechanical companies was proposed by Paolillo, Silva, and Pasini (2016). Unfortunately, the study was carried out in large-scale industries. Their model showed that safety motivation mediates the relationship between safety climate and participation. Previously, Sinclair, Martin, and Sears (2008) stated that safety motivation and knowledge are the

intervening factors that mediate the influence of safety climate on safety behavior. Therefore, we argue that there is an opportunity for further development of the safety behavior model, specifically for SMEs in metal manufacture. The purposes of this study were to investigate the effect of safety climate, motivation, and knowledge on safety compliance and participation in Indonesian metal manufacturing SMEs.

## Conceptual Model

This study adopted the model by Neal *et al.* (2000), as shown in Figure 1. The model states that safety climate influences knowledge, motivation, and participation. On the other hand, it has an indirect influence on safety compliance. It should be noted that this model was developed based on a large-scale industry in Australia, and an adjustment should be made for the field under study. We hypothesized that there should be a direct effect on safety compliance, which is due to the differences between the safety climate characteristics of large industries and SMEs. Informal and personal working conditions in SMEs might lead to individual work climate (Hasle and Limborg, 2006; Perrini, Russo, and Tencati, 2007; Martin, 2012). Subsequently, the implementation of safety measures may be difficult due to the extreme flexibility of work rules (Mihail, 2004; Rothenberg *et al.*, 2016).

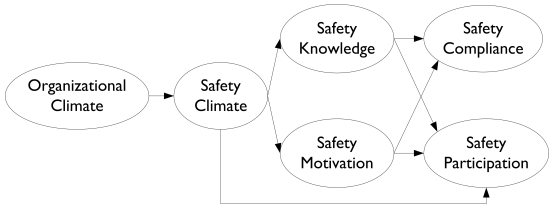


**Figure 1.** Safety behavior model.
**Source:** Neal *et al.* (2000)

Conversely, work climate is influenced by the subjectivity of workers, colleagues, and superiors or employers. Therefore, we proposed that safety climate may directly influence safety behavior in SMEs, as shown in Figure 2, which is consistent with previous studies (Hong *et al.*, 2011; Saat *et al.*, 2016; Subramaniam *et al.*, 2016). The model was also adjusted based on the consideration that the cordial relationship between workers, and between them and their superiors leads to a lack of social hierarchy in SMEs (Marlow and Patton, 2002; Sørensen *et al.*, 2007; Croucher *et al.*, 2013). This is consistent with the study carried out by Turner, Stride, Carter, McCaughey, and Carroll (2012), which stated that safety climate (namely, decision latitude and social support) directly affects safety behavior.

Previous studies on safety behavior in SMEs indicated varying results for the effects of safety climate on compliance and participation (Subramaniam *et al.*, 2016, Saat *et al.*, 2016, Neal *et al.* 2000). We hypothesized that there should be direct effects of safety climate on safety behaviors, which is based on a study on safety behavior in small-scale industries carried out by Guo, Yiu, and Gonzalez (2018), where safety climate is represented by social support and production pressure.

The integration of person and situation-related factors in SMEs needs to be carried out due to their unique characteristics. Mihail (2004) and Rothenberg *et al.* (2016) stated that the safety climate of SMEs is relatively informal and personal. Subsequently, it is difficult to objectively implement safety measures, given the excessive flexibility of work rules. Furthermore, the commitment of SME management is generally based on the personality, beliefs, or values of owners-managers in order to ensure that most decisions regarding effective working conditions are their responsibility (Croucher, *et al.*, 2013). The high level of cordial relations tends to compromise safety rules and procedures, which, in turn, can compromise occupational safety and health (OSH) implementation (Croucher, *et al.*, 2013). Therefore, the proposed model aims to examine the direct impact of safety climates on compliance and participation.

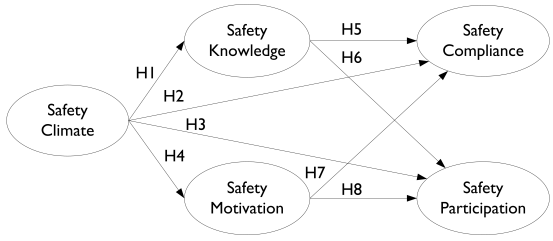


**Figure 2.** Proposed Conceptual Model.
**Source:** Adapted from Neal *et al.* (2000)

In short, we proposed eight hypotheses, as shown in in Figure 2, namely:

- *H1:* Safety climate positively influences safety knowledge.
- *H2:* Safety climate positively influences safety compliance.
- *H3:* Safety climate positively influences safety participation.
- *H4:* Safety climate positively influences safety motivation.
- *H5:* Safety knowledge positively influences safety compliance.
- *H6:* Safety knowledge positively influences safety participation.
- *H7:* Safety motivation positively influences safety compliance.
- *H8:* Safety motivation positively influences safety participation.

## Method

### *Respondents*

This study involved 100 respondents from 23 metal SMEs with voluntary participations (mean age = 35, 40 years,

SD = 7,76 years and average experience = 10,96 years, SD = 7,03 years). The sample size was considered to be sufficient according to Hair, Hult, Ringle, and Sarstedt (2017), based on the number of independent and latent variables. The demographic data of the respondents are shown in Table 1.

**Table 1.** Demographic data of respondents

| Description | N | % | Total (%) |
|---|---|---|---|
| *Age group (year)* | | | |
| 16-29 | 24 | (24) | |
| 30-39 | 43 | (43) | |
| 40-49 | 30 | (30) | |
| 50-59 | 3 | (3) | |
| 60-69 | 0 | (0) | |
| | | | (100) |
| *Work experience (year)* | | | |
| Less than 3 | 15 | (15) | |
| 3 to 7 | 19 | (19) | |
| More than 7 | 66 | (66) | |
| | | | (100) |
| *Education* | | | |
| No Formal Education | 0 | (0) | |
| Elementary School | 12 | (12) | |
| High School (Junior) | 17 | (17) | |
| High School (Senior) | 56 | (56) | |
| University/College | 15 | (15) | |
| | | | (100) |
| *Relationship with the owner* | | | |
| Family | 21 | (21) | |
| Neighbor | 10 | (10) | |
| Friend | 6 | (6) | |
| Other | 63 | (63) | |
| | | | (100) |

**Source:** Authors

## *Questionnaire*

A questionnaire was developed based on previous studies, consisting of 3 questions on safety climate (Neal *et al.*, 2000; Neal and Griffin, 2006), 6 questions on safety knowledge (Guo, Yiu, and Gonzalez, 2016; Mohammadfam *et al.*, 2017; Guo *et al.*, 2018), 5 questions on safety motivation (Neal and Griffin, 2006; Vinodkumar and Bhasi, 2010; Guo *et al.*, 2016, 2018), 7 questions on safety compliance (Guo *et al.*, 2016; Lu and Kuo, 2016; Subramaniam *et al.*, 2016; Guo et al., 2018), and 5 questions on safety participation (Guo *et al.*, 2016; Subramaniam *et al.*, 2016; Guo *et al.*, 2018). The question items were constructed using a modified Likert scale, starting from 1 (strongly disagree) to 5 (strongly agree), as well as from 1 (never) to 6 (always), respectively, as shown in Table 2.

**Table 2.** The item in the questionnaire

| Constructs | Question Item | Reference |
|---|---|---|
| Safety Climate (SCI) | 3 | Neal *et al.* (2000), Neal and Griffin (2006) |
| Safety Motivation (SM) | 5 | Neal and Griffin (2006), Vinodkumar and Bhasi (2010), Guo *et al.* (2016), Guo *et al.* (2018) |
| Safety Knowledge (SK) | 6 | Guo *et al.* (2016), Mohammadfam *et al.* (2017), Guo *et al.* (2018) |
| Safety Compliance (SC) | 7 | Guo *et al.* (2016), Lu and Kuo (2016), Subramaniam *et al.* (2016), Guo *et al.* (2018) |
| Safety Participation (SP) | 5 | Subramaniam *et al.* (2016), Guo *et al.* (2016), Guo *et al.* (2018) |

**Source:** Authors

The questionnaire was formatted in Bahasa (Indonesian language) using a back-translation procedure, which involved three bilinguals who translated the original version to English. A comparison between the original and back-translated versions was applied to test the validity of the translation. The descriptive items or questions for each factor in the developed model are shown in Table 3.

**Table 3.** Descriptive analysis

| Constructs/Associated Items | | Initial | Mean | Standard Deviation |
|---|---|---|---|---|
| *Safety Climate* | | SCI | 3,70 | 1,28 |
| 1 | The SME emphasizes the implementation of health and safety in the work area | SCI1 | 3,62 | 1,35 |
| 2 | Safety is treated high priority by the SME | SCI2 | 4,01 | 1,17 |
| 3 | The SME sees safety as something important | SCI3 | 3,47 | 1,33 |
| *Safety Motivation* | | SM | 3,66 | 1,23 |
| 1 | I enjoy work when working safely at work | SM1 | 3,92 | 1,15 |
| 2 | I feel uncomfortable when it does not work safely | SM2 | 3,66 | 1,26 |
| 3 | I feel guilty when I do not work safely | SM3 | 3,57 | 1,21 |
| 4 | I feel the need to make efforts to reduce accidents and incidents at work | SM4 | 3,48 | 1,26 |
| 5 | I find it useful when maintaining or enhancing my safety | SM5 | 3,69 | 1,28 |
| *Safety Knowledge* | | SK | 4,00 | 0,82 |
| 1 | I know how to use work tools and machinery in a safe manner | SK1 | 4,10 | 0,73 |
| 2 | I know how to maintain or improve health and safety at work | SK2 | 4,16 | 0,68 |
| 3 | I know how to reduce the risk of accidents and incidents at work | SK3 | 4,11 | 0,69 |

| | Constructs/Associated Items | Initial | Mean | Standard Deviation |
|---|---|---|---|---|
| 4 | I am aware of the hazard precautions when doing work | SK4 | 4,13 | 0,77 |
| 5 | I understand the safety rules of my job | SK5 | 3,54 | 1,25 |
| 6 | I understand my job safety procedures | SK6 | 3,50 | 1,24 |
| *Safety Compliance* | | SC | 3,73 | 1,86 |
| 1 | How often do I wear a safety helmet in the designated areas? | SC1 | 3,26 | 2,25 |
| 2 | How often do I wear eye protection in the designated areas? | SC2 | 3,74 | 1,91 |
| 3 | How often do I wear the right PPE (e.g., gloves, safety shoes) when working on or near the electricity? | SC3 | 4,44 | 1,57 |
| 4 | How often do I wear PPE (e.g., safety belt) when working at height? | SC4 | 3,05 | 2,17 |
| 5 | How often do I follow the correct safety rules when doing work? | SC5 | 3,99 | 1,77 |
| 6 | How often do I follow the correct safety procedures while doing work? | SC6 | 3,93 | 1,74 |
| 7 | How often do I not neglect safety even when I am in a hurry? | SC7 | 3,67 | 1,65 |
| *Safety Participation* | | SP | 4,09 | 1,30 |
| 1 | How often do I talk and encourage colleagues to become involved in resolving safety issues? | SP1 | 4,18 | 1,18 |
| 2 | How often do I try to change the way of work to make it safer? | SP2 | 3,90 | 1,38 |
| 3 | How often do I take action to stop a safety breach to protect the safety of my coworkers? | SP3 | 3,77 | 1,38 |
| 4 | How often do I report to the SMEs' manager when there are safety-related problems? | SP4 | 4,31 | 1,24 |
| 5 | How often do I volunteer to carry out work or activities to help improve safety in the workplace? | SP5 | 4,29 | 1,30 |

**Source:** Authors

### *Procedure*

After obtaining permission from the owners of the SMEs, the workers were requested to answer the questionnaires. Informed consent was obtained before the respondents filled out the questionnaire, and they were assisted when they encountered any difficulties.

### *Data analysis*

First, the validity and reliability analyses were carried out to ensure the quality of the model. Its validity was assessed using factor loading, in which the value of 0,7 or higher indicated that it was good. Second, the confirmatory factor analysis (CFA) was carried out using the Partial Least Squares Structural Equation Modeling (PLS-SEM) to ensure that the related items were grouped in a construct, in accordance with the path relation to determine their significant influences. Third, the variance inflation factor (VIF) was applied to ascertain whether there was no common method bias in the construct's collinearity statistics. Finally, the model's goodness of fit was assessed using the chi-square, and the Standardized Root Mean Square Residual (SRMR). The PLS-SEM was used to analyze the data obtained by using Smart-PLS.3 to detect abnormal distribution.

## Results and Discussion

This study was aimed to evaluate the effect of situation (safety climate) and person-related factors (safety motivation and knowledge) on safety behavior (safety compliance and participation). Additionally, person-related factors served as a mediator between safety climate and behavior. The results of this study showed that safety climate was affected by safety knowledge, motivation, compliance, and participation. Subsequently, safety knowledge and motivation mediated the relationship between safety climate and behavior. Safety knowledge only affected compliance, whereas motivation tended to affect both compliance and participation. There was no common method bias among all the constructs.

The validity of our test results refers to a measurement model that was evaluated based on the loading factor shown in Table 4. Statistically, the loading factor conforms to the validity test when the outer loading has a minimum of 0,7 (Hair *et al.*, 2017). However, most of the values obtained were greater than 0,7, which showed that the model was extremely valid. The CFA (*i.e.*, greater than 0,757) showed that the constructs, namely safety climate, motivation, knowledge, compliance, and participation, were properly explained by the indicators.

The results from the reliability test are shown in Table 5. The Cronbach's alpha needed to be greater than 0,6, while the average variance extracted (AVE) needed to be more than 0,5, and the composite reliability had to be a minimum of 0,7 (Hair *et al.*, 2017). All parameters met the stipulated requirements.

The empirical model is shown in Figure 3, while the results are shown in Table 6. A coefficient of determination ($R^2$) of 0,696 and 0,483 showed that the variance in safety compliance and participation is moderately explained by the independent variables, namely, safety climate, knowledge, and motivation.

We found that safety climate had a positive influence on both compliance and participation. This result is consistent with the studies carried out by Seo *et al.* (2015), Shin *et al.* (2015), and Panuwatwanich *et al.* (2016). The positive effect proves that an improved safe atmosphere in SMEs tends to increase the workers' compliance and participation. These results are in line with the studies carried out on SMEs in several countries, such as in Malaysia and China (Liu, Mei, and Shen, 2010; Saat *et al.*, 2016; Subramaniam *et al.*, 2016). Subramaniam *et al.* (2016) carried out detailed research on the safety climate construct based on management commitment, training, and safety regulations. Conversely, Saat *et al.* (2016) defined it as a form of worker involvement, training, management commitment,

**Table 4.** Outer loading of indicators

| Indicators | Constructs | | | | |
|---|---|---|---|---|---|
| | Safety Climate (SCl) | Safety Motivation (SM) | Safety Knowledge (SK) | Safety Compliance (SC) | Safety Participation (SP) |
| SCl1 | 0,946 | | | | |
| SCl2 | 0,915 | | | | |
| SCl3 | 0,932 | | | | |
| SM1 | | 0,861 | | | |
| SM2 | | 0,834 | | | |
| SM3 | | 0,954 | | | |
| SM4 | | 0,935 | | | |
| SM5 | | 0,907 | | | |
| SK1 | | | 0,757 | | |
| SK2 | | | 0,815 | | |
| SK3 | | | 0,778 | | |
| SK4 | | | 0,766 | | |
| SK5 | | | 0,898 | | |
| SK6 | | | 0,906 | | |
| SC1 | | | | 0,950 | |
| SC2 | | | | 0,914 | |
| SC3 | | | | 0,802 | |
| SC4 | | | | 0,899 | |
| SC5 | | | | 0,962 | |
| SC6 | | | | 0,963 | |
| SC7 | | | | 0,780 | |
| SP1 | | | | | 0,782 |
| SP2 | | | | | 0,905 |
| SP3 | | | | | 0,894 |
| SP4 | | | | | 0,778 |
| SP5 | | | | | 0,861 |

**Source:** Authors

**Table 5.** Reliability of factors

| Factors | Cronbach's Alpha | Composite Reliability | Average Variance Extracted (AVE) |
|---|---|---|---|
| Safety Climate (SCl) | 0,924 | 0,951 | 0,867 |
| Safety Motivation (SM) | 0,940 | 0,955 | 0,808 |
| Safety Knowledge (SK) | 0,905 | 0,926 | 0,676 |
| Safety Compliance (SC) | 0,959 | 0,967 | 0,807 |
| Safety Participation (SP) | 0,901 | 0,926 | 0,716 |

**Source:** Authors

and communication. On the contrary, Liu *et al.* (2010) reported that it generally affects safety behavior. Additionally, Saat *et al.* (2016) and Liu *et al.* (2010) elaborated a systematic review of safety behavior in SME studies in Malaysia and China. Subramaniam *et al.* (2016) carried out an empirical study based on SME behavior in Malaysia. However, because China and Malaysia are developing countries, there is a possibility that the characteristics of their SMEs are similar to those in Indonesia. Therefore, the result from this research enriches literature centered on SMEs in developing countries.

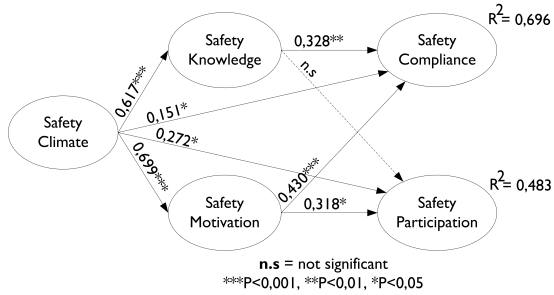


**Figure 3.** Empirical model.
**Source:** Authors

Safety climate has a positive influence on both knowledge and motivation. This confirms that shared perceptions regarding safety procedures, policies, and practices in SMEs positively impact knowledge and motivation. This finding is consistent with the research carried out by Guo *et al.* (2018) regarding small-scale industries, which stated that social support and production pressure influence both knowledge and motivation as aspects of safety climate.

**Table 6.** Result of structural model

| Hypothesis | Path | $\beta$ | T Statistics | P Values | Sig. |
|---|---|---|---|---|---|
| H1 | Safety Climate -> Safety Knowledge | 0,617 | 8,499 | 0,000 | *** |
| H2 | Safety Climate -> Safety Compliance | 0,151 | 2,004 | 0,045 | * |
| H3 | Safety Climate -> Safety Participation | 0,272 | 2,285 | 0,022 | * |
| H4 | Safety Climate -> Safety Motivation | 0,699 | 10,656 | 0,000 | *** |
| H5 | Safety Knowledge -> Safety Compliance | 0,328 | 3,481 | 0,001 | ** |
| H6 | Safety Knowledge -> Safety Participation | 0,182 | 1,448 | 0,148 | n.s |
| H7 | Safety Motivation -> Safety Compliance | 0,430 | 4,292 | 0,000 | *** |
| H8 | Safety Motivation -> Safety Participation | 0,318 | 1,963 | 0,050 | * |

**Note:** $\beta$ = path coefficient, ***P < 0,001, **P < 0,01, *P < 0,05, n.s = not significant
**Source:** Authors

Furthermore, we found that safety knowledge has a positive influence on compliance. This is consistent with the studies carried out by Amponsah-Tawaih and Adu (2016) and Guo *et al.* (2016, 2018). However, safety knowledge did not influence safety participation. This result is different from the one obtained from the initial model developed by Neal *et al.* (2000), which shows that an increased understanding of safety improves compliance with safety rules and work procedures, excluding participation or involvement.

Safety motivation has a positive effect on both compliance and participation. This result is consistent with the studies carried out by Vinodkumar and Bhasi (2010), Shin *et al.* (2015), and Mohammadfam *et al.* (2017). This implies that, when the workers are motivated, they tend to be consistent

with safety procedures and work settlement. Therefore, increased motivation triggers participation in terms of helping colleagues, promoting, and improving workplace safety initiatives.

Meanwhile, this study shows mediating constructs (namely, knowledge and motivation) from safety climate to safety behavior. This result is consistent with the research carried out by Sinclair *et al*. (2008), which stated that motivation and knowledge are the intervening factors that mediate the influence of safety climate on safety behavior.

In short, situation-related (safety climate) and person-related factors (motivation and knowledge) affect safety behavior (compliance and participation). The managerial implications of this research are to improve the safety behavior of SMEs workers through enhancing safety climate, safety motivation, and safety knowledge. Conversely, to improve safety behavior performance, SMEs need to consider the improvement all of them.

In the context of PLS-SEM, the common-method variance is detected through the full collinearity assessment approach (Kock, 2015). The variance inflation factor (VIF) shows the collinearity assessment. Its values need to be lower than 5. However, if it is higher, it implies a potential collinearity problem (Hair, Ringle, and Sarstedt, 2011). Table 7 shows the value of the VIF for all constructs, and all their correlation has a VIF value of less than 5, which indicates there is no common-method bias.

**Table 7.** The variance inflation factor (VIF)

| Constructs | SCl | SC | SM | SP | SK |
|---|---|---|---|---|---|
| Safety Climate (SCI) | | 1,983 | 1,000 | 1,983 | 1,000 |
| Safety Compliance (SC) | | | | | |
| Safety Motivation (SM) | | 3,618 | | 3,618 | |
| Safety Participation (SP) | | | | | |
| Safety Knowledge (SK) | | 2,984 | | 2,984 | |

**Source:** Authors

Finally, the goodness of fit (GoF) for the model is shown in Table 8. The chi-square is 933,598, which implies a high level of fit. Based on the research carried out by Wetzels, Odekerken-Schröder, and Oppen (2009), the chi-square started from 0,25, which is either less than, equal to, or greater than 0,36, which is presumed to be large. The standardized root means square residual (SRMR) is 0,093. However, when the SRMR is ≤ 0,10, the model is reported to have a good fit because Henseler *et al*. (2014) stated that it serves as a goodness of fit measure for PLS-SEM.

This study has certain limitations: firstly, it has a limited number of samples, which is due to restricted permits; second, the data collection was limited to the East Java province. Further study involving more samples is therefore needed. Irrespective of its limitations, this study generally offers a valuable novel contribution in field of SMEs, particularly those in Indonesia. Moreover, this study provides empirical data on safety climate, motivation, knowledge, and relationships. The managerial implications are based on the fact that, to improve the safety behavior of SME workers, it is necessary to consider both situation-related and person-related factors.

**Table 8.** The goodness of fit (GoF)

| GoF method | Value | Cut off value | Goodness |
|---|---|---|---|
| Chi-square | 933,598 | ≥ 0,36 *) | Large |
| SRMR | 0,093 | ≤ 0,10 **) | Good fit |

**Note:** *) Based on Wetzels *et al*. (2009). **) Based on Henseler *et al*. (2014).
**Source:** Authors

## Conclusions

Safety climate has a positive influence on knowledge, motivation, compliance, and participation. In addition, knowledge and motivation mediate the relationship between safety climate and behavior (namely, compliance and participation). Safety knowledge affects only compliance, whereas motivation affects both compliance and participation.

## Acknowledgements

The authors would like to thank The Indonesia Endowment Fund for Education (LPDP) - Ministry of Finance for funding research through a doctoral program scholarship.

## References

Al-Hemoud, A. M., and Al-Asfoor, M. M. (2006). A behavior-based safety approach at a Kuwait research institution. *Journal of Safety Research*, *37*(2), 201-206. 10.1016/j.jsr.2005.11.006

Amponsah-Tawaih, K. and Adu, M. A. (2016). Work pressure and safety behaviors among health workers in Ghana: The moderating role of management commitment to safety. *Safety and Health at Work*, *7*(4), 340-346. 10.1016/j.shaw.2016.05.00

Ansori, N., Widyanti, A., and Sutalaksana, I. Z. (2018). *Safety Outcomes in Small-Size and Medium-Size Metal Enterprises in Indonesia: Are They Different?* [Paper presentation] International Conference on Industrial Engineering and Engineering Management (IEEM), Thailand. 10.1109/IEEM.2018.8607746

Baser, F., Ture, H., Abubakirova, A., Sanlier, N., and Cil, B. (2016). Structural modeling of the relationship among food safety knowledge, attitude, and behavior of Hotel Staff in Turkey. *Food Control, 73*(B), 438-444. 10.1016/j.foodcont.2016.08.032

Campbell, J. P., McCloy, R. A., Oppler, S. H., and Sager, C. E. (1993). A theory of performance. In N. Schmitt, W. C. Borman, and Associates (Eds.) *Personnel selection in organizations* (pp. 35-70). San Francisco: Jossey-Bass.

Christian, M. S., Bradley, J. C., Wallace, J. C., and Burke, M. J. (2009). Workplace safety: A meta-analysis of the roles of

person and situation factors. *Journal of Applied Psychology*, *94*, 1103-1127. 10.1037/a0016172

Croucher, R., Stumbitz, B., Quinlan, M., and Vickers, I. (2013). *Can better working conditions improve the performance of SMEs? An international literature review*. Geneva, Italy: International Labor Office.

Geller, E.S. (2001). *Psychology of safety Handbook*. Boca Raton, FL: CRC Press.

Griffin, M. A. and Neal, A. (2000). Perceptions of safety at work: a framework for linking safety climate to safety performance, knowledge, and motivation. *Journal of Occupational Health Psychology, 5*(3), 347-358. 10.1037/1076-8998.5.3.347

Guo, B. H. W., Yiu, T. W., and Gonzalez, V. A. (2016). Predicting safety behavior in the construction industry: Development and test of an integrative model. *Safety Science*, *84*, 1-11. 10.1016/j.ssci.2015.11.020

Guo, B. H. W., Yiu, T. W., and Gonzalez, V. A. (2018). Does company size matter? Validation of an integrative model of safety behavior across small and large construction companies. *Journal of Safety Research*, *64*, 73-81. 10.1016/j.jsr.2017.12.003

Hair, J. F., Ringle, C. M., and Sarstedt, M. (2011). PLS-SEM: Indeed a silver bullet. *Journal of Marketing Theory and Practice, 19,* 139-151. 10.2753/MTP1069-6679190202

Hair, J. F., Hult, G. T. M., Ringle, C. M., and Sarstedt, M. (2017). *A primer on partial least squares structural equation modeling* (*PLS-SEM*). Thousand Oaks, CA: SAGE Publishing.

Harncharoen, K., Isahak, M., Kaewboonchoo, O., Low, W.Y., and Ratanasiripong, P. (2016). Workplace Environment and Quality of Life of SME Workers: A Systematic Review. *Asia Journal of Public Health, 7*(2), 64-81. https://www.ph.mahidol.ac.th/phep/kitiphong_2016.pdf

Hasle, P., and Limborg, H. J. (2006). A review of the literature on preventive occupational health and safety activities in small enterprises. *Industrial Health*, *44*(1), 6-12. 10.2486/indhealth.44.6

Henseler, J., Dijkstra, T. K., Sarstedt, M., Ringle, C. M., Diamantopoulos, A., Straub, D. W., and Calantone, R. J. (2014). Common Beliefs and Reality About PLS: Comments on Ronkko and Evermann (2013). *Organizational Research Methods*, *17*(2), 182–209. 10.1177/1094428114526928

Hong, K. T., Surienty, L., and Hung, D. K. M. (2011). Safety management practices and safety behavior: A preliminary investigation in Malaysian Small and Medium Enterprises in Northern Corridor Economic Region (NCER). *Journal Occupational Safety and Health*, *8*, 1-11.

Huda, U. F., Sukmawati, A., and Sumertajaya, I. M. (2016). Model perilaku keselamatan kerja karyawan pada industri berisiko tinggi. *Jurnal Manajemen Teknologi*, *15*, 51-66. 10.12695/jmt.2016.15.1.4

Khandan, M., Maghsoudipour, M., Vosoughi, S., and Kavousi, A. (2013). Safety climate and prediction of ergonomic behaviour. *International Journal of Occupational Safety and Ergonomics, 19*(4), 523-530. 10.1080/10803548.2013.11077018

Kheni, N. A., Gibb, A. G. F., and Dainty, A. R. J. (2010). Health and safety management within Small and Medium Sized Enterprises (SMEs) in developing countries: Study of contextual influences, *Journal of Construction Engineering and Management, 136*(10), 1104-1115. 10.1061/_ASCE_CO.1943-7862.0000218

Kock, N. (2015). Common method bias in PLS-SEM: A full collinearity assessment approach. *International Journal of e-Collaboration* (*IJeC*), *11*(4), 1-10. 10.4018/ijec.2015100101

Kopelman, R. E., Brief, A. P., and Guzzo, R. A. (1990). The role of climate and culture in productivity. In Schneider, B. (Ed.), *Organizational Climate and Culture* (pp. 282-318). San Francisco, CA: Jossey-Bass.

Legg, S. J., Olsen, K. B., Laird, I. S., and Hasle, P. (2015). Managing safety in small and medium enterprises, *Safety Science*, *71*(C), 189-196. 10.1016/j.ssci.2014.11.007

Liu, S., Mei, Q., and Shen, B. (2010). *A safety management mode for Small and medium sized enterprise based of safety behavior*. [Paper presentation] International Conference on E-Business and E-Government. 10.1109/ICEE.2010.598

Lu, C. and Kuo, S. (2016). The effect of job stress on self-reported safety behavior in container terminal operations: The moderating role of emotional intelligence. *Transportation Research, F*(7), 10-26. 10.1016/j.trf.2015.12.008

Martin, E. (2012). Employment relationship in the small firm: Revisiting orientations to work, *International Journal of Hospitality Management, 31*(4), 1318-1326. 10.1016/j.ijhm.2012.03.015

Marlow, S. and Patton, D. (2002). Minding the gap between employers and employees: The challenge for owner-managers of smaller manufacturing firms. *Employee Relations, 24*(5), 523-539. 10.1108/01425450210443294

Mihail, D. M. (2004). Labour flexibility in Greek SMEs. *Personnel Review*, *33*(5), 549-560. 10.1108/00483480410550152

Mohammadfam, I., Ghasemi, F., Kalatpour, O., and Moghimbeigi, A. (2017). Constructing a bayesian network model for improving safety behavior of employees at workplaces. *Applied Ergonomics*, *58*, 35-47. 10.1016/j.apergo.2016.05.006

Neal, A. and Griffin, M. A. (2006). A study of the lagged relationships among safety climate, safety motivation, safety behavior, and accidents at the individual and group levels. *Journal of Applied Psychology*, *91*(4), 946-953. 10.1037/0021-9010.91.4.946

Neal, A., Griffin, M.A., and Hart, P.M. (2000). The impact of organizational climate on safety climate and individual behavior. *Safety Science*, *34*(1-3), 99-109. 10.1016/S0925-7535(00)00008-4

Panuwatwanich, K., Al-Haadir, S., and Stewart, R.A. (2016). Influence of safety motivation and climate on safety behavior and outcomes: Evidence form the Saudi Arabian Construction Industry. *International Journal of Occupational Safety and Ergonomics*, *23*(1), 60-75. 10.1080/10803548.2016.1235424

Perrini, F., Russo, A., and Tencati, A. (2007). CSR strategies of SMEs and large firms, Evidence from Italy. *Journal of Business Ethics, 74*(3), 285-300. 10.1007/s10551-006-9235-x

Paolillo, A., Silva, S. A., and Pasini, M. (2016). Promoting safety participation through diversity and inclusion climates. *International Journal of Workplace Health Management*, *9*(3), 308-327. 10.1108/IJWHM-01-2015-0002

Rothenberg, A. D., Gaduh, A., Burger, N. E., Chazali, C., Tjandraningsih, I., Radikun, R., Sutera, C., and Weilant, S. (2016). Rethinking Indonesia's informal sector. *World Development*, *80*, 96-113. 10.1016/j.worlddev.2015.11.005

Saat, M. Z. M., Subramaniam, C., and Shamsudin, F. M. (2016). A proposed relationship between organizational safety practices and safety performance in the manufacturing of small and medium enterprises in Malaysia. *Sains Humanika*, *8*, 91-97. 10.11113/sh.v8n4-2.1066

Seo, H. C., Lee, Y. S., Kim, J. J., and Jee, N. Y. (2015). Analyzing safety behavior of temporary construction workers using structural equation modeling. *Safety Science*, *77*, 160-168. 10.1016/j.ssci.2015.03.010

Shin, D., Gwak, H., and Lee, D. (2015). Modeling the predictors of safety behavior in construction workers. *International Journal of Occupational Safety and Ergonomics*, *21*(3), 298-311. 10.1080/10803548.2015.1085164

Sinclair, R. R., Martin, J. E., and Sears, L. E. (2008). Labor unions and safety climate: Perceived union safety values and retail employee safety outcomes. *Accident Analysis and Prevention*, *42*(5), 1477-1487. 10.1016/j.aap.2009.11.003

Sørensen, O. H., Hasle, P., and Bach, E. (2007). Working in small enterprises – Is there a special risk? *Safety Science*, *45*(10), 1044-1059. 10.1016/j.ssci.2006.09.005

Subramaniam, C., Shamsudin, F. M., Zin, M. L., Ramalu, S. S., and Hassan, Z. (2016). The influence of safety management practices on safety behavior: A study among manufacturing SMES in Malaysia. *International Journal of Supply Chain Management*, *5*, 148-160. http://repo.uum.edu.my/21443/1/IJCM%205%204%202016%20148%20160.pdf

Suprianto, R., and Evendi, A. (2015). Kepatuhan Pemakaian Alat Pelindung Diri pada Pekerja Las di Indramayu. *Jurnal Kesehatan Masyarakat*, *1*, 14-18. https://docplayer.info/35683794-Kepatuhan-pemakaian-alat-pelindung-diri-pada-pekerja-las-di-indramayu.html

Turner, N., Stride, C. B., Carter, A. J., McCaughey, D., and Carroll, A. E., (2012). Job Demands–Control–Support model and employee safety performance. *Accident Analysis and Prevention*, *45*, 811-817. 10.1016/j.aap.2011.07.005

Vinodkumar, M. N., and Bhasi, M. (2010). Safety management practices and safety behavior: Assessing the mediating role of safety knowledge and motivation. *Accident Analysis and Prevention*, *42*(6), 2082-2093. 10.1016/j.aap.2010.06.021

Wallace, J. C. (2016). Creating a safety conscious organization and workforce. *Organizational Dynamics*, *45*(4), 305-312. 10.1016/j.orgdyn.2016.10.006

Wetzels, M., Odekerken-Schröder, G., and Oppen, C. V. (2009). Using PLS path modeling for assessing hierarchical construct models: Guidelines and empirical illustration. *MIS Quarterly*, *33*(1), 177-195. 10.2307/20650284

Xu, X. and Shi, J. (2017). Research on the factors affecting safety behavior based on interpretative structural modeling. *Cluster Computing*, *20*, 1573-7543. 10.1007/s10586-017-1228-2

Research Article / Mechanical Engineering, Mechatronics, and Materials Science https://doi.org/10.15446/ing.investig.v41n3.85756

# Design and Analysis of a Bulge Test Device

## Diseño y análisis de un dispositivo para ensayos Bulge

Luis Humberto Martínez Palmeth[1], María Angelica Gonzales Carmona[2], and José Miranda Castro[3]

**ABSTRACT**

The aim of this work is to present the methodological process to design a device capable of performing Bulge tests. This kind of device allows obtaining more information about the plastic behavior of a material than the one provided by a traditional tensile test. The engineering specifications of the device were evaluated through the QFD methodology. Then, a basic design of the device was performed based on available analytical models such as thick-walled pressure vessel theory, annular plate theory, and a basic plasticity model for the biaxial stress state. Later, a detailed design of the device was proposed, which was evaluated by means of a 3D model of finite elements and a linear-static analysis for the main components. Finally, a 2D axisymmetric model and a dynamic non-linear analysis were performed to validate the proposed design. The main novelty of the work consists of articulating the methodology of the mechanical design process and the conception, design, and validation of a Bulge device while solving the deficiencies found in the literature regarding the design and validation processes of this type of devices.

**Keywords:** mechanical design, Bulge test, sheet metal, mechanical characterization, plastic behavior

**RESUMEN**

El objetivo de este trabajo es presentar el proceso metodológico para diseñar un dispositivo capaz de realizar ensayos Bulge. Este tipo de dispositivos permite obtener más información del comportamiento plástico de un material que la proporcionada por un ensayo de tensión tradicional. Se evaluaron los requerimientos de diseño del dispositivo a través de la metodología QFD. Seguidamente se realizó un diseño básico del dispositivo basado en modelos analíticos disponibles como la teoría de recipientes a presión de pared gruesa, la teoría de placas anulares y un modelo de plasticidad básico para el estado biaxial de esfuerzo. Luego, se propuso un diseño detallado del dispositivo, el cual fue evaluado mediante un modelo 3D de elementos finitos y un análisis lineal-estático para los componentes principales. Finalmente, se realizaron un modelo axisimétrico 2D y un análisis no-lineal para validar el diseño propuesto. La novedad principal del trabajo consiste en articular la metodología del proceso de diseño mecánico y la concepción, diseño y validación de un dispositivo Bulge, solventando las carencias encontradas en la literatura en cuanto a procesos de diseño y validación de este tipo de dispositivos.

**Palabras clave:** diseño mecánico, ensayo Bulge, lámina metálica, caracterización mecánica, comportamiento plástico

**Received:** March 18th, 2020
**Accepted:** March 15th, 2021

## Introduction

From the literature of manufacturing processes, it is widely known that the aerospace and automotive industries, to name a few, are based on metal forming processes such as forging, extrusion, stamping, bending, etc. (Groover, 2019). In order to design these processes, it is necessary to know the elasto-plastic behavior of the employed materials. To this effect, the material must be experimentally characterized. This helps to prevent and correct failure during manufacturing processes or phenomena such as springback of the parts. Plastic behavior is characterized by the curve equivalent of stress against equivalent plastic strain, $\sigma_{eq}$ vs $\varepsilon_{eq}^{p}$ (Calladine, 2016). The most frequently used method to obtain this curve are tensile tests, where it is possible to obtain information about the elastoplastic behavior of materials, up to the beginning of the localized necking. This limits the obtained information on the plastic behavior to low levels of equivalent plastic strain, around 30%, in the most ductile materials. However, to properly design a forging or deep drawing process, information must be available up to an equivalent plastic strain around 80%, which is impossible to obtain through a tensile test in the most ductile materials (Rees, 2012). On the other hand, by means of a Bulge test, the phenomenon of localized necking is delayed, and equivalent plastic strain levels can be obtained around 60%, which offers more information about the plastic behavior of materials (Lăzărescu, Nicodim, Ciobanu, Comşa, and Banabic, 2013).

In Figure 1, plastic behavior curves for AA5754-O, obtained by means of tensile and Bulge tests, are compared. The

[1]Ph.D. in Mechanical Engineering, Universidad de Sevilla, España. Affiliation: Assistant professor, Universidad Surcolombiana, Colombia. E-mail: luis.martinez@usco.edu.co
[2]Ph.D. in Mechanical Engineering, Universidad Federal de Pernambuco, Brazil. Affiliation: Assistant professor, Institución Universitaria ITSA, Colombia. E-mail: magonzalezc@itsa.edu.co
[3]Mechanical Engineering, Universidad Antonio Nariño, Colombia. Affiliation: Independent researcher. E-mail: josemiranda@uan.edu.co

**How to cite:** Martínez-Palmeth, L. H. González-Carmona, M. A. Miranda-Castro, J. (2021). Design and Analysis of a Bulge Test Device. *Ingeniería e Investigación*, *41*(3), e85756. 10.15446/ing.investig.v41n3.85756

maximum value of equivalent plastic strain reached was around 18% for the tensile test, while the Bulge test reported levels of 40%. All the above reflects the need to have an experimental capacity that allows performing this type of test. Therefore, in this paper, the methodological and design processes followed to obtain a device capable of carrying out Bulge test are presented.

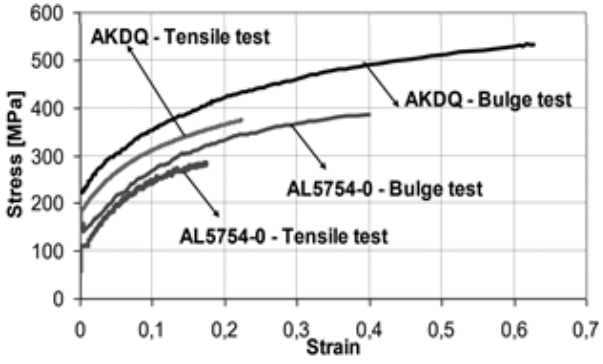


**Figure 1.** Comparison between curves $\sigma eq$ vs $\varepsilon eqp$ obtained by tensile and Bulge tests.
**Source:** Altan, Palaniswamy, Bortot, Heidl, and Bechtold, 2006.

## Methods

Bulge tests consist of taking a sheet metal with a circular shape, pressing it by means of dies (die and blank holder) and then applying pressurized fluid, which causes the specimen test to deform. As the pressure increases due to a hydraulic pumping system, the specimen continues to deform until it breaks.

Figure 2 shows a test scheme and how a sheet metal adopts a spherical shape that induces a biaxial stress and strain states at the pole of bulge (Lăzărescu *et al.*, 2013).

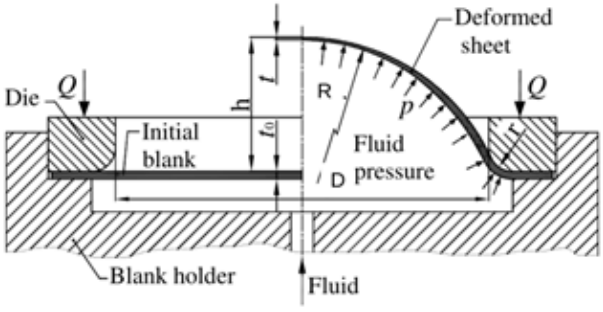


**Figure 2.** Diagram of a Bulge test.
**Source:** Lăzărescu *et al.*, 2013.

First, a bibliographic review of the literature was carried out, where some experimental prototypes designed to perform Bulge test were found (López-Panal, 2015; Moses and Payam, 2015; Mersch, 2013; Wei Koh, 2008; Vasilescu, 2016). From this review, initial range values were obtained for some design parameters, such as the operating pressure ($p$), initial sheet thickness ($t_o$), die aperture ($D$), the outer diameter of the tools ($D_t$), tool thickness ($t_t$), and drawbead diameter ($D_b$). A summary of these parameters can be found in Table 1. All prototypes are cylindrical, thick-walled vessels, subject to high pressure, and they have at least 3 pieces, while some have a protective structure for users. All prototypes are designed to test sheet metals for automotive purposes (High Strength Steel (HSS) and Advanced High Strength Steel (AHSS)). These prototypes must induce stresses around 1 200 MPa in the specimens (Davies, 2012). These parameters serve as input for the Quality Function Deployment (QFD), which was used in this work as a methodology to define engineering specifications for prototypes and guide the morphology of design alternatives (Ullman, 2017).

**Table 1.** Values of design parameters values found in the literature

| | $P$ (MPa) | $D$ (mm) | $D_t$ (mm) | $D_b$ (mm) | $t_t$ (mm) | $t_o$ (mm) |
|---|---|---|---|---|---|---|
| Range values | 21-60 | 100-152 | 188-230 | 113-191 | 14 - 30 | 2 |

**Source:** Authors

A matrix was obtained by applying the QFD methodology. It is shown in Table 2, where customer needs (7 in total) and their weighting are described, as well as engineering specifications (9 in total), which are generated from customer needs.

**Table 2.** Matrix generated through the QFD methodology: customer needs vs. engineering specifications

| QFD matrix for the experimental prototype designed.<br><br>9 = strongly related.<br>3 = moderately related.<br>1 = weakly related.<br>blank = not related at all. | Laboratory Assistants; technicians, technologists, engineers, students. | Maximum stress reached | Maximum Sheet thickness | Safety factors | Number of operations to perform a test. | Time to prepare the device for testing. | Number of parts that make up the device | Number of manufacturing processes | Outer diameter of the device | Total height of the device |
|---|---|---|---|---|---|---|---|---|---|---|
| | | ↑ | ↑ | ↑ | ↓ | ↓ | ↓ | ↓ | ↓ | ↓ |
| | | MPa | mm | Qty | Qty | s | Qty | Qty | mm | mm |
| **Able to break metal sheets for automotive and aerospace use** | 30 | 9 | 3 | 3 | | | | | | |
| **Easy to use** | 15 | | | | 9 | 9 | 9 | | | |
| **Safe to use** | 20 | | | 9 | 3 | | | | | |
| **Low maintenance** | 5 | | | | | | 3 | | | |
| **Easy to manufacture** | 10 | | | | | | 3 | 9 | | |
| **Economic** | 15 | | | | | | 3 | 9 | 9 | 9 |
| **Compact** | 5 | | | | | | 3 | | 9 | 9 |

| [6] | ◊ | 1 - the prototype does not meet the requirement at all. |
|---|---|---|
| [7] | ○ | 2 - the product complies slightly with the requirement. |
| [8] | ● | 3 - the product meets the requirement partially. |
| [9] | □ | 4 - the product meets the requirement almost always. |
| [10] | ▪ | 5 - the product meets the |

| 1 | 2 | 3 | 4 | 5 |
|---|---|---|---|---|
| | | | ●□ | ◊○▪ |
| | ◊ | ○ | □▪ | ● |
| | | ◊▪ | ●□ | ○ |
| | | | | ◊○▪●□ |
| ○ | ▪ | ◊ | ●□ | |
| ○ | ▪ | ◊ | □ | ● |
| ▪ | ○ | | ◊● | □ |

**Source:** Authors

The percentage weight of the customer's needs must amount to 100% by adding the weights given in the table for each need. For example, for low maintenance, the percentage weight is 5%. Considering the above, the most important need is the ability to break materials with automotive and aerospace applications (30% weight). The main objective of these specifications is to translate the customer's needs into engineering language, thus allowing to quantify needs. To evaluate the adequacy of proposed engineering specifications in relation to the customer's needs, the scale shown in Table 2 was adopted, where the number 9 means that a engineering specification is closely related to the need, and, if it is blank, it means that this specification does not contribute in any way to satisfy the customer's need. From Table 2, there are four requirements that greatly influence the design: the number of parts in the device, the external diameter of the device, the

number of manufacturing processes needed to fabricate the device, and the desired safety factor.

Likewise, another part of the QFD matrix is seen in Table 3. In addition to customer needs, there is the level of compliance with experimental prototypes found in the literature in relation to requirements (1 to 5). This scale allows identifying the flaws and benefits of each design (benchmark). In this case, it can be observed that some prototypes presented in the literature (Mersch, 2013; Wei Koh, 2008) are alternatives that adequately meet most of the requirements. In this work, these designs have been taken as a base to develop the design process and meet the initial requirements.

In Figure 10, a CAD model for the proposed design is presented. The device consists of two parts: a die and a blank holder. The die has a drawbead, whose main function is to prevent that specimen from slipping once the test has started, since the working fluid is pressurized, and the specimen starts to deform.

**Table 3.** Matrix generated through the QFD methodology: customer needs vs. weighting of the experimental designs found

| | QFD matrix for the experimental prototype designed.<br><br>9 = strongly related.<br>3 = moderately related.<br>1 = weakly related.<br>blank = not related at all. | Laboratory Assistants: technicians, technologists, engineers, students. | Engineering Specifications | | | | | | | | |
|---|---|---|---|---|---|---|---|---|---|---|---|
| | | | Maximum stress reached | Maximum Sheet thickness | Safety factors | Number of operations to perform a test. | Time to prepare the device for testing. | Number of parts that make up the device | Number of manufacturing processes | Outer diameter of the device | Total height of the device |
| | | | ↑ | ↑ | ↑ | ↓ | ↓ | ↓ | ↓ | ↓ | ↓ |
| | | | MPa | mm | Qty | Qty | s | Qty | Qty | mm | mm |
| Customer Needs | Able to break metal sheets for automotive and aerospace use | 30 | 9 | 3 | 3 | | | | | | |
| | Easy to use | 15 | | | | 9 | 9 | 9 | | | |
| | Safe to use | 20 | | | 9 | 3 | | | | | |
| | Low maintenance | 5 | | | | | | 3 | | | |
| | Easy to manufacture | 10 | | | | | | 3 | 9 | | |
| | Economic | 15 | | | | | | 3 | 9 | 9 | 9 |
| | Compact | 5 | | | | | | 3 | | 9 | 9 |

**Source:** Authors

The blank holder has a hole in its lower part where for the pressurized fluid, as well as a cavity to contain fluid. Finally, the blank holder has a groove to house a gasket in order to ensure tightness during the test.

To achieve the proposed design for the die and blank holder, the following steps were followed:

- An initial wall thickness was estimated for a hollow cylindrical container considering safety factors, the material to be used, and thick-walled pressure vessel theory.
- The grade, number, and dimension of the bolts necessary for the most critical test conditions were calculated.
- A functional geometry was proposed (with drawbead, bolt flange, groove, and fluid inlet hole)
- Stresses and strains in the die and blank holder were verified using a finite element model (linear and static analysis).
- A simulation of the closing stage of tools (die and blank holder) was carried out in the presence of a specimen through a finite element analysis (non-linear dynamic analysis).
- Finally, a suitable gasket was selected for the device (this procedure is not presented in this article).
- Once all the above was defined, stresses and strains in tools were verified again.

## Preliminary design: analytical models

### *Bulge Test*

Having defined the engineering specifications, the construction parameters of device had to be estimated. To achieve this, an analytical model of a Bulge test had to be evaluated. In this work a model proposed by Rees was used (Rees, 2012), where the maximum equivalent stress ($\sigma_{eq}$) present in specimen test can be estimated. This stress is a function of fluid pressure during the test ($p$). Additionally, the maximum equivalent plastic strain ($\varepsilon_{eq}^{p}$), present in specimen test can be estimated as a function of the maximum height reached by the specimen during the test ($h$). The model includes other parameters such as the final thickness of the specimen ($t$), the radius of curvature for the specimen near maximum height ($R$), and die aperture ($D$). In Figure 3, there is a scheme with the most significant model parameters.

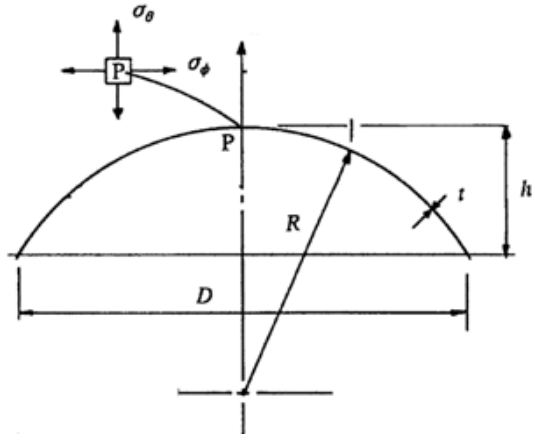


**Figure 3.** Hydraulic Bulge test geometry.
**Source:** Rees, 2012.

As shown above, a sheet metal takes an approximate spherical shape when subjected to hydrostatic pressure, which generates a biaxial stress condition at the highest point ($P$) of the sheet metal. Additionally, the specimen is very thin compared to its radius ($\frac{t}{R} \ll \frac{1}{10}$), and it can be considered as a thin-walled pressure vessel (Mott and Untener, 2017).

Therefore, stresses in the material are related to internal pressure through Equation 1:

$$\sigma = \sigma_\theta = \sigma_\phi = \frac{pR}{2t} \quad (1)$$

where $\sigma$ is the stress at the highest point of the dome ($P$), which is equal in all directions, since it is assumed that sheet metal adopts an approximately spherical shape, even though a small error is induced by assuming this (Rees, 2012).

If volume conservation is assumed during the deformation process of sheet metal, the initial material volume can be related to the final material volume. Assuming that the thickness of sheet metal is thinned in the same way (*i.e.* throughout all of sheet metal), a small error is induced (Djavanroodi, Riahi, and Janbakhsh, 2013). Thus, an expression is obtained for the final sheet metal thickness ($t$):

$$t = \frac{D^2 t_o}{8Rh} \quad (2)$$

By estimating the final sheet metal thickness, the plastic strain of sheet metal at the highest point ($P$) of the specimen can be quantified. Similarly, it is necessary to obtain an expression that relates the radius adopted by the sheet metals under pressure ($R$) and some test parameters such as the height of the dome ($h$) and die aperture ($D$). An equation was proposed by Hill (Djavanroodi *et al.*, 2013):

$$R = \frac{h^2 + (D/2)^2}{2h} \quad (3)$$

Based on Equations (I) to (3) and taking values in Table 1 as reference (limits), values were defined for the operating pressure ($p$) and die aperture ($D$) that allow reaching stress values in the specimens ($\sigma$) of around 700 MPa, enough to break most HSS and AHSS. The value of 700 MPa was set for economic reasons, given that, if a higher level of stress is required, a hydraulic unit capable of providing more pressure is needed, and, therefore, the device becomes more expensive. On the other hand, die aperture can be enlarged to achieve a higher stress level for a given system pressure. The problem with this is that it increases the cost of the device and its size.

According to the literature, the maximum possible thickness for sheet metal to be considered thin is 2 mm. Because of this, the maximum initial thickness ($t_o$) to be considered was this value. The maximum height of the dome ($h$) depends on the ductility of the material. Additionally, during the design process of the device, it can serve as a parameter. In the literature, it is found that, for ductile and automotive materials, the maximum height is in the range of 35-55 mm. Therefore, a maximum design value of $h$ = 60 mm was chosen. This allows the proposed device to test very ductile materials, even if they are not for automotive use. Die aperture ($D$) was estimated to be the range of 100-152 mm (see Table I). A value was chosen to make the device as small as possible, but without making the operating pressure value too high, thus resulting in a suitable value of $D$ = 130 mm.

Therefore, the design parameters were defined as follows: $\sigma$ = 700 MPa, $t_o$ = 2 mm, $h$ = 60 mm, $D$ = 130 mmm. The selected values for maximum dome height ($h$) and die aperture ($D$) were then replaced in Equation (3), and the radius of the sphere ($R$) was obtained. Next, the $R$ value and the initial sheet metal thickness ($t_o$) were replaced in Equation (2), and the final sheet metal thickness value ($t$) was calculated. Finally, the $t$, $R$, and $\sigma$ values were replaced in Equation (1), thus obtaining the system pressure ($p$). The values selected for the parameters in the proposed design are shown in Table 4.

**Table 4.** Proposed values for the design parameters

| $p$ (MPa) | $t_o$ (mm) | $D$ (mm) | $h$ (mm) | $R$ (mm) | $t$ (mm) | $\sigma_{vm}$ (MPa) |
|---|---|---|---|---|---|---|
| 23,20 | 2,00 | 130,00 | 60 | 65,21 | 1,1 | 700,5 |

**Source:** Authors

## *Blank Holder*

The basic design of the device began with the dimensioning of the blank holder. To this effect, the thick-walled pressure vessel theory was used. This part was modeled as a hollow cylindrical vessel subjected to an internal working pressure; tangential ($\sigma_t$) and radial ($\sigma_r$) stresses had to be calculated using the following Equations (Budynas and Nisbett , 2015):

$$\sigma_t = \frac{r_i^2 p}{r_o^2 - r_i^2}\left(1 + \frac{r_o^2}{r^2}\right) \quad (4)$$

$$\sigma_r = \frac{r_i^2 p}{r_o^2 - r_i^2}\left(1 - \frac{r_o^2}{r^2}\right) \quad (5)$$

The basic *a priori* design parameter was the internal radius of the vessel, $r_i = D/2$ = 65 mm, as set out in the methodological design. Additionally, a minimum safety factor was set, $n$ = 4, as advised in literature (Mott and Untener, 2017). SAE/AISI 1 020 steel was selected in an annealed state, which has an elastic limit of $S_y$ = 294 MPa and a tensile strength of $S_{ut}$ = 411 MPa. This material was selected due to commercial and economic limitations. Results obtained by using Equations (4) and (5) are shown in Table 5.

**Table 5.** Preliminary stress analysis values for blank holder

| $p$ (MPa) | $r_i$ (mm) | $t$ (mm) | $r_o$ (mm) | $r$ (mm) | $\sigma_t$ (MPa) | $\sigma_r$ (MPa) | $n$ |
|---|---|---|---|---|---|---|---|
| 23,2 | 65 | 32 | 97 | 65 | 61 | 23,2 | 4 |

**Source:** Authors

As it can be seen, the safety factor agrees with the values reported in the literature for this type of pressure vessel. For this, the must be a thickness of $t$ = 32 mm on the thinnest wall. At the same time, the outer diameter of the raw material was defined, which in this case must be at least $r_o$ = 194 mm (7⅝ inches).

### *Die*

To achieve initial sizing of the die, it was modeled as a plate subjected to bending load as shown in Figure 4. It was assumed that Die is fixed near the bolts and that pressure is applied to the die faceup (specimen testing transmits pressure to the die).

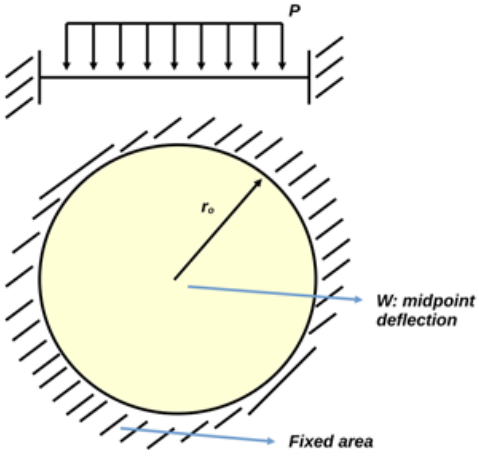


**Figure 4.** Scheme of the analytical model used for the die's pre-dimensioning.
**Source:** Authors

For this configuration, the maximum deflection ($w_{\max}$) and maximum stress ($\sigma_{\max}$) present in die were obtained through the following Equations (Young, Budynas, and Sadegh, 2012):

$$w_{\max} = \frac{pr_o^4}{64Z} \tag{6}$$

$$\sigma_{\max} = \frac{3(1+v)pr_o^2}{8h^2} \tag{7}$$

where $Z$ is calculated by:

$$Z = \frac{Et^3}{12(1-v^2)} \tag{8}$$

For the model, the operating pressure ($p$) was 23,2 MPa, and the die aperture ($D = r_o$) was 65 mm. The usual values of elastic constants for steels were used, $E$ = 200 GPa and $v$ = 0,3 (Young's modulus and Poisson's ratio). The values in Table 6 were obtained using Equations (6), (7), and (8).

**Table 6.** Preliminary stress analysis values for the die

| $p$ (MPa) | $r_o$ (mm) | $t$ (mm) | $\sigma_y$ (MPa) | $W$ (mm) | $\sigma$ (MPa) | $n$ |
|---|---|---|---|---|---|---|
| 23,2 | 65 | 25 | 294 | 0,0226 | 76 | 4 |

**Source:** Authors

Here, it was observed that a thickness of 25 mm was needed for the die to obtain a safety factor of 4. This configuration generates a maximum stress of 76 MPa in the fixed area.

### *Bolted joints*

Once the basic designs for the tools were defined, the number of bolts needed to provide an appropriate clamping force on the specimen had to be calculated, in order to prevent the bolted joint from separating during testing at maximum design pressure. Furthermore, there had to be enough bolts to avoid failure by tension (Brown, Morrow, Durbin, and Baca, 2008). All the above was quantified using three safety factors: the bolt yielding factor ($n_p$), the bolt load factor ($n_L$), and the joint separation factor ($n_o$). The objective was to define the degree, quantity, and nominal diameter of bolts to be used in device. This was achieved by finding the combination of parameters that satisfied all safety factors mentioned above.

Table 7 shows the most important parameters for the design of bolted joint, such as the maximum design pressure and the number of bolts in the design. SAE 8 grade bolts were selected with a nominal diameter of 1/2 in, since they have a minimum proof resistance of 270 MPa.

**Table 7.** Parameters for bolted joint design

| Design data | | Bolt SAE grade 8 | | Bolted joint properties | | Safety factors | | |
|---|---|---|---|---|---|---|---|---|
| P (MPa) | # bolt | d (mm) | Sp (MPa) | C | Ti (N· m) | $n_p$ | $n_L$ | $n_o$ |
| 23,2 | 14 | 12,7 | 270 | 0,13 | 216 | 1,2 | 6,5 | 2,9 |

**Source:** Authors

Calculations showed that the stiffness constant for the joints (C) was 0,13, and the tightening torque ($T_i$) was 216 N·m, which resulted in the safety factors shown in Table 7. Finally, the bolted joints would have a total of 14 bolts for maximum design pressure.

## Design evaluation: computational tools

### *FE model for tools (blank holder and die)*

As a result of the process, the design shown in Figure 10 was obtained. As can be seen, this design has sections where stress concentrations occur. It is necessary to propose a finite element model that allows a more accurate evaluation of stresses, strains, and displacements that may occur in the tools. To this effect, CADs, finite element models, and their respective simulations were made with Solidworks® to evaluate mechanical behavior of tools under maximum load conditions. Static-linear analyses were performed, as well as their respective convergence analysis. The material selected for the tools was an AISI 1 020 in an annealed state, modeled by an isotropic behavior. A mesh based on curvature was also used.

In Figure 5, the evolution of von Mises stress is shown at critical points vs. the number of elements present in each model. Critical points are presented at point D for the blank holder and at point A for the die (Figures 7 and 9, respectively).

As noted, in the case of the die, at least 100 000 elements had to be used to obtain an acceptable response, whereas the blank holder was quite unaffected by the size of the mesh in the model. This is due to the critical places for tools to occur

in different zones. For the blank holder, the critical point is at the bottom of tank, just where fillet radius is quite large. This means that when meshing with curvature control while having few elements in the model, there are few elements in the critical zone. As the number of elements in the model increases, there are more elements in this critical zone. Therefore, the blank holder is sensitive to the total number of elements in the model. As for the die, the critical point occurs in the holes made for the bolts because the fillet radius is smaller, and the meshing control is based on curvature. From the beginning, the critical zone is meshed with many elements. This means that, as the number of elements in the model increases, the critical zone does not necessarily have more elements. Therefore, the die is insensitive to the number of elements in the model.

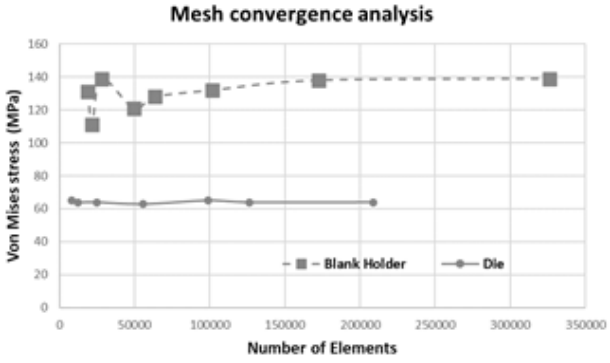


**Figure 5.** Mesh sensitivity analysis in models.
**Source:** Authors

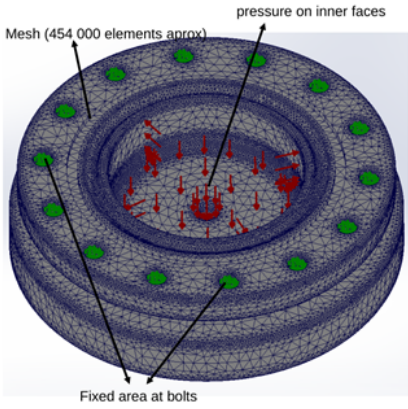


**Figure 6.** Meshing, boundary conditions, and loads on the blank Holder.
**Source:** Authors

## *Blank Holder Analysis*

This stage began with the computational evaluation of the detailed design of the blank holder. The model was fixed in the bolt area, and pressure was applied to the internal faces of its blank holder, as shown in Figure 6, where the mesh used for the evaluation of stresses and strains can also be observed.

On the other hand, in Figure 7, the stress field on the blank holder is presented. The greatest stress values occurred at

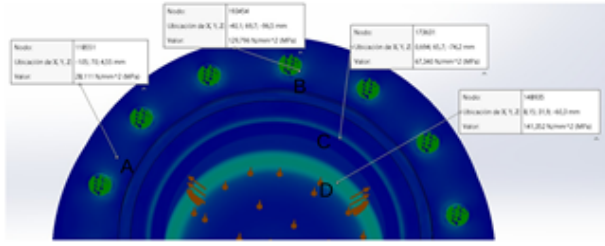


**Figure 7.** Stress field on the blank holder.
**Source:** Authors

the bottom of the blank holder. The critical point was at point D. The largest von Mises stress was around 141 MPa, thus obtaining a safety factor of about 2 (the yield limit was 294 MPa). This value was half of that predicted by the analytical model, but it was still safe because the device would fail at the bolted joint first before breaking the blank holder. The safety factor value in the analytical model was not obtained because stress concentration was not considered, as it was done in the numerical model. It was also observed that, at point C, located at the vessel wall, the stress was 67 MPa. This agrees with the value predicted in Equation (4) for tangential stress.

## *Die analysis*

In Figure 8, the loads and boundary conditions can be observed, as well as the mesh used for the evaluation of stresses and strains. The die is fixed near the bolts. The effect of force exerted by the specimen on the inner face of the die is modeled with a point load applied to its centroid.

In Figure 9, the stress field for the die is presented, where the maximum von Mises stress occurs in a place close to the holes for the bolts and whose maximum value is around 63 MPa (point A in the Figure). This value agrees with the results of the analytical model mentioned in the preliminary design section (Table 6). Therefore, the same safety factor was obtained, which is around 4.

Considering the above, it has been verified that the finite element models proposed for both tools were correctly performed and evaluated since both analytical and numerical models converge in practically equal results.

## *Bulge test simulation*

Figure 10 shows the proposed design of the device and its main features (die, blank holder, bolt holes, gasket groove, drawbead, and fluid inlet hole). The objective of this simulation is to verify that a stress of 700 MPa can be reached in the specimens with proposed parameters $(p, D, t_o, h)$. Additionally, the purpose of this process is to simulate the closing stage of tools to validate aspects of the design such as the drawbead.

To this effect, a finite element model for the Bulge test (device and test specimen) were made. Computational simulations were performed in the Solidworks® simulation environment. A 2D axisymmetric model of the original 3D model was constructed, which generally reduces the computational cost

of simulations. A non-linear dynamic analysis was chosen to simulate the Bulge test. The meshing was performed based on curvature with meshing control on the test specimen, as can be seen in Figure 11. About 10 000 elements were used in the model.

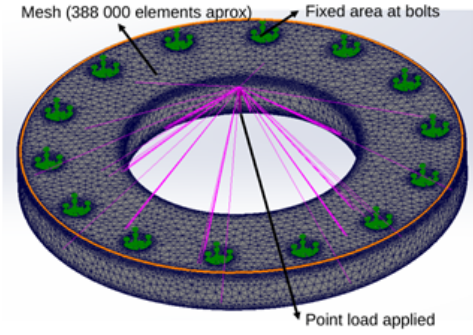


**Figure 8.** Meshing, boundary conditions, and loads on the die.
**Source:** Authors

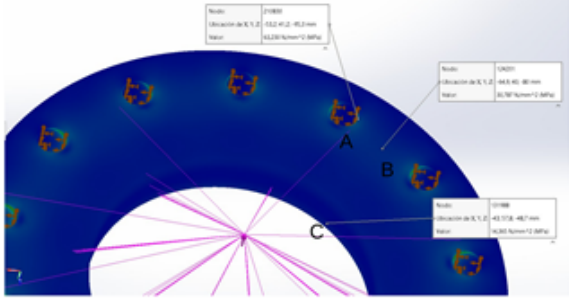


**Figure 9.** Stress field on the die.
**Source:** Authors

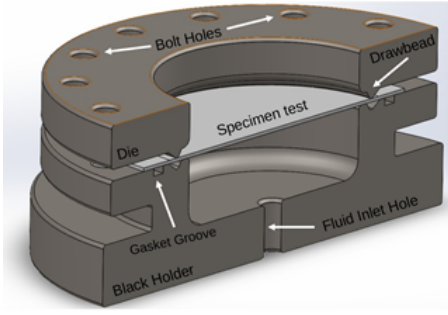


**Figure 10.** CAD model of the proposed device.
**Source:** Authors

Figure 11 shows the boundary conditions and loads proposed in the model. Initially, there is symmetry with respect to the vertical axis in the center of the device. For the blank holder, there is a restriction of zero movement in all directions. All these restrictions were made to facilitate the convergence of the simulations. Also, what happens to the specimen is more important for this study instead of what happens to the tools, which were previously validated. For the die, there is a restriction of movement in the vertical axis of about 1,5 millimeters downward, and horizontal movement is not allowed. This is the first stage of the simulation and is maintained until the end. Finally, pressure is applied on the inner face of the specimen, which is the second stage of the simulation.

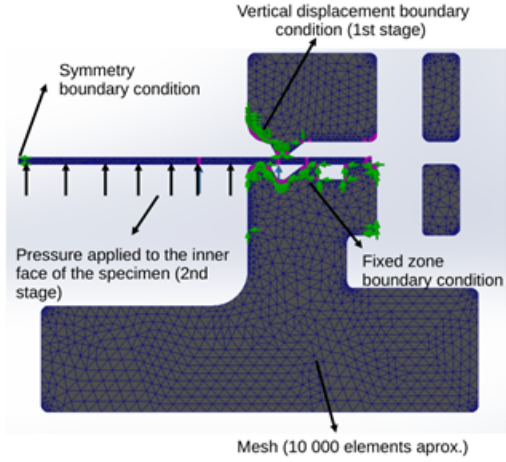


**Figure 11.** Mesh used in the simulations and mesh control in the specimen and in the contact area.
**Source:** Authors

For the computational simulations of the Bulge test, a material with tensile strength of about 700 MPa was chosen, which is the maximum stress induced with the proposed device. For this, DP600 steel was chosen. To model the plastic behavior of the specimen, the Solidworks® von Mises plasticity model was used, which allowed modeling the plastic hardening part with a mixed behavior between isotropic and kinematic hardening for flow curve.

In the first instance, the model (von Mises) selected of the specimen was suitable for modeling materials with isotropic material behavior. However, it is well known that sheet metals exhibit an anisotropic behavior. Therefore, if it is required to consider such behavior, plastic behavior data are needed in three preferred directions, which usually are in the 0°, 45°, and 90° angles with respect to the original rolling direction (Martínez, Martínez, Vallellano, Centeno, and García, 2013). However, since the model receives a single behavior curve, we decided to take an averaged curve of the three previously mentioned directions, which were taken from the work by Ozturk, Toros, and Kilic (2009). The values used are reported in Table 8.

Once the computational simulations of the Bulge test were carried out, it was found that the proposed design can perform the test without problems. One of the usual problems in this type of design is that the drawbead induces premature failure of the test piece in the clamping area, which did not happen in this case. The maximum displacement reached during the simulation was around 28,9 mm at the height of the dome. In the literature, dome heights reported for DP600 steels are in accordance with the simulation results (Ramazani, Abbasib, Prahl, and Blecka, 2012).

The stress field in the specimen was also obtained during this stage, which is shown in Figure 12 for the last solution

**Table 8.** Experimental data of DP600 steel

| Tensile direction | Sut [MPa] | Sy [MPa] | Elongation [%] |
|---|---|---|---|
| **0°** | 687,25 | 350,84 | 21 |
| **45°** | 713,29 | 348,94 | 22,5 |
| **90°** | 720,87 | 355,17 | 22,2 |
| **Average** | 707,14 | 351,65 | 21,9 |

**Source:** Authors

step in the simulation. The maximum stress value that was reported in the highest zone of the specimen (biaxial zone) were 700 MPa, with which the process of failure should begin in the specimen, since fractures occur in the biaxial zone practically at the same time as in the localized necking (Martínez, Martínez, and Vallellano, 2019; Martínez, Martínez, Borrego, Morales, and Vallellano, 2019).

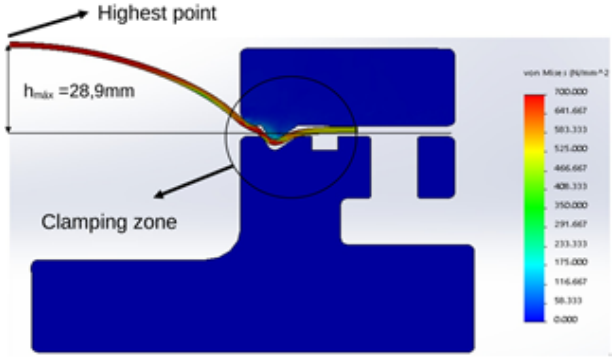


**Figure 12.** Stress field in the specimen during the simulation.
**Source:** Authors

## Conclusions

In this work, the QFD methodology was applied, and a relevant matrix was proposed for the process of conception and basic and detailed design of a device that allows performing Bulge tests. Likewise, we found the engineering specifications that the device must have to perform tests on sheet metals for the automotive and aerospace industries. Results show that there are 9 potential customer needs and 7 engineering specifications. The most important engineering specification is the number of parts in the device, which greatly affects its cost. Additionally, size was found to indirectly influence the cost of the equipment by influencing the operating pressure of the system, which can drastically increase the costs associated with the use of the equipment.

Then, the prototype's basic design was proposed, based on analytical models of Bulge test and the theory of thick-walled pressure vessels. From these models, a pre-dimensioning was obtained, conditional on the safety factor of 4 that was used. It was found that a wall thickness of at least 25 mm was required for tools when using AISI 1020 steel to reach a pressure of 23 MPa. This allows inducing a stress of at least 700 MPa during specimen testing. When designing the bolted joint, it was found that it is sufficient to use 14 SAE grade 8 bolts, which affect the structural integrity of the tools. Subsequently, with this pre-sizing, a detailed design was made. It includes a drawbead, a groove for a gasket, and an oil reservoir for fluid testing. This detailed design is computationally valid, and it was found that the radius of agreement of the bottom of the blank holder and the number of holes to accommodate bolts in the die are design constraints and create a strong stress concentration. However, while performing static analysis of stresses and strains, it was verified that the safety factors are below 4. On the other hand, it was found that the curvature-based meshing used in Solidworks is very efficient and allows keeping the number of total elements of a model at low levels while still obtaining adequate stress and strain values.

Finally, the functionality of the proposed design was evaluated, through the computational simulation of the Bulge test, which was performed in the Solidworks® simulation environment through a non-linear dynamic analysis. An isotropic behavior of the material (DP600 steel) was assumed. The results of the simulations allowed the proposed design to be approved since the simulations were carried out completely and without causing failure of the specimen in undesired areas. The simulations consisted of two stages. The first stage was the closing of the tools, and the second stage was the deformation of the specimen under pressure, which caused a deformation of about 29 mm in height at the center of the specimen, which was validated with experimental information obtained from literature for DP600 steel. During the simulations, no fracture of the specimen was observed outside the ideal fault zone (close to the dome). This demonstrated that, by means of a 2D axisymmetric model, proper functioning of the proposed tools can be verified. These tools will be manufactured and used to carry out a bulge test for future research.

## References

Altan, T., Palaniswamy, H., Bortot, P., Heidl, W., and Bechtold, A. (2006). Determination of sheet material properties using biaxial bulge tests. In Neugebauer, R. (Ed.) *Proceedings of the 2nd International Conference on Accuracy in Forming Technology* (p. 15). Chemnitz, Germany: Verlag Wissenschaftliche Scripten.

Brown, K., Morrow, C., Durbin, S., and Baca, A. (2008). *Guideline for bolted joint design and analysis.* Albuquerque, NM: Sandia National Laboratories.

Budynas, R. and Nisbett, K. (2015). *Shigley's mechanical engineering design*. New York, NY: McGraw-Hill Education.

Calladine, C. (2016). *Engineering Plasticity: The Commonwealth and International Library: Structures and Solid Body Mechanics Division*. Amsterdam, Netherlands: Elsevier.

Davies, G. (2012). *Materials for automobile bodies.* Oxford: Butterworth-Heinemann, Elsevier.

Djavanroodi, F., Riahi, M., and Janbakhsh, M. (2013). Utilization of bulge and uniaxial tensile tests for determination of flow stress curves of selected anisotropic alloys. *Proceedings*

*of the Institution of Mechanical Engineers, Part L: Journal of Materials: Design and Applications, 227*(1), 38-51. 10.1177/1464420712451963

Groover, M. (2019). *Fundamentals of modern manufacturing: materials processes, and systems* (7th Edition). Hoboken, NJ: John Wiley and Sons.

Hu, J., Duncan, J., and Marciniak, Z. (2002). *Mechanics of sheet metal forming.* Amsterdam, Netherlands: Elsevier.

Kulak, G., Fisher, J., and Struik, J. (2001). *Guide to Design Criteria for Bolted and Riveted Joints.* Chicago, IL: American Institute of Steel Construction.

Lăzărescu, L., Nicodim, I., Ciobanu, I., Comşa, D., and Banabic, D. (2013). Determination of material parameters of sheet metals using the hydraulic bulge test. *Acta Metallurgica Slovaca, 19*(1), 4-12. 10.12776/ams.v19i1.81

Lenzen, M. and Merklein, M. (2018). Improvement of Numerical Modelling Considering Plane Strain Material Characterization with an Elliptic Hydraulic Bulge Test. *Journal of Manufacturing and Materials Processing, 2*(1), 1-20. 10.3390/jmmp2010006

López-Panal, A. (2015.). *Diseño y puesta a punto del ensayo bulge de caracterización de chapa* [Thesis, Universidad de Sevilla, Sevilla, Spain]. http://bibing.us.es/proyectos/abreproy/5587/fichero/Memoria.pdf

Martínez-Donaire, A., Martínez-Palmeth, L., Borrego, M., Morales-Palma, D., and Vallellano, C. (2019). Analysis of the failure of H240LA steel sheets subjected to stretch-bending conditions. *Procedia Manufacturing, 41,* 626-633. 10.1016/j.promfg.2019.09.051

Martínez-Palmeth, L., Martínez-Donaire, A., and Vallellano, C. (2019). Formability limits of high-strength H240LA steel sheets under stress/strain gradients. *Mechanics of Materials, 132,* 47-56. 10.1016/j.mechmat.2019.02.014

Martínez-Palmeth, L., Martínez-Donaire, A., Vallellano Martin, C., Centeno Baez, G., and García-Lomas, F. (2013). Experimental Study of the Formability of H240LA Steel Sheets under Stretch-Bending Conditions. *Key Engineering Materials, 549*, 349-355. 10.4028/www.scientific.net/KEM.549.349

Moses, S. and Payam, M. (2015). Learning Experience in Designing a Hydraulic Bulge Test Setup for Material Properties Characterization. In ASEE (Eds.) *122nd ASEE Annual Conference and Exposition American Society for Engineering* (pp. 1-26). Seattle, WA: ASEE.

Mott, R. and Untener, J. (2017). *Applied strength of materials.* Boca Raton, FL: CRC Press, Tailor and Francis.

Nasser, A., Yadav, A., Pathak, P., and Altan, T. (2010). Determination of the flow stress of five AHSS sheet materials (DP 600, DP 780, DP 780-CR, DP 780-HY and TRIP 780) using the uniaxial tensile and the biaxial Viscous Pressure Bulge (VPB) tests. *Journal of Materials Processing Technologies, 210*(3), 429-436 10.1016/j.jmatprotec.2009.10.003

Ozturk, F., Toros, S., and Kilic, S. (2009). Tensile and spring-back behavior of DP600 advanced high strength steel at warm temperatures. *Journal of Iron and Steel Research International, 16,* 41-46. 10.1016/S1006-706X(10)60025-8

Mersch, J. P. (2013). *On the Hydraulic Bulge Testing of Thin Sheets* [Master's thesis, University of Texas]. https://repositories.lib.utexas.edu/bitstream/handle/2152/23655/MERSCH-THESIS-2013.pdf?sequence=1&isAllowed=y

Ramazani, A., Abbasib, M., Prahl, U., and Blecka, W. (2012). Failure analysis of DP600 steel during the cross-die test. *Computational Materials Science, 64*, 101-105. 10.1016/j.commatsci.2012.01.031

Rees, D. (2012). *Basic engineering plasticity: an introduction with engineering and manufacturing applications*. Amsterdam, Netherlands: Elsevier.

Ullman, D. (2017). *The mechanical design process*. New York, NY: McGraw-Hill.

Vasilescu, M. (2016). *Development of a Hydraulic Bulge Test to Determine the Work Hardening Behaviour of Sheet Materials*. Windsor, Ontario, Canada: Department of Mechanical, Automotive and Materials Engineering, University of Windsor.

Wei Koh, C. (2008). *Design of a Hydraulic Bulge Test Apparatus*. [Master's thesis, Massachusetts Institute of Technology]. http://hdl.handle.net/1721.1/43132

Young, W., Budynas, R. G., and Sadegh, A. (2012). *Roark's Formulas for Stress and Strain.* New York, NY: McGraw-Hill Education.

Research Article / Systems and Computer Engineering https://doi.org/10.15446/ing.investig.v41n3.79308

# Full Model Selection Problem and Pipelines for Time-Series Databases: Contrasting Population-Based and Single-point Search Metaheuristics

## Problema de selección de modelo completo y tuberías para bases de datos de series de tiempo: contrastando metaheurísticas basadas en población y de un solo punto de búsqueda

Nancy Pérez-Castro[1], Héctor Gabriel Acosta-Mesa[2], Efrén Mezura-Montes[3], and Nicandro Cruz-Ramírez[4]

**ABSTRACT**

The increasing production of temporal data, especially time series, has motivated valuable knowledge to understand phenomena or for decision-making. As the availability of algorithms to process data increases, the problem of choosing the most suitable one becomes more prevalent. This problem is known as the Full Model Selection (FMS), which consists of finding an appropriate set of methods and hyperparameter optimization to perform a set of structured tasks as a pipeline. Multiple approaches (based on metaheuristics) have been proposed to address this problem, in which automated pipelines are built for multitasking without much dependence on user knowledge. Most of these approaches propose pipelines to process non-temporal data. Motivated by this, this paper proposes an architecture for finding optimized pipelines for time-series tasks. A micro-differential evolution algorithm ($\mu$-DE, population-based metaheuristic) with different variants and continuous encoding is compared against a local search (LS, single-point search) with binary and mixed encoding. Multiple experiments are carried out to analyze the performance of each approach in ten time-series databases. The final results suggest that the $\mu$-DE approach with *rand/1/bin* variant is useful to find competitive pipelines without sacrificing performance, whereas a local search with binary encoding achieves the lowest misclassification error rates but has the highest computational cost during the training stage.

**Keywords:** full model selection, time series, metaheuristics

**RESUMEN**

La creciente producción de datos temporales, especialmente de series de tiempo, ha motivado la extracción analítica de conocimiento valioso para comprender fenómenos o para la toma de decisiones. A medida que aumenta la disponibilidad de algoritmos para procesar datos, el problema de elegir el más adecuado se vuelve más frecuente. Este problema se conoce como la Selección del Modelo Completo (SMC), que consiste en encontrar un conjunto apropiado de métodos y la optimización de hiperparámetros para realizar un conjunto de tareas estructuradas como una tubería. Se han propuesto múltiples enfoques (basados en metaheurísticas) para abordar este problema, en los que se construyen tuberías automatizadas para realizar múltiples tareas sin mucha dependencia del conocimiento del usuario. La mayoría de estos enfoques proponen tuberías para procesar datos no temporales. Motivado por esto, este artículo propone una arquitectura para encontrar tuberías optimizadas para tareas de series de tiempo. El algoritmo de micro-Evolución Diferencial ($\mu$-ED, metaheurística basada en población) con diferentes variantes y codificación continua, es comparado contra una búsqueda local (BL, búsqueda de un solo punto) con codificación binaria y mixta. Se realizan múltiples experimentos para analizar el rendimiento de cada enfoque en diez bases de datos de series de tiempo. Los resultados finales sugieren que el enfoque de $\mu$-ED con la variante *rand/1/bin* es útil para encontrar tuberías competitivas sin sacrificar el rendimiento, mientras que la BL con codificación binaria logra las tasas de error de clasificación incorrecta más bajas, pero tiene el costo computacional más alto durante la etapa de entrenamiento.

**Palabras clave:** selección del modelo completo, series de tiempo, metaheurísticas

**Received:** April 25th, 2019
**Accepted:** March 18th, 2021

[1]Ph.D. Artificial Intelligence, University of Veracruz Artificial Intelligence Research Institute, México. Affiliation: Graduate of the PhD in Artificial Intelligence, University of Veracruz Artificial Intelligence Research Institute, México. E-mail: naperez@uv.mx
[2]Ph.D. Artificial Intelligence, University of Sheffield, Sheffield, UK. Affiliation: Research Professor, University of Veracruz Artificial Intelligence Research Institute, México. E-mail: heacosta@uv.mx.
[3]Ph.D. Computer Science, Center for Research and Advanced Studies of the National Polytechnic Institute (CINVESTAV-IPN), México. Affiliation: Research Professor, University of Veracruz Artificial Intelligence Research Institute, México. E-mail: emezura@uv.mx
[4]Ph.D. Artificial Intelligence, University of Sheffield, Sheffield, UK. Affiliation: Research Professor, University of Veracruz Artificial Intelligence Research Institute, México. E-mail: ncruz@uv.mx

**How to cite:** Pérez-Castro, N., Acosta-Mesa, H. G., Mezura-Montes, E., Cruz-Ramírez, N. (2021). Full Model Selection Problem and Pipelines for Time-Series Databases: Contrasting Population-Based and Single-Point Search Metaheuristics. *Ingeniería e Investigación*, *41*(3), e79308. https://doi.org/10.15446/ing.investig.v41n3.79308

## Introduction

In recent years, the ability to generate and store data has far outpaced the capability to analyze and exploit it (Rydning 2018). According to Gantza and Reisel (2012), just 3% of global data are currently tagged and ready for manipulation, and only 0,5% of this is used for analysis, at least in 2012.

Therefore, the interest in analyzing and extracting useful information to understand phenomena or for decision-making has brought the attention of practitioners and the research community. The increasing production of temporal data, especially time series, has motivated the analysis for extracting valuable knowledge through knowledge discovery in databases (KDD) processes and data mining (DM) techniques (Sun, Yang, Liu, Chen, Rao, and Bai 2019, Boullé, Dallas, Nakatsukasa, and Samaddar 2020).

Time series are an important class of temporal data objects, and they can be easily obtained from scientific research (Fu 2011) and other domains such as medicine, engineering, earth and planetary sciences, physics and astronomy, mathematics, environmental sciences, biochemistry, genetic and molecular biology, agricultural and biological sciences, among others.

Figure 1 shows a scientific document analysis by subject areas where time series have been used, especially in classification tasks during the last seven years, obtained from the Elsevier-Scopus database, where 7 973 articles were considered.

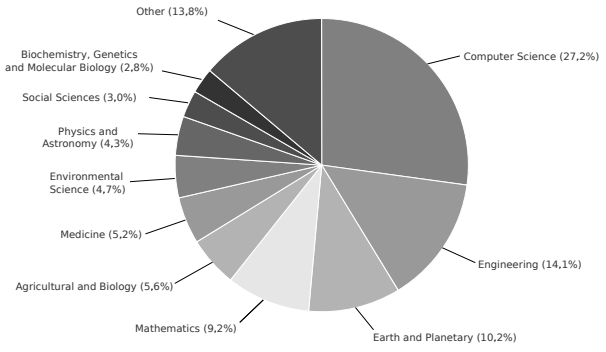


**Figure 1.** Analysis of the time-series usage that has been reported in scientific documents in the last seven years.
**Source:** Authors

Time series $T = (t_1, \ldots, t_n) \in \mathcal{R}$ is the result of the observation of the underlying procedure in which a set of values is collected through measurements made into uniformly spaced time-instants. Therefore, a time series can be defined as an ordered sequence of $n$ real-valued variables (Esling and Agon 2012, Jastrzebska 2019).

A wide variety of DM techniques has been proposed and applied to dealing diverse tasks in domains where time series can be involved (Gong, Chen, Yuan, and Yao 2019, Jastrzebska 2019, Ali, Alqahtani, Jones, and Xie 2019).

However, classical DM techniques often perform poorly in the presence of time-series data, because most of them treat time-series as unrelated data, thus resulting in inaccurate or inconsistent models (Rashid and Hossain 2012).

To overcome the disadvantages of traditional DM techniques with time series, a set of techniques has been proposed which are part of Temporal Data Mining (TDM). TDM has a huge array of techniques for tackling tasks such as query by content, clustering, classification, segmentation, and others (Yang 2017).

When time series data are involved in the data mining process, the quality of the mined data can depend on two important issues: the first is the choice of the appropriate algorithm for a given task, while the second is the proper hyper-parameter selection that may produce a relatively good performance.

Both issues are known as algorithm selection (AS), and model selection (MS), and these are often solved separately. Nevertheless, there are some proposals which have addressed both AS and MS at the same time under the issue known as full model selection (FMS) (Escalante, Montes, and Sucar 2009).

Therefore, FMS consists of finding an appropriate set of methods and their hyperparameter optimization for multitasking. This combination can be represented as a kind of pipeline, characterized by avoiding the dependency on user knowledge (Hutter, Kotthoff, and Vanschoren 2019).

Multiple approaches have been proposed to find automated pipelines according to the hyperparameter optimization process (Yu and Zhu 2020). These approaches can be categorized into three main classes: a) approaches based on exhaustive traditional search (Bergstra and Bengio 2012), b) approaches based on Bayesian optimization (Shahriari, Swersky, Wang, Adams, and de Freitas 2016), and c) approaches based on metaheuristics (Hutter *et al.* 2019).

The first class of these approaches can be impractical and costly because the search focuses on exhaustive exploration defined for a particular block of the pipeline. In contrast to exhaustive approaches, Bayesian approaches keep track of past evaluation results, which they use to find better model settings than random search in fewer iterations. The major drawback of Bayesian optimization approaches is that inference time grows cubically in the number of observations.

Metaheuristics represent a flexible option that has been increasingly used to build optimized pipelines. Population-based metaheuristics such as evolutionary or swarm intelligence algorithms have been adopted to propose an automatic framework that finds streamlined pipelines (Sun, Pfahringer, and Mayo 2013, Olson, Urbanowicz, Andrews, Lavender, Kidd, and Moore 2016, de Sá, Pinto, Oliveira, and Pappa 2017).

Most of the population-based metaheuristic approaches have focused on building pipelines for databases in which the temporary factor is not considered. Therefore, approaches dealing with FMS while involving the building of time series pipelines are scarce.

Single-point search, a part of metaheuristics, has been used for search optimized structures or hyperparameter selection (Aly, Guadagni, and Dugan 2019). Local search is an example of a single-point search that has turned out to be a practical option to solve complex problems despite being the most straightforward.

In this paper, an architecture is proposed for finding an optimized pipeline for time series databases in which the FMS problem is related. It is empirically studied from two points of view: the first, from a population-based approach, where $\mu$-DE is used as a search engine; and the second, from a single-point search, where a local search is adopted.

The main objectives of this work are to empirically study the proposed architecture, varying the search engine and solution encoding; and to offer an alternative that automatically assists the selection of an optimized pipeline for time series database tasks, *i.e.*, to solve the FMS problem for time series.

## Related works

From the literature review, it is essential to note that FMS is not a new trend. Since the 90s, solutions have emerged to deal with the issue of selecting an algorithm from a portfolio of options in order to carry out a single task (Rice 1976).

Subsequently, the need arises to incorporate more tasks into said selection (multi-task) and deal with hyperparameter optimization, resulting in machine learning pipelines (Hutter *et al*. 2019).

Nowadays, learning pipelines are developed to be truly usable by a non-expert. Against this background, a need for automated machine learning (AutoML, a recently coined term) systems can be used to handle various tasks and solve the FMS problem, a challenging and time-consuming process.

Grid search, random search, Bayesian optimization, and metaheuristics are four conventional approaches to building AutoML systems for diverse applications (Bergstra and Bengio 2012). Grid search and random search are traditional hyperparameter optimization methods that could prove impractical to explore high-dimensional spaces at a high computational cost.

Bayesian optimization has been effective in this realm and has even outperformed manual hyperparameter tuning by expert practitioners. Auto-WEKA (Hall *et al*. 2009), mlr (Bischl *et al*. 2016) and auto-SKLearn (Pedregosa *et al*. 2011) are approaches based on Bayesian optimization, and their prime objective is to find the best combination between complete learning pipelines and their respective parameters.

Both approaches follow a hierarchical method that first chooses a particular algorithm and, only after this step, optimizes its parameters. Thus, algorithms may be left out which, with the right hyperparameters, could generate better results than the selected ones.

On the other hand, metaheuristics, especially evolutionary and swarm intelligence algorithms, have gained a particular interest in the research community by allowing the construction of machine learning pipelines that can be complex and extensive.

In the rest of this section, a set of metaheuristics-based approaches for AutoML are described.

### *Metaheuristics-based approaches*

In 2009, Escalante *et al*. (2009) proposed a machine learning pipeline that included selecting a preprocessing algorithm, a feature selection algorithm, a classifier and, all their hyperparameters. Their approach used a modified Particle Swarm Optimization (PSO) to deal with the limited configuration space and was called PSMS system. Although the authors found that they could apply their method to different datasets without domain knowledge, most of the datasets used had unrelated attributes. In order to avoid overfitting, the authors proposed using k-cross-validation, and then the approach was extended with a custom assembling strategy that combined the best solutions from multiple generations (Escalante, Montes, and Sucar 2010).

Later, Sun *et al*. extended the idea of PSMS and proposed the unification of the PSO algorithm and the Genetic Algorithm (GA) (2013). This approach was called GPS (which stands for GA-PSO-FMS). A GA were was used to optimize the pipeline structure, while the PSO for the hyperparameter optimization of each pipeline. The pipeline proposed by the authors included selecting from a pool of methods such as data sampling, data cleansing, feature transformation, feature selection, and classification. The datasets used for evaluating GPS were characterized by a high number of instances, thus causing an increase in the computational cost during the loss function evaluation. Therefore, the authors proposed the use of an internal binary tree structure to speed up the GPS system.

Another interesting line of research is the application of multi-objective evolutionary algorithms. One of these approaches is the Multi-objective Support Vector Machine Model Selection (MOSVMMS) (Rosales-Pérez, Escalante, Gonzalez, Reyes-Garcia, and Coello-Coello 2013), where the search is guided by a Non-dominated Sorted Genetic Algorithm-II (NSGA-II).

The authors built a pipeline formed by feature selection, pre-processing, and classification tasks focused only in the SVM classifier. The models were evaluated under bias and variance trade-off as prime objective functions. This approach was only tested on thirteen binary classification problems. Two extensions of this approach were reported, the first called Multi-Objective Model Type Selection (MOMTS), where a multi-objective evolutionary algorithm based on decomposition (MOEA/D) was used instead of the NSGA-II (Rosales-Pérez, Gonzalez, Coello-Coello, Escalante, and Reyes-Garcia 2014). MOMTS focused only on selecting classification models without other involved tasks. However, the authors explored the idea of measuring complexity models through the Vapnik-Chervonenkis dimension, which could have a high computational cost as the dimension of the datasets grows.

For that reason, the second extension proposed by Rosales-Pérez, Gonzalez, Coello, Escalante, and Reyes-Garcia was the Surrogate Assisted Multi-Objective Model Selection (SAMOMS) (2015), in which a pipeline structure is considered, (preprocessing, feature selection, and classification). They proposed a surrogate assistant to speed up the fitness evaluation.

The Tree-Based Pipeline Optimization Tool (TPOT) is an open-source software package for configuring pipelines in a more flexible manner (Olson *et al*. 2016). TPOT uses a genetic programming algorithm for optimizing structures and hyperparameters. The main operator included in TPOT has supervised classification, feature preprocessing operators, and feature selection operators, all of them taken from scikit-learn. The main drawback of TPOT is considering unconstrained search, where resources can be spent on generating and evaluating invalid solutions.

So far, these approaches do not present evidence of the treatment of time-series databases. Most of them use a fixed pipeline length in sequential steps. TPOT is, to date, the approach that stands out for optimizing the design of pipes. Early efforts for an approach that suggests automated pipelines for time series can be found a previous work proposed by Pérez-Castro, Acosta-Mesa, Mezura-Montes, and Cruz-Ramírez (2015). The authors proposed using a micro version of differential evolution to solve the FMS problem, and they suggested optimized pipelines. In that work, smoothing, time series representation, and classification through the k-nearest neighbor algorithm are only considered. This work is an extension of the work mentioned above.

## FMS problem in time-series databases

The FMS term, conceived by Escalante *et al*. (2009), consists of selecting a combination of suitable methods to obtain a learning pipeline for a particular database with a low generalization error.

In this paper, the FMS problem in time series databases is tackled as a single-objective optimization problem, defined by Equation (1), based on the definition made by Díaz-Pacheco, Gonzalez-Bernal, Reyes-García, and Escalante-Balderas (2018), which consists of searching for suitable pipeline composed by a smoothing $s^*_\lambda \in S$, a time series representation $r^*_\lambda \in R$, a numerosity reduction $e^*_\lambda \in E$, and classification method $c^*_\lambda \in C$ with their related hyper-parameter setting $\lambda$ from the corresponding domain space $\wedge$.

For each pipeline, a loss function $\mathcal{L}$ is estimated over a labeled time-series database $D = \{(\vec{x}_1,y_1),\ldots,(\vec{x}_n,y_n)\}$, where for $i = 1,\ldots,n$, let $\vec{x}_i \in X^d$, which denotes an ordered sequence of $n$ real-valued variables (univariate time series), and $y_i \in Y$ for the corresponding label value.

In order to build pipelines with a low generalization error, database $D$ is divided into $k$ disjoint partitions ($D^{(i)}_t$ and $D^{(i)}_v$ for $i = 1,2,\ldots,k$).

$$s^*_\lambda, r^*_\lambda, e^*_\lambda, c^*_\lambda \in \underset{s^{(i)}\in S, r^{(i)}\in R, e^{(i)}\in E, c^{(i)}\in C, \lambda\in\wedge}{\arg\min} \frac{1}{k}\sum_{i=1}^{k}\mathcal{L}(s_\lambda, r_\lambda, e_\lambda, c_\lambda, D^i_t, D^i_v) \quad (1)$$

Where, $S$ is the set of available smoothing methods; $R$ is the set of available time series representation methods; $E$ is the set of available numerosity reduction methods; $C$ is the set of available classifiers; $\lambda$ is a vector of hyperparameters; $D_t$ is a training data partition; $D_v$ is a validation partition; $\mathcal{L}$ is a loss function computed on the validation set; and *argmin* returns the lowest values estimated by the loss function.

## Methodology overview

### *Materials*

#### *Benchmark databases*

In this article, a part of the well-known collection of univariate time series databases is used (Keogh *et al*. 2011). The essential characteristics of those databases are summarized in Table 1.

**Table 1.** Time-series databases description

| No. | Name | No. of classes | Training set size | Testing set size | Time-series length |
|---|---|---|---|---|---|
| 1. | Beef | 5 | 30 | 30 | 470 |
| 2. | CBF | 3 | 30 | 900 | 128 |
| 3. | Coffee | 2 | 28 | 28 | 286 |
| 4. | ECG200 | 2 | 100 | 100 | 96 |
| 5. | FaceFour | 4 | 24 | 88 | 350 |
| 6. | Gun-Point | 2 | 50 | 150 | 150 |
| 7. | Lightning-2 | 2 | 60 | 61 | 637 |
| 8. | Lightning-7 | 7 | 70 | 73 | 319 |
| 9. | OliveOil | 4 | 30 | 30 | 570 |
| 10. | Trace | 4 | 100 | 100 | 275 |

**Source:** Authors

A brief description of each database is presented below:

- *Beef:* This database consists of five classes of beef spectrograms acquired from raw samples, cooked using two different cooking regimes. Each beef class represents a differing degree of contamination with offal (Al-Jowder, Kemsley, and Wilson 2002).
- *CBF:* Cylinder-Bell-Funnel is a simulated database where each class is standard normal noise plus an offset term that differs for each category (Saito 2000).
- *Coffee:* The coffee database consists of two spectrograms class that distinguish between Robusta and Arabica coffee beans (Bagnall, Davis, Hills, and Lines 2012).
- *ECG200:* The electrocardiogram (ECG) database contains the measurements recorded by one electrode during one heartbeat. The two classes correspond

to a normal heartbeat and a myocardial infarction, respectively (Olszewski 2001).

- *FaceFour:* This database was built from face profile images. Each time series was obtained by converting a local (outer) angle at every point x of the face profile contour, starting from the head profile's neck area (Keogh *et al*. 2011).

- *Gun-Point:* This database was obtained from motions with hands involving one female actor and one male actor. Two classes were identified: Gun-Draw (actors point the gun at a target for approximately one second) and Gun-Point (actors point with their index fingers to a goal for about one second). Each time series corresponds to the centroid of the actor's right hands in the x-axis (Ratanamahatana and Keogh 2005).

- *Lightning-2 and Lightning-7:* The FORTE satellite detects transient electromagnetic events associated with lightning using a suite of optical and radio-frequency (RF) instruments. Data is collected with a sample rate of 50 MHz for 800 microseconds that are transformed into spectrograms, which are collapsed in frequency to produce a power density time series, with 3 181 samples in each time series. These are then smoothed to produce time series of length 637 and 319 (Eads *et al*. 2002).

- *OliveOil:* This is another example of the food spectrographs used in chemometrics to classify food types. Each class of this database corresponds to virgin olive oils originating from four European producing countries.

- *Trace:* It is a synthetic database created by Davide Roverso and designed to simulate instrumentation failures in a nuclear power plant. All instances are linearly interpolated to have the same length of 275 data point (Roverso 2000).

It can be seen that most databases describe real phenomena. A behavior analysis of time-series databases was carried out. This analysis consisted of observing three characteristics: a) class separation (CS), b) noise level (NL), and c) the similarity between the training and testing sets (SBS). The mean, median, and average of these per class for each database were computed and plotted from raw databases. From the visualization, the three characteristics of the above-listed were ranked. CS 1 means non-separable, and a value of 3 means easily separable. NL can take values between 1-5, where 1 means low noise and five high noise. SBM was measured in a range of 1 to 3, where 1 represents low similarity, and 3 means high similarity. The results of this analysis are summarized in Table 2.

It is important to note that the data was not pre-processed for the experimental stage.

**Table 2.** Characteristics of visual analysis in time-series databases

| No. | Name | CS | NL | SBS |
|---|---|---|---|---|
| 1. | Beef | 2 | 1 | 3 |
| 2. | CBF | 2 | 2 | 2 |
| 3. | Coffee | 2 | 1 | 3 |
| 4. | ECG200 | 3 | 2 | 3 |
| 5. | FaceFour | 3 | 1 | 2 |
| 6. | Gun-Point | 2 | 1 | 1 |
| 7. | Lightning-2 | 2 | 3 | 1 |
| 8. | Lightning-7 | 1 | 4 | 1 |
| 9. | OliveOil | 2 | 4 | 3 |
| 10. | Trace | 2 | 2 | 1 |

**Note:** Acronyms: CS (Class Separation); NL (Noise Level); SBS (similarity between the training and testing sets)
**Source:** Authors

*Pipeline tasks: available methods*

In this work, four main tasks are considered to build a learning pipeline for time series which involves solving the FMS problem.

1. *Smoothing:* It is usually used to soften out the irregular roughness to see a clearer signal. This task does not provide a model, but it can be a promising first step in describing various series components (Giron-Sierra 2018). It is common to use the term filter to describe the smoothing procedure. Moving Average (Baijal, Singh, Rani, and Agarwal 2016), the Savitzky-Golay filter (Savitzky and Golay 1964), and Local Regression (with and without weights) are considered with related hyper-parameters (Cleveland and Loader 1996).

2. *Time-series representation:* This task consists of transforming the time series to another domain to reduce dimensionality, followed by an indexing mechanism. Piecewise Aggregate Approximation (PAA) (Keogh, Chakrabarti, Pazzani, and Mehrotra 2001), Symbolic Aggregate approXimation (SAX) (Lin, Keogh, Wei, and Lonardi 2007) and Principal Component Analysis (PCA) are available methods (Page, Lischeid, Epting, and Huggenberger 2012).

3. *Numerosity reduction:* It is a procedure used to reduce data volume by using suitable forms of data representation. The Monte Carlo 1 (MC1) and INSIGHT approaches were included (Garcia, Derrac, Cano, and Herrera 2012, Buza, Nanopoulos, and Schmidt-Thieme 2011).

4. *Clasification:* It is a machine learning supervised task that consists of identifying the category to which a new observation belongs, based on a training set of data containing examples whose category membership is known. Some classifiers were considered, such as k-nearest neighbors, Naive Bayes, among others (Bishop 2006).

Table 3 shows a summary of the available methods for each pipeline tasks and their related hyperparameters.

**Table 3.** Description of available methods for each pipeline task and the description of their hyperparameters (values in square brackets indicate lower and upper limits)

| ID | Method | Type | Hyper-parameters | Description |
|---|---|---|---|---|
| 1 | SG | S | $k \in [1;5]$ | Polynomial order |
| | | | $f \in [1;TSL]$ | Frame size |
| 2 | MA | S | $span \in [2;TSL]$ | Span size |
| 3 | LRw | S | $\%span \in [0{,}1;1{,}0]$ | Percentage span size |
| 4 | LRe | S | $\%span \in [0{,}1;1{,}0]$ | Percentage span size |
| 1 | SAX | R | $nseg \in [2;TSL/2]$ | Number of segments |
| | | | $a \in [2;20]$ | Alphabet |
| 2 | PAA | R | $nseg \in [2;TSL/2]$ | Number of segments |
| 3 | PCA | R | $\%red \in [0{,}2;0{,}9]$ | Percentage of reduction |
| 1 | INSIGHT | NR | $\%ins \in [0{,}5;1]$ | Percentage of instances |
| 2 | MC1 | NR | $\%ins \in [0{,}5;1]$ | Percentage of instances |
| | | | $nitera \in [1;500]$ | Number of iteration |
| 1 | KNN-ED | C | $k \in [1;7]$ | Number of neighbors |
| 2 | KNN-LBDTW | C | $k \in [1;7]$ | Number of neighbors |
| | | | $r \in [0{,}0;0{,}05]$ | Percentage of warping |
| 3 | NB | C | $tk \in [1;4]$ | Type of kernel |
| 4 | DT | C | $tsc \in [1;3]$ | Split criterion |
| | | | | 1 = gdi |
| | | | | 2 = twoing |
| | | | | 3 = deviance |
| | | | $maxCat \in [2;20]$ | Maximum levels |
| 5 | AB | C | $n \in [2;500]$ | Number of learners |
| 6 | SVM | C | $-t \in [0;3]$ | Type of kernel |
| | | | | 0 = linear |
| | | | | 1 = polynomial |
| | | | | 2 = radial |
| | | | | 3 = sigmoid |
| | | | $-d \in [1;50]$ | Degree in kernel function |
| | | | $-g \in [1;100]$ | Gamma in kernel function |
| | | | $-r \in [0;100]$ | Coef0 in kernel function |
| | | | $-c \in [1;1\,000]$ | Cost |

**Note:** Acronyms: S (Smoothing); R (Representation); NR (Numerosity Reduction); C (Classification); TLS (Time-series length); SG (Savitzky-Golay Filter); MA (Moving Average); LRw (Local Regression-lowess); LRe (Local Regression-loess); SAX(Aggregate approXimation); PAA (Piecewise Aggregate Approximation); PCA (Principal Component Analysis); INSIGHT (Instance Selection based on Graph-coverage and Hubness for Time-series); MC1 (Monte Carlo 1); KNN-ED (K-Nearest Neighbor-Euclidean Distance); KNN-LBDTW (K-Nearest Neighbor-Lower Bounding Dynamic Time Warping); NB (Naive Bayes); DT (Decision Tree); AB (AdaBoost); SVM (Support Vector Machine)
**Source:** Authors

### *Encoding pipeline solutions*

A candidate solution for the learning pipeline for time-series databases is represented as a vector in this work. Each vector can be formed by continuous values, binary values, or mixed values (continuous and discrete values).

*Continuous encoding:* Each potential solution is encoded as a continuous vector which is formed as in Equation (2).

$$\vec{x_i} = [x_{j,s}; h_{j,1,\ldots,ns}; x_{j,r}; h_{j,1,\ldots,nr}; x_{j,e}; h_{j,1,\ldots,ne}; x_{j,c}; h_{j,1,\ldots,nc}] \quad (2)$$

Where $j$ depicts each position within a particular vector; and $x_{j,s} \in [1;4]$, $x_{j,r} \in [1;3]$, $x_{j,e} \in [1;2]$, and $x_{j,c} \in [1;6]$ represent the ID of the selected smoothing, time-series representation, numerosity reduction, and classification available methods, respectively.

$h_{j,1,\ldots,ns}$, $h_{j,1,\ldots,nr}$, $h_{j,1,\ldots,ne}$, and $h_{j,1,\ldots,nc}$ encode the set of hyperparameters related to the overall available methods, where $ns$, $nr$, $ne$, and $nc$ represent the number of hyperparameters per type of task into the learning pipeline that has different limits. Each position can take random continuous values according to Equation (3), which determines a value between the lower and upper bounds of each hyperparameter, described in Table 3.

$$f(x_i) = lb_i + (ub_i - lb_i) * rand \quad (3)$$

In Equation (3), $lb_i$ is a lower bound, $ub_i$ an upper bound, and *rand* represents a random value between 0 and 1. Figure 3 shows an example of the structure of a continuous vector solution. Black boxes represent the positions that encode the selected method according to the task in the learning pipeline (smoothing, time-series representation, numerosity reduction, and classification), and the white boxes encode their related hyperparameters. For continuous encoding, vectors of 24 dimensions are considered to represent a learning pipeline, which is equivalent to a candidate solution of FMS problem for time-series databases.

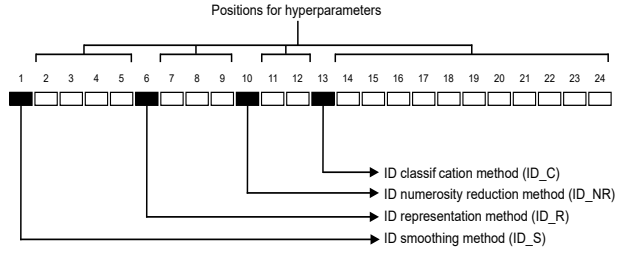


**Figure 2.** Graphical representation of a solution encoding used in contentious or mixed encoding.
**Source:** Authors

*Mixed encoding:* Mixed encoding consists of a vector of 24 dimensions, as shown in Figure 2. However, for this option, both continuous and discrete values are permitted.

Continuous values are generated by Equation (3), according to the limits of each position. In contrast, discrete values are generated by *randi*(), the function of MATLAB language that returns integer values drawn from a discrete uniform distribution, where limits are also respected.

*Binary encoding:* Binary encoding consists of a vector formed by binary values (0 or 1). These values can be grouped into binary strings that represent continuous or discrete values.

The length of a particular binary string depends on the boundary of values to be expressed. Binary string length $l_j$ is computed with Equation (4), where *int* expresses a integer value, $log_2$ is the log base 2, *ub* the upper boundary, *lb* the lower boundary, and *precision* is a constant that means the number of decimal places to encode.

$$l_j = int[\log_2[(ub_j - lb_j) \cdot 10^{precision}] + 0{,}9] \quad (4)$$

Then, the overall binary vector length $bvl$ to encode a potential pipeline solution is the concatenation of each binary string. Equation (5) states how it is computed, where $D$ is the amount of continuous or discrete values that can be encoded as binary strings, and $l_j$ is the maximum length of these binary strings.

$$bvl = \sum_{j=1}^{D} l_j \tag{5}$$

If a mixed vector structure is considered containing 24 values that represent a potential pipeline solution, which respects the boundaries of the values presented in Table 3, then vector with a length of 169 positions is required. It can be seen in Figure 3 that the first three binary values correspond to a binary string representing integer values between 1 and 4 that are the number of available smoothing methods. The next binary strings encode the rest of the values.

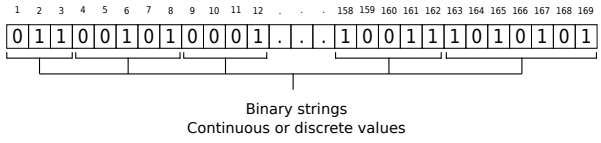


**Figure 3.** Graphical representation of a binary encoding.
**Source:** Authors

A decoding process is needed to compute the quality of each binary encode solution. Decoding is performed for each binary string $x_s$ of complete binary vector according to Equation (6), where $lb_j$ is the lower boundary used for this binary string, $ub_j$ is the upper boundary used for this binary string, $x_{int}$ is the result of traditional binary to decimal conversion, and $l_j$ is the binary string length performed obtained from (4).

$$x_s = lb_j + \frac{x_{int}(ub_j - lb_j)}{2^{l_j} - 1} \tag{6}$$

*Fitness function*

The Cross Validation Error Rate (CVER) is used as the fitness function $f_x$ to evaluate the quality of a learning pipeline under a particular time-series database. Equation (7) describes $f_x$, where $a$ represents the portion of instances in the time-series database that was incorrectly classified, and $b$ is the total number of instances in such database. $k$ depicts the number of stratified subsamples (folds) chosen randomly but with roughly equal size in the cross validation method that is adopted to avoid over-fitting.

$$f(x) = CVER = \frac{1}{k}\sum_{i=1}^{k}(\frac{a}{b})_i \tag{7}$$

## *Methods: search engines*

*Micro Differential Evolution* ($\mu$*-DE*)

Population-based metaheuristics such as evolutionary algorithms have a reduced population version that has proven to be efficient for solving large scale optimization problems (Olguín-Carbajal *et al.* 2019, Salehinejad, Rahnamayan, and Tizhoosh 2017). The reduced population versions usually are denoted with the prefix $\mu$. Besides the small population, $\mu$ algorithms are characterized by a restart mechanism to avoid stagnation.

The $\mu$-DE cycle and conventional operations, based on the scaled difference between two vectors of a population set, remain the same as in the classical DE. Usually, the population size in $\mu$-DE can take a value between four and six vectors (Viveros Jiménez, Mezura Montes, and Gelbukh 2012, Caraffini, Neri, and Poikolainen 2013). Regarding the restart mechanism, $\mu$-DE requires randomly replacing the $N$ worst vectors each $R$ generations. In this paper, the $\mu$-DE proposed by Parsopoulos (2009) is used as a population-based metaheuristic.

Algorithm 1 summarizes the main steps of the adopted $\mu$-DE. Step six shows the mutation and combination process, for that, different variants such as *rand/1/bin*, *rand/1/exp*, *best/1/bin*, and *best/1/exp* are used in the experimentation.

**Algorithm 1** $\mu$-DE

**Require:** $NP \in [3;6]$ (Size of population), $G$ (maximum number of generations), $CR \in [0;1]$ (Crossover Rate) , $F > 0$ (scale factor), $N \in \mathbb{N}$ (number of restart solutions), $R \in \mathbb{N}$ (replacement generation).
1: Generate an initial population of size $NP$.
2: Compute fitness function of initial population by Equation (7).
3: Restarts $N$ worst solution each $R$ generations.
4: **repeat**
5: For each target vector, three vectors must be selected randomly.
6: Generate a trial vector trough mutation and combination operators.
7: Replace the worst vectors, according to fitness function values.
8: this
9: **until** $G$ is reached
**Ensure:** Final best vector found.

This results in four versions to solve FMS problem, called P-DEMS1 (Population-Differential Evolution Model Selection 1, using *rand/1/bin*), P-DEMS2 (Population-Differential Evolution Model Selection 2, using *rand/1/exp*), P-DEMS3 (Population-Differential Evolution Model Selection 3, using *best/1/bin*), and P-DEMS4 (Population-Differential Evolution Model Selection 4, using *best/1/exp*).

*Local search* (*LS*)

LS, a single-point optimization metaheuristic, is considered to be the oldest and most straightforward method (Talbi 2009). However, it has recently been used to train complex structures of neural networks and examine their hyperparameters for successful image classification (Aly *et al.* 2019). The LS algorithm used in this paper is briefly described in Algorithm 2.

For each iteration of the LS, a single solution $s$ is replaced by a neighbor as long as the objective function is improved. Otherwise, the original solution is preserved. The search stops when all candidate neighbors are worse than the current solution, meaning that a local optimum is reached.

**Algorithm 2** LS

**Require:** $N_k$ (Neighborhood size), $I$ (Maximum number of iterations)
1: Set $i = 0$
2: $s_0$; /* *Generate an initial solution* */
3: **while** $i < I$ **do**
4: $s = s_0$
5: Generate ($N(s)$); /* *Generation of candidate neighbors*/
6: **if** there is a better neighbor **then**
7: $s = s\prime$; /* *Select a better neighbor* $s\prime \in N(s)$*/
8: **end if**
9: **end while**
10: $i = i + 1$
**Ensure:** Final solution found (local optima)

Step five (Algorithm 2) corresponds to the operator that generates the $N$ neighbors of a slightly varied solution, according to the type of solution encoding. The neighbors are generated based on $nvar \in [1; D]$ modifications that equivalent to the selected random positions. For example, Figure 4a shows a binary vector where $nvar = 3$. Thus, 3 positions are switched (0 instead 1 or vice-versa).

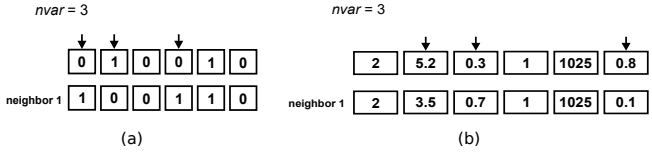


**Figure 4.** Examples of neighbors generated by LS. (a) Using a binary encode. (b) Using mixed encode.
**Source:** Authors

On the other hand, when mixed encoding is used, the *nvar* selected values are replaced with new values that are within boundaries of their corresponding variables (Figure 4b).

Two versions of LS are adopted as search engines: S-LSMS1 (Single-Local Search Model Selection, where binary encoding is used) and S-LSMS2 (Single-Local Search Model Selection, where mixed encoding is used).

### *Methodology architecture*

In this section, the general architecture adopted for evaluating both population-based and single-point search approaches for solving the FMS problem to find a suitable learning pipeline for time-series databases is described.

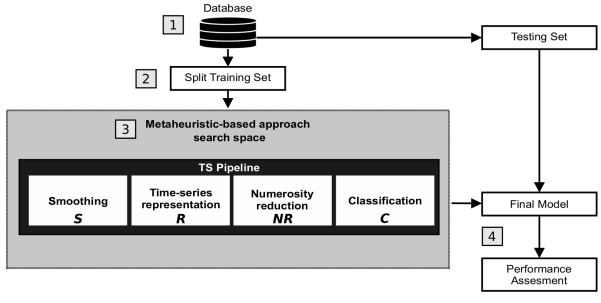


**Figure 5.** General methodology for FMS approaches in time series.
**Source:** Authors

The architecture can be summarized into four main steps (Figure 5).

1. A training time-series database is considered as input data.
2. The training database is split into $k$ stratified subsets (each subset contains approximately the same percentage of samples of each target class as the complete set) that are available during the search process.
3. This step consists of the search process guided by the metaheuristics, either the population-based or single-point versions. Regarding population-based options (based on Algorithm 1), these generate random solutions according to continuous encoding. The overall population is evaluated thought the fitness function (Equation 6) under the stratified subsets generated in the second step. The solutions evolve throughout an established number of iterations, and, in the end, the best solution is obtained. Regarding single-point search (based on Algorithm 2), a unique solution is generated (binary or mixed encoding) which improves throughout the iterations. In the end, the best solution is also obtained.
4. The final best solution found in the search process is evaluated with the test database.

## Experiments and results

This section presents a set of experiments where the PM (population-based metaheuristics) versions and SM (single-point-based metaheuristics) are used as the search engines to solve the FMS problem and find a suitable pipeline for time-series databases.

The experimentation is presented in five subsections: (1) a comparison of the final statistical results of each metaheuristic, (2) a convergence plot analysis, (3) a diversity analysis of the PM versions, (4) an analysis of the final obtained models, and (5) a frequency analysis of the methods' usage. Each metaheuristic was evaluated in the ten time-series databases described in Table 1. Considering the high computation time required by the approaches, five independent runs for each metaheuristic were carried out. The termination condition was 3 000 evaluations. The configuration used by each involved metaheuristics is described in Table 4, based on (Viveros-Jiménez *et al.* 2012, Escalante *et al.* 2009).

### *Final Statistical Results*

Table 5 shows the final numerical results of CVER obtained by the six metaheuristics versions. The reported values correspond to the average of five trials evaluated in the testing set of each database.

Due to the fact that the samples have a non-normal distribution, and multiple comparisons are needed, the non-parametric Friedman test was used (García, Fernández, Luengo, and Herrera 2010). The related samples are the performances of the metaheuristics measured across the same data

sets. The Friedman tests evaluates the following null hypothesis: all methods obtain similar results with non-significant differences.

**Table 4.** Experimental settings for each metaheuristic approach

| Metaheuristic approach | Algorithm | Setting |
|---|---|---|
| PM | $\mu$-DE versions | I = 500, NP = 6, CR = 0.1, F = 0:9, N = 2, R = 10 |
| SM | LS versions | I = 500, Nk =6 |

**Note:** Acronyms: PM (Population-based Metaheuristic); SM (Single-point-based Metaheuristics); $\mu$-DE (micro Differential Evolution); LS (Local Search); I (Iterations); NP (Population Size); CR (Crossover Rate); F (Scaled Factor); N (Number of restart solutions); R (Replacement generation); Nk (Number of neighbors)
**Source:** Authors

In the Friedman test, numerical results are converted to ranks. Thus, it ranks the metaheuristics for each problem separately. The best performing metaheuristic should have rank 1, the second best, rank 2, etc., as shown in Table 5. When there are ties, average ranks are computed. With six compared metaheuristics and ten databases, the p-value computed by the Friedman test was 0,183, which means that the null hypothesis is accepted. Thus, there are no significant differences found among the compared metaheuristics.

However, according to the average rank shown in Table 5, the S-LSMS1 (SM with binary representation) was the highest rank in most of the databases. It was followed by the P-DEMS1 (PM based on $\mu$-DE, where the base vector is randomly chosen, and a binomial crossover is used).

To enhance statistical validation, the Tukey *post-hoc* test based on the Friedman results was applied by using the best and median values obtained over the five runs for each metaheuristic over the whole databases. Figures 6 and 7 show the results of this test, where the x-axis exhibits the confidence interval of mean ranks (given by the Friedman test) and the y-axis shows the name of each metaheuristic compared. Using the best and median values, the test yielded a p-value = 0,005 and a p-value = 0,250, respectively. In the case of Figure 6, there was a significant difference between S-LSMS1 and P-DEMS4.

Meanwhile, in Figure 7, there are no significant differences between the metaheuristics. Finally, a pairwise comparison was conducted to determine which of the metaheuristics exhibit a different performance against a selected control metaheuristic, namely S-MSLS1 because it was the best ranked.

The non-parametric 95% confidence Wilcoxon rank sum test was applied to the numerical results of the six metaheuristics for each database. Table 4 shows the numerical results of the pairwise comparison. The metaheuristics are sorted according to the average rank provided by the Friedman test.

The results in Table 6 show that the S-LSMS1 technique was able to provide the most competitive results among

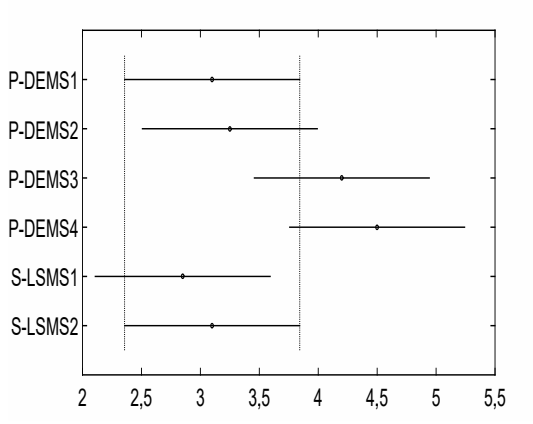


**Figure 6.** Tukey *post-hoc* test using the best values over the whole set of databases
**Source:** Authors

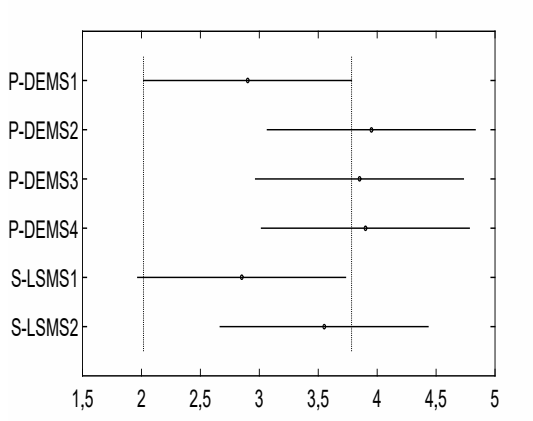


**Figure 7.** Tukey post-hoc test using the median values over the whole set of databases.
**Source:** Authors

the compared metaheuristics. S-LSMS1 outperformed P-DEMS1 in two (out of ten) databases Lightning-7 and Trace, while P-DEMS1 outperformed S-LSMS1 in Coffee and Gun-Point. S-LSMS1 outperformed P-DEMS2 in four databases (Beef, ECG200, Lightning-7, and Trace), while P-DEMS2 outperformed S-LSMS1 in just the Coffee database.

S-LSMS1 outperformed S-LSMS2 in Beef and Lightning-7, and was beaten in the Coffee database. S-LSMS1 outperformed P-DEMS4 in four databases (Beef, ECG200, Lightning-7, and Trace) and was outperformed in just one (Coffee). In summary, S-LSMS1 was able to obtain the best numerical values at least in eight of ten databases (Beef, CBF, ECG200, FaceFour, Lightning-2, Lightning-7, OliveOil, and Trace). Finally, P-DEMS3 was outperformed by S-LSMS1 in three databases (ECG200, Lightning-7, and Trace) and outperformed in just one (Coffee).

## *Analysis of convergence plots*

To further understand the behavior of each compared metaheuristic, the convergence plots of a set of representative databases are analyzed.

**Table 5.** Comparison of averaging performance among the six metaheuristics for each database

| Database | P-DEMS1 | P-DEMS2 | P-DEMS3 | P-DEMS4 | S-LSMS1 | S-LSMS2 |
|---|---|---|---|---|---|---|
| Beef | 0,053±0,102 (3) | 0,087±0,038 (4) | *0,000±0,000 (1,5) | 0,160±0,060 (5) | *0,000±0,000 (1,5) | 0,367±0,227 (6) |
| CBF | *0,000±0,000 (3) | *0,000±0,000 (3) | *0,000±0,000 (3) | *0,000±0,000 (3) | *0,000±0,000 (3) | 0,030±0,027 (6) |
| Coffee | *0,000±0,000 (3) | *0,000±0,000 (3) | *0,000±0,000 (3) | *0,000±0,000 (3) | 0,268±0,157 (6) | 0,000+0,000 (3) |
| ECG200 | *0,000±0,000 (2) | 0,800±0,447 (4) | 1,000±0,000 (5,5) | 1,000±0,000 (5,5) | *0,000±0,000 (2) | *0,000±0,000 (2) |
| FaceFour | *0,000±0,000 (3,5) | *0,000±0,000 (3,5) | *0,000±0,000 (3,5) | *0,000±0,000 (3,5) | *0,000±0,000 (3,5) | *0,000±0,000 (3,5) |
| Gun_Point | *0,000±0,000 (1) | 0,395±0,221 (4) | 0,493±0,000 (5,5) | 0,493±0,000 (5,5) | 0,388±0,217 (3) | 0,212±0,253 (2) |
| Lightning-2 | *0,000±0,000 (3) | *0,000±0,000 (3) | *0,000±0,000 (3) | *0,000±0,000 (3) | *0,000±0,000 (3) | 0,069±0,154 (6) |
| Lightning-7 | 0,766±0,035 (5) | 0,762±0,028 (4) | 0,786±0,019 (6) | 0,761±0,012 (3) | *0,019±0,019 (1) | 0,082±0,046 (2) |
| OliveOil | 0,013±0,030 (2,5) | 0,033±0,047 (5) | 0,027±0,043 (4) | 0,013±0,018 (2,5) | *0,000±0,000 (1) | 0,133±0,122 (6) |
| Trace | 0,800±0,447 (3,5) | 0,800±0,447 (3,5) | 1,000±0,000 (5,5) | 1,000±0,000 (5,5) | *0,000±0,000 (1,5) | *0,000±0,000 (1,5) |
| Average rank | 2,950 | 3,700 | 4,050 | 3,950 | *2,550 | 3,800 |

**Note:** Acronyms: P-DEMS1 (Population-Differential Evolution Model Selection 1 with *rand/1/bin*); P-DEMS2 (Population-Differential Evolution Model Selection 2 with *rand/1/exp*); P-DEMS3 (Population-Differential Evolution Model Selection 3 with *best/1/bin*), and P-DEMS4 (Population-Differential Evolution Model Selection 4 with *best/1/exp*); S-LSMS1 (Single-Local Search Model Selection with binary encoding); S-LSMS2 (Single-Local Search Model Selection with mixed encoding). Values to the right of ± represent the standard deviation, the values in parentheses represent the ranks computed by the Friedman test, and values in parentheses to the left mean the lowest values found or the best ranking.
**Source:** Authors

**Table 6.** Comparison between the control metaheuristic S-LSMS1 and the rest of metaheuristics

| Database | S-LSMS1 1° (Control) | P-DEMS1 2° | P-DEMS2 3° | S-LSMS2 4° | P-DEMS4 5° | P-DEMS3 6° |
|---|---|---|---|---|---|---|
| Beef | *0,000±0,000 | 0,053±0,102 (=) | 0,087±0,038 (-) | 0,367±0,227 (-) | 0,160±0,060 (-) | *0,000±0,000 (=) |
| CBF | *0,000±0,000 | *0,000±0,000 (=) | *0,000±0,000 (=) | 0,030±0,027 (=) | *0,000±0,000 (=) | 0,000±0,000 (=) |
| Coffee | 0,268±0,157 | *0,000±0,000 (+) | *0,000±0,000 (+) | *0,000±0,000 (+) | *0,000±0,000 (+) | *0,000±0,000 (+) |
| ECG200 | *0,000±0,000 | *0,000±0,000 (=) | 0,800±0,447 (-) | *0,000±0,000 (=) | 1,000±0,000 (-) | 1,000±0,000 (-) |
| FaceFour | *0,000±0,000 | *0,000±0,000 (=) | *0,000±0,000 (=) | *0,000±0,000 (=) | *0,000±0,000 (=) | *0,000±0,000 (=) |
| GunPoint | 0,388±0,217 | 0,000±0,000 (+) | 0,395±0,221 (=) | 0,212±0,253 (=) | 0,493±0,000 (=) | 0,493±0,000 (=) |
| Lightning-2 | *0,000±0,000 | *0,000±0,000 (=) | *0,000±0,000 (=) | 0,069±0,154 (=) | *0,000±0,000 (=) | *0,000±0,000 (=) |
| Lightning-7 | *0,019±0,019 | 0,766±0,035 (-) | 0,762±0,028 (-) | 0,082±0,046 (-) | 0,761±0,012 (-) | 0,786±0,019 (-) |
| OliveOil | *0,000±0,000 | 0,013±0,030 (=) | 0,033±0,047 (=) | 0,133±0,122 (=) | 0,013±0,018 (=) | 0,027±0,043 (=) |
| Trace | *0,000±0,000 | 0,800±0,447 (-) | 0,800±0,447 (-) | *0,000±0,000 (=) | 1,000±0,000 (-) | 1,000±0,000 (-) |
| Number of (-) | | 2 | 4 | 2 | 4 | 3 |
| Number of (+) | | 2 | 1 | 1 | 1 | 1 |
| Number of (=) | | 6 | 5 | 7 | 5 | 6 |

**Note:** Acronyms: P-DEMS1 (Population-Differential Evolution Model Selection 1 with *rand/1/bin*); P-DEMS2 (Population-Differential Evolution Model Selection 2 with *rand/1/exp*); P-DEMS3 (Population-Differential Evolution Model Selection 3 with *best/1/bin*), and P-DEMS4 (Population-Differential Evolution Model Selection 4 with *best/1/exp*); S-LSMS1 (Single-Local Search Model Selection with binary encoding); S-LSMS2 (Single-Local Search Model Selection with mixed encoding). (-) means that there was a significant difference favoring the control metaheuristic. (+) implies that there was a significant difference favoring the compared metaheuristic. (=) means that no significant difference was observed between the compared metaheuristics. Values in parentheses to the left mean the best values found.
**Source:** Authors

The average of five independent runs for each database is plotted. From Figures 8 to 13, convergence plots for Beef, CBF, Gun Point, Lightning-2, OliveOil, and Trace are shown. The x-axis represents the number of performing iterations for each metaheuristic, and the y-axis represents the fitness function value obtained for each iteration.

The x-axis was plotted in the logarithmic scale for a better display of the results. The results suggest that, in the case of the $\mu$-DE, to obtain a fast and competitive solution, the best option is P-DEMS1, which uses a random base vector and binomial crossover.

However, in cases such as in the Trace database, PDEMS1 was trapped in local optima. Regarding SMs, S-LSMS2 (mixed representation) achieves fast convergence with respect to S-LSM1 (binary representation), but the first is usually caught in local optima, e.g., Beef, CBF, Lightning-2, or OliveOil, while S-LSM2 finds better values.

Finally, an important finding is that P-DEMS1 had a faster fitness improvement in early iterations, *i.e.*, before 100 iterations in most databases. However, S-LSMS1 was capable of finding competitive final results at the end of the search process.

### *Diversity analysis of population-based metaheuristics*

According to Yang, Li, Cai, and Guan (2015), the population diversity has a strong influence on the performance of evolutionary algorithms. Therefore, a brief analysis of population diversity in PM versions is presented. The diversity measure

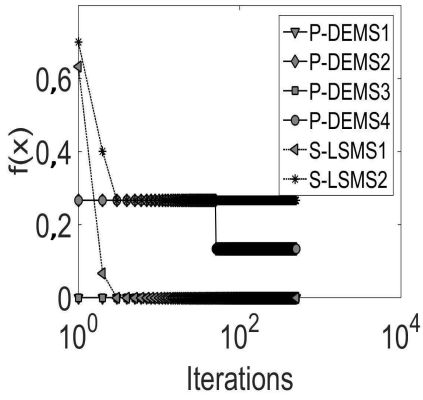


**Figure 8.** Convergence plots comparison for the Beef database
**Source:** Authors

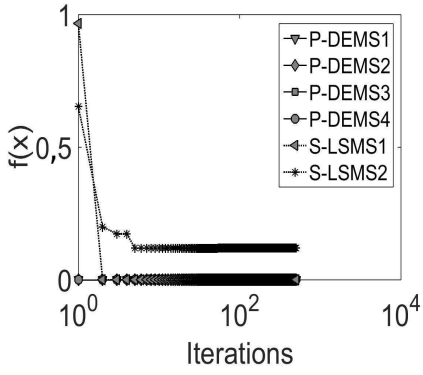


**Figure 9.** Convergence plots comparison for the CBF database.
**Source:** Authors

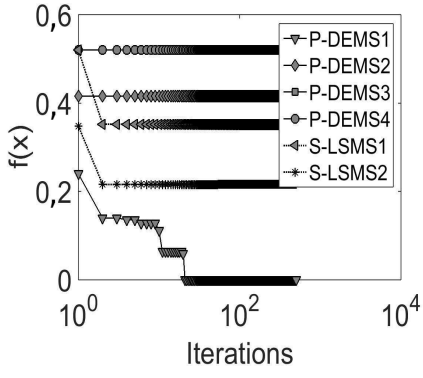


**Figure 10.** Convergence plots comparison for the Gun-Point database.
**Source:** Authors

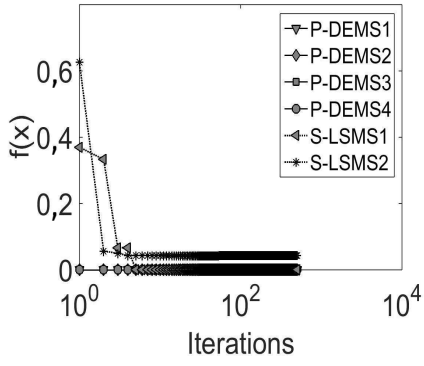


**Figure 11.** Convergence plots comparison for the Lightning-2 database.
**Source:** Authors

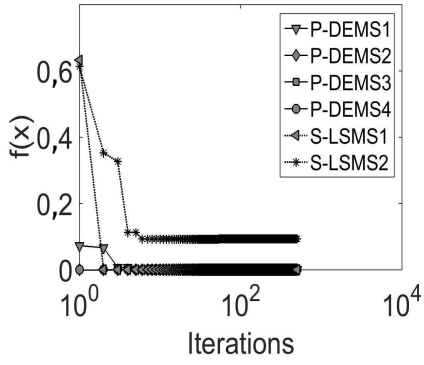


**Figure 12.** Convergence plots comparison for the OliveOil database
**Source:** Authors

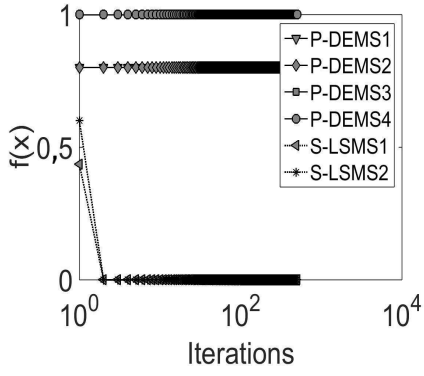


**Figure 13.** Convergence plots comparison for the Trace database.
**Source:** Authors

is based on the distance between vectors in the variable space. For each iteration, a centroid is computed in the current population.

Then, the Euclidean distance is calculated between each vector of the population and the centroid vector. With the aim of measuring the individuals' dispersion, the standard deviation over the whole distances at the current population is computed. The diversity measure was computed for each PM over the five independent runs per each database.

Figure 14 shows the averaging diversity measure of each PM over the ten databases. A high diversity in P-DEMS 1 is observed against the other $\mu$-DE versions. It can be said that the use of a random base vector instead of the best one, as well as the binomial instead of the exponential crossover, favors a better diversity maintenance.

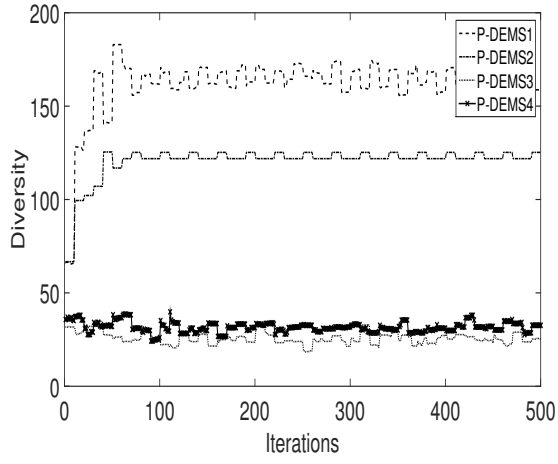


**Figure 14.** Average diversity measure in population-based metaheuristics.
**Source:** Authors

### *Analysis of final pipeline-models*

Table 7 shows the best pipelines suggested by each compared approach for each database. The third column details the pipeline models. Despite the fact that differences were observed in the solution models, there are interesting similarities.

Regarding the smoothing task, Moving Average was the most preferred. PAA was the most commonly used and suggested method for time series representation, while INSIGHT was the most popular numerosity reduction technique.

As for the classification task, the decision tree and the AdaBoost (with decision trees as the weak learners) appeared as the most suitable. From the resulting final models, it can be seen that there were some evaluated databases with different models with similar performance values.

Databases such as Beef, Gun-Point, and Lightning-7 were detected as possible multimodal problems. They reported more diversification in the selected methods and their related hyperparameters.

Runtime varies considerably due to the different features of the temporal databases and the selected methods for carrying out a specific sub-task. Overall, P-DEMS3 reported the lowest runtime computational cost, while S-LSMS1 was the most expensive approach.

However, S-LSMS1 reported the best performance during training and competitive results in the testing phase. Figure 15 shows a graphical example of the suggested pipeline that was applied to the CBF database. It can be seen that the average behavior of the original CBF database remains after the processing originated by the applied pipeline. A significant dimensionality reduction was observed.

### *Frequency analysis of considered method by metaheuristics*

In order to enhance the analysis of the preferred solutions, a selection frequency analysis of the methods considered by the approaches for the FMS problem in time-series databases was made. Figure 16 shows the average frequency, for each recognized method, computed from five trials over all databases for each metaheuristic.

The frequency results for population-baed meteheuristics were based on 601 200 evaluated pipeline-models, while single-point search metaheuristics were based on 300 600 models. Regarding the smoothing options, Moving Average method, was the most solicited by population-based meteheuristics, while the Savitzky-Golay filter was the most preferred by single-point search metaheuristics.

For time-series representation, the PAA method was the most preferred for both population-based and single-based metaheuristics. INSIGHT was the most selected numerosity reduction method. Regarding the classifiers, it can be confirmed that Adaboost was the most suitable classifier, while KNN1 was the less preferred.

## Conclusions and future work

In this paper, a comparison study between two metaheuristic approaches to deal with FMS and pipelines building for time-series databases was presented. The first approach was based on the micro-version of a differential evolution algorithm, named as $\mu$-DEMS in this work, from which four variants were tested based on *rand*/*1*/*bin* (P-DEMS1), *rand*/*1*/*exp* (P-DEMS2), *best*/*1*/*bin* (P-DEMS3), and *best*/*1*/*exp* (PDEMS4).

The second approach focused on evaluating local search behavior S-LSMS, the most straightforward single-point search metaheuristics. Two versions were assessed, one of them with binary encoding and the second one with mixed encoding.

Six complete pipeline-model search options were evaluated, out of which four are P-DEMS variants and two are S-LSMS variants. Each of the variants was evaluated in ten different time-series databases.

The set of experiments was divided into five parts: the statistical analysis of the numerical results, the analysis of the convergence graphs, a diversity analysis focused only on the population variants, the analysis of the final pipeline models, and the study of the selection frequency of the methods involved. From these experiments, some important conclusions and findings are listed below:

Statistical analysis suggests that S-LSMS1 (binary encoding version) is the best option when working with time-series databases that have high dimensionality, are noisy, and whose number of classes is higher than two, such as Lightning-2, Lightning-7, and OliveOil. S-LSMS1 has the advantage of being simple in its structure, and only requires two parameters to be set. However, it has the disadvantage of having a high computational cost.

**Table 7.** Best final pipelines obtained by each approach for all databases

| Database | Approach | Pipeline |
|---|---|---|
| Beef | P-DEMS 1 | ($\uparrow_g$) SG, PAA, MCI, AB |
| | P-DEMS 2 | ($\bullet_r$) MA, PAA,MCI, AB |
| | P-DEMS 3 | ($\bullet_g$) MA, SAX, INSIGTH, AB |
| | P-DEMS 4 | ($\bullet_b$) MA, PAA, MCI, AB |
| | S-LSMS 1 | ($\bullet_g$) LRe, PAA, MCI, AB |
| | S-LSMS 2 | ($\uparrow_r$) SG, PCA, INSIGTH, AB |
| CBF | P-DEMS 1 | ($\bullet_g$) LRe, PCA, MCI, TREE |
| | P-DEMS 2 | ($\bullet_g$) MA, PAA, MCI, AB |
| | P-DEMS 3 | ($\bullet_g$) MA, PAA, MCI, TREE |
| | P-DEMS 4 | ($\bullet_g$) MA, PAA, MCI, AB |
| | S-LSMS 1 | ($\bullet_g$) LRw, PAA, INSIGTH, AB |
| | S-LSMS 2 | ($\bullet_g$) SG, SAX, INSIGTH, TREE |
| Coffee | P-DEMS 1 | ($\bullet_g$) SG, SAX, INSIGTH, TREE |
| | P-DEMS 2 | ($\bullet_g$) MA, PAA, INSIGTH, TREE |
| | P-DEMS 3 | ($\downarrow_g$) MA, PAA, INSIGTH, TREE |
| | P-DEMS 4 | ($\downarrow_g$) MA, PAA, INSIGTH, TREE |
| | S-LSMS 1 | ($\downarrow_r$) LRw, PCA, MC1, KNN-LBDTW |
| | S-LSMS 2 | ($\downarrow_g$) SG, PAA, INSIGTH, TREE |
| ECG200 | P-DEMS 1 | ($\uparrow_g$)SG, SAX, INSIGTH, TREE |
| | P-DEMS 2 | ($\downarrow_g$) MA, PAA, INSIGTH, TREE |
| | P-DEMS 3 | ($\downarrow_b$) MA, PAA, INSIGTH, NB |
| | P-DEMS 4 | ($\downarrow_b$) MA, PAA, INSIGTH, NB |
| | S-LSMS 1 | ($\uparrow_g$)LRw, PAA, MC1, TREE |
| | S-LSMS 2 | ($\bullet_g$)SG, SAX, INSIGTH, TREE |
| FaceFour | P-DEMS 1 | ($\uparrow_g$) SG, PAA, INSIGTH, AB |
| | P-DEMS 2 | ($\bullet_g$) LRe, PAA, INSIGTH, AB |
| | P-DEMS 3 | ($\downarrow_g$) LRe, PAA, INSIGTH, AB |
| | P-DEMS 4 | ($\downarrow_g$) LRe, PAA, INSIGTH, AB |
| | S-LSMS 1 | ($\bullet_g$) LRe, PAA, MC1, AB |
| | S-LSMS 2 | ($\bullet_g$) LRe, SAX, INSIGTH, AB |
| Gun Point | P-DEMS 1 | ($\bullet_g$) SG, SAX, INSIGTH, TREE |
| | P-DEMS 2 | ($\downarrow_g$) LRe, SAX, INSIGTH, TREE |
| | P-DEMS 3 | ($\downarrow_b$) SG, PCA, MC1, AB |
| | P-DEMS 4 | ($\downarrow_b$) SG, PCA, MC1, AB |
| | S-LSMS 1 | ($\uparrow_g$) LRw, PCA, INSIGTH, TREE |
| | S-LSMS 2 | ($\uparrow_g$) SG, PCA, MC1, TREE |
| Lightnigng-2 | P-DEMS 1 | ($\uparrow_g$) LRw, PCA, INSIGTH, TREE |
| | P-DEMS 2 | ($\uparrow_g$) LRw, PCA, INSIGTH, TREE |
| | P-DEMS 3 | ($\uparrow_g$) LRw, PCA, INSIGTH, TREE |
| | P-DEMS 4 | ($\uparrow_g$) LRw, PCA, INSIGTH, TREE |
| | S-LSMS 1 | ($\uparrow_g$) MA, SAX, INSIGTH, TREE |
| | S-LSMS 2 | ($\uparrow_g$) SG, PCA, INSIGTH, TREE |
| Light-nigng-7 | P-DEMS 1 | ($\downarrow_b$) MA, SAX, MCI, NB |
| | P-DEMS 2 | ($\downarrow_b$) LRw, PCA, INSIGTH, SVM |
| | P-DEMS 3 | ($\downarrow_b$) LRw, PCA, INSIGTH, SVM |
| | P-DEMS 4 | ($\downarrow_b$) LRw, PCA, INSIGTH, SVM |
| | S-LSMS 1 | ($\uparrow_g$) SG, PCA, INSIGTH, AB |
| | S-LSMS 2 | ($\uparrow_g$) MA, SAX, INSIGTH, TREE |
| OliveOil | P-DEMS 1 | ($\uparrow_g$) MA, PCA, MCI, AB |
| | P-DEMS 2 | ($\bullet_g$) MA, PAA, MCI, AB |
| | P-DEMS 3 | ($\bullet_g$) MA, PAA, MCI, AB |
| | P-DEMS 4 | ($\bullet_g$) MA, PAA, MCI, AB |
| | S-LSMS 1 | ($\uparrow_g$) LRw, PCA, INSIGTH, AB |
| | S-LSMS 2 | ($\uparrow_g$) SG, SAX, INSIGTH, AB |
| Trace | P-DEMS 1 | ($\downarrow_g$) LRw, SAX, INSIGTH, AB |
| | P-DEMS 2 | ($\downarrow_g$) MA, PAA, INSIGTH, AB |
| | P-DEMS 3 | ($\downarrow_b$) MA, PAA, INSIGTH, NB |
| | P-DEMS 4 | ($\downarrow_b$) MA, PAA, INSIGTH, NB |
| | S-LSMS 1 | ($\uparrow_g$) MA, PAA, INSIGTH, AB |
| | S-LSMS 2 | ($\uparrow_g$)SG, SAX, INSIGTH, TREE |

**Note:** Acronyms: S (Smoothing); R (Representation); NR (Numerosity Reduction); C (Classification); TLS (Time-series length); SG (Savitzky-Golay Filter); MA (Moving Average); LRw (Local Regression-lowess); LRe (Local Regression-loess); SAX(Aggregate approXimation); PAA (Piecewise Aggregate Approximation); PCA (Principal Component Analysis); INSIGHT (Instance Selection based on Graph-coverage and Hubness for Time-series); MC1 (Monte Carlo 1); KNN-ED (K-Nearest Neighbor-Euclidean Distance); KNN-LBDTW (K-Nearest Neighbor-Lower Bounding Dynamic Time Warping); NB (Naive Bayes); DT (Decision Tree); AB (AdaBoost); SVM (Support Vector Machine); P-DEMS1 (Population-Differential Evolution Model Selection 1 with rand/1/bin); P-DEMS2 (Population-Differential Evolution Model Selection 2 with rand/1/exp); P-DEMS3 (Population-Differential Evolution Model Selection 3 with best/1/bin), and P-DEMS4 (Population-Differential Evolution Model Selection 4 with best/1/exp); S-LSMS1 (Single-Local Search Model Selection with binary encoding); S-LSMS2 (Single-Local Search Model Selection with mixed encoding). Symbols in parentheses mean the spent runtime during training and the subscripts represent the performance of the pipeline in terms of classification error. (↑) means high runtime > 933 minutes, (•) means medium runtime > 272 and < 873 minutes, (↓) means low runtime < 272 minutes. Subscripts next to symbols: $g$ means good, $r$ means regular, and $b$ means bad performance.
**Source:** Authors

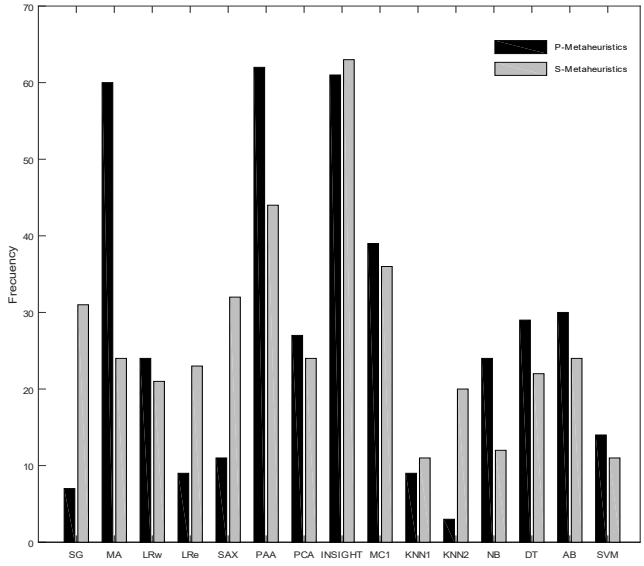


**Note:** Acronyms: P-Metaheuristics (Population-based Metaheuristics); S-Metaheuristics (Single point search Metaheuristics); SG (Savitzky-Golay Filter); MA (Moving Average); LRw (Local Regression-lowess); LRe (Local Regression-loess); SAX(Aggregate approXimation); PAA (Piecewise Aggregate Approximation); PCA (Principal Component Analysis); INSIGHT (Instance Selection based on Graph-coverage and Hubness for Time-series); MC1 (Monte Carlo 1); KNN1 (K-Nearest Neighbor-Euclidean Distance); KNN2 (K-Nearest Neighbor-Lower Bounding Dynamic Time Warping); NB (Naive Bayes); DT (Decision Tree); AB (AdaBoost); SVM (Support Vector Machine).

**Figure 15.** Frequency analysis of included into pipeline task by metaheuristics.
**Source:** Authors

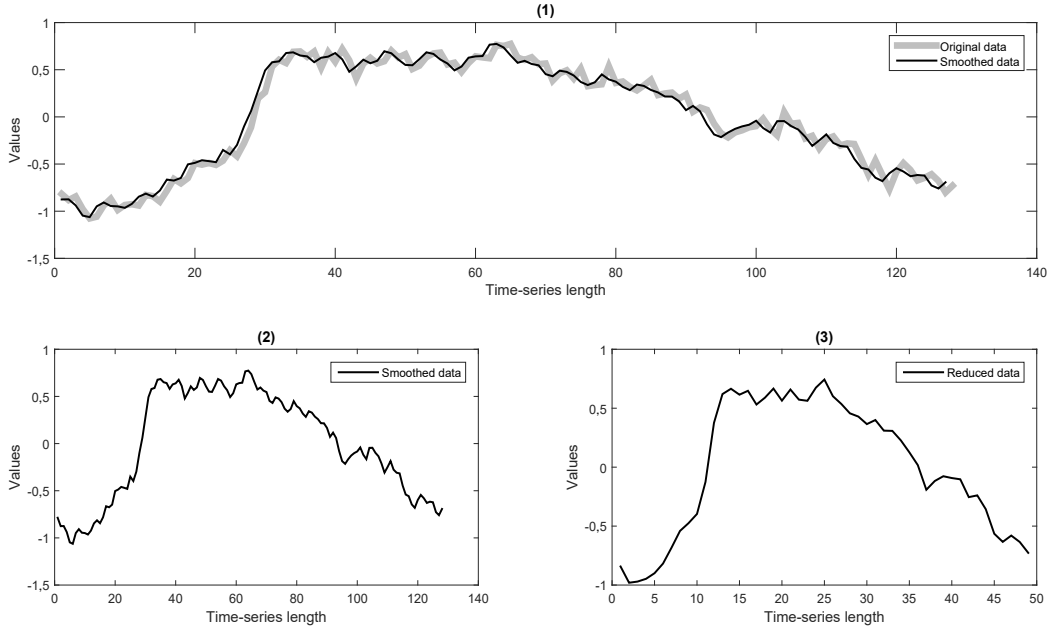


**Note:** (1) The average behavior of the original testing database is plotted that is compared to the average smoothed testing test. (2) The averaged smoothed testing database is plotted before the time-series representation process. (3) The averaged smoothed testing database is plotted after the time-series representation and numerosity reduction processes were applied.

**Figure 16.** Example of pipeline-model applied to CBF database. Model: S:MA{span=67}, R:PAA{nseg=21}. R:MC1{%ins=0.81403,nitera=400}, C:AB{n=436}.
**Source:** Authors

On the other hand, if the database is dichotomous, the noise is moderate, and its dimensionality length is below an approximate value of 350. Therefore, population-based metaheuristics P-DEMS1, which uses *rand/1/bin*, turns out to be the best option. Besides, it achieved competitive results around the first 100 iterations.

Regarding the exploration capacity, it was observed that the population-based metaheuristic P-DEMS1 with the *rand/1/bin* variant provides a better diversity of pipeline models.

With respect to the final pipeline-models, it can be seen that, for most of the databases, a complete model was found which contained the most straightforward methods for the tasks of smoothing, dimensionality reduction, and number reduction. These methods are Moving Average, PAA, and INSIGHT, respectively. On the side of the classification task, AdaBoost was the most common method.

An important finding was discovering different complete pipeline model configurations with similar performance for the same database. Therefore, some temporary databases can be seen as a multi modal problem.

As part of future work, a complexity measure could be considered as a fitness function to then tackle the FMS problem as a multi-objective problem. Additionally, a mechanism to build more flexible pipelines where the length and order can incorporated, in addition to searching for a way to fairly compare it against other state-of-the-art approaches.

## Acknowledgements

The authors would like to acknowledge support from the Mexican National Council for Science and Technology (CONACyT) through scholarship number 259655 and project No. 220522.

## References

Al-Jowder, O., Kemsley, E., and Wilson, R. H. (2002). Detection of adulteration in cooked meat products by mid-infrared spectroscopy. *Journal of Agricultural and Food Chemistry, 50*(6), 1325-1329. 10.1021/jf0108967

Ali, M., Alqahtani, A., Jones, M. W., and Xie, X. (2019). Clustering and classification for time series data in visual analytics: A survey. *IEEE Access, 7*, 181314-181338. 10.1109/ACCESS.2019.2958551

Aly, A., Guadagni, G., and Dugan, J. B. (2019). Derivative-free optimization of neural networks using local search. In IEEE (Eds.) *2019 IEEE 10th Annual Ubiquitous Computing, Electronics Mobile Communication Conference* (*UEMCON*) (pp. 0293-0299). New York, NY: IEEE. 10.1109/UEMCON47517.2019.8993007

Bagnall, A., Davis, L., Hills, J., and Lines, J. (2012). Transformation based ensembles for time series classification. In SIAM (Eds.) *Proceedings of the 2012 SIAM international conference on data mining* (pp. 307-318). Philadelphia, PA: Society for Industrial and Applied Mathematics. 10.1137/1.9781611972825.27

Baijal, S., Singh, S., Rani, A., and Agarwal, S. (2016). Performance evaluation of S-Golay and MA filter on the basis of white and flicker noise. In *Proceedings of Second International Symposium on Signal Processing and Intelligent Recognition Systems* (*SIRS-2015*) (pp. 245-255). New York, NY: Springer. 10.1007/978-3-319-28658-7_21

Bergstra, J. and Bengio, Y. (2012). Random search for hyper-parameter optimization. *The Journal of Machine Learning Research*, 13(2), 281-305. https://www.jmlr.org/papers/volume13/bergstra12a/ber\gstra12a

Bischl, B., Lang, M., Kotthoff, L., Schiffner, J., Richter, J., Studerus, E., Casalicchio, G., and Jones, Z. M. (2016). mlr: Machine learning in R. *The Journal of Machine Learning Research*, 17(170), 1-5. http://jmlr.org/papers/v17/15-066.html

Bishop, C. M. (2006). *Pattern recognition and machine learning*. New York, NY: Springer.

Boullé, N., Dallas, V., Nakatsukasa, Y., and Samaddar, D. (2020). Classification of chaotic time series with deep learning. *Physica D: Nonlinear Phenomena, 403*, 132261. 10.1016/j.physd.2019.132261

Buza, K., Nanopoulos, A., and Schmidt-Thieme, L. (2011). Insight: Efficient and effective instance selection for time-series classification. In Huang, J. Z., Cao, L., and Srivastava, J. (Eds.) *Pacific-Asia Conference on Knowledge Discovery and Data Mining* (pp. 149-160). Heidelberg/Berlin, Germany: Springer.

Caraffini, F., Neri, F., and Poikolainen, I. (2013). Micro-differential evolution with extra moves along the axes. In IEEE (Eds.) *2013 IEEE Symposium on Differential Evolution* (*SDE*) (pp. 46-53). New York, NY: IEEE. 10.1109/SDE.2013.6601441

Cleveland, W. S. and Loader, C. (1996). Smoothing by local regression: Principles and methods. In Hardle, W., and Scmiek, M. G. (Eds.) *Statistical Theory and Computational Aspects of Smoothing* (pp. 10-49). Heidelberg, Germany: Physica-Verlag HD. 10.1007/978-3-642-48425-4_2

de Sá, A. G. C., Pinto, W. J. G. S., Oliveira, L. O. V. B., and Pappa, G. L. (2017). RECIPE: A grammar-based framework for automatically evolving classification pipelines. In McDermott, J., Castelli, M., Sekanina, L., Haasdijk, E., and García-Sánchez, P. (Eds.) *European Conference on Genetic Programming* (pp. 246-261), Springer International Publishing, Cham. 10.1007/978-3-319-55696-3_16

Díaz-Pacheco, A., Gonzalez-Bernal, J. A., Reyes-García, C. A., and Escalante-Balderas, H. J. (2018). Full model selection in big data. In Castro, F., Miranda-Jiménez, S., and González-Mendoza, M. (Eds.) *Advances in Soft Computing* (pp. 279-289). Springer International Publishing, Cham. 10.1007/978-3-030-02837-4_23

Eads, D. R., Hill, D., Davis, S., Perkins, S. J., Ma, J., Porter, R. B., and Theiler, J. P. (2002). Genetic algorithms and support vector machines for time series classification. In Bosacchi, B., Fogel, D. B., and Bezdek, J. C. (Eds.) *Applications and Science of Neural Networks, Fuzzy Systems, and Evolutionary Computation V* (vol. 4787, pp. 74-85). Bellingham, WA: International Society for Optics and Photonics. 10.1117/12.453526

Escalante, H. J., Montes, M., and Sucar, E. (2010). Ensemble particle swarm model selection. In IEEE (Eds.)*The 2010 International Joint Conference on Neural Networks* (*IJCNN*) (pp. 1-8). New York, NY: IEEE. 10.1109/IJCNN.2010.5596915

Escalante, H. J., Montes, M., and Sucar, L. E. (2009). Particle swarm model selection. *Journal of Machine Learning Research, 10*(2), 405-440. http://jmlr.org/papers/v10/escalante09a.html

Esling, P. and Agon, C. (2012). Time-series data mining. *ACM Computing Surveys* (*CSUR*)*, 45*(1), 1-12. 10.1145/2379776.2379788

Fu, T.-c. (2011). A review on time series data mining. *Engineering Applications of Artificial Intelligence, 24*(1), 164-181. 10.1016/j.engappai.2010.09.007

Gantza, J. and Reisel, D. (2012). The digital universe in 2020: Big data, bigger digital shadows, and biggest growth in the far east. *IDC iView: IDC Analyze the Future, 2007*(2012), 1-16. https://www.speicherguide.de/download/dokus/IDC-Digital-Universe-Studie-iView-11.12.pdf

Garcia, S., Derrac, J., Cano, J., and Herrera, F. (2012). Prototype selection for nearest neighbor classification: Taxonomy and empirical study. *IEEE transactions on pattern analysis and machine intelligence, 34*(3), 417-435. 10.1109/TPAMI.2011.142

García, S., Fernández, A., Luengo, J., and Herrera, F. (2010). Advanced nonparametric tests for multiple comparisons in the design of experiments in computational intelligence and data mining: Experimental analysis of power. *Information Sciences, 180*(10), 2044-2064. 10.1016/j.ins.2009.12.010

Giron-Sierra, J. (2018). *Digital Signal Processing with Matlab Examples, Volume 3: Model-Based Actions and Sparse Representation*. Singapore: Springer Singapore.

Gong, Z., Chen, H., Yuan, B., and Yao, X. (2019). Multiobjective learning in the model space for time series classification. *IEEE Transactions on Cybernetics, 49*(3), 918-932. 10.1109/TCYB.2018.2789422

Hall, M., Frank, E., Holmes, G., Pfahringer, B., Reutemann, P., and Witten, I. H. (2009). The weka data mining software: An update. *ACM SIGKDD Explorations Newsletter, 11*(1), 10-18. 10.1145/1656274.1656278

Hutter, F., Kotthoff, L., and Vanschoren, J. (2019). *Automated Machine Learning: Methods, Systems, Challenges*. New York, NY: Springer. 10.1007/978-3-030-05318-5

Jastrzebska, A. (2019). Time series classification through visual pattern recognition. *Journal of King Saud University - Computer and Information Sciences*. 10.1016/j.jksuci.2019.12.012

Keogh, E., Chakrabarti, K., Pazzani, M., and Mehrotra, S. (2001). Dimensionality reduction for fast similarity search in large time series databases. *Knowledge and Information Systems, 3*(3), 263-286. 10.1007/PL00011669

Keogh, E., Zhu, Q., Hu, B., Hao, Y., Xi, X., Wei, L., and Ratanamahatana, C. A. (2011). The UCR Time Series Classification/Clustering Homepage. https://www.cs.ucr.edu/~eamonn/time_series_data/

Lin, J., Keogh, E., Wei, L., and Lonardi, S. (2007). Experiencing sax: a novel symbolic representation of time series. *Data Mining and Knowledge Discovery, 15*(2), 107-144. 10.1007/s10618-007-0064-z

Olguín-Carbajal, M., Herrera-Lozada, J. C., Sandoval-Gutierrez, J., Vasquez-Gomez, J. I., Serrano-Talamantes, J. F., Chavez-Estrada, F. A., Rivera-Zarate, I., and Hernandez-Boláos, M. (2019). A micro-differential evolution algorithm for continuous complex functions. *IEEE Access, 7*, 172783-172795. 10.1109/ACCESS.2019.2954296

Olson, R. S., Urbanowicz, R. J., Andrews, P. C., Lavender, N. A., Kidd, L. C., and Moore, J. H. (2016). Automating biomedical data science through tree-based pipeline optimization. In Squillero, G., and Burelli, P. (Eds.) *European Conference on the Applications of Evolutionary Computation* (pp. 123-137). Cham, Germany: Springer. 10.1007/978-3-319-31204-0_9

Olszewski, R. T. (2001). Generalized feature extraction for structural pattern recognition in time-series data (Doctoral thesis, Carnegie Mellon University, Pittsburgh, PA). https://apps.dtic.mil/sti/pdfs/ADA457624.pdf

Page, R. M., Lischeid, G., Epting, J., and Huggenberger, P. (2012). Principal component analysis of time series for identifying indicator variables for riverine groundwater extraction management. *Journal of Hydrology, 432*, 137-144. 10.1016/j.jhydrol.2012.02.025

Parsopoulos, K. E. (2009). Cooperative micro-differential evolution for high-dimensional problems. In ACM (Eds.) *GECCO '09: Proceedings of the 11th Annual Conference on Genetic and Evolutionary Computation* (pp. 531-538). New York, NY: ACM. 10.1145/1569901.1569975

Pedregosa, F., Varoquaux, G., Gramfort, A., Michel, V., Thirion, B., Grisel, O., Blondel, M., Prettenhofer, P., Weiss, R., Dubourg, V., Vanderplas, J., Passos, A., and Cournapeau, D. (2011). Scikit-learn: Machine learning in python. *The Journal of Machine Learning Research, 12*, 2825-2830.

Pérez-Castro, N., Acosta-Mesa, H., Mezura-Montes, E., and Cruz-Ramírez, N. (2015). Towards the full model selection in temporal databases by using micro-differential evolution. an empirical study. In IEEE (Eds.) *2015 IEEE International Autumn Meeting on Power, Electronics and Computing* (*ROPEC*) (pp. 1-6). New York, NY: IEEE. 10.1109/ROPEC.2015.7395161

Rashid, A. and Hossain, M. A. (2012) Challenging issues of spatio-temporal data mining. *Computer Engineering and Intelligent Systems, 3*(4), 55-63. https://www.iiste.org/Journals/index.php/CEIS/article/view/1484

Ratanamahatana, C. A. and Keogh, E. (2005). Three myths about dynamic time warping data mining. In SIAM (Eds.) *Proceedings of the 2005 SIAM International Conference on Data Mining* (pp. 506-510). Philadelphia, PA: Society for Industrial and Applied Mathematics. 10.1137/1.9781611972757.50

Rice, J. R. (1976). The algorithm selection problem. In Rubinoff, M. and Yovits, M. C. (Eds.) *Advances in computers* (vol. 15, pp. 65-118). Amsterdam, Netherlands: Elsevier. 10.1016/S0065-2458(08)60520-3

Rosales-Pérez, A., Escalante, H. J., Gonzalez, J. A., Reyes-Garcia, C. A., and Coello-Coello, C. A. (2013). Bias and variance multi-objective optimization for support vector machines model selection. In Sanches, J. A. M., Micó, L., and Cardoso, J. S. (Eds.) *Iberian Conference on Pattern Recognition and Image Analysis* (pp. 108-116). Berlin/Heidelberg, Germany: Springer. 10.1007/978-3-642-38628-2_12

Rosales-Pérez, A., Gonzalez, J. A., Coello-Coello, C. A., Escalante, H. J., and Reyes-Garcia, C. A. (2015). Surrogate-assisted multi-objective model selection for support vector machines. *Neurocomputing, 150*, 163-172. 10.1016/j.neucom.2014.08.075

Rosales-Pérez, A., Gonzalez, J. A., Coello-Coello, C. A., Escalante, H. J., and Reyes-Garcia, C. A. (2014). Multi-objective model type selection. *Neurocomputing, 146*, 83-94. 10.1016/j.neucom.2014.05.077

Roverso, D. (2000). Multivariate temporal classification by windowed wavelet decomposition and recurrent neural networks. In ANS (Eds.) *3rd ANS international topical meeting on nuclear plant instrumentation, control and human-machine interface* (vol. 20, pp. 527-538). La Grange Park, IL: American Nuclear Society.

Rydning, D. R.-J. G.-J. (2018). The digitization of the world from edge to core. http://cloudcode.me/media/1014/idc.pdf

Saito, N. (2000). Local feature extraction and its applications using a library of bases. In Coifman, R. (Ed.) *Topics in Analysis and Its Applications: Selected Theses* (pp. 269-451). 10.1142/9789812813305_0005

Salehinejad, H., Rahnamayan, S., and Tizhoosh, H. R. (2017). Micro-differential evolution: Diversity enhancement and a comparative study. *Applied Soft Computing, 52*, 812-833. 10.1016/j.asoc.2016.09.042

Savitzky, A. and Golay, M. J. E. (1964). Smoothing and differentiation of data by simplified least squares procedures. *Analytical Chemistry, 36*(8), 1627-1639. 10.1021/ac60214a047

Shahriari, B., Swersky, K., Wang, Z., Adams, R. P., and de Freitas, N. (2016). Taking the human out of the loop: A review of bayesian optimization. *Proceedings of the IEEE, 104*(1), 148-175. 10.1109/JPROC.2015.2494218

Sun, J., Yang, Y., Liu, Y., Chen, C., Rao, W., and Bai, Y. (2019). Univariate time series classification using information geometry. *Pattern Recognition, 95*, 24-35. 10.1016/j.patcog.2019.05.0406

Sun, Q., Pfahringer, B., and Mayo, M. (2013). Towards a framework for designing full model selection and optimization systems. In Zhou, Z.-H., Roli, F., and Kittler, J. (Eds.) *International Workshop on Multiple Classifier Systems* (pp. 259-270). Springer, Berlin, Heidelberg. 10.1016/j.patcog.2019.05.040

Talbi, E. (2009). *Metaheuristics: From Design to Implementation*. John Wiley & Sons.

Viveros-Jiménez, F., Mezura-Montes, E., and Gelbukh, A. (2012). Empirical analysis of a micro-evolutionary algorithm for numerical optimization. *International Journal of Physical Sciences, 7*(8), 1235-1258. 10.5897/IJPS11.303

Yang, M., Li, C., Cai, Z., and Guan, J. (2015). Differential evolution with auto-enhanced population diversity. *IEEE transactions on cybernetics, 45*(2), 302-315. 10.1109/TCYB.2014.2339495

Yang, Y. (2017). Chapter 2 - temporal data mining. In Y. Yang (Ed.) *Temporal Data Mining Via Unsupervised Ensemble Learning* (pp. 9-18). Amsterdam, Netherlands: Elsevier. 10.1016/B978-0-12-811654-8.00002-6

Yu, T. and Zhu, H. (2020). Hyper-parameter optimization: A review of algorithms and applications. https://arxiv.org/pdf/2003.05689.pdf

Research Article / Education in Engineering https://doi.org/10.15446/ing.investig.v41n3.88685

# Verification of a Fabless Device Model Using TCAD Tools: from Bipolar Transistor Formation to I-V Characteristics Extraction

## Verificación de un modelo de dispositivo sin defectos utilizando herramientas TCAD: desde la formación de transistores bipolares hasta la extracción de características I-V

Vaidotas Barzdenas[1], Gediminas Grazulevicius[2], John Liobe[3], Aleksandr Vasjanov[4], and Leonid Kladovscikov[5]

**ABSTRACT**

This paper describes the analysis of processes used in micro- and nano-electronic device manufacturing. It also presents an exemplary and novel laboratory exercise in which an epitaxial planar *n* + *pn* bipolar transistor with junction isolation is illustrated and analyzed step-by-step. Only seven photolithography steps are used to obtain this bipolar transistor structure: for buried layer formation, for junction transistor isolation and collectors regions formation, for base region formation, for emitter and collector *n*+ region formation, for contact windows, for first aluminum metallization, and, finally, for passivation. Silvaco TCAD software tools are used to implement all of these manufacturing processes and to simulate the resulting I-V characteristics of all presented semiconductor structures. This type of laboratory work provides students with basic knowledge and a consistent understanding of bipolar transistor manufacturing, as well as facilitating theoretical understanding, analysis, and simulation of various semiconductor manufacturing processes without the need for costly and lengthy technological manufacturing experiments. This article also presents the conclusions and other benefits of such laboratory work, as well as possible recommendations for further improvement or expansion.

**Keywords:** electronics engineering education, laboratory learning environment, learning technology, TCAD tools

**RESUMEN**

Este artículo describe el análisis de los procesos utilizados en la fabricación de dispositivos de micro y nanoelectrónica. También presenta un ejercicio de laboratorio ejemplar y novedoso en el que se ilustra y analiza paso a paso un transistor bipolar plano *n* + *pn* epitaxial con aislamiento de unión. Solo se utilizan siete pasos de fotolitografía para obtener esta estructura de transistor bipolar: para la formación de capas enterradas, para el aislamiento del transistor de unión y la formación de regiones colectoras, para la formación de regiones base, para la formación de regiones emisoras y colectoras *n*+, para ventanas de contacto, para la primera metalización de aluminio, y finalmente para pasivación. Las herramientas de software Silvaco TCAD se utilizan para implementar todos estos procesos de fabricación y para simular las características I-V resultantes de todas las estructuras de semiconductores presentadas. Este tipo de trabajo de laboratorio proporciona a los estudiantes conocimientos básicos y una comprensión constante de la fabricación de transistores bipolares. Asimismo, este estudio facilita la comprensión teórica, el análisis y la simulación de varios procesos de fabricación de semiconductores sin la necesidad de experimentos de fabricación tecnológicos costosos y largos. Este artículo también presenta las conclusiones y otros beneficios de dicho trabajo de laboratorio, así como posibles recomendaciones para una su mejora o expansión.

**Palabras clave:** educación en ingeniería electrónica, entorno de aprendizaje de laboratorio, tecnología de aprendizaje, herramientas TCAD

**Received:** June 29th, 2020
**Accepted:** March 1st, 2021

[1]Ph.D. in the area of Electrical and Electronics Engineering, Vilnius Gediminas Technical University (VilniusTech), Lithuania. Affiliation: Professor, Vilnius Gediminas Technical University (VilniusTech), Lithuania.
Email: vaidotas.barzdenas@vilniustech.lt
[2]Ph.D. in the area of Electrical and Electronics Engineering, Vilnius Gediminas Technical University (VilniusTech), Lithuania. Affiliation: Associate Professor, Vilnius Gediminas Technical University (VilniusTech), Lithuania.
Email: gediminas.grazulevicius@vilniustech.lt
[3]Ph.D. in the area of Electrical and Computer Engineering, University of Rochester, USA. Affiliation: Senior Research Fellow, Vilnius Gediminas Technical University (VilniusTech), Lithuania. Email: john-charles.liobe@vilniustech.lt
[4]Ph.D. in the area of Electrical and Electronics Engineering, Vilnius Gediminas Technical University (VilniusTech), Lithuania. Affiliation: Associate Professor, Vilnius Gediminas Technical University (VilniusTech), Lithuania.
Email: aleksandr.vasjanov@vilniustech.lt
[5]Ph.D. in the area of Electrical and Electronics Engineering, Vilnius Gediminas Technical University (VilniusTech), Lithuania. Affiliation: Lecturer, Vilnius Gediminas Technical University (VilniusTech), Lithuania.
Email: leonid.kladovscikov@vilniustech.lt

**How to cite:** Barzdenas, V., Grazulevicius, G., Liobe, J., Vasjanov, A., and Kladovscikov, L. (2021). Verification of a Fabless Device Model Using TCAD Tools: from Bipolar Transistor Formation to I-V Characteristics Extraction. *Ingeniería e Investigación*, *41*(3), e88685. 10.15446/ing.investig.v41n3.88685

## Introduction

One of the most characteristic features of today's scientific and technical progress is the extent to which electronic devices are used in many human activities, ranging from personal health to public safety, aerospace and defense. The elemental basis of such electronic devices consists of transistors, diodes, resistors, capacitors, and other elements designed and implemented in advanced micro- and later in nano-electronics. Based on recent scientific research, the economic analysis of market trends, and their contribution to social challenges, the European Union's (EU) Key Enabling Technologies (KET) include micro- and nano-electronics, nanotechnology, photonics, advanced materials, industrial biotechnology, and advanced manufacturing technologies (European Commission, 2012). These technologies are an engine of economic and technological development, as well as a major driver of innovation. In 2015, the global KET market was estimated at more than 1 trillion euros, while export of KET products from the EU accounted for up to 23% of exports worldwide. KETs also have great potential for growth and employment: in the coming years, 10-20% of growth potential can be expected (European Commission, 2013; European Commission, 2015). As a result, the European Commission, like other leading economy countries, has developed a strategy to boost the advancement of these high-impact technologies and create new workplaces, thereby boosting growth in other industries and sectors (European Commission, 2018).

At least 10% of the global GDP depends on products and services created by the micro- and nano-electronics industries (Annegarn, *et al.*, 2012). These industries' innovations and their stimulating role is a major driver of growth in all electronics, information technology, automotive, aerospace, medical, and other economic industries. Therefore, the rapid growth of these sectors is also affecting the creation of new workplaces and the need for new employees, with a deeper knowledge. For example, according to the data of the statistical office of the EU (Eurostat), the number of Information and Communication Technology (ICT) professionals covering electronics, information technology, and telecommunications has increased by as much as 39,1% between 2011 and 2018, which is more than 6 times higher than the increase in overall employment of all sectors (6,5%). Similarly, more than two-thirds (63,1%) of ICT professionals in the EU had a university degree (Eurostat, 2018). The United States Bureau of Labor Statistics also projects the need for computer science and ICT professionals. According to forecasts, the employment opportunities of these specialists will increase by 12% between 2018 and 2028, *i.e.* much faster than the average for all other occupations. It is also forecasted that, during this period, about 0,55 million workplaces of this occupation will be created in the USA (United States Department of Labor, 2019).

Such rapid growth and development pose increasingly difficult challenges for higher education institutions. One of the major trials in a rapidly growing industry is to engage and motivate students to study engineering sciences. Most higher education institutions try to solve this problem by giving lectures and various seminars/workshops in secondary schools; organizing events, competitions, and tours with commercial enterprises; improving teacher competencies; and developing effective teaching methods and increasing their diversity. The second challenge, which we mentioned in our previous article and book (Barzdenas, Grazulevicius, and Vasjanov, 2020; Barzdenas, Navickas, 2012) is to provide quality education with minimal or no investment, as the costs of rapidly evolving technologies are very high. These costs, which include capital equipment, human resources, and time, are so expensive that higher education institutions cannot even make a dent with their limited financial resources. For these reasons, teachers are forced to look for virtual software tools that allow at least for the partial replacement of costly equipment. One such tool for virtual simulation of various micro- and nano-electronic structures and devices are various Technology Computer-Aided Design (TCAD) software tools. However, with the help of TCAD software tools, it is necessary to adopt various teaching methods to provide students with interesting tasks to motivate their better understanding of the common and newly developed structures of micro- and nano-electronic devices, as well as their working principles. Therefore, via laboratory projects and lectures, it is advisable to examine examples covering all stages of the manufacturing of these devices, that is, from an unprocessed silicon wafer to the simulation and analysis of the final structure of a semiconductor device and its electrical parameters and characteristics.

In this article, we describe the analysis of the processes used in micro- and nano-electronic device manufacturing. We also an example of a laboratory work where students use Silvaco TCAD software tools to apply a step-by-step approach to the design and simulation of an epitaxial planar $n + pn$ transistor with junction isolation.

## Design flow

Bipolar integrated circuits typically use $n + pn$ transistors because their parameters are better than their $pnp$ transistor counterparts. There are two reasons for this. First, the solubility of phosphorus, the impurity of choice for $n$-type materials, is higher in silicon than that of boron, which is conversely the dopant-of-choice for p-type materials. This leads to a higher impurity density in the emitter region and a higher emitter current transfer coefficient for $n+pn$ transistors. Another reason is that the majority charge carrier of $n + pn$ transistors are electrons whose mobility in silicon is several times higher than that of holes. This results in a higher current transfer coefficient. Additionally, with higher mobility, the transistors have better frequency characteristics and a higher operating speed. Therefore, in the presented laboratory work, we will simulate the manufacturing processes of $n+pn$ bipolar transistors and show supporting Athena and Atlas software code with the explanation of its function.

The purpose of this laboratory work is to simulate the main manufacturing processes of an epitaxial planar $n + pn$ transistor with junction isolation, as well as to extract the I-V characteristics of the obtained semiconductor structure. The

main design stages of the technological process, described below, are as follows: silicon substrate preparation, formation of a $n$+ buried layer, silicon epitaxial layer growth, formation of junction isolation and collector region, formation of base region, formation of emitter and collector $n$+ regions, photolithography for contact windows, first aluminum metallization, passivation, description of transistor electrodes, analysis of transistor structure parameters, and simulation of I-V characteristics. All of these twelve stages performed in the laboratory work are shown in Figure 1.

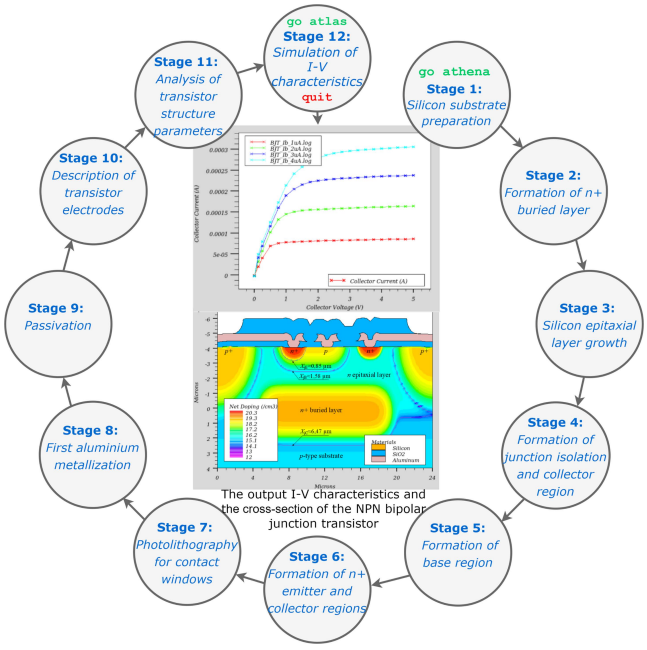


**Figure 1.** $n + pn$ bipolar junction transistor (BJT) step-by-step manufacturing and analysis flowchart.
**Source:** Authors

Note: The authors would like to point out that the code below was generated and validated using Silvaco TCAD 2012 software for both Windows and Linux operating systems. It should also be noted that the word lifting symbol (-) in the code in this article means that these lines of code must be interpreted as a single line.

1. *Silicon substrate preparation:* The simulation of a planar epitaxy $n + pn$ bipolar transistor and technological processes of other semiconductor structures with the Silvaco TCAD software can be performed by using the Athena software. This can be done by entering the following program code in the top of the Deckbuild program window:

```
1 # The first line, go Athena, invokes the Silvaco Athena
1 process simulator
2 go athena
```

Simulation of semiconductor structures and their technological processes begins with a description of the silicon wafer's dimensions. Since modern silicon wafers have a maximum diameter of 300 mm or 450 mm, and one transistor has the geometry of several or tens of micrometers, only the part of the wafer where the transistor structures will be formed is selected for simulation. The dimensions of the wafer are indicated along the axes of abscissas and ordinates. Our simulated transistor will have a starting point of the abscissa axis of 0 µm, an end point of 24 µm, and a start point of the ordinate axis of 0 µm and an end point of 4 µm. Later, the mesh (grid line) of the described wafer is formed. This is necessary because Athena uses the finite element method in its calculations. In this method, differential and integral equations are calculated at the intersection of the grid of abscissas and ordinates, so the denser the grid, the more accurate the calculations will be. However, it should be noted that grid density determines the calculation time, *i.e.* the denser it is, the longer the calculation time. Considering the accuracy of the simulation of the transistor structure and the calculation time, the following grid is chosen for further calculations: the abscissa axis will have a step grid of 0,5 µm at 0 µm and 24 µm point, and a denser step grid of 0,1 µm at 6 µm and 18 µm point, since $pn$ junctions of the transistor will be created in this interval. Similarly, in the ordinate axis, a 0,1 µm grid is selected at the wafer's surface, and a 0,5 µm grid at the 4 µm point. The program code for the selected wafer and its grid description is as follows:

```
3 # x dimension definition
4 line x loc=0.0 spacing=0.5
5 line x loc=6.0 spacing =0.1
6 line x loc=18.0 spacing =0.1
7 line x loc=24.0 spacing =0.5
8 # y dimension definition
9 line y loc=0.0 spacing =0.1
10 line y loc=4.0 spacing =0.5
```

Subsequently, the wafer material and its crystallographic structure, doping impurities and their concentration, or the specific resistance $\rho$ of the wafer are indicated. A silicon (Si) wafer with a (100) crystallographic structure, doped with boron and a specific resistance of $\rho = 10\Omega\times$ cm, was chosen. The description code for such a silicon wafer is as follows:

```
11 # (100) silicon wafer doped with boron and having a
11 resistivity of 10 Ω·cm
12 init silicon orient=100 boron resistivity=10 two.d
```

2. *Formation of n+ buried layer:* After preparing the surface of the Si wafer, a 10-minute thermal oxidation process is carried out in an atmosphere of wet oxygen at 1100 °C. The program code for thermal oxidation in wet oxygen is as follows:

```
13 # Wet oxidation at 1100 °C for 10 minutes
14 diffuse time=10 temperature=1100 wetO2 press=2 hcl=3
```

We obtain 0,38 µm thick oxide, which is then coated with a photoresist in a centrifuge. Here, due to centrifugal forces, the photoresist spreads on a flat surface with a thin layer of 0,5 mm uniform thickness. The photoresist coating of the wafer with $SiO_2$ layer is as follows:

```
15 # The surface is covered with the photoresist AZ1250J
16 deposit name.resist=AZ1350J thickness=0.5 div=10
```

Thereafter, the technological process of photolithography should include the following processing operations: drying,

exposing, heating, developing, and hardening of the photoresist. The photolithography process is replaced by the geometric etching used in Athena to simplify the program code. This etching removes the area of the photoresist specified by the coordinate points. The program code for geometric etching of the photoresist is as follows:

```
17 # Window to form the n+ buried layer
18 etch name.resist=AZ1350J start x=6.0 y=-0.8
19 etch cont x=6.0 y=-0.2
20 etch cont x=18.0 y=-0.2
21 etch done x=18.0 y=-0.8
```

$SiO_2$ is etched with fluoric acid HF using ammonium fluoride $NH_4F$ as an additive to improve the etching quality. The selectivity of such a mordant to the photoresist is very high (more than 100). The program code for isotropic etching is as follows:

```
22 # Etching speed configurations
23 rate.etch machine=HF wet.etch name.resist=AZ1350J n.m
23 isotropic=1
24 rate.etch machine=HF wet.etch oxide n.m isotropic=100
25 # Etching time setting
26 etch machine=HF time=5 min
```

The remaining photoresist layer is removed in concentrated sulphuric or nitric acid. The removal of the photoresist is described below:

```
27 # Photoresist removal
28 etch name.resist=AZ1350J all
```

It is now possible to perform the initial formation of the $n$+ buried layer. At a depth of about 0,25 mm of the silicon wafer, a diffusion of arsenic (As) impurities at 1000 °C for 5 minutes is performed:

```
29 # Diffusion of arsenic into the silicon wafer
30 diffusion time=5 temp=1000 c.arsenic=1.0e21
```

After this diffusion, the remaining $SiO_2$ layer is etched using the following program code:

```
31 # Etching the remaining SiO2 layer
32 etch oxide all
```

3. *Silicon epitaxial layer growth:* An epitaxial layer of 5 $\mu$m thick doped with $n$-type arsenic ($N_D$ = 5 x $10^{15}$ $cm^{-3}$) is caused to grow on the wafer by using the chloride method in an epitaxial vertical reactor for 10 minutes at 1000 °C. The program code for this epitaxial process is as follows:

```
33 # Growth of the arsenic-doped silicon epitaxial layer
34  epitaxy time=10 temp=1000 t.final=1100 c.arsenic=5e15
34  thickness=5 div=50
```

4. *Formation of junction isolation and collector region*: The wafer is thermally oxidized, and, during the second photolithography step, windows are etched in the areas where the two-stage boron diffusion will occur. The first diffusion is the doping of boron impurities at 1100 °C for 10 minutes, and the second diffusion is the redistribution of boron impurities at 1200 °C under a dry oxygen atmosphere. The duration of the second stage is chosen so that the boron impurities penetrate the entire thickness of the epitaxial layer. In this way, an $n$ conductivity collector area is isolated by the $p$+ conductivity areas. The program code for this stage is as follows:

```
35 # Wet oxidation at 1100 °C for 10 minutes
36 diffuse time=10 temperature=1100 wetO2 press=2 hcl=3
37 # The surface is covered with the photoresist AZ1250J
38 deposit name.resist=AZ1350J thickness=0.5 div=10
39 # Window in the photoresist to form the isolation area:
39 left window
40 etch name.resist=AZ1350J start x=0.0 y=-5.6
41 etch cont x=0.0 y=-5.0
42 etch cont x=0.5 y=-5.0
43 etch done x=0.5 y=-5.6
44 # Window in the photoresist to form the isolation area:
44 right window
45 etch name.resist=AZ1350J start x=23.5 y=-5.6
46 etch cont x=23.5 y=-5.0
47 etch cont x=24.0 y=-5.0
48 etch done x=24.0 y=-5.6
49 # Etching speed configurations
50 rate.etch machine=HF wet.etch name.resist=AZ1350J n.m
50 isotropic=1
51 rate.etch machine=HF wet.etch oxide n.m isotropic=100
52 # Etching time setting
53 etch machine=HF time=5 min
54 # Photoresist removal
55 etch name.resist=AZ1350J all
56 # Diffusion of boron into silicon wafer
57 diffusion time=10 temp=1100 c.boron=1.0e21
58 # Redistribution of boron impurities
59 diffusion time=40 temp=1200 dryo2 press=1 hcl=2
60 # Etching the remaining SiO2 layer
61 etch oxide all
```

5. *Formation of base region:* Thermal oxide is grown with a thickness of about 0,38 mm. The third photolithography step is used to open the window of the base of the transistor in the oxide. Through this window, boron diffusion is also carried out in two stages. The target reference parameters of the base layer are: a depth $X_{jB}$ ofabout 1,5-2,0 mm, a sheet resistance $R_{sB}$ of about 250-300 Ω/□, and a surface concentration $N_{0B}$ of about 4-5 x $10^{18}$ $cm^{-3}$. During the second stage of diffusion, the oxide layer that has grown in the base area is etched. The program code for this stage is as follows:

```
62 # Wet oxidation at 1100°C for 10 minutes
63 diffuse time=10 temperature=1100 wetO2 press=2 hcl=3
64 # The surface is covered with the photoresist AZ1250J
65 deposit name.resist=AZ1350J thickness=0.5 div=10
66 # Window in the photoresist for base doping
67 etch name.resist=AZ1350J start x=12.5 y=-5.4
68 etch cont x=12.5 y=-4.8
69 etch cont x=17.0 y=-4.8
70 etch done x=17.0 y=-5.4
71 # Etching speed configurations
72 rate.etch machine=HF wet.etch name.resist=AZ1350J n.m
72 isotropic=1
73 rate.etch machine=HF wet.etch oxide n.m isotropic=100
74 # Etching time setting
75 etch machine=HF time=5 min
76 # Removal of the photoresist
77 etch name.resist=AZ1350J all
78 # Diffusion of boron into silicon wafer
79 diffusion time=10 temp=1100 c.boron=3e19
80 # Redistribution of boron impurities
81 diffusion time=15 temp=1200 dryo2 press=1 hcl=2
82 # Etching of the remaining SiO2 layer
83 etch oxide all
```

6. *Formation of emitter and collector n+ regions:* During the fourth photolithography step, windows for emitter diffusion and collector resistance reduction are formed. The $n$+ emitter is obtained through one-stage diffusion of phosphorus in an oxidizing medium for 5 minutes at 1000 °C. The target reference parameters of the emitter layerare as follows: the depth $X_{jE}$ is about 0,7-0,9 mm, the sheet resistance $R_{sE}$ is about 8–10 Ω/□, and the surface concentration $N_{0E}$ is about 1,5-2,0 x $10^{20}$ $cm^{-3}$. The program code for this stage is described below:

```
84 # Wet oxidation at 1100 °C for 10 minutes
85 diffuse time=10 temperature=1100 wetO2 press=2 hcl=3
86 # The surface is covered with the photoresist AZ1250J
87 deposit name.resist=AZ1350J thickness=0.5 div=10
88 # Window in the photoresist for emitter doping
89 etch name.resist=AZ1350J start x=16.0 y=-5.2
90 etch cont x=16.0 y=-4.6
91 etch cont x=17.0 y=-4.6
92 etch done x=17.0 y=-5.2
93 # Window in the photoresist to form the ohmic collector
93 contact
94 etch name.resist=AZ1350J start x=8.0 y=-5.2
95 etch cont x=8.0 y=-4.6
96 etch cont x=9.0 y=-4.6
97 etch done x=9.0 y=-5.2
98 # Etching speed configurations
99 rate.etch machine=HF wet.etch name.resist=AZ1350J n.m
99 isotropic=1
100 rate.etch machine=HF wet.etch oxide n.m isotropic=100
101 # Etching time setting
102 etch machine=HF time=5 min
103 # Photoresist removal
104 etch name.resist=AZ1350J all
105 # Diffusion of phosphorus into silicon wafer
106 diffusion time=5 temp=1000 c.phos=1e21
107 # Etching of the remaining SiO2 layer
108 etch oxide all
```

7. *Photolithography for contact windows:* The silicon wafer is thermally oxidized. The thickness of the oxide is about 0,38 mm. During the fifth photolithography step, windows are etched in areas where the transistor terminals, including the emitter, the base, the collector, and the junction isolation, create ohmic contacts between aluminum and silicon. After the oxide etching, the photoresist is removed. The program code for this stage is as follows:

```
109 # Wet oxidation at 1100 °C for 10 minutes
110 diffuse time=10 temperature=1100 wetO2 press=2 hcl=3
111 # The surface is covered with the photoresist AZ1250J
112 deposit name.resist=AZ1350J thickness=0.5 div=10
113 # Window in the photoresist to form the emitter
113 electrode
114 etch name.resist=AZ1350J start x=16.25 y=-5.1
115 etch cont x=16.25 y=-4.4
116 etch cont x=16.75 y=-4.4
117 etch done x=16.75 y=-5.1
118 # Window in the photoresist to form the base electrode
119 etch name.resist=AZ1350J start x=12.75 y=-5.1
120 etch cont x=12.75 y=-4.4
121 etch cont x=13.25 y=-4.4
122 etch done x=13.25 y=-5.1
123 # Window in the photoresist to form the collector
123 electrode
124 etch name.resist=AZ1350J start x=8.25 y=-5.1
125 etch cont x=8.25 y=-4.4
126 etch cont x=8.75 y=-4.4
127 etch done x=8.75 y=-5.1
128 # Etching speed configurations
129 rate.etch machine=HF wet.etch name.resist=AZ1350J n.m
129 isotropic=1
130 rate.etch machine=HF wet.etch oxide n.m isotropic=100
131 # Etching time setting
132 etch machine=HF time=5 min
133 # Photoresist removal
134 etch name.resist=AZ1350J all
```

8. *First aluminum metallization*: Before covering the aluminum layer through chemical vapor deposition, the wafer is cleaned by means of a chemical or plasma treatment. The projected Al layer thickness is 0,5 mm:

```
135 # Chemical vapor deposition of aluminum
136 rate.depo machine=cvd aluminum n.m cvd dep.rate=250
136 step.cov=0.80
137 deposit machine=cvd time=2 minutes div=10
```

During the sixth photolithography step, windows for the transistor electrodes and other integrated circuit elements such as junction isolation are formed in the photoresist. The aluminum layer is then etched. Conductive paths, which are conductors connecting elements of integrated circuits, remain in the contact windows and on the insulating layer of silicon dioxide. The width of these conductive paths depends on the minimum size of photolithography and/or the maximum densities of the flowing current. Aluminum is etched in acid and alkaline solutions. In the case of a positive photoresist, Al is etched at 60-70 °C in phosphoric acid, and acetic, nitric acid additives are used to improve the etching quality. The etching speed of Al is about 550-600 nm/min, when the mordant solution contains 80% $H_3PO_4$, 5% $HNO_3$, 5% $CH_3COOH$, and 10% deionized $H_2O$, and the temperature is 60 °C. Then, after removing the photoresist, annealing of the Al contacts is performed at 500 °C to improve the quality of the ohmic contacts. The program code for this stage is as follows:

```
138 # The surface is covered with the photoresist AZ1250J
139 deposit name.resist=AZ1350J thickness=0.5 div=10
140 # Window in the photoresist to form the electrode
141 etch name.resist=AZ1350J start x=10.0 y =-5.6
142 etch cont x=10.0 y=-4.9
143 etch cont x=11.5 y=-4.9
144 etch done x=11.5 y=-5.6
145 # Window in the photoresist to form the electrode
146 etch name.resist=AZ1350J start x=14.5 y =-5.6
147 etch cont x=14.5 y=-4.9
148 etch cont x=15.0 y=-4.9
149 etch done x=15.0 y=-5.6
150 # Etching speed configurations: phosphoric acid
150 solution
151 rate.etch machine=H3PO4 wet.etch name.resist=AZ1350J
151 n.m isotropic=15
152 rate.etch machine=H3PO4 wet.etch aluminum n.m
152 isotropic=550
153 # Etching time setting
154 etch machine=H3PO4 time=1 min
155 # Photoresist removal
156 etch name.resist=AZ1350J all
157 # Surface tension and viscosity of aluminum
158 material aluminum gamma.reflo=860 reflow visc.0=2e-17
158 visc.E=4.45
159 # Aluminum annealing
160 bake time=5 min temp=500 reflow
```

9. *Passivation*: Finally, a continuous layer of silicon dioxide is deposited on the wafer's surface. Subsequently, the passivation photolithography step is performed to open windows for the final contacts/electrodes. These processes conclude the batch processing of transistors and integrated circuits with a

single metallization on a silicon wafer. The program code is as follows:

```
161 # Chemical vapor deposition of SiO2
162 rate.depo machine=SiO2 oxide n.m cvd
162 dep.rate=125 step.cov=0.80
163 deposit mach=SiO2 time=8.0 minute div=10
164 # Photolithography to open the contacts
165 # The surface is covered with the photoresist AZ1250J
166 deposit name.resist=AZ1350J thickness=0.5 div=10
167 # Window in the photoresist to form the emitter contact
168 etch name.resist=AZ1350J start x=0 y=-6.5
169 etch cont x=0 y=-5.9
170 etch cont x=2.0 y=-5.9
171 etch done x=2.0 y=-6.5
172 # Window in the photoresist to form the collector
172 contact
173 etch name.resist=AZ1350J start x=22 y=-6.5
174 etch cont x=22 y=-5.9
175 etch cont x=24.0 y=-5.9
176 etch done x=24.0 y=-6.5
177 # Etching speed configurations
178 rate.etch machine=HF wet.etch name.resist=AZ1350J n.m
178 isotropic=1
179 rate.etch machine=HF wet.etch oxide n.m isotropic=100
180 # Etching time setting
181 etch machine=HF time=10 min
182 # Photoresist removal
183 etch name.resist=AZ1350J all
```

*10. Description of transistor electrodes:* Once the transistor electrodes are formed, their names need to be specified to simulate the electrical characteristics of the created device. This is done by specifying the midpoints of the following electrodes in the abscissa axis:

```
184 # Electrode names
185 electrode name=collector x=8.5
186 electrode name=emitter x=16.5
187 electrode name=base x=13.0
```

*11. Analysis of transistor structure parameters:* During the manufacturing of the integrated device, the technological process must be monitored. The quality of oxidation, photolithography, and surface cleaning are visually checked. The parameters of the diffusion area are controlled by measuring sheet resistances $R_s$, impurity concentrations $N_0$, and/or junction depths $X_j$. These parameters can also be fixed with Athena. The depths $X_j$ of the resulting $pn$ junctions at the middle of the emitter, *i.e.* the 16,5 abscissa point (x.val = 16,5) is found using the following program codes:

```
188 # Extraction of the emitter depth XjE
189 extract name="Emitter depth" xj material="Silicon"
189 mat.occno=1 x.val=16.5 junc.occno=1
190 # Extraction of the base depth XjB
191 extract name="Base depth" xj material="Silicon"
191 mat.occno=1 x.val=16.5 junc.occno=2
192 # Extraction of the collector depth XjC
193 extract name="Collector depth" xj material="Silicon"
193 mat.occno=1 x.val=16.5 junc.occno=3
```

The *junc.occno* parameter specifies the order of the semiconductor layers from the substrate surface at the selected point (x.val = 16,5). Since, within the structure of the $n+pn$ transistor, the emitter area is the first layer of the wafer's surface, then *junc.occno* = 1. Meanwhile, the base area is the second layer, and the collector is the third one, so these parameters are set to *junc.occno* = 2, *junc.occno* = 3, respectively.

After the calculations, the following results will be displayed in the bottom executable window of the Deckbuild:

```
EXTRACT > extract name="Emitter depth" xj material="Silicon"
mat.occno=1 x.val=16.5 junc.occno=1
Emitter depth = 0.83842 um from top of first Silicon layer
X.val=16.5
EXTRACT > extract name="Base depth" xj material="Silicon"
mat.occno=1 x.val=16.5 junc.occno=2
Base depth = 1.5771 um from top of first Silicon layer
X.val=16.5
EXTRACT > extract name="Collector depth" xj material="Silicon"
mat.occno=1 x.val=16.5 junc.occno=3
Collector depth = 6.47272 um from top of first Silicon layer
X.val=16.5
```

Calculations show that the emitter's depth ($X_{jE}$) is approximately equal to 0,84 µm, the base $X_{jB} \approx 1{,}58$ µm, and the collector $X_{jC} \approx 6{,}47$ µm.

The sheet resistances $R_s$ are determined using the following program codes:

```
194 # Extraction of the emitter sheet resistance depth RsE
195 extract name="Emitter sheet resistance" sheet.res
195 material="Silicon" mat.occno=1 x.val=16.5
195 region.occno=1
196 # Extraction of the base sheet resistance depth RsB
197 extract name="Base sheet resistance" sheet.res
197 material="Silicon" mat.occno=1 x.val=13.0
197 region.occno=1
198 # Extraction of the collector sheet resistance depth
198 RsC
199 extract name="Collector sheet resistance" sheet.res
199 material="Silicon" mat.occno=1 x.val=8.5
199 region.occno=1
```

The calculations of the sheet resistance $R_s$ give the following results: $R_{sE} \approx 8{,}92\ \Omega/\square$, $R_{sB} \approx 302{,}93\ \Omega/\square$, $R_{sC} \approx 6{,}84\ \Omega/\square$.

The surface impurity concentrations $N_0$ of the formed $n+pn$ transistor areas are determined using the following program codes:

```
200 # Extraction of the emitter surface impurity
200 concentration N0E
201 extract name="Emitter surface concentration" surf.conc
201 impurity="Net Doping" material="Silicon" mat.occno=1
201 x.val=16.5
202 # Extraction of the base surface impurity
202 concentration N0B
203 extract name="Base surface concentration" surf.conc
203 impurity="Net Doping" material="Silicon" mat.occno=1
203 x.val=13.0
204 # Extraction of the collector surface impurity
204 concentration N0C
205 extract name="Collector surface concentration"
205 surf.conc impurity="Net Doping" material="Silicon"
205 mat.occno=1 x.val=8.5
```

The calculations of the transistor areas $N_0$ gives the following results: $N_{0E} \approx 1{,}96 \times 10^{20}$ cm$^{-3}$, $N_{0B} \approx 2{,}43 \times 10^{18}$ cm$^{-3}$, collector $N_{0C} = 1{,}82 \times 10^{20}$ cm$^{-3}$.

Finally, after fixing all the necessary parameters, the designed structure of the n+pn transistor with junction isolation is saved in the file *complete_BJT.str* and represented by the TonyPlot:

```
206 # Saving and plotting of the final structure
207 structure outfile = complete_BJT.str
208 tonyplot complete_BJT.str -set settings.set
```

It should be noted that the TonyPlot has a specified text setting file (*settings.set*). This file stores the graph settings, text sizes, label names, etc. Therefore, when a Tonyplot graph is configured for the first time, this information is saved and reused as a template when creating new graphs and images. An example of this file is provided in Appendix A at the end of this article.

When all commands discussed above are saved in the Deckbuild program window, calculations are performed. During this process, the TonyPlot will show the structure of a planar epitaxial bipolar $n+pn$ transistor and the impurity distribution in the semiconductor volume. It can be seen in Figure 2.

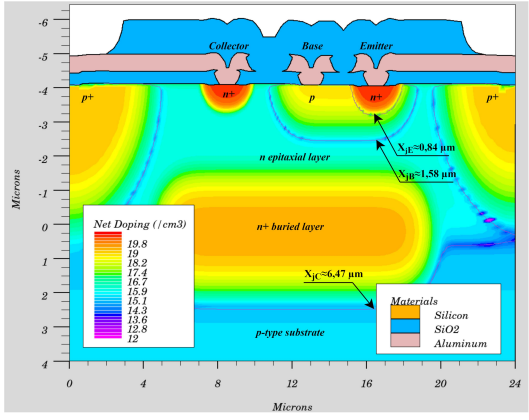


**Figure 2.** Cross-section view of the $n + pn$ bipolar junction transistor.
**Source:** Authors

Previously, $X_j$ setup program codes were provided, but this can also be done graphically. To do this, select the sequence of commands *Plot* → *Display* → *Junction* in the TonyPlot window, and when it is executed, *pn* junction boundaries will be plotted. To set these boundaries accurately, it is advisable to use a ruler that can be selected by executing the *Tools* → *Ruler* command sequence. After making measurements at the middle of the emitter, *i.e.* at 16,5 µm abscissa point, it can be seen that $X_{jE} \approx 0{,}84$ µm, $X_{jB} \approx 1{,}58$ µm, and $X_{jC} \approx 6{,}47$ µm. The results of the measurements are presented in Figures 2 and 3.

The *Tools* → *Cutline* command sequence is used to determine the impurity distribution in the desired areas of the semiconductor structure. After executing this command and selecting the vertical cursor, the desired point of the abscissa axis (in this case, the middle of the emitter, $x$ = 16,5 µm) generates a graph of the net doping Neff (Figure 3). Neff is the modulus of the difference between donor $N_D$ and acceptor $N_A$ impurities, *i.e.* $N_{eff} = |N_D\text{-}N_A|$. This graph can also be used to determine the $X_j$ depths of *pn* junctions. Knowing that *pn* junctions are formed at a depth where the concentration of doped donor impurities is equal to the concentration of acceptor impurity (*i.e.* $N_{eff} = |N_D\text{-}N_A| = 0$), the minima of this graph will correspond to the previously calculated and measured values of $X_{jE}$, $X_{jB}$, and $X_{jC}$.

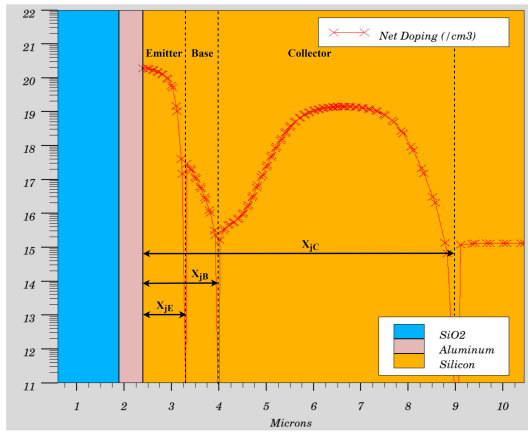


**Figure 3.** Doping profiles of the $n + pn$ bipolar junction transistor.
**Source:** Authors

12. *Simulation of I-V characteristics:* Here is the program code for simulation of the output I-V characteristics family of a planar epitaxial bipolar $n + pn$ transistor:

```
209 # The first line, go Atlas, invokes the Silvaco Atlas
209 device simulator
210 go atlas
211 # Loading of the n+pn bipolar transistor structure
212 init infile=complete_BJT.str
213 # Description of bipolar transistor models
214 models conmob fldmob consrh auger print
215 # Setting of the base current values
216 solve init
217 solve vbase=0.1 vstep=0.1 vfinal=0.7 name=base
218 contact name=base current
219 solve ibase=1.e-6 outfile=BJT_1uA
220 solve ibase=2.e-6 outfile=BJT_2uA
221 solve ibase=3.e-6 outfile=BJT_3uA
222 solve ibase=4.e-6 outfile=BJT_4uA
223 # Changing the collector voltage at a given base
223 current
224 load infile=BJT_1uA
225 log outfile=BJT_1uA.log
226 solve vcollector=0.0 vstep=0.25 vfinal=5.0
226 name=collector
227 load infile=BJT_2uA
228 log outfile=BJT_2uA.log
229 solve vcollector=0.0 vstep=0.25 vfinal=5.0
229 name=collector
230 load infile=BJT_3uA
231 log outfile=BJT_3uA.log
232 solve vcollector=0.0 vstep=0.25 vfinal=5.0
232 name=collector
233 load infile=BJT_4uA
234 log outfile=BJT_4uA.log
235 solve vcollector=0.0 vstep=0.25 vfinal=5.0
235 name=collector
236 # Saving and plotting of the output I-V
236 characteristic-curve
237 tonyplot -overlay BJT_1uA.log BJT_2uA.log BJT_3uA.log
237 BJT_4uA.log -set BJT_settings.set
238 quit
```

An example of the *BJT_settings.set* settings file is given in Appendix B.

Figure 4 shows the family of the output I-V characteristics of a bipolar $n + pn$ transistor. These characteristics show that the current of the collector $I_C$ is controlled by the current of the base $I_B$. When $V_C$ = 2 V, and when the $I_B$ current changes from 1 µA to 2 µA, the collector current $I_C$ increases from 50

μA to 100 μA, that is, the base current transfer coefficient $\beta$ is about 50.

## Conclusions

The design and analysis of the manufacturing processes were performed for an epitaxial planar $n + pn$ bipolar transistor with junction isolation, using only the seven photolithography steps. The basic design parameters of the transistor are given below. The crystallographic orientation of the silicon wafer is (100), doped with boron, and the specific resistance is $\rho$ = 10 Ω x cm. The epitaxial layer of silicon is 5 μm thick, $n$-type, and has a surface concentration of $N_D = 5 \times 10^{15}$ cm$^{-3}$. The depth of the emitter is approximately equal to $X_{jE} \approx 0{,}84$ μm, the base $X_{jB} \approx 1{,}58$ μm, and the buried layer (collector) $X_{jC} \approx 6{,}47$ μm. Sheet resistance is, respectively, $R_{sE} = 8{,}92$ Ω/□, $R_{sB} = 302{,}93$ Ω/□ and $R_{sC} = 6{,}84$ Ω/□, and the surface concentrations $N_{0E} \approx 1{,}96 \times 10^{20}$ cm$^{-3}$, $N_{0B} \approx 2{,}43 \times 10^{18}$ cm$^{-3}$, and $N_{0C} = 1{,}82 \times 10^{20}$ cm$^{-3}$, respectively.

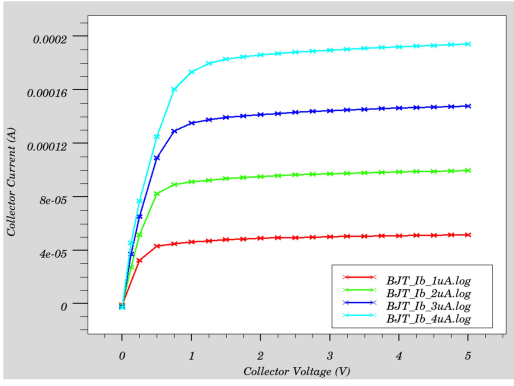


**Figure 4.** Output I-V characteristics of the n+pn bipolar junction transistor.
**Source:** Authors

## Discussions

At first glance, this kind of laboratory work may be considered 'dry', when merely entering the specified program code and realizing the supplied transistor structure without much further consideration. If students mechanically or monotonously enter the program code without delving into its meaning, syntax, and sequence, they do not acquire new knowledge, and, thus, the laboratory work becomes boring for them. To avoid this scenario, it is also necessary to present additional interesting tasks or control questions or tests that will allow students to understand the essence of this laboratory work and consolidate their knowledge. Therefore, each laboratory work session should be divided into separate stages that define the basic steps or groups of steps in the manufacturing of the micro- and nano-electronics device being developed. For example, the laboratory work presented in this article distinguishes 12 main stages: silicon substrate preparation, formation of a $n$+ buried layer, silicon epitaxial layer growth, formation of junction isolation and collector region, formation of base region, formation of emitter and collector $n$+ regions, photolithography for contact windows, first aluminum metallization, passivation, description of transistor electrodes, analysis of transistor structure parameters, and simulation of I-V characteristics. All these stages are shown in Figure 1. At each of these stages, the student is given additional tasks, which are presented in the form of a test. These tasks include both theoretical questions that examine the student's knowledge gained during the lectures and practical questions/tasks, which allows them to assess their skills and understanding. For example, in the silicon substrate preparation stage, students are asked test questions about the silicon monocrystalline ingot growth technologies, the slicing methods of the silicon ingot, the standard wafer diameters and thickness, the basic process steps for wafer preparation, and similar questions, which are discussed in detail during the lectures. Meanwhile, the practical questions ask a variety of questions related to the TCAD program code that were performed during laboratory work: how the dimensions of the silicon wafer are described, what the purpose of the mesh and its density is, among others. Practical questions also include asking students to create teacher-provided examples of silicon wafers with an appropriate or specific mesh. Meanwhile, in the final simulation of I-V characteristics, students answer theoretical questions related to the physical phenomena of BJTs, their regions of operation, different configurations for connecting BJTs, transistor testing methods, and so on. This article presents the program code for the output I-V characteristics family of BJTs. However, with a simple modification of this program code, the input I-V characteristics family can be obtained. Such modifications are given to students in practical tasks. From the obtained I-V characteristics, students can determine the basic parameters of BJTs: the common-emitter current transfer factor $\beta$, saturation and cut-off voltage points, transconductance, early voltage point, and others. The ability to simulate and analyze the I-V characteristics of transistors enables students to understand the theory of transistor operation, their basic parameters, and the technical specifications provided by manufacturers. This acquired knowledge and abilities allow students to properly use bipolar transistors to design various electronic devices.

After completing all these additional tasks, the student gets an assessment and proceeds to the next stage of this laboratory work. By completing all the stages and additional tasks, the student gets a final total grade.

Since these tasks do not require complex and expensive equipment, but only software tools, they can also be done remotely. In the case of most TCAD software packages, students can log in to their dedicated accounts or use licenses for these software tools remotely. Distance learning opens a wide range of opportunities for students and teachers alike. Students can learn and complete tasks with their own potential and at their own pace and time, and teachers, in turn, can come up with more interesting homework, course projects, or complex tasks that involve teams of students. This will enable students to further expand their knowledge and gain new research and experimentation experience while developing project management and people skills.

As mentioned earlier, teachers can also provide interesting

course projects that students can do individually or in teams. For these projects, it is appropriate to give tasks from scientific publications that provide images or photos of real micro- and nano-electronic device structures. Students make an accurate computer simulation of these structures and analyze the obtained results by using the TCAD software tools and data from scientific publications. Two main advantages of such tasks could be highlighted. The first advantage is that students are convinced of the simulation accuracy of the TCAD software tools, and the second advantage is that students analyze scientific literature, which promotes scientific cognition and allows students to evaluate the possibilities of the practical application of scientific achievements. An example of one simple course project is shown in Figure 5.

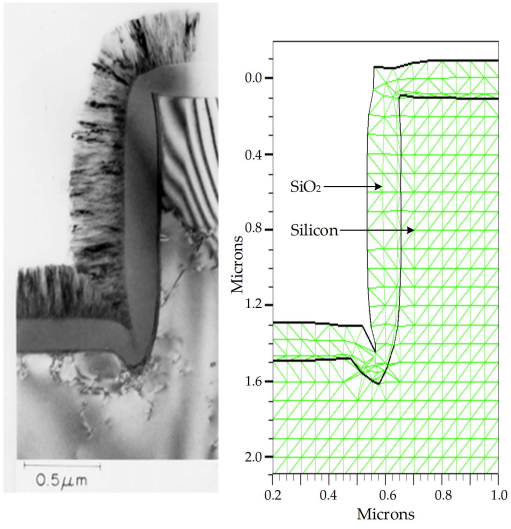


**Figure 5.** Oxidation in wet oxygen at 950 °C for 40 minutes: a) semiconductor structure photo (Marcus and Sheng, 1982); b) results of TCAD computer simulation.
**Source:** Authors

This figure shows the growth specificity of silicon oxide, which depends on surface relief, various defects, and the formation of stresses. Students select appropriate materials and technological process parameters specified in the scientific article, and they simulate this structure and perform analysis with TCAD software tools. The results of this effort are submitted to the lecturer and presented to other students.

Valuable references which can be used as sources of theoretical material when coming up with tasks for students can be found in the referenced books and publications (Armstrong and Maiti, 2007; Maiti and Maiti, 2013; Maiti, 2017; Plummer, Deal, and Griffin, 2000; Sarkar, 2013).

This type of laboratory work, along with proposed tasks and control questions or tests, has been positively received by students at the Vilnius Gediminas Technical University. We have disclosed this in our previous article (Barzdenas, Grazulevicius, and Vasjanov, 2020) by providing capturing student feedback over several years. At the end of each laboratory work, a voluntary student survey is conducted to collect immediate feedback. Figure 6 and Table 1 show a subset of eight questions from this questionnaire. The answers of 83 fifth-year respondents were collected. For example, 81,93% and 85,54% of the respondents answered positively to the questions "Did you like carrying out this lab work?" and "Did this lab work provide you with new knowledge or skills?". Such a large number of positive responses indicates that students are both particularly receptive about the use of such laboratory work in the study process, and that it promotes the assimilation of the theoretical material introduced during lectures.

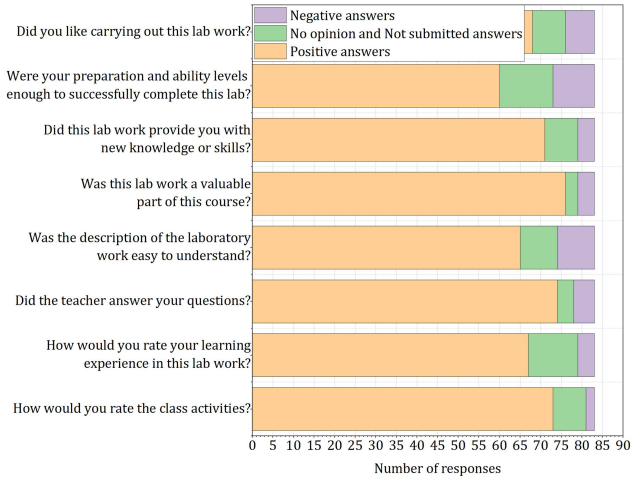


**Figure 6.** Graphical representation of the survey results.
**Source:** Authors

**Table 1.** Summary of the student survey results, $N = 83$

| Question | Positive answers | No opinion and not submitted answers | Negative answers |
|---|---|---|---|
| How would you rate the class activities? | 73 | 8 | 2 |
| How would you rate your learning experience in this lab work? | 67 | 12 | 4 |
| Did the teacher answer your questions? | 74 | 4 | 5 |
| Was the description of the laboratory work easy to understand? | 65 | 9 | 9 |
| Was this lab work a valuable part of this course? | 76 | 3 | 4 |
| Did this lab work provide you with new knowledge or skills? | 71 | 8 | 4 |
| Were your preparation and ability levels enough to successfully complete this lab? | 60 | 13 | 10 |
| Did you like carrying out this lab work? | 68 | 8 | 7 |

**Source:** Authors

## Conclusions

This paper presents an exemplary laboratory work cycle of manufacturing processes for micro- and nano-electronics

devices. The aim of this laboratory work is to simulate the structure and I-V characteristics of an epitaxial planar $n + pn$ bipolar transistor with junction isolation using Silvaco TCAD software tools. Seven photolithography steps were used to obtain the structure of this transistor: buried layer formation, junction transistor isolation and collector region formation, base region formation, emitter and collector $n+$ region formation, contact windows, first aluminum metallization, and passivation. This laboratory work also provides examples of the determination of sheet resistances, surface impurity concentrations, and junction depths of individual regions of the resulting bipolar transistor. Such laboratory work, which covers all device manufacturing processes and the simulation of their electrical characteristics, enables students to have a consistent view of the manufacturing process of such devices in order for them to deepen their knowledge gain new research and experimentation experience. In turn, this knowledge and these skills will enable students to contribute significantly in the future to the ever-growing development of micro- and nano-electronics and other industries and sectors.

## Appendix A

```
### Semiconductor structure image/view settings ###
# View mesh on/off
show mesh off
# Material edges enabled/disabled
show edges on
# Materials display on/off
show materials on
# Impurity concentration distributions on/off
show contours on
# Junction depths on/off
show junctions on
### Settings of impurity concentrations ###
# Show the effective impurity concentration
contours 1 impurity "Net Doping"
# Show impurity concentrations in silicon only
contours 1 materials 1
contours 1 materials "Silicon" 1
# Color step of impurity concentration divisions
contours 1 nsteps 33
# Impurity concentrations outline on/off
contours 1 outline off
# Color palette of impurity concentrations
contours 1 color 0
# Enable impurity concentration settings
contours 1 apply
```

## Appendix B

```
### Label position settings ###
# Collector current label at the bottom right
key electrical at 1
# Base currents label at the top left
key overlay at 4
# Enable label position settings
key apply
### Output I-V characteristics graph settings ###
# Show graph points
show points on
# Show graph lines
show lines on
# Graph type setting
xygraph type 0 convert 0
# Graph y-axis scale setting
xygraph yaxis scale linear
# x-axis type setting
xygraph xaxis "Collector voltage" linear
# y-axis type setting
xygraph yaxis "Collector current" linear
# Show x-axis title
show label xaxis on
# Show y-axis title
show label yaxis on
# x-axis title description
label xaxis "Collector voltage, V"
# y-axis title description
label yaxis "Collector current, A"
```

## References


Annegarn, M., Baldi, L., Hartman, R., Lehner, N., Matheron, G., and Van Roosmalen, F. (2012, November). *Innovation for the future of Europe: Nanoelectronics beyond 2020*. Paris: Aeneas and Catrene. https://ec.europa.eu/digital-single-market/en/news/innovation-future-europe-nanoelectronics-beyond-2020

Armstrong, G. A. and Maiti, C. K. (2007). *Technology computer aided design for Si, SiGe and GaAs integrated circuits* (Vol. 21). London: IET.

Barzdenas, V., Grazulevicius, G., and Vasjanov, A. (2020). TCAD tools in undergraduate studies: A laboratory work for learning deep submicron CMOS processes. *The International Journal of Electrical Engineering and Education, 57*(2), 133-163. 10.1177/0020720919846811

Barzdenas, V. and Navickas, R. (2012). *Microtechnologies: A Laboratory Manual*. Vilnius: Technika.

European Commission (2012). *Key Enabling Technologies. A bridge to growth and jobs. Press release*. https://ec.europa.eu/commission/presscorner/detail/en/MEMO_12_484

European Commission (2013). *Status Implementation Report – Second High-Level Expert Group on Key Enabling Technologies* (*KETs*). https://ec.europa.eu/growth/content/status-implementation-report----second-high-level-expert-group-key-enabling-technologies-kets_en

European Commission (2015). *High-Level Expert Group on Key Enabling Technologies. Final Report KETs: Time to Act*. https://ec.europa.eu/growth/content/high-level-expert-group-kets-publishes-final-recommendations-0_en

European Commission (2018). *What are KETs and why are they important? Internal Market, Industry, Entrepreneurship and SMEs*. https://ec.europa.eu/growth/industry/policy/key-enabling-technologies/description_en

Eurostat (2018). *ICT specialists in employment – Statistics Explained*. https://ec.europa.eu/eurostat/statistics-explained/index.php/ICT_specialists_in_employment

Maiti, C. K. and Maiti, A. (2013). Teaching technology computer aided design (TCAD) online. In Information Resources Management Association (Eds.) *Industrial Engineering: Concepts, Methodologies, Tools, and Applications* (pp. 1043-1063). Hershey, PA: IGI Global.

Maiti, C. K. (2017). *Introducing Technology Computer-Aided Design* (*TCAD*)*: Fundamentals, Simulations, and Applications*. Boca Raton, FL: CRC Press.

Marcus, R. B. and Sheng, T. T. (1982). The oxidation of shaped silicon surfaces. *Journal of the Electrochemical Society, 129*(6), 1278. 10.1149/1.2124118

Plummer, J. D., Deal, M., and Griffin, B. P. (2000). *Silicon VLSI Technology: Fundamentals, Practice, and Modeling*. Upper Saddle River, NJ: Prentice Hall.

Sarkar, C. K. (Ed.) (2013). *Technology computer aided design: simulation for VLSI MOSFET*. Boca Raton, FL: CRC Press.

United States Department of Labor (2019). *Computer and information technology occupations: Occupational Outlook Handbook*. https://www.bls.gov/ooh/computer-and-information-technology/home.htm

# Instructions for Authors

Editorial Committee reserves the copyright to printing any material and its total or partial reproduction, as well as the right to accept submitted material or reject it. It also reserves the right to make any editorial modification which it thinks fit. In such event, the author of the submitted material in question will receive the evaluators' recommendations for changes to be made in writing. If an author accepts them, the revised (or rewritten) article must be submitted with the suggested changes having been made by the date fixed by the journal to guarantee its publication in the programmed issue.

## The process to be followed for publishing an article in the journal

The article must be uploaded into the journal's OJS website, see the guidelines for article submission in the Authors guide section in our website http://www.revistas.unal.edu.co/index.php/ingeinv/article/view/59291/56815. Any manuscript must be sent using journal's template (6 pages length max.) and must be accompanied by the license agreement, addressed to the journal's editor, Prof. Andrés Pavas, stating that all authors involved in the work in question agree to it being submitted for consideration in the *Ingeniería e Investigación journal*.

Article and License templates are available on:
http://www.revistas.unal.edu.co/index.php/ingeinv/index

Once an article has been received by the journal, the corresponding author will be notified by e-mail and the peer-review process will be begun. Following this evaluation, authors will then be informed whether their article has been accepted or not. If accepted, authors must deal with the respective corrections recommended by the evaluators and the Editorial Committee's final decision. If it is to be published.

## Content

All articles being considered by the committee for possible publication in the *Ingeniería e Investigación journal* must consist of the following parts:

- Title, abstract and keywords must be written in Spanish and English. The title must clearly explain the contents of the article in question, written in normal title form and be preferably brief. The abstract should contain around 200 words in Spanish and English, as well as including the methods and materials used, results obtained and conclusions drawn.
- An Introduction must be given. It must describe article's general purpouse, including its main objective, referring to any previous work and the scope of the current article.
- Conclusions must be drawn. This section must provide the implication of the results found and their relationship to the proposed objective.
- Bibliographical references must be given (an explanation and example of how to set them out is given later on).
- Acknowledgements (Optional). These should be brief and mention any essential support received for carrying out the work being reported.
- Appendix (Optional).

Scientific and technological research articles must also include:

- Experimental development. This must be written giving sufficient details for the subject to be fully understood by readers, including descriptions of any procedures involved.
- Results. These must give a clear explanation and interpretation of the findings. If it is necessary, a brief, focused discussion about how given results can be interpreted.

It is required that the bibliographical references for all articles are included at the end of the article, given in alphabetical order of first authors' surnames and mentioned in the text and, since May 2014, it is asked that the authors use the American Psychological Association (APA) style for citation and references:

*- Articles published in journals:*

Author, A. A., Author, B. B., & Author, C. C. (year). Article title. Journal Title, volume number(issue number), page numbers.

Del Sasso, L. A., Bey, L. G. & Renzel, D. (1958). Low-scale flight ballistic measurements for guided missiles. *Journal of the Aeronautical Sciences, 15*(10), 605-608

Author, A. A., & Author, B. B. (year). Article title. Journal Title, volume number(issue number), page numbers. Retrieved from http://www.xxxxxxxxxxxxxxxx

Gaona, P. A. (2014). Information visualization: a proposal to improve search and access digital resources in repositories. Ingeniería e Investigación, 34(1), 83-89. Retrieved from http://www.revistas.unal.edu.co/index.php/ingeinv/article/ view/39449

*- Books:*

Author, A. A. & Author, B. B. (year). Title of work. Location: Publisher.

Turner, M. J., Martin, H. C. & Leible, R. C. (1964). Further development and applications of the stiffness method, Matrix Methods of Structural Analysis. New York: the Macmillan Co.

*- Conference papers and symposium contributions:*

Uribe, J. (1973, September). The effects of fire on the structure of Avianca building, Paper presented at National Seminar concerning Tall Buildings, Bogotá, Colombian School of Engineering.

*- Theses or undergraduate projects:*

Patton, F. D. (1906). Multiple modes of shear failure in rock-related materials (Ph.D. thesis, University of Illinois).

## Further information can be obtained by:

Contacting the Editorial Team (Email: revii_bog@unal.edu.co) or Prof. Andrés Pavas (Editor-in-Chief.
Email: fapavasm@unal.edu.co)

The *Ingeniería e Investigación* journal's office is located at: Ciudad Universitaria, Facultad de Ingeniería, Edificio CADE. Telefax: (57-1) 3165000 Ext. 13674. Bogotá - Colombia.